Functional and Evolutionary Characterisation of Antimicrobial Effectors Secreted by *Verticillium dahliae* to Shape Host Microbiota

Doctoral thesis

for

the award of the doctoral degree

of the Faculty of Mathematics and Natural Sciences

of the University of Cologne

submitted by

Anton Kraege

Accepted in the year 2026

Table of Contents

Thesis Summary

Plants are continuously colonized by diverse microbial communities, collectively known as the plant microbiota, which inhabit all parts of the plant including roots, shoots, and leaves. The assembly of these communities is shaped by both environmental factors, such as soil properties and microbial pools, and host-derived factors, including root exudates that attract or repel specific taxa. Together with their host, these microbes form a functional unit known as the holobiont, in which host and microbial activities are tightly interconnected. The microbiota contributes to plant health by protecting against pathogens, for instance through direct antagonism or by stimulating host defences. Under pathogen attack, plants can recruit beneficial microbes from the bulk soil to enhance protection, a process termed the “cry for help” response. Research over recent years has shown that plant pathogens have evolved sophisticated strategies to overcome not only plant immune responses, but also microbiota-mediated defences. Many pathogens secrete antimicrobial effector proteins that manipulate host-associated microbial communities to facilitate disease development. In this thesis research I aimed to investigate the functional and evolutionary roles of antimicrobial effectors in shaping plant–microbe interactions and promoting pathogen success.

During my doctoral research, I investigated the functional and evolutionary roles of antimicrobial effectors in shaping plant–microbe interactions and pathogen success. We first characterized the *Verticillium dahliae* effector Av2, demonstrating that it suppresses the plant’s “cry for help” recruitment of antagonistic *Pseudomonas* bacteria, providing the first evidence that pathogens can actively undermine microbiota-mediated host defences. We then examined the effector Ave1, revealing that it perturbs host-associated microbial communities across natural soils and that its contribution to fungal virulence is strongly influenced by the composition of the soil microbiota, highlighting the context-dependent interaction between effectors, microbial communities, and pathogen success. Expanding to an evolutionary perspective, we developed an antimicrobial activity predictor and, revealed that antimicrobial effector repertoires in filamentous fungi are larger and more conserved than previously recognized. Additionally, we found that many fungal effectors with immunomodulatory functions possess conserved antimicrobial activity, supporting the idea that ancient antimicrobial molecules were repeatedly co-opted as immunomodulators during fungal adaptation to plant-associated niches. Focusing on the cerato-platanin effector family in *V. dahliae*, structural clustering revealed four effectors, including Ave1, with conserved antimicrobial activity *in vitro*, a trait maintained across fungi with diverse lifestyles. Together, these findings position antimicrobial effectors as ancient molecules that have been repeatedly co-opted by plant pathogens in the ongoing arms race between plants and pathogens.

Zusammenfassung

Pflanzen werden kontinuierlich von vielfältigen mikrobiellen Gemeinschaften besiedelt, die zusammen als Pflanzenmikrobiota bezeichnet werden und alle Teile der Pflanze bewohnen, einschließlich Wurzeln, Triebe und Blätter. Die Zusammensetzung dieser Gemeinschaften wird sowohl von Umweltfaktoren wie Bodeneigenschaften und mikrobiellen Pools als auch von Faktoren des Wirtspflanzen bestimmt, darunter Wurzelausscheidungen, die bestimmte Taxa anziehen oder abweisen. Zusammen mit ihrem Wirt bilden diese Mikroben eine funktionelle Einheit, die als Holobiont bezeichnet wird und in der die Aktivitäten des Wirts und der Mikroben eng miteinander verbunden sind. Die Mikrobiota trägt zur Gesundheit der Pflanzen bei, indem sie sie vor Krankheitserregern schützt, beispielsweise durch direkten Antagonismus oder durch Stimulierung der Abwehrkräfte des Wirts. Bei einem Befall durch Krankheitserreger können Pflanzen nützliche Mikroben aus dem Boden rekrutieren, um ihren Schutz zu verbessern, ein Prozess, der als „Cry-for-help“ bezeichnet wird. Forschungen der letzten Jahre haben gezeigt, dass Pflanzenpathogene ihrerseits ausgefeilte Strategien entwickelt haben, um nicht nur die Immunantworten der Pflanzen, sondern auch die durch die Mikrobiota vermittelten Abwehrmechanismen zu überwinden. Viele Krankheitserreger sezernieren antimikrobielle Effektorproteine, die die mit dem Wirt assoziierten mikrobiellen Gemeinschaften manipulieren, um die Etablierung ihrer Nische und die Entwicklung der Krankheit zu erleichtern.

Im Rahmen meiner Doktorarbeit untersuchte ich die funktionellen und evolutionären Rollen antimikrobieller Effektoren bei der Gestaltung von Pflanzen-Mikroben-Interaktionen und dem Erfolg von Pathogenen. Zunächst charakterisierten wir den *Verticillium dahliae*-Effektor Av2 und zeigten, dass er den „Cry-for-help“ der Pflanze zur Rekrutierung antagonistischer Pseudomonas-Bakterien unterdrückt. Damit lieferten wir den ersten Beweis dafür, dass Pathogene die durch die Mikrobiota vermittelte Abwehr des Wirts aktiv untergraben können. Anschließend untersuchten wir den Effektor Ave1 und stellten fest, dass er die mit dem Wirt assoziierten mikrobiellen Gemeinschaften in natürlichen Böden stört und dass sein Beitrag zur Virulenz von Pilzen stark von der Zusammensetzung der Bodenmikrobiota beeinflusst wird, was die kontextabhängige Interaktion zwischen Effektoren, mikrobiellen Gemeinschaften und dem Erfolg von Krankheitserregern unterstreicht. Ausgehend von einer evolutionären Perspektive entwickelten wir einen Prädiktor für antimikrobielle Aktivität und konnten mit diesem Tool zeigen, dass das Repertoire an antimikrobiellen Effektoren in Fadenpilzen größer und konservierter ist als bisher angenommen. Darüber hinaus fanden wir heraus, dass viele Pilzeffektoren mit immunmodulatorischen Funktionen eine konservierte antimikrobielle Aktivität besitzen, was die Annahme stützt, dass alte antimikrobielle Moleküle während der Anpassung der Pilze an pflanzenassoziierte Nischen wiederholt als Immunmodulatoren

kooptiert wurden. Mit Fokus auf die Cerato-Platanin-Effektor-Familie in *V. dahliae* wurden durch strukturelle Clusterbildung vier Effektoren identifiziert, darunter Ave1, die in vitro eine konservierte antimikrobielle Aktivität aufweisen, eine Eigenschaft, die bei Pilzen mit unterschiedlichen Lebensweisen erhalten bleibt. Zusammen genommen positionieren diese Erkenntnisse antimikrobielle Effektoren als uralte Moleküle, die von Pflanzenpathogenen im andauernden Wettrüsten zwischen Pflanzen und Pathogenen wiederholt genutzt wurden.

General Introduction

The plant microbiota

Plants are continuously colonized by diverse microbial communities that populate all tissues, collectively referred to as the plant microbiota (Trivedi et al., 2020). These communities are predominantly composed of bacteria, followed by fungi, and supplemented with other microbes that belong to other groups such as protists, archaea, nematodes, and algae (Sokol et al., 2022). Plant microbiota are commonly separated in an above-ground part, called the phyllosphere microbiota, and a blow-ground part including the root surface and the soil zone directly influenced by root exudates, called the rhizosphere microbiota (Trivedi et al., 2020). The microbiota inside plant tissues is collectively termed the endosphere microbiota and includes both roots and shoots, thus containing part of both the rhizosphere and phyllosphere microbiota.

The assembly of the plant microbiota is a process influenced by both environmental and host-derived factors. While some members of the plant microbiota are vertically transmitted across generations via seeds, a substantial portion stems from environmental sources. Althought airborne transmission contributes to the microbiota assembly, the bulk of microbes originates from the bulk soil microbiota surrounding the roots (Chialva et al., 2022; Sokol et al., 2022). The bulk soil therefore constitutes the primary microbial reservoir, providing an immense diversity of microbes. Soil physicochemical properties, such as pH, organic carbon content, nutrient availability, temperature, and redox potential strongly influence the microbial pool available for recruitment by the plant (Chialva et al., 2022; Fierer, 2017). Root exudates serve as key modulators of this microbial recruitment. These chemically diverse secretions act both as nutrient sources and as signalling molecules through which plants attract, repel, or modulate specific microbial taxa (McLaughlin et al., 2023). Exudation profiles are dynamic and can respond to plant developmental stage, environmental fluctuations, and stress conditions such as drought or pathogen attack. The impact of host recruitment on the microbiota is illustrated by the observation of plant-species specific core microbiota, defined as particular microbial taxa that can consistently be found associated with a particular plant across environments (Almario et al., 2022; Lundberg et al., 2012). Host selection is also reflected in compartment-specific microbiota within a plant, where microbial diversity tends to decline from bulk soil to the rhizosphere and phyllosphere (Trivedi et al., 2020). Besides all these deterministic factors, microbial community assembly and structure is also affected by stochastic processes such as priority effects; the order of microbial arrival (Carlström et al., 2019; Debray et al., 2022; Zhou & Ning, 2017).

The plant microbiota contributes to plant health

Within plant microbiota, microbes exhibit a range of lifestyles, engaging in mutualistic, commensal, or pathogenic interactions with their host. Mutualistic interactions directly influence plant performance, for instance through facilitating nutrient uptake, modulating hormone levels, suppressing pathogens, inducing systemic immunity and enhancing tolerance to abiotic stresses (Trivedi et al., 2020). By performing these roles, the microbiota actively contributes to plant growth, survival, and adaptability. Together with their host, the microbiota forms a complex biological unit, often referred to as the holobiont, which integrates host and microbial functions into a single evolutionary, ecological, and functional entity (Mesny et al., 2023; Vandenkoornhuyse et al., 2015). An important function of plant microbiota is their capacity to protect plants from pathogens. Mutualistic members of the plant microbiota provide basal protection by inhibiting pathogen establishment and activating host immunity (Berendsen et al., 2012; Pieterse et al., 2014). Consequently, the plant microbiota has been described as an additional layer of the plant immune system (Du et al., 2024; Hacquard et al., 2017; Pieterse et al., 2014). Under pathogen attack, plants can alter their root secretions leading to the recruitment of beneficial microorganisms from the soil in order to limit disease progression, a phenomenon termed the “cry for help” response (Berendsen et al., 2018). For example, during infection by *Fusarium oxysporum*, cucumber plants can increase the exudation of tryptophan, which promotes the recruitment of *Bacillus amyloliquefaciens* that can mitigate disease progression (Liu et al., 2017). When such plant-mediated recruitment occurs repeatedly over time, it can lead to persistent shifts in soil microbial communities that reduce pathogen fitness. In some cases, these shifts may contribute to the development of disease-suppressive soils, whereas in other systems they result in pathogen- and host-specific suppressive states (Mesny et al., 2024; Spooren et al., 2024). A well-studied example of the latter is take-all decline that can develop upon long-term wheat monocultures, where continuous wheat cultivation under recurrent pathogen pressure selects for antagonistic *Pseudomonas* species producing antibiotics such as 2,4-diacetylphloroglucinol or phenazine-1-carboxylic acid, thereby suppressing the take-all pathogen *Gaeumannomyces graminis* var. *tritici* (Raaijmakers & Weller, 1998; Spooren et al., 2024).

The plant immune system

Plants rely on a sophisticated immune system to detect and defend themselves against diverse pathogens (Cook et al., 2015; Jones & Dangl, 2006). In the classical “zigzag” model, immune activation begins when pattern-recognition receptors (PRRs) sense conserved microbe-associated molecular patterns (MAMPs), initiating pattern-triggered immunity (PTI),

which includes ROS production, ion fluxes, kinase activation, hormone signaling, defence gene expression, and cell wall fortifications (Cook et al., 2015; Jones & Dangl, 2006; Ngou et al., 2021). To successfully invade, host-adapted pathogens deploy effector proteins that can suppress these defences, resulting in effector-triggered susceptibility (ETS) (Rovenich et al., 2014). Plants, in turn, have evolved resistance (R) proteins that recognise these effectors or their activities and activate a stronger response termed effector-triggered immunity (ETI) (Jones & Dangl, 2006). Pathogens can evade such recognition by altering or losing recognized effectors, or by evolving novel ones, capable of interfering with host recognition or downstream immune responses. This dynamic interplay between pathogens and plants is described as a molecular arms race, in which pathogens modify or replace effectors to evade detection, while plants continually adapt to detect effectors or their activities (Cook et al., 2015; Jones et al., 2024; Jones & Dangl, 2006). Recognising the tight integration of PTI and ETI, and the principal dichotomy between PAMPs and effectors being flawed, and accordingly the dichotomy between PTI and ETI, the Invasion model proposed that plants detect “invasion patterns” (IPs), molecules produced by pathogens or generated during the invasion process, via invasion pattern receptors (IPRs), leading to an invasion pattern-triggered response (IPTR) that pathogens manipulate using effectors (Cook et al., 2015). Indeed, several studies have revealed mechanistic overlap between PTI and ETI responses (Ngou et al., 2021; Pruitt, Gust, et al., 2021; Pruitt, Locci, et al., 2021; Yuan et al., 2021).

Pathogen effectors facilitate host colonisation through diverse contributions

During host colonization, pathogens secrete a cocktail of effectors that deregulate host immunity and enable successful infection (Lo Presti et al., 2015). Because of their central role in plant–pathogen interactions, effectors have been a focal point of phytopathology research. Initially, the term effector was exclusively assigned to pathogen-encoded small cysteine-rich *in planta*-secreted proteins that were thought to interfere with host immunity, at the level of pathogen perception by immune receptors, downstream immune signalling, or at the level of the execution of immunity (Bozkurt et al., 2011; de Jonge et al., 2010; Lo Presti et al., 2015; Rovenich et al., 2014). Examples illustrating these classical functions include *Cladosporium fulvum* Ecp6, which sequesters chitin oligosaccharides to prevent recognition by chitin immune receptors, *Ustilago maydis* Tin2, which disrupts anthocyanin biosynthesis and may to suppress tissue lignification, or the bacterial effectors effector HopF2 from *Pseudomonas syringae* that supresses immunity by targeting mitogen-activated protein kinase signalling (de Jonge et al., 2010; Sánchez-Vallet et al., 2020; Tanaka et al., 2014; Zhou et al., 2014). However, pathogens secrete also larger proteins and non-proteinaceous molecules such as

metabolites and small RNAs to facilitate host infection, broadening the definition of effectors to include these types of molecules as well (Weiberg et al., 2013). Furthermore, effectors were recognised to manipulate other aspects of host physiology beyond immune suppression to promote pathogen virulence. For instance, the *Pseudomonas syringae* effectors HopM1 and AvrE modulate ABA signaling, inducing stomatal closure and promoting water-soaking to promote bacterial colonization of host tissues (Hu et al., 2022; Roussin-Léveillée et al., 2022), whereas *Xanthomonas* uses transcription activator-like effectors to upregulate host sugar transporters and enrich the apoplast with accessible nutrients (Chen et al., 2010). While effectors are classically associated with pathogenic interactions, it has been shown that effector secretion is not restricted to pathogens, but that mutualistic and commensal endophytes also rely on effectors to facilitate successful host colonization (Rovenich et al., 2014). For example, the root endophyte *Serendipita indica* secretes the nuclease SiNucA to modify the apoplastic nucleotide pool, leading to the production of deoxyadenosine that is taken up by host cells and induces controlled cell death, thereby facilitating mutualistic root colonization (Dunken et al., 2024).

Although many fungal effectors occur in a lineage-specific manner and share no to little sequence similarity with other effector proteins, consistent with rapid diversification driven by host–pathogen arms races, several widely conserved effector families have been identified (Sperschneider et al., 2015). These conserved effectors occur across fungi with pathogenic, mutualistic, or saprophytic lifestyles, as well as in some opportunistic animal pathogens, indicating that their distribution is broader than expected for strict plant virulence factors. For instance, LysM effectors, a class of secreted chitin-binding proteins, are found in diverse fungi across ecological niches (Kombrink & Thomma, 2013). Similarly, necrosis- and ethylene-inducing-like proteins (NLPs) occur in bacteria, fungi, and oomycetes (Seidl & Van den Ackerveken, 2019). Cerato-platanins (CPs) are proposed to contribute to virulence in certain plant pathogens through carbohydrate- or chitin-binding activities that may modify host cell walls or shield fungal chitin from recognition, yet this protein family is also widely present in fungi that do not colonize plants (Baccelli et al., 2014; Luti et al., 2020). The presence of such conserved effector families across microbes that inhabit diverse ecological niches suggests that certain effector proteins may fulfil biological functions that are unrelated to plant manipulation (Snelders et al., 2018)

Effectors for the manipulation for host microbiota

Building on the broad conservation of certain effector families across fungi with diverse lifestyles, it has been hypothesized that some effectors may function in microbial antagonism,

either in addition to, or independently of, their host-immunomodulating roles (Kombrink & Thomma, 2013; Snelders et al., 2018). For example, LysM effectors have been proposed to protect fungal hyphae and through peptidoglycan binding activity immobilize certain bacteria, thereby enhancing competitive fitness in the microbial environment (Kombrink & Thomma, 2013). Likewise, the *Zymoseptoria tritici* effector Zt6 exhibits ribonuclease activity that is both phytotoxic and antimicrobial. Expressed during spore germination, Zt6 may suppress microbial competitors near germinating spores, although its effects on fungal colonization and plant-associated microbial communities remain untested (Kettles et al., 2018). Together with the broad distribution of conserved effector families in non-plant-colonizing fungi, these observations suggest that antimicrobial activity could be a common feature of certain effectors, distinct from their direct host-targeted functions, and raise the possibility that some effectors might actively manipulate host microbiota (Snelders et al., 2018).

Direct experimental evidence for a role of effectors to shape microbial communities was provided using the soil-borne pathogen *Verticillium dahliae*. The effector Ave1, initially identified through recognition by the Ve1 receptor of tomato, has been shown to manipulate host microbiota in tomato as well as in cotton plants to facilitate successful host colonisation (de Jonge et al., 2012; Snelders et al., 2020). Experiments comparing wild type and *Ave1* deletion strains showed that *V. dahliae* uses Ave1 to suppress antagonistic bacteria, including members of the Sphingomonadales, which have been shown to reduce disease severity when applied to seeds (Snelders et al., 2020). Subsequent studies identified additional antimicrobial effectors with life stage-specific expression patterns, indicating that these effectors act at different stages of the fungal life cycle. Ave1L2 is expressed *in planta*, suppressing antagonistic Actinobacteria, whereas AMP2 is expressed exclusively during soil-dwelling stages (Snelders et al., 2020, 2023). Antimicrobial effectors can also target fungi, as exemplified by AMP3 that inhibits fungal members of the host mycobiome during late infection stages in decaying plant tissues (Snelders et al., 2021). Beyond *V. dahliae*, antimicrobial effectors have been identified in multiple other plant pathogens, suggesting that the deployment of antimicrobial effectors is a widespread strategy to manipulate microbial communities and facilitate pathogen colonisation (Chang et al., 2021; Chavarro-Carrero et al., 2024; Gómez-Pérez et al., 2023; Mesny et al., 2024; Ökmen et al., 2023).

Some effector folds are evolutionary ancient

Structural studies revealed structurally conserved yet sequence-unrelated effector families in several fungal pathogens (Derbyshire & Raffaele, 2023; Seong & Krasileva, 2023). For example, MAX and KP6 folds, initially described in *Magnaporthe oryzae* and *Zymoseptoria*

tritici, respectively, are conserved across diverse plant-pathogenic fungi despite their overall low sequence similarity (de Guillen et al., 2015, 2025; Derbyshire & Raffaele, 2023; Seong & Krasileva, 2023). The KP6 fold has also been observed in non-pathogenic fungi, indicating that these structural folds occur broadly across fungal lineages (Seong & Krasileva, 2023). Interestingly, some folds are more abundant in particular plant pathogens, suggesting lineage-specific expansions (Derbyshire & Raffaele, 2023; Seong & Krasileva, 2023). For instance, around 70% of all effectors of the wheat powdery mildew fungus *Blumeria graminis* displays an RNase-like fold (Cao et al., 2023; Pennington et al., 2019a). The conservation of structural folds across pathogenic and non-pathogenic fungi suggests that certain folds have an ancient origin, and that their sequences have diverged extensively, likely due to rapid diversification driven by host–pathogen arms races (Seong & Krasileva, 2023).

The soil-borne plant pathogenic fungus *Verticillium dahliae*

V. dahliae is a soil-borne vascular wilt fungus with a broad host range, infecting hundreds of dicotyledonous plant species, including crops such as tomato, potato, lettuce, olive, and cotton (Fradin & Thomma, 2006; Klosterman et al., 2009). The fungus persists in the soil through melanized resting structures called microsclerotia, which can survive for many years under adverse conditions. Microsclerotia germinate in response to nutrient-rich root exudates, after which *V. dahliae* penetrates roots, traverses the cortex, and enters xylem vessels (Fradin & Thomma, 2006). Within the vasculature, the fungus produces conidiospores that are passively transported to distal tissues with the transpiration stream, enabling systemic colonization and the development of typical *Verticillium* wilt symptoms, including chlorosis, necrosis, and wilting (Fradin & Thomma, 2006). During plant senescence, new microsclerotia are formed that are released into the soil as plant tissue drops to the floor and decomposes.

Although *V. dahliae* is a presumed asexual fungus, it generates genetic diversity through chromosomal rearrangements and segmental duplications (Cook et al., 2020; de Jonge et al., 2013; Faino et al., 2016; Depotter et al., 2019). These processes produce hypervariable regions known as adaptive genomic regions (AGRs), which vary between strains and are more flexible than the stable core regions that make up the rest of the genome (de Jonge et al., 2013; Cook et al., 2020). AGRs are enriched in repetitive elements and effector genes compared with core regions (Cook et al., 2020; de Jonge et al., 2013). Overall, similar to many other filamentous pathogens, *V. dahliae* has a compartmentalised genome, containing AGRs with increased plasticity compared with core genomic regions, an observation often referred to as a ‘two-speed genome’ (Raffaele & Kamoun, 2012; Torres et al., 2021). Recent studies have also identified the population of AGRs by giant transposons called *Starships* that harbour

horizontally transferred effector genes from other fungal plant pathogens, driving virulence evolution in *V. dahliae* (Sato et al., 2025).

Controlling *V. dahliae* is challenging: crop rotation is largely ineffective because of its broad host range and long-lived microsclerotia (Fradin & Thomma, 2006). Additionally, fungicide treatments are generally ineffective once the fungus entered the xylem (Fradin & Thomma, 2006). Generally, genetic resistance is preferred, but effective resistance remains rare and has been identified in few plant species only. In tomato, the *Ve1* gene encodes a cell surface-localized receptor that recognizes the antimicrobial effector Ave1 to trigger an immune response (de Jonge et al., 2012; Kawchuk et al., 2001). In addition, a second resistance locus, V2, was identified in wild tomato species and can provide resistance against *V. dahliae* strains that escape Ve1-mediated recognition (Usami et al., 2017). Comparative genomics between *V. dahliae* strains that are either recognized by or able to overcome V2 immunity led to the identification of the effector Av2, which activates immunity in V2-carrying plants (Chavarro-Carrero et al., 2021). Based on recognition by tomato resistance loci, *V. dahliae* strains are classified into different races: strains producing Ave1 are classified as race 1, whereas race 2 strains have evolved to evade detection by losing the *Ave1* gene (de Jonge et al., 2012; Faino et al., 2016). Similarly, strains that evade V2-mediated immunity through loss of Av2 are classified as race 3 strains (Chavarro-Carrero et al., 2021).

Thesis outline

During my doctoral research I investigated the antimicrobial effectors of *V. dahliae* to broadening our understanding of antimicrobial effectors and effector evolution. In **Chapter 2**, entitled “Undermining the cry for help: The phytopathogenic fungus *Verticillium dahliae* secretes an antimicrobial effector protein to undermine host recruitment of antagonistic *Pseudomonas* bacteria”, we functionally characterise the *V. dahliae* effector *Av2*, showing that it is utilised by the pathogen to supress the plant’s cry for help recruitment of antagonistic bacteria (Figure 1a). More specifically, our findings reveal that Av2 undermines the host recruitment of antagonistic *Pseudomonas* spp. during *V. dahliae* infection, thereby demonstrating that pathogens do not only respond to and reshape plant microbiota, but also sabotage microbiota-mediated host defence responses by compromising the cry for help recruitment.

We were furthermore interested in understanding how antimicrobial effectors shape pathogen virulence as well as plant-associated microbial communities across diverse soil environments (Figure 1b). Therefore, in **Chapter 3** entitled “Differential contributions of an antimicrobial

effector from *Verticillium dahliae* to virulence and tomato microbiota assembly across natural soils" we investigated the contribution of the antimicrobial effector Ave1 to fungal virulence and manipulation host microbiota across natural soils. Profiling microbiota of *V. dahliae*–infected tomato plants revealed that the contribution of Ave1 to virulence differs markedly among types of soil. Although Ave1 consistently perturbs host microbiota, the specific microbial taxa that are affected depend strongly on the soil-derived community. Together, these findings demonstrate that Ave1 influences microbiota across environments, but its effect on fungal virulence is contingent on the particular microbial assemblage recruited from the soil.

In **Chapter 4**, entitled "Plant-associated fungi co-opt ancient antimicrobials for host manipulation", we show that many fungal effectors with immunomodulating functions possess conserved antimicrobial properties suggesting that fungi repurposed ancient antimicrobial effectors to serve multiple roles during host colonisation (Figure 1c, d). Upon developing the Antimicrobial Activity Predictor for Effector Candidates (AMAPEC), we are able to observe that antimicrobial effector repertoires in filamentous fungi are larger than expected, and that many antimicrobial effectors are conserved across fungi. Moreover, many effectors have been shown to exhibit immunomodulating functions in fungal plant pathogens. Combined with their presence in non–plant-associated fungi, these results point to an ancient antimicrobial origin for these effectors and support the idea that during evolution fungi repurposed them as immunomodulators, mediating ancient fungal lifestyle transitions to plant symbionts.

We expand on this hypothesis by focusing on the broadly conserved cerato-platanin effector family in *V. dahliae* in **Chapter 5** entitled "Conserved antimicrobial activity of the fungal cerato-platanin protein family uncovered through structural clustering of *Verticillium dahliae* effectors" (Figure 1c, d). By structural clustering of effectors in *V. dahliae* we identify a cluster of four effectors with a similar fold, comprising Ave1 and three members that can be assigned to the cerato-platanin protein family. Interestingly, we show antimicrobial activity of all four members *in vitro*. Furthermore, we demonstrate that this antimicrobial activity of cerato-platanins is conserved across fungi with diverse lifestyles.

In **Chapter 6**, the general discussion of my thesis, I provide an overall discussion of the findings obtained during my PhD research and place these findings into a broader context.

Overall, this thesis advances our understanding of how antimicrobial effector proteins contribute to pathogen success against microbiota-mediated plant defence mechanisms and their evolutionary role in fungal adaptation to pathogenic lifestyles. It demonstrates that fungal pathogens not only respond to and reshape plant-associated microbiota, but can also actively undermine host defence by compromising the "cry for help" recruitment of antagonistic microbes. In addition, this work highlights the evolutionary dimension of antimicrobial effectors,

revealing their ancient origins in microbial antagonism and showing how these ancestral activities have been repeatedly co-opted during fungal adaptation to plant-associated niches. Together, these findings position antimicrobial effectors as ancient molecules that have been repeatedly harnessed by pathogens in the ongoing arms race between plants and pathogens.

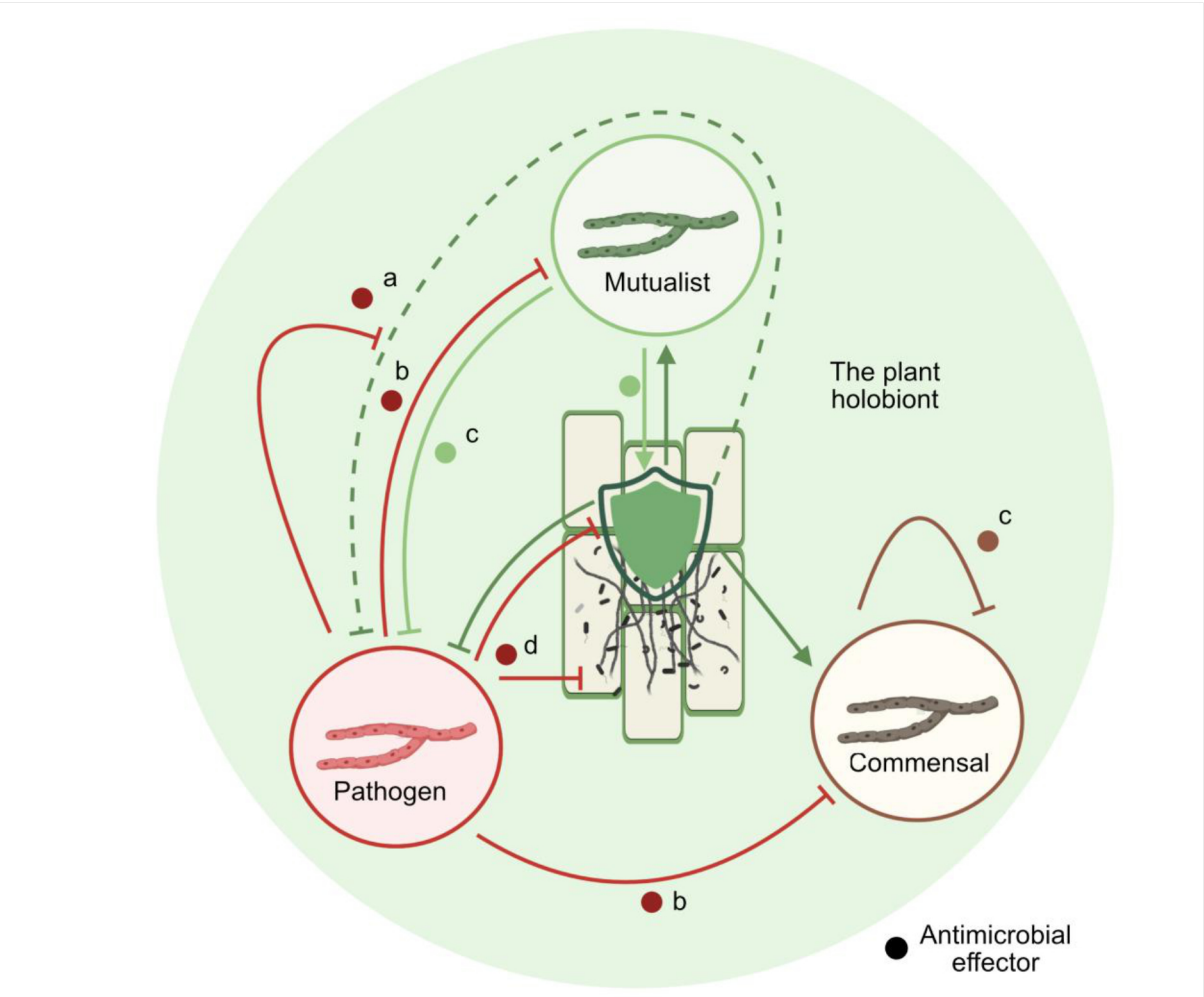

Figure 1. Overview of the of the main findings presented in this thesis. (**a**) Upon pathogen infection, plants deploy a microbiota-mediated defence strategy termed the "cry for help", in which mutualistic microbes are recruited to antagonize invading pathogens. We show that pathogenic fungi in turn utilise antimicrobial effectors to undermine this recruitment and target the beneficial microbes, ultimately keeping antagonists out of the microbiota and facilitating host colonization (for details, see Chapter 2). (**b**) By investigating the effects of antimicrobial effectors across different microbiota compositions, we demonstrate that these effectors can inhibit both antagonistic and non-antagonistic microbes, and that their contribution to virulence is strongly environment-dependent (for details, see Chapter 3). (**c**) We show that effectors that are broadly conserved across fungi with different lifestyles possess antimicrobial properties, indicating that these proteins originally evolved as tools for microbial competition long before fungi engaged in interactions with terrestrial plants (for details, see Chapter 4 & 5). (**d**) Many fungal effectors with immunomodulating functions possess conserved antimicrobial properties suggesting that fungi repurposed ancient antimicrobial effectors to serve multiple roles during host colonisation (for details, see Chapter 4 & 5).

Chapter 2

Undermining the cry for help: the phytopathogenic fungus *Verticillium dahliae* secreats an antimicrobial effector protein to undemine host recruitment of antagonistic *Pseudomonas* bacteria

Anton Kraege[1,#], Wilko Punt[1,#], Andrea Doddi[1,2], Jinyi Zhu[1], Natalie Schmitz[1], Nick C. Snelders[1,3,$], Bart P.H.J. Thomma[1,$,]

[1]University of Cologne, Institute for Plant Sciences, Cluster of Excellence on Plant Sciences (CEPLAS), 50674 Cologne, Germany;

[2]Sapienza University of Rome, Department of Environmental Biology, 00185 Rome, Italy;

[3]University of Utrecht, Theoretical Biology and Bioinformatics Group, 3584CH Utrecht, The Netherlands;

[#]These authors contributed equally

[$]These authors contributed equally

[*]Corresponding author. Email: bthomma@uni-koeln.de

This article was published in *New Phytologist* (2026), 249: 406-417

doi: doi.org/10.1111/nph.70686

Research

New Phytologist

Undermining the cry for help: the phytopathogenic fungus *Verticillium dahliae* secretes an antimicrobial effector protein to undermine host recruitment of antagonistic *Pseudomonas* bacteria

Anton Kraege[1]*, Wilko Punt[1]*, Andrea Doddi[1,2], Jinyi Zhu[1], Natalie Schmitz[1], Nick C. Snelders[1,3†] and Bart P. H. J. Thomma[1†]

[1]Institute for Plant Sciences, Cluster of Excellence on Plant Sciences (CEPLAS), University of Cologne, 50674, Cologne, Germany; [2]Department of Environmental Biology, Sapienza University of Rome, 00185, Rome, Italy; [3]Theoretical Biology and Bioinformatics Group, Department of Biology, University of Utrecht, 3584CH, Utrecht, the Netherlands

Author for correspondence:
Bart P. H. J. Thomma
Email: bthomma@uni-koeln.de

Received: *22 September 2025*
Accepted: *8 October 2025*

New Phytologist (2026) **249:** 406–417
doi: 10.1111/nph.70686

Key words: AMP, antimicrobial, intermicrobial interaction, microbe–microbe interaction, microbiota, plant pathogen.

Summary

- During pathogen attack, plants recruit beneficial microbes in a 'cry for help' to mitigate disease development. Simultaneously, pathogens secrete effectors to promote host colonisation through various mechanisms, including targeted host microbiota manipulation.
- Inspired by *in silico* antimicrobial activity prediction, we investigated the antimicrobial activity of Av2, an effector of *Verticillium dahliae*, *in vitro*. Furthermore, its role in *V. dahliae* virulence was assessed through microbiota sequencing of inoculated plants, microbial co-cultivation assays, and inoculations in a gnotobiotic plant cultivation system.
- Av2 appears structurally unique and lacks domains that hint towards its function. We show that Av2 inhibits bacterial growth and acts as a virulence factor during host colonisation. Microbiota sequencing revealed involvement of Av2 in suppression of *Pseudomonas* spp. recruitment upon plant inoculation with *V. dahliae*, indicating that Av2 suppresses the cry for help. We show that several *Pseudomonas* spp. are antagonistic to *V. dahliae* and sensitive to Av2 treatment.
- We conclude that *V. dahliae* secretes Av2 to suppress the plant's cry for help by inhibiting the recruitment of antagonistic *Pseudomonas* spp. to pave the way for successful plant invasion.

Introduction

Plants associate with a plethora of microbes above and below ground, collectively called the microbiota, that can positively impact plant productivity and health (Berendsen *et al.*, 2018; Trivedi *et al.*, 2020). Through the secretion of root exudates, plants shape their microbiota and actively recruit beneficial microbes to mitigate biotic and abiotic stresses (López *et al.*, 2008; Berendsen *et al.*, 2018). Under pathogen attack, plants can modify these exudates to selectively attract protective microbes in order to limit disease progression. This targeted recruitment in response to pathogen infection is known as the plant's 'cry for help' (Berendsen *et al.*, 2018; Yuan *et al.*, 2018; Liu *et al.*, 2024; Spooren *et al.*, 2024). For example, cucumber plants increase the exudation of tryptophan during *Fusarium oxysporum* infection, which promotes the recruitment of beneficial *Bacillus amyloliquefaciens* that can mitigate disease progression (Liu *et al.*, 2017).

Ultimately, the cry for help, which results in the recruitment of beneficial microbes, may have a legacy effect in cases when it leads to an increased population of these microbes in the soil, resulting in the establishment of disease-suppressive soils that protect future plants grown in the same soil (Rolfe *et al.*, 2019; Mesny *et al.*, 2024). However, the development of such a legacy effect typically requires years and many plant generations to fully establish (Rolfe *et al.*, 2019). Arguably, the most famous example of such a legacy effect concerns the decline of take-all disease, caused by the fungal plant pathogen *Gaeumannomyces tritici*, in wheat over years of monoculture that has been associated with the recruitment of 2,4-diacetylphloroglucinol-producing *Pseudomonas* spp. (Raaijmakers & Weller, 1998).

To detect pathogens, plants have evolved a complex immune system that recognises a multitude of microbe-derived molecules to activate appropriate defence responses (Jones & Dangl, 2006). Initial immune responses are triggered upon recognition of conserved microbe-associated molecular patterns (MAMPs), such as chitin or flagellin, by plant membrane-localised MAMP recognition receptors that activate pattern-triggered immunity (PTI) responses (Jones & Dangl, 2006; Cook *et al.*, 2015). In response,

*These authors contributed equally to this work.
†These authors contributed equally to this work.

host-adapted pathogens have evolved strategies to suppress or overcome such PTI responses, which include the secretion of virulence factors, also known as effectors (Rovenich *et al.*, 2014). In turn, particular host genotypes evolved to recognise effectors, or their activities, by resistance (R) proteins that include cell surface and cytoplasmic receptors that activate effector-triggered immunity (Jones & Dangl, 2006; Cook *et al.*, 2015).

Most effectors characterised to date deregulate host immune responses or target other aspects of host physiology through various biochemical activities and mechanisms (Rovenich *et al.*, 2014). For example, the effector Ecp6 is secreted by *Cladosporium fulvum* to sequester chitin oligosaccharides that are released from its cell walls to prevent recognition by chitin immune receptors (Sánchez-Vallet *et al.*, 2013). Intriguingly, several research groups have recently uncovered a novel function of effectors besides the modulation of host physiology by showing that several pathogens secrete effectors that target host-associated microbiota through the display of selective antimicrobial activity in order to promote host colonisation (Snelders *et al.*, 2020; Gómez-Pérez *et al.*, 2023).

Several antimicrobial effectors have been functionally characterised in the soil-borne fungus *Verticillium dahliae*, a presumed asexual filamentous fungus that causes vascular wilt disease on hundreds of host plants (Fradin & Thomma, 2006). The fungus generates genetic diversity through large-scale chromosomal rearrangements and segmental duplications, leading to hypervariable regions between *V. dahliae* strains that are called adaptive genomic regions (AGRs) (de Jonge *et al.*, 2013; Faino *et al.*, 2016; Cook *et al.*, 2020). These AGRs are enriched in repeats and in effector genes and display a unique chromatin profile that sets these regions apart from core genomic regions (Cook *et al.*, 2020). Interestingly, despite being dispersed across the genome, these AGRs were found to physically interact in the nucleus, possibly contributing to their differential behaviour (Torres *et al.*, 2024). Overall, similar to other filamentous pathogens, *V. dahliae* has a compartmentalised genome-containing AGRs with increased plasticity compared with core genomic regions, an observation often referred to as a 'two-speed genome' (Raffaele & Kamoun, 2012; Torres *et al.*, 2021).

The first *V. dahliae* effector for which antimicrobial activity was shown is the AGR-encoded lineage-specific effector Ave1 that was identified by comparative genomics between *V. dahliae* strains that are controlled by *Ve1*-mediated resistance in tomato and resistance-breaking strains that are virulent towards *Ve1* plants (de Jonge *et al.*, 2012). Besides being recognised by the tomato Ve1 immune receptor as an avirulence factor, Ave1 contributes to fungal virulence on plants lacking *Ve1* by targeting antagonistic bacteria of the Sphingomonadales order (Snelders *et al.*, 2020). Notably, Ave1 is not the only *V. dahliae* effector protein with antibacterial activity, as a search for effectors with homology to known antimicrobial proteins within the *V. dahliae* secretome yielded the AMP2 effector that is expressed in soil extract. AMP2 revealed complementary activity to Ave1, suggesting that *V. dahliae* exploits different effectors to cope with the diversity of microbial competitors in soil (Snelders *et al.*, 2020). The antimicrobial activity of *V. dahliae* effector proteins is not restricted to bacteria, as the defensin-like effector AMP3 was found to target the mycobiota (Snelders *et al.*, 2021). Intriguingly, and in contrast to Ave1 and AMP2, AMP3 is exclusively expressed at late infection stages when resting structures are formed in decaying plant tissue while host immune responses fade and opportunists and fungal decay organisms invade host tissues (Snelders *et al.*, 2021).

Over the years, only two *R* loci were identified that confer resistance against *V. dahliae* in tomato. Besides the recognition of Ave1 by the Ve1 receptor, the fungal effector Av2 is recognised in *V2* tomato plants, although the corresponding *R* gene has not yet been cloned (Usami *et al.*, 2017; Chavarro-Carrero *et al.*, 2021). Similar to Ave1, Av2 is a small (73 amino acid mature protein; net charge +1.8) secreted protein produced only by a subset of *V. dahliae* strains. Apart from homologues found in other *Verticillium* spp., the only homologues of this effector were found in the *Fusarium* genus (Chavarro-Carrero *et al.*, 2021). *Verticillium dahliae Av2* occurs in two allelic variants that differ in one non-synonymous single nucleotide polymorphism (SNP) that are both recognised in *V2* plants, and so far its intrinsic function for the pathogen has remained enigmatic (Chavarro-Carrero *et al.*, 2021). In this study, we aimed to characterise the virulence function of *Av2* through a combination of *in silico* and functional analysis.

Materials and Methods

Detection of *V. dahliae Av2* expression in soil extract

For each treatment, 10^6 conidiospores of *Verticillium dahliae* Kleb. strain JR2 were added to 10 ml potato dextrose broth (PDB) and incubated while shaking with 130 rpm at 28°C for 2 d (Ecotron, Infors-HT, Bottmingen, Switzerland). Subsequently, the mycelium was collected using sterilised miracloth (Merck, Darmstadt, Germany) and washed with sterilised water. Next, the mycelium was transferred to new flasks containing 10 ml of soil extract that was prepared by adding 40 g of potting soil (Balster Einheitserde, Frödenberg, Germany) to 200 ml of sterilised water followed by incubation at room temperature for 2 d, after which soil particles were pelleted by centrifugation for 30 min at 4000 ***g*** and the supernatant was collected. The flasks were then incubated while shaking with 130 rpm at 28°C for 5 d (Ecotron, Infors-HT, Bottmingen, Switzerland). Next, mycelium was recollected using sterilised miracloth and washed with sterilised water. RNA was extracted using TRIzol reagent (Thermo Fisher Scientific, Waltham, MA, USA) of which 1 µg was transcribed into cDNA using the PrimeScript™ RT reagent Kit with gDNA Eraser (Takara Bio USA, San Jose, CA, USA). Real-time PCR was performed using SsoAdvance Universal SYBR Green Supermix (BioRad, Hercules, CA, USA) on a CFX Opus Real-Time PCR System (BioRad) and the expression of effector genes was normalised using the *V. dahliae* glyceraldehyde 3-phosphate dehydrogenase gene (*VdGAPDH*) as a reference.

Heterologous expression of Av2 homologues

The *Av2* alleles encoding *V. dahliae* Av2 and Av2^{V73E} (from strains TO22 and JR2, respectively) and their homologues from *Fusarium oxysporum* f. sp. *pisi* and *F. redolens* (*Fop*Av2 and *Fr*Av2,

respectively) were codon-optimised for expression in *E. coli* and cloned into the pET15b vector (Merck, Darmstadt, Germany) such that the proteins are produced without a signal peptide and as a fusion protein with an N-terminal His_6 tag. All vectors were ordered from BioCat GmbH (Heidelberg, Germany). While *Vd*Av2 and $Av2^{V73E}$ were produced in *E. coli* strain BL21 (Thermo Fisher Scientific), *Fop*Av2 and *Fr*Av2 were produced in *E. coli* strain SHUFFLE T7 (New England Biolabs, Ipswich, MA, USA). A preinoculum of bacterial cultures was incubated overnight in Lysogeny broth (LB) supplemented with 50 μg ml^{-1} ampicillin at 37°C for BL21 and at 30°C for SHUFFLE T7 while shaking at 170 rpm (Ecotron, Infors-HT, Bottmingen, Switzerland). Subsequently, the preinoculum was transferred to 1 l of LB supplemented with ampicillin (50 μg ml^{-1}) and incubated at 37°C (BL21) or 30°C (SHUFFLE T7) until the OD_{600} reached 0.6–0.8. Next, isopropyl-1-thio-β-D-galactopyranoside (IPTG) was added to a final concentration of 1 mM, and the culture was incubated for 4 h at 37°C (BL21) or 30°C (SHUFFLE T7). Next, cells were pelleted through centrifugation (21 000 ***g***) at 4°C and resuspended in 6 M guanidine, 10 mM TRIS–HCl, and 10 mM β-mercaptoethanol (pH 8.0) and incubated overnight at 4°C while rotating continuously. After centrifugation at 21 000 ***g*** for 30 min, proteins were purified from the supernatant by immobilised metal affinity chromatography (IMAC) on a custom-packed 5 ml Ni^{2+} CYTIVIA column (XK16/20 Column, Cytiva, Marlborough, MA, USA) with His60 Ni Superflow Resin (Takara Bio USA, San Jose, CA, USA). Fractions containing the protein of interest were identified by sodium dodecyl sulphate-polyacrylamide gel electrophoresis (SDS-PAGE) analysis, combined, and dialysed in a stepwise fashion. To this end, the protein was dialysed in a stepwise manner over several 18-h intervals. Initially, dialysis was performed against 4 M guanidine, 50 mM BIS-TRIS, 10 mM reduced glutathione, and 2 mM oxidised glutathione (pH 7.0). This was followed by dialysis against 3 M guanidine, 50 mM BIS-TRIS, 10 mM reduced glutathione, and 2 mM oxidised glutathione (pH 6.5). Subsequently, the protein was dialysed against 2 M guanidine, 100 mM BIS-TRIS, 250 mM ammonium sulfate, 10 mM reduced glutathione, and 2 mM oxidised glutathione (pH 6.5), followed by 1 M guanidine, 100 mM BIS-TRIS, 125 mM ammonium sulfate, 10 mM reduced glutathione, and 2 mM oxidised glutathione (pH 5.8). The final dialysis step was performed in 100 mM BIS-TRIS, 125 mM ammonium sulfate, 10 mM reduced glutathione, and 2 mM oxidised glutathione (pH 5.8). Ultimately, the protein was dialysed against potassium phosphate buffer (pH 6.5). Final protein concentrations were determined with Nanodrop (Thermo Fisher Scientific) based on absorbance at 280 nm and adjusted to a final concentration of 16 μM.

In vitro antimicrobial activity assays

All bacteria used in the assays originated from a tomato culture collection (Punt *et al.*, 2025). After growth of bacterial isolates on tryptone soy agar (TSA) at 28°C, single colonies were selected and grown overnight in tryptone soy low salt broth (TSB LS) at 28°C while shaking at 200 rpm (Ecotron, Infors-HT, Bottmingen, Switzerland). Subsequently, optical density was measured at 600 nm (OD_{600}) and adjusted to 0.05 by dilution with TSB LS. One hundred microlitres of bacterial culture were mixed with 100 μl of Av2 protein variants (16 μM) in clear 96-well plates (BRAND SCIENTIFIC GMBH, Wertheim, Germany) with three replicates for each treatment. The plates were incubated in a CLARIOstar® plate reader (BMG LABTECH, Ortenberg, Germany) at 28°C with double orbital shaking every 15 min (10 s at 300 rpm), after which the OD_{600} was measured (Snelders *et al.*, 2020).

Plant disease assays

Inoculation of tomato plants to determine the virulence of *V. dahliae* was performed as described previously (Fradin *et al.*, 2009). Briefly, conidiospores of *V. dahliae* wild-type or *Av2* deletion strain (Chavarro-Carrero *et al.*, 2021) were harvested after 10 d of cultivation on potato dextrose agar (PDA). The conidiospore suspensions were centrifuged at 10 000 ***g*** for 10 min, and the pellets were resuspended in water. This washing step was repeated twice before spores were counted, and the concentration was adjusted to 10^6 conidiospores ml^{-1}. For the inoculation, 10-d-old tomato (*Solanum lycopersicum* L.) MoneyMaker plants were carefully uprooted, roots were rinsed in water, and placed into the inoculum for 6 min. Next, plants were placed back into soil and placed in the glasshouse at 22°C during 16 h : 8 h day/night periods with a maximum of 80% relative humidity, and symptoms were monitored at 14 d post inoculation (dpi). To this end, canopy areas were measured and fungal biomass inside the tomato stem was determined. For the latter, samples were frozen in liquid nitrogen, ground to a fine powder, and DNA was isolated using phenol–chloroform extraction (Chavarro-Carrero *et al.*, 2021). *Verticillium dahliae* biomass was quantified through real-time PCR using *V. dahliae*-specific primers targeting the internal transcribed spacer (ITS) region of the ribosomal DNA (Snelders *et al.*, 2020). The tomato *Rubisco* gene was used for sample calibration (Snelders *et al.*, 2020).

Tomato stem microbiota sequencing

Tomato stem samples were collected, washed with sterile water, frozen in liquid nitrogen, and manually ground using a mortar and pestle. Total DNA was extracted following a phenol–chloroform-based extraction procedure (Chavarro-Carrero *et al.*, 2021), and DNA concentrations were determined using a Qubit fluorometer (Thermo Fisher Scientific). Sequence libraries were prepared following amplification of the V5–V7 region of the bacterial 16S rDNA (799F and 1139R) as described previously (Wippel *et al.*, 2021) and sequenced (paired-end 300 bp) on an Illumina MiSeq V3 Platform (Cologne Center for Genomics, Cologne, Germany). Sample barcoding was done as described previously (Fadrosh *et al.*, 2014).

Microbiota analysis

Sequencing data were processed using R v.4.2.0 as described previously (Callahan *et al.*, 2016; Snelders *et al.*, 2020). Briefly, reads were demultiplexed using CUTADAPT (v.4.1; Martin, 2011). Afterwards reads were trimmed and filtered to an average paired read length of 412 bp with the Phred score of 30. From the trimmed reads, OTUs were inferred using the DADA2 method (v.1.24; Callahan *et al.*, 2016). Taxonomy was assigned using the Ribosomal Database Project (RDP, v.18; Cole *et al.*, 2014). The PYLOSEQ package (v.1.40.0; McMurdie & Holmes, 2013) was used to calculate β-diversity (weighted unifrac distance) after the data was normalised with the METAGENOMESEQ package (v.1.38.0; Paulson *et al.*, 2013) using cumulative sum scaling. PERMANOVA was performed with the VEGAN (v.2.6-4; Oksanen *et al.*, 2004) package. Differential abundance analysis was done using the DESeq2 package (v.1.36.0; Love *et al.*, 2014) using a negative binomial Wald test and a significance *P*-adjusted threshold < 0.05.

Homology analysis of Av2

In order to find functional domains within the Av2 sequence, the online version of InterProScan was used with the amino acid sequence of Av2. Structural prediction of Av2 was done using ALPHAFOLD2 (v.2.0 Jumper *et al.*, 2021) with default settings. To find structural homologues, the Av2 structure was queried against the AlphaFold structural database (Varadi *et al.*, 2022) using the Foldseek search server (van Kempen *et al.*, 2023). Protein surface charge was calculated and visualised using PyMOL (The PyMOL Molecular Graphics System, v.3.0 Schrödinger, LLC) using the APBS electrostatics plugin (Jurrus *et al.*, 2018).

In vitro competition assay

Conidiospores of *V. dahliae* strain TO22 and the *VdAv2* deletion strain were harvested from a PDA plate using sterile water and diluted to a concentration of 2×10^6 conidiospores ml^{-1} in ½-strength Murashige & Skoog (½MS) medium (Duchefa, Haarlem, the Netherlands). Plant-associated *Pseudomonas* spp. (Punt *et al.*, 2025) were cultured overnight in ½MS medium. Next, overnight cultures were adjusted to OD_{600} of 0.05 in ½MS and added to the conidiospores, and 500 µl of the microbial mixture was added into a 12-well flat bottom polystyrene tissue culture plate (Sarstedt, Nümbrecht, Germany). Following 48 h of incubation at RT with shaking at 150 rpm (Ecotron, Infors-HT, Bottmingen, Switzerland), genomic DNA was extracted using the SmartExtract DNA kit (Eurogentec, Maastricht, the Netherlands), and *V. dahliae* biomass was quantified through real-time PCR using *V. dahliae*-specific primers targeting the ITS region of the ribosomal DNA (Snelders *et al.*, 2020). A spike-in DNA sequence was added during DNA extraction for sample calibration (Guo *et al.*, 2020). Genomic sequences of the tested *Pseudomonas* spp. (Punt *et al.*, 2025) were used to infer rooted species trees based on single-copy orthologous genes (Emms & Kelly, 2019).

Gnotobiotic tomato cultivation for *V. dahliae* inoculations

For tomato cultivation, a previously developed Flowpot system was used (Kremer *et al.*, 2021; Punt *et al.*, 2025). A 1:1 blend of potting soil (Balster Einheitserdewerk, Fröndenberg, Germany) and vermiculite (LIMERA Gartenbauservice, Geldern-Walbeck, Germany) was autoclaved three times on a liquid cycle and filled into 50 ml syringes (Terumo Europe, Leuven, Belgium). To check for substrate sterility, 500 mg of substrate was added to 10 ml of 100 mM $MgCl_2$ and shaken at 300 rpm at room temperature for 1 h (Ecotron, Infors-HT, Bottmingen, Switzerland). Subsequently, the samples were diluted 1000-fold, and 50 µl of the dilution was plated onto Reasoner's 2A agar, TSA, and LB agar and incubated in darkness at room temperature for 4 d before microbial growth was assessed. The substrate-filled syringes were flushed with 40 ml of sterile H_2O followed by 40 ml of ½MS. Next, surface-sterilised tomato seeds (MoneyMaker) were placed into each syringe, and six syringes were placed into an autoclaved Microbox container ($SacO_2$, Deinze, Belgium) and placed in the glasshouse at 22°C during 16 h : 8 h day/night periods with a maximum of 80% relative humidity. After 2 wk, tomato plants were carefully uprooted under sterile conditions and inoculated with 10^6 conidiospores ml^{-1} of either wild-type TO22 or the corresponding *Av2* deletion strain. Subsequently, the plants were placed back into the syringe and the syringes into the container in the glasshouse. Symptoms of disease were scored at 14 dpi. For biomass quantification, stems of the plants were frozen in liquid nitrogen and ground to a fine powder. DNA was isolated using phenol–chloroform extraction (Chavarro-Carrero *et al.*, 2021). *Verticillium dahliae* biomass was quantified through real-time PCR using *V. dahliae*-specific primers targeting the ITS region of the ribosomal DNA. The tomato *Rubisco* gene was used for sample calibration.

Results

Av2 selectively inhibits bacterial growth *in vitro*

Most functionally characterised effectors target host physiology and are strictly *in planta* expressed, while microbiota-manipulating effectors can be expressed *in planta* as well as during fungal life cycle stages outside the plant host (Snelders *et al.*, 2020, 2021). In order to functionally characterise *Av2*, its expression was analysed by querying previously generated RNA sequencing datasets (de Jonge *et al.*, 2012; Cook *et al.*, 2020), revealing that *Av2* is not only expressed during host colonisation (1695 transcripts per million (TPM), 16, de Jonge *et al.*, 2012) but also during *in vitro* growth on PDA (3256 TPM, 4 d old, Cook *et al.*, 2020). Furthermore, *Av2* is expressed in conditions mimicking soil colonisation (Supporting Information Fig. S1). A similarly broad expression pattern, including expression in soil, has previously been observed for the *V. dahliae Ave1* effector gene (Fig. S1, Snelders *et al.*, 2020), suggesting that Av2 may act as an antimicrobial too. Interestingly, *in silico* analysis using the Antimicrobial Peptide Scanner (v.2; Veltri *et al.*, 2018)

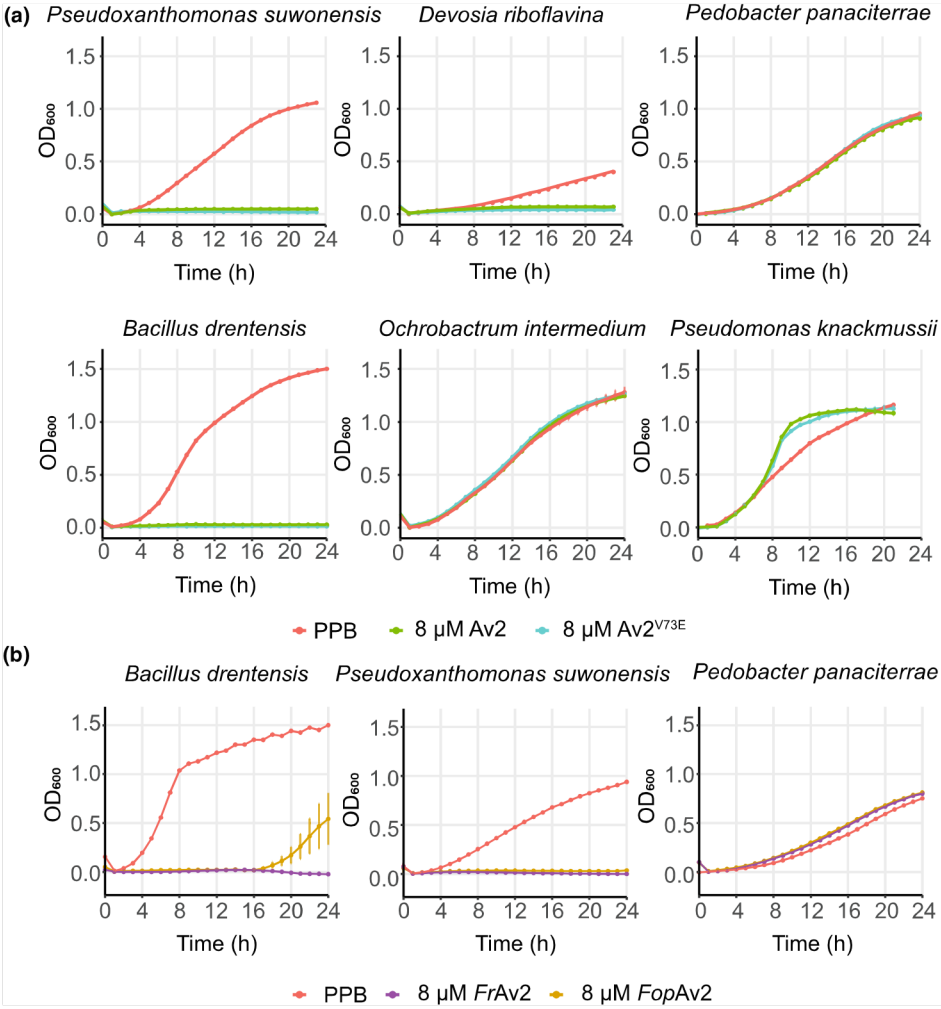

Fig. 1 Av2 effector variants from *Verticillium dahliae* and homologues from *Fusarium* spp. display selective antibacterial activity. (a) The Av2 effector as well as the effector variant $Av2^{V73E}$ selectively inhibits growth in a panel of phylogenetically diverse plant-associated bacteria *in vitro*. (b) Av2 homologues from *Fusarium redolans* (*Fr*Av2) and *F. oxysporum* f. sp. *pisi* (*Fop*Av2) display an overlapping activity spectrum with the *V. dahliae* Av2 variants. Phosphate buffer (PPB) was used as a control. Graphs display time-course measurements of bacterial densities in the presence or absence of effector proteins with 15 min intervals over 24 h and display the average OD_{600} of three biological replicates ± SD.

predicted antimicrobial activity for Av2 with a probability of 99.6%.

To validate the predicted antimicrobial activity of Av2 *in vitro*, the two previously identified variants, Av2 and $Av2^{V73E}$, were expressed heterologously in *E. coli*, purified, and used in antimicrobial activity assays. Additionally, Av2 homologues from two *Fusarium* spp. were produced, purified, and tested for antimicrobial activity as well. To this end, a panel of 10 phylogenetically diverse plant-associated bacteria was incubated with either of the Av2 variants at a concentration of 8 μM, or buffer as a control, and bacterial growth was assessed. Interestingly, three out of 10 bacteria showed reduced growth when incubated with either of the two *V. dahliae* Av2 variants, namely *Bacillus drentensis*, *Pseudoxanthomonas suwonensis*, and *Devosia riboflavina* (Fig. 1a). A subset of bacteria was also tested with the Av2 homologues from *Fusarium*, which showed activity against *Bacillus drentensis*, *Pseudoxanthomonas suwonensis* while *Devosia riboflavina* was not tested (Fig. 1b). Importantly, no differences in inhibitory activity were observed between any of the Av2 variants, including the homologues, suggesting they have overlapping activity spectra. Thus, all Av2 proteins display selective antimicrobial activity against bacteria *in vitro*.

To explore the potential mode of action of Av2, InterProScan was used to query for functional domains, but no such domains were detected. Furthermore, the structure of Av2 was predicted using AlphaFold2, resulting in a structural model with a low confidence score (pLDDT = 53.8), indicating limited reliability of the predicted structure (Fig. S2a). Nevertheless, FoldSeek was used to search for structural similarities between Av2 and previously characterised proteins, but no significant structural homologues were identified. These results suggest that, in addition to sharing sequence similarity only with *Fusarium* homologues, Av2 lacks detectable structural similarity to any known protein in the AlphaFold Protein Structure Database. To further investigate whether any compositional features could provide functional insight, the amino acid composition of Av2 was compared to that of other secreted proteins of *V. dahliae* (Fig. S2c). Consistent with the structural model that revealed positively charged surface regions (Fig. S2b), Av2 displayed a net positive charge of +2.33, in contrast to the average net charge of −10.1 for the secretome.

Av2 contributes to *V. dahliae* virulence through microbiota manipulation

Next, we hypothesised that *Av2* is utilised by *V. dahliae* for microbiota manipulation during host colonisation as well as during soil-colonising stages. To investigate this hypothesis, we

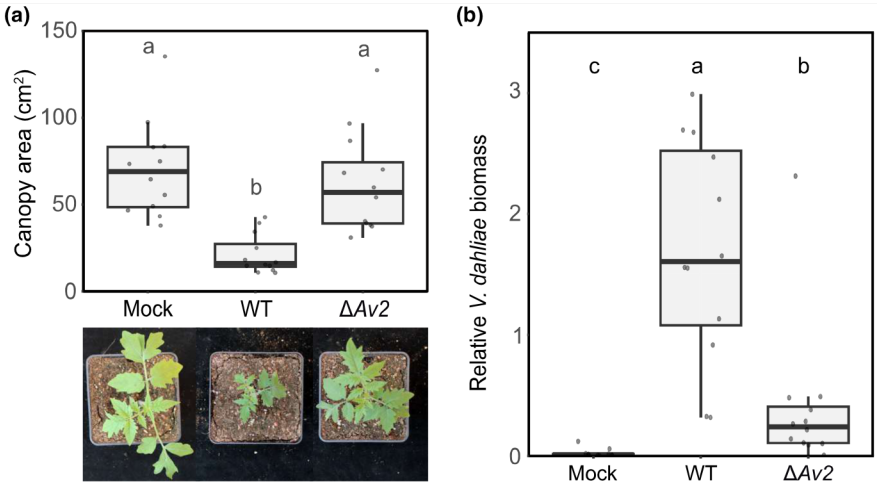

Fig. 2 Av2 contributes to *Verticillium dahliae* virulence on tomato. (a) Canopy area measurements of inoculated plants show stronger stunting upon inoculation with wild-type *V. dahliae* strain TO22 (WT) compared with the corresponding *Av2* deletion strain (Δ*Av2*). Mock-inoculated plants were treated with sterile water. Different letters represent significant differences (one-way ANOVA and Tukey's *post hoc* test; $P < 0.05$). Boxes indicate the interquartile range of the values, the median values are indicated by horizontal lines, and the whiskers extend to the minimum and maximum values. (b) *Verticillium dahliae* biomass in tomato stems was quantified with real-time PCR and normalised to *Rubisco* abundance. Different letters represent significant differences (one-way ANOVA and Tukey's *post hoc* test; $P < 0.05$).

pursued microbiota sequencing through bacterial 16S ribosomal DNA profiling of tomato plants. To this end, tomato plants were inoculated with either wild-type *V. dahliae* strain TO22 or the corresponding *Av2* deletion strain (Chavarro-Carrero *et al.*, 2021), while water treatment was used as a control. Interestingly, while tomato plants inoculated with wild-type *V. dahliae* showed severely stunted growth by 10 d after inoculation compared with mock-inoculated plants (Fig. 2a), plants inoculated with the *Av2* deletion strain only showed mild symptoms of disease, and significantly less stunting occurred than in plants inoculated with the wild-type fungus. Importantly, significantly more fungal biomass was recorded in tomato plants inoculated with the wild-type fungus than in plants inoculated with the *Av2* deletion strain (Fig. 2b), showing that *Av2* contributes to *V. dahliae* virulence during host colonisation.

To address the hypothesis that *Av2* contributes to virulence through microbiota manipulation, tomato plants were inoculated in a peat-based gnotobiotic system (Punt *et al.*, 2025). If microbiota manipulation is the genuine function of the effector, *Av2* should not contribute to fungal virulence when plants are grown axenically, in the absence of microbes, while its contribution should become noticeable upon microbial reintroduction. To reintroduce microbes into sterile soil while maintaining physicochemical properties similar to the sterilised substrate, 10% unsterilised soil was mixed with 90% sterilised soil. Importantly, plating confirmed that sterilisation effectively removed the microbial population from the substrate, whereas reintroduction resulted in microbial colonisation of the originally sterilised substrate (Fig. S3). Next, tomato seedlings were inoculated with wild-type *V. dahliae* strain TO22 or the corresponding *Av2* deletion strain and cultivated in the two substrates. Importantly, at 2 wk after inoculation, tomato plants inoculated with wild-type *V. dahliae* were significantly smaller than the mock-inoculated plants, while plants inoculated with the *Av2* deletion strain developed similar to tomato plants grown in potting soil (Figs 2a, 3), showing that *V. dahliae* can establish infections on tomato plants also in a gnotobiotic system on sterilised substrate. As previously observed for other plant species, tomato plants grown axenically generally developed slower than those grown in the presence of a microbiota on recolonised substrate (Kremer *et al.*, 2021; Punt *et al.*, 2025). However, when tomato plants were grown on sterile substrate, no difference could be observed between tomato plants inoculated with wild-type *V. dahliae* or with the *Av2* deletion strain, showing that *Av2* only contributes to virulence in the presence of a microbiota. This finding suggests that microbiota manipulation is the genuine virulence function of the Av2 effector, and that the effector lacks plant virulence targets.

Av2 suppresses the recruitment of Pseudomonadales

To perform microbiota sequencing through bacterial 16S ribosomal DNA profiling, tomato stem samples were collected at 10 d post *V. dahliae* inoculation, before the onset of wilting symptoms, and the V5–V7 region of the bacterial 16S rDNA was amplified and sequenced. Subsequent analysis did not reveal major changes in microbial diversity (α-diversity) between plants inoculated with *V. dahliae* wild-type and mock-inoculated plants (Fig. 4a). Interestingly, however, plants inoculated with the *V. dahliae Av2* deletion strain showed a significant reduction in microbial diversity that coincided with a strong increase in the relative abundance of Proteobacteria (Fig. 4c). PCA based on weighted unifrac distance revealed differential grouping of the tomato stem endosphere microbiota for the three different treatments (PERMANOVA, $P < 0.001$; Fig. 4b). To investigate which bacterial orders drove the separation of the samples in the PCA, pairwise bacterial abundance comparisons were performed

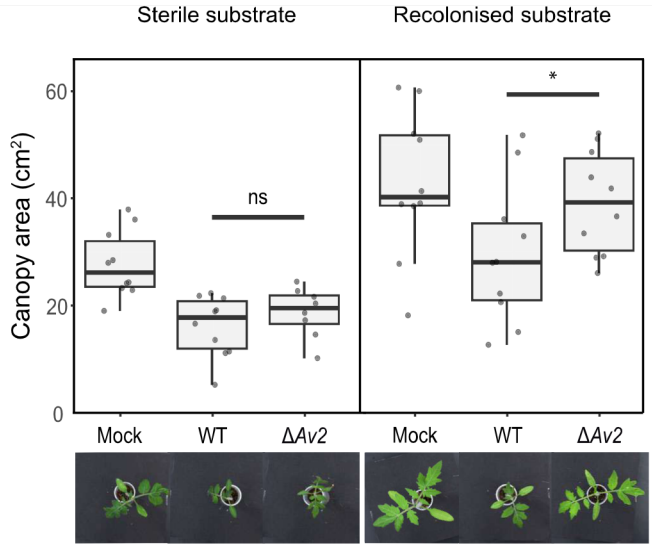

Fig. 3 Av2 contributes to *Verticillium dahliae* virulence on tomato plants solely in the presence of microbes. Canopy area measurements of inoculated tomato plants grown in Flowpots show stronger stunting upon inoculation with wild-type *V. dahliae* strain TO22 (WT) compared with the corresponding *Av2* deletion strain (Δ*Av2*) in recolonised substrate but not in sterile substrate. Mock-inoculated plants were treated with sterile water. Statistical analyses were performed for each of the substrates, and the star indicates significant differences, whereas ns indicates no significant difference (unpaired two-sided Student's *t*-test; $P < 0.05$). Boxes indicate the interquartile range of the values, the median values are indicated by horizontal lines, and the whiskers extend to the minimum and maximum values. Photographs display phenotypes of representative plants for each of the treatments at 14 d post inoculation.

between plants inoculated with *V. dahliae* wild-type and the *Av2* deletion strain. Several bacterial orders were significantly more abundant in plants inoculated with the *Av2* deletion strain, namely Pseudomonadales, Burkholderiales, Mycobacteriales, and Micromonsporales, suggesting that these orders are particularly affected by the activity of the Av2 effector protein (Fig. 4d). Of these bacterial orders, the Pseudomonadales displayed the largest increase in abundance ($\log_2$-fold change 1.67). Only a few genera appeared to drive the differential abundance of these bacterial orders. Within the Pseudomonadales, only the genera *Pseudomonas* and *Acinetobacter* were significantly more abundant upon inoculation with the *Av2* deletion strain, while within the order of Burkholderiales, only the genus *Massilia* showed a significant increase (Fig. 4e). The genus *Pseudomonas* especially caught our attention because of its high relative abundance in the tomato microbiota, with *c.* 20% and 50% in plants inoculated with the wild-type *V. dahliae* and the *Av2* deletion strain, respectively. Intriguingly, while we anticipated a reduction in *Pseudomonas* abundance in plants inoculated with wild-type *V. dahliae* compared with mock-inoculated plants, we observed no difference in *Pseudomonas* abundance between the two treatments (Figs 4f, S5). This significant increase of *Pseudomonas* in plants inoculated with the *Av2* deletion strain also explains the decrease in alpha diversity of this treatment (Fig. 4a). Given that we only saw a strong recruitment of *Pseudomonas* during the infection by the *Av2* deletion strain, we conclude that this effector is utilised by *V. dahliae* to suppress the recruitment of this bacterial genus by the host upon pathogen invasion.

Verticillium dahliae utilises Av2 to inhibit antagonistic *Pseudomonas* spp.

The targeted recruitment of *Pseudomonas* by tomato plants upon *V. dahliae* colonisation, and the role of *Av2* in the prevention of such recruitment, suggests that *Pseudomonas* acts as an antagonist of the fungus. To investigate whether the interaction between *V. dahliae* and *Pseudomonas* involves direct antagonism and to elucidate the role of *Av2* in this interaction, competition assays were performed between *V. dahliae* and *Pseudomonas* strains isolated from tomato plants (Punt *et al.*, 2025). To this end, wild-type *V. dahliae* strain TO22 and the corresponding *Av2* deletion strain were incubated with a panel of 15 *Pseudomonas* species. Interestingly, wild-type *V. dahliae* grew significantly better than the *Av2* deletion strain in the presence of any of the four *Pseudomonas* species *P. crudilactis*, *P. laurentiana*, *P. plecoglossicida*, or *P. vancouverensis* (Figs 5a, S4). No difference in growth between the two *V. dahliae* strains could be observed when cocultured with the remaining *Pseudomonas* species under these conditions. The reduced growth of the *Av2* deletion strain when cocultured with particular *Pseudomonas* species demonstrates that several *Pseudomonas* spp. are antagonists of *V. dahliae* growth and suggests that *Av2* is utilised by the fungus to counter these antagonists.

To test whether Av2 inhibits the growth of antagonistic *Pseudomonas* spp., their sensitivity towards Av2 was assessed *in vitro*. Interestingly, all antagonistic *Pseudomonas* spp. that showed reduced antagonism in the presence of *Av2* were inhibited when incubated with 8 μM Av2 or Av2^{V73E} (Fig. 5b). By contrast, most of the *Pseudomonas* spp. for which no difference in antagonism was recorded in the cocultivation with *V. dahliae* were unaffected by Av2 or Av2^{V73E}, suggesting that *V. dahliae* coopted Av2 to selectively suppress antagonistic *Pseudomonas* spp. (Fig. 5c). To investigate the phylogenetic placement of the diverse *Pseudomonas* spp. isolates and assess potential clustering of the species that act as *V. dahliae* antagonists and are inhibited by Av2, 2495 orthologous genes present in all species were extracted from their genomic sequences and used to infer a phylogenetic tree. Interestingly, *Pseudomonas* spp. that showed increased antagonism towards the *Av2* deletion strain compared with wild-type *V. dahliae* do not seem to cluster but appear in two clades (Fig. 5c). Further insight into the molecular function of Av2 could reveal whether this phylogenetic split is caused by the evolution of resistance against Av2 within the *Pseudomonas* genus or is due to physiological similarities among the inhibited antagonistic species. In conclusion, our findings suggest that *V. dahliae* exploits Av2 to suppress the cry for help recruitment of beneficial *Pseudomonas* spp. during plant colonisation.

Discussion

The plant microbiota has been shown to be crucial for plant health and to act as an additional layer of defense against

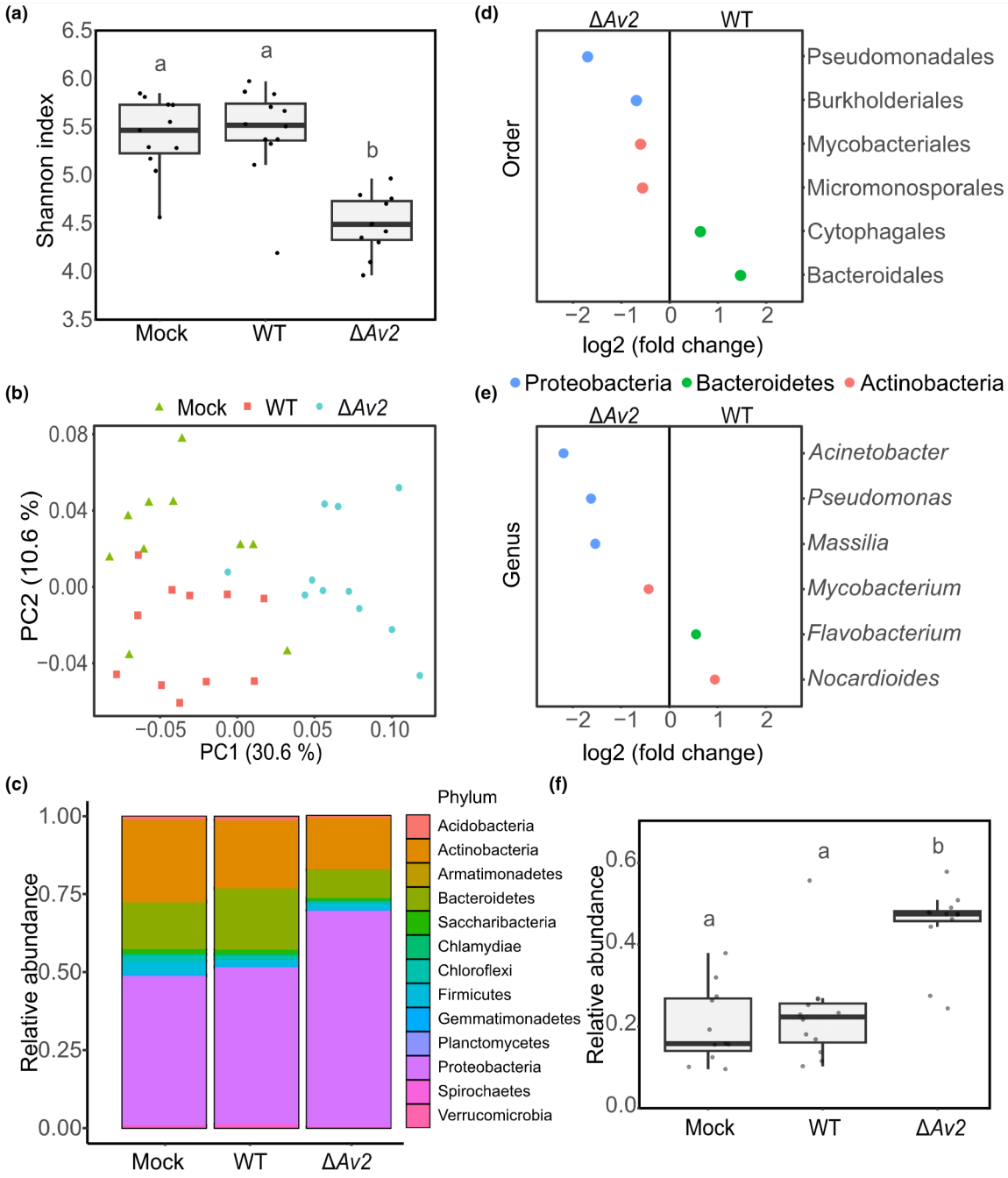

Fig. 4 *Verticillium dahliae* Av2 suppresses *Pseudomonas* recruitment during host colonisation. (a) α-diversity of tomato endosphere microbiota 10 d after inoculation as determined with 16S ribosomal DNA profiling. The α-diversity is significantly lower for microbiomes of plants inoculated with the *Av2* deletion strain (Δ*Av2*) compared with the other treatments. Different letters represent significant differences (one-way ANOVA and Tukey's *post hoc* test; $P < 0.05$). Boxes indicate the interquartile range of the values, the median values are indicated by horizontal lines, and the whiskers extend to the minimum and maximum values. (b) PCA based on weighted unifrac distance reveals separation of tomato stem endosphere microbiota upon inoculation with either water (Mock), wild-type *V. dahliae*, or the *Av2* deletion strain (PERMANOVA, $P < 0.001$). (c) Relative abundance of bacterial phyla shows increased Proteobacteria abundance in plants inoculated with the *Av2* deletion strain. (d) Differentially abundant bacterial orders in the stem endosphere of tomato plants upon inoculation with either wild-type *V. dahliae* or the *Av2* deletion strain (Wald test, adjusted $P < 0.05$). (e) Differential abundance analysis of bacteria at the genus level in the tomato stems upon inoculation with either wild-type *V. dahliae* or the *Av2* deletion strain. (f) Relative abundance comparison of *Pseudomonas* in tomato stems upon inoculation with either water, wild-type *V. dahliae*, or the *Av2* deletion strain. Different letters represent significant differences (one-way ANOVA and Tukey's *post hoc* test; $P < 0.05$). The boxplot follows the same structures as in panel a.

invading pathogens (Trivedi *et al.*, 2020). In a phenomenon known as the 'cry for help', plants respond to pathogen invasion by dynamically altering their microbiota through modulating the composition of their root exudates to selectively recruit beneficial, disease-suppressing microorganisms and thereby mitigate disease progression (Rolfe *et al.*, 2019). Here, we characterise the

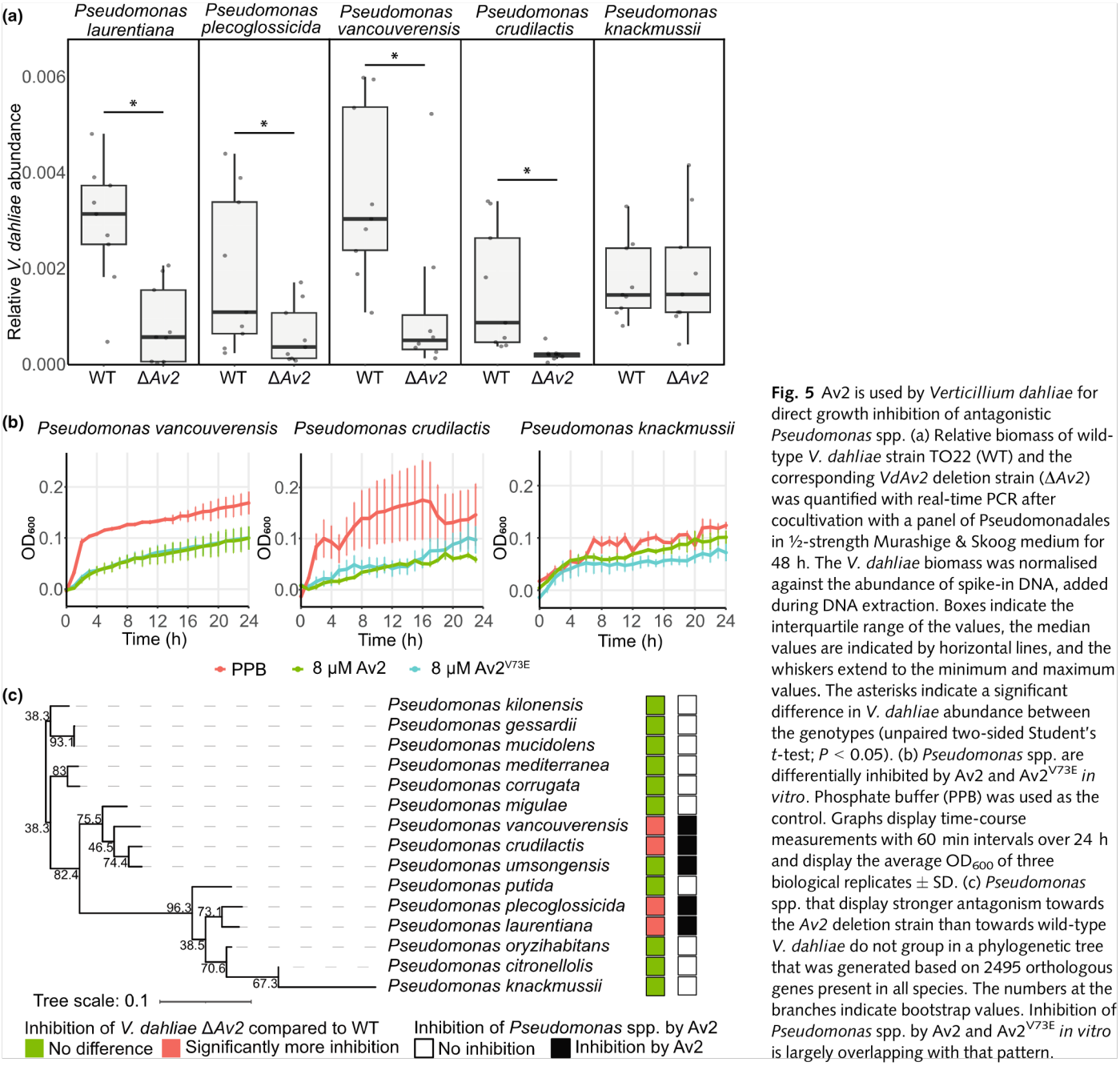

Fig. 5 Av2 is used by *Verticillium dahliae* for direct growth inhibition of antagonistic *Pseudomonas* spp. (a) Relative biomass of wild-type *V. dahliae* strain TO22 (WT) and the corresponding *VdAv2* deletion strain (Δ*Av2*) was quantified with real-time PCR after cocultivation with a panel of Pseudomonadales in ½-strength Murashige & Skoog medium for 48 h. The *V. dahliae* biomass was normalised against the abundance of spike-in DNA, added during DNA extraction. Boxes indicate the interquartile range of the values, the median values are indicated by horizontal lines, and the whiskers extend to the minimum and maximum values. The asterisks indicate a significant difference in *V. dahliae* abundance between the genotypes (unpaired two-sided Student's *t*-test; $P < 0.05$). (b) *Pseudomonas* spp. are differentially inhibited by Av2 and Av2^{V73E} *in vitro*. Phosphate buffer (PPB) was used as the control. Graphs display time-course measurements with 60 min intervals over 24 h and display the average OD_{600} of three biological replicates ± SD. (c) *Pseudomonas* spp. that display stronger antagonism towards the *Av2* deletion strain than towards wild-type *V. dahliae* do not group in a phylogenetic tree that was generated based on 2495 orthologous genes present in all species. The numbers at the branches indicate bootstrap values. Inhibition of *Pseudomonas* spp. by Av2 and Av2^{V73E} *in vitro* is largely overlapping with that pattern.

V. dahliae effector *Av2* as an antimicrobial effector that actively suppresses the plant's cry for help. We show that in tomato, *Av2* suppresses the recruitment of antagonistic *Pseudomonas* spp. into the rhizosphere. As a result, plants inoculated with wild-type *V. dahliae* exhibit *Pseudomonas* spp. levels comparable to mock-inoculated controls, whereas infection with an *Av2*-deletion mutant leads to strong *Pseudomonas* spp. enrichment that correlates with significantly reduced fungal colonisation. This activity is distinct from previously characterised antimicrobial effectors such as Ave1 and Ave1L2, which promote pathogen virulence by depleting antagonistic Sphingomonadales and Actinobacteria from the host plant microbiota (Snelders *et al.*, 2020, 2023), or the suite of antimicrobial proteins secreted by *Albugo candida*, which collectively target core members of the *Arabidopsis thaliana* microbiota to facilitate host colonisation (Gómez-Pérez *et al.*, 2023). Although the overall structural model confidence is low, we observed positively charged surface areas which could point towards potential membrane activity, a mechanism previously described to various antimicrobial peptides (Oliveira Júnior *et al.*, 2025). However, given the limited reliability of the structural prediction, this interpretation remains highly speculative. Our findings reveal a further sophisticated level of pathogen interference, demonstrating that pathogens can not only respond to and reshape the plant microbiome but also sabotage

microbiota-mediated host defence responses by compromising the cry for help recruitment during infection. *Pseudomonas* species are well known for their role in plant disease suppression and are frequently enriched during plant cry for help responses (Wang & Song, 2022). For example, beneficial *Pseudomonas* spp. are recruited in response to take-all disease in wheat, where they protect the host through direct antagonism against the pathogen (Raaijmakers & Weller, 1998). We observed antagonism by *P. crudilactis*, *P. laurentiana*, *P. plecoglossicida* and *P. vancouverensis* against the *V. dahliae Av2* deletion mutant *in vitro*, indicating that these *Pseudomonas* spp. are capable of suppressing *V. dahliae* during infection. Furthermore, the same *Pseudomonas* spp. that exhibited enhanced antagonism towards the *Av2* deletion mutant were directly inhibited by Av2. This reciprocal antagonism aligns with previous findings showing that antimicrobial effectors target beneficial bacteria that are able to antagonise the pathogen (Snelders *et al.*, 2020, 2023; Chavarro-Carrero *et al.*, 2024). Interestingly, *Pseudomonas* species inhibited by Av2 span two distinct phylogenetic groups, suggesting that some *Pseudomonas* species have evolved resistance to overcome suppression by Av2. This may suggest that a co-evolutionary arms race takes place between *V. dahliae* and host-associated microbiota members reminiscent of the development of antibiotic resistance. Given the abundance of microbes that produce antimicrobial molecules (Mullis *et al.*, 2019; Mesny *et al.*, 2025), the resistance of *Pseudomonas* spp. to Av2 may be part of a broader antimicrobial resistance developed through diverse microbial interactions, with *V. dahliae* playing only a minor role in this process. Elucidating how particular *Pseudomonas* species have overcome Av2 sensitivity may provide valuable insight into the mode of action of the effector and selective pressures shaping pathogen–microbe interactions in the rhizosphere. Within the *V. dahliae* population, two closely related homologues of the *Av2* effector have been identified, differing by only a single amino acid (Chavarro-Carrero *et al.*, 2021). Since this variation does not seem to affect recognition by the V2 immune receptor (Chavarro-Carrero *et al.*, 2021), we hypothesised that it might affect the antimicrobial activity that is exerted by the effector protein. However, our *in vitro* activity assays revealed no significant differences in antimicrobial activity between the two variants, suggesting that the amino acid substitution does not affect this function. In these assays, we also observed that the antimicrobial activity of Av2 extends beyond *Pseudomonas* spp., although it remains to be determined what the biological relevance of this broader activity is for *V. dahliae*. *Av2* homologues have furthermore been reported in other species of the *Verticillium* genus and in *Fusarium* (Chavarro-Carrero *et al.*, 2021). Intriguingly, recent evidence indicates that *V. dahliae* acquired *Av2* via horizontal gene transfer from *Fusarium* species (Sato *et al.*, 2025). Although sequence variation exists among these homologues, our assays did not reveal any functional differences in antimicrobial activity. It is important to note, however, that only a limited panel of bacterial strains was tested, and the possibility remains that sequence variation modulates activity against untested microbial targets. The conservation of the antimicrobial function observed for Av2 is reminiscent of Ave1, which was also horizontally acquired by *V. dahliae*, in this case from plants (de Jonge *et al.*, 2012; Snelders *et al.*, 2020). Interestingly, plant homologues of *Ave1*, known as plant natriuretic peptides (PNP), likely exhibit similar antimicrobial activity *in vitro*, as both *A. thaliana* PNP-A and Ave1 inhibit the growth of *Bacillus subtilis* (Snelders *et al.*, 2020). These parallels raise the possibility that conserved antimicrobial effectors, regardless of their evolutionary origin, fulfil similar ecological roles in shaping microbial communities. Since both *Fusarium* spp. and *V. dahliae* are soil-borne fungal pathogens that infect plants via the roots and disperse within their hosts via the vasculature (Di Pietro *et al.*, 2003; Fradin & Thomma, 2006), further investigation into the role of *Av2* in *Fusarium* spp. could help clarify whether its conserved antimicrobial activity similarly contributes to the colonisation strategy shared by these pathogens.

Taken together, our findings broaden the understanding of how pathogens manipulate their hosts by revealing that antimicrobial effectors can actively suppress the pathogen-induced cry for help response. By blocking the recruitment of protective microbes, pathogens undermine a critical layer of microbiota-mediated immunity. This adds to growing evidence that the plant microbiota is a strategic battleground in host–pathogen interactions (Mesny *et al.*, 2024). As more antimicrobial effectors are identified and characterised (Kettles *et al.*, 2018; Snelders *et al.*, 2020, 2021, 2023; Chang *et al.*, 2021; Gómez-Pérez *et al.*, 2023; Ökmen *et al.*, 2023; Chavarro-Carrero *et al.*, 2024; Mesny *et al.*, 2025), it will become increasingly clear how deeply the molecular arms race between plants and pathogens extends into the plant's microbial sphere. Finally, given that the cry for help recruitment of beneficial microbes may ultimately lead to the establishment of disease-suppressive soils (Mesny *et al.*, 2024), future research will have to reveal whether Av2 suppresses such long-term legacy effects in the soil microbiome.

Acknowledgements

BPHJT acknowledges funding by the Alexander von Humboldt Foundation in the framework of an Alexander von Humboldt Professorship endowed by the German Federal Ministry of Education and Research is furthermore supported by the Deutsche Forschungsgemeinschaft (DFG, German Research Foundation) under Germany's Excellence Strategy – EXC 2048/1 – Project ID: 390686111. Open Access funding enabled and organized by Projekt DEAL.

Competing interests

None declared.

Author contributions

AK, WP, NCS, and BPHJT conceived the project. AK, WP, JZ, NCS, and BPHJT designed the experiments. AK, WP, AD, JZ, and NS performed the experiments. AK, WP, AD, JZ, NS, and BPHJT analysed the data. AK, WP, and BPHJT wrote the manuscript. All authors read and approved the final manuscript.

AK and WP, and NCS and BPHJT contributed equally to this work.

ORCID

Andrea Doddi https://orcid.org/0000-0003-3149-6304
Anton Kraege https://orcid.org/0000-0002-4741-5671
Wilko Punt https://orcid.org/0000-0003-4047-1117
Nick C. Snelders https://orcid.org/0000-0002-2576-1928
Bart P. H. J. Thomma https://orcid.org/0000-0003-4125-4181
Jinyi Zhu https://orcid.org/0000-0003-1736-8680

Data availability

The 16S profiling data have been deposited in the NCBI GenBank database under BioProject PRJEB90267.

References

Berendsen RL, Vismans G, Yu K, Song Y, de Jonge R, Burgman WP, Burmølle M, Herschend J, H M Bakker PA, J Pieterse CM. 2018. Disease-induced assemblage of a plant-beneficial bacterial consortium. *The ISME Journal* **12**: 1496–1507.

Callahan BJ, McMurdie PJ, Rosen MJ, Han AW, Johnson AJA, Holmes SP. 2016. DADA2: high-resolution sample inference from Illumina amplicon data. *Nature Methods* **13**: 581–583.

Chang HX, Noel ZA, Chilvers MI. 2021. A β-lactamase gene of *Fusarium oxysporum* alters the rhizosphere microbiota of soybean. *The Plant Journal* **106**: 1588–1604.

Chavarro-Carrero EA, Snelders NC, Torres DE, Kraege A, López-Moral A, Petti GC, Punt W, Wieneke J, García-Velasco R, López-Herrera CJ *et al.* 2024. The soil-borne white root rot pathogen *Rosellinia necatrix* expresses antimicrobial proteins during host colonization. *PLoS Pathogens* **20**: e1011866.

Chavarro-Carrero EA, Vermeulen JP, Torres D, Usami T, Schouten HJ, Bai Y, Seidl MF, Thomma BPHJ. 2021. Comparative genomics reveals the *in planta*-secreted *Verticillium dahliae* Av2 effector protein recognized in tomato plants that carry the V2 resistance locus. *Environmental Microbiology* **23**: 1941–1958.

Cole JR, Wang Q, Fish JA, Chai B, McGarrell DM, Sun Y, Brown CT, Porras-Alfaro A, Kuske CR, Tiedje JM. 2014. Ribosomal Database Project: data and tools for high throughput rRNA analysis. *Nucleic Acids Research* **42**(D1): D633–D642.

Cook DE, Kramer HM, Torres DE, Seidl MF, Thomma BPHJ. 2020. A unique chromatin profile defines adaptive genomic regions in a fungal plant pathogen. *eLife* **9**: e62208.

Cook DE, Mesarich CH, Thomma BPHJ. 2015. Understanding plant immunity as a surveillance system to detect invasion. *Annual Review of Phytopathology* **53**: 541–563.

Di Pietro A, Madrid MP, Caracuel Z, Delgado-Jarana J, Roncero MIG. 2003. *Fusarium oxysporum*: exploring the molecular arsenal of a vascular wilt fungus. *Molecular Plant Pathology* **4**: 315–325.

Emms DM, Kelly S. 2019. OrthoFinder: phylogenetic orthology inference for comparative genomics. *Genome Biology* **20**: 238.

Fadrosh DW, Ma B, Gajer P, Sengamalay N, Ott S, Brotman RM, Ravel J. 2014. An improved dual-indexing approach for multiplexed 16S rRNA gene sequencing on the Illumina MiSeq platform. *Microbiome* **2**: 1–7.

Faino L, Seidl MF, Shi-Kunne X, Pauper M, Van Den Berg GCM, Wittenberg AHJ, Thomma BPHJ. 2016. Transposons passively and actively contribute to evolution of the two-speed genome of a fungal pathogen. *Genome Research* **26**: 1091–1100.

Fradin EF, Thomma BPHJ. 2006. Physiology and molecular aspects of Verticillium wilt diseases caused by *V. dahliae* and *V. albo-atrum*. *Molecular Plant Pathology* **7**: 71–86.

Fradin EF, Zhang Z, Ayala JCJ, Castroverde CDM, Nazar RN, Robb J, Liu CM, Thomma BPHJ. 2009. Genetic dissection of Verticillium wilt resistance mediated by tomato Ve1. *Plant Physiology* **150**: 320–332.

Gómez-Pérez D, Schmid M, Chaudhry V, Hu Y, Velic A, Maček B, Ruhe J, Kemen A, Kemen E. 2023. Proteins released into the plant apoplast by the obligate parasitic protist Albugo selectively repress phyllosphere-associated bacteria. *New Phytologist* **239**: 2320–2334.

Guo X, Zhang X, Qin Y, Liu YX, Zhang J, Zhang N, Wu K, Qu B, He Z, Wang X *et al.* 2020. Host-associated quantitative abundance profiling reveals the microbial load variation of root microbiome. *Plant Communications* **1**: 100003.

Jones JDG, Dangl JL. 2006. The plant immune system. *Nature* **444**(Issue 7117): 323–329.

de Jonge R, Bolton MD, Kombrink A, Van Den Berg GCM, Yadeta KA, Thomma BPHJ. 2013. Extensive chromosomal reshuffling drives evolution of virulence in an asexual pathogen. *Genome Research* **23**: 1271–1282.

de Jonge R, Van Esse HP, Maruthachalam K, Bolton MD, Santhanam P, Saber MK, Zhang Z, Usami T, Lievens B, Subbarao KV *et al.* 2012. Tomato immune receptor Ve1 recognizes effector of multiple fungal pathogens uncovered by genome and RNA sequencing. *Proceedings of the National Academy of Sciences, USA* **109**: 5110–5115.

Jumper J, Evans R, Pritzel A, Green T, Figurnov M, Ronneberger O, Tunyasuvunakool K, Bates R, Žídek A, Potapenko A *et al.* 2021. Highly accurate protein structure prediction with AlphaFold. *Nature* **596**: 583–589.

Jurrus E, Engel D, Star K, Monson K, Brandi J, Felberg LE, Brookes DH, Wilson L, Chen J, Liles K *et al.* 2018. Improvements to the APBS biomolecular solvation software suite. *Protein Science* **27**: 112–128.

van Kempen M, Kim SS, Tumescheit C, Mirdita M, Lee J, Gilchrist CLM, Söding J, Steinegger M. 2023. Fast and accurate protein structure search with Foldseek. *Nature Biotechnology* **42**: 243–246.

Kettles GJ, Bayon C, Sparks CA, Canning G, Kanyuka K, Rudd JJ. 2018. Characterization of an antimicrobial and phytotoxic ribonuclease secreted by the fungal wheat pathogen *Zymoseptoria tritici*. *New Phytologist* **217**: 320–331.

Kremer JM, Sohrabi R, Paasch BC, Rhodes D, Thireault C, Schulze-Lefert P, Tiedje JM, He SY. 2021. Peat-based gnotobiotic plant growth systems for Arabidopsis microbiome research. *Nature Protocols* **16**: 2450–2470.

Liu Y, Chen L, Wu G, Feng H, Zhang G, Shen Q, Zhang R. 2017. Identification of root-secreted compounds involved in the communication between cucumber, the beneficial *Bacillus amyloliquefaciens*, and the soil-borne pathogen *Fusarium oxysporum*. *Molecular Plant–Microbe Interactions* **30**: 53–62.

Liu Y, Zhang H, Wang J, Gao W, Sun X, Xiong Q, Shu X, Miao Y, Shen Q, Xun W *et al.* 2024. Nonpathogenic *Pseudomonas syringae* derivatives and its metabolites trigger the plant "cry for help" response to assemble disease suppressing and growth promoting rhizomicrobiome. *Nature Communications* **15**: 1–14.

López M, Tejera NA, Iribarne C, Lluch C, Herrera-Cervera JA. 2008. Trehalose and trehalase in root nodules of *Medicago truncatula* and *Phaseolus vulgaris* in response to salt stress. *Physiologia Plantarum* **134**: 575–582.

Love MI, Huber W, Anders S. 2014. Moderated estimation of fold change and dispersion for RNA-seq data with DESeq2. *Genome Biology* **15**: 1–21.

Martin M. 2011. Cutadapt removes adapter sequences from high-throughput sequencing reads. *EMBnet.Journal* **17**: 10–12.

McMurdie PJ, Holmes S. 2013. phyloseq: an R package for reproducible interactive analysis and graphics of microbiome census data. *PLoS ONE* **8**: e61217.

Mesny F, Bauer M, Zhu J, Thomma BPHJ. 2024. Meddling with the microbiota: fungal tricks to infect plant hosts. *Current Opinion in Plant Biology* **82**: 102622.

Mesny F, Wolf V, López-Moral A, Kraege A, Punt W, Park J, Zhu J, Sato Y, Thomma BP. 2025. Plant-associated fungi co-opt ancient antimicrobials for host manipulation. *BioRxiv*. doi: 10.1101/2024.01.04.574150.

Mullis MM, Rambo IM, Baker BJ, Reese BK. 2019. Diversity, ecology, and prevalence of antimicrobials in nature. *Frontiers in Microbiology* **10**: 2518.

Ökmen B, Katzy P, Huang L, Wemhöner R, Doehlemann G. 2023. A conserved extracellular Ribo1 with broad-spectrum cytotoxic activity enables smut fungi to compete with host-associated bacteria. *New Phytologist* **240**: 1976–1989.

Oksanen J, Simpson G, Blanchet F, Kindt R, Legendre P, Minchin P, O'Hara R, Solymos P, Stevens M, Szoecs E *et al.* 2004. vegan: community ecology package. [WWW document] URL https://github.com/vegandevs/vegan.

Oliveira Júnior NG, Souza CM, Buccini DF, Cardoso MH, Franco OL. 2025. Antimicrobial peptides: structure, functions and translational applications. *Nature Reviews Microbiology* **23**: 687-700.

Paulson JN, Colin Stine O, Bravo HC, Pop M. 2013. Differential abundance analysis for microbial marker-gene surveys. *Nature Methods* **10**: 1200–1202.

Punt W, Park J, Roevenich H, Kraege A, Schmitz N, Wieneke J, Snelders NC, Fiorin GL, López-Moral A, Chavarro-Carrero EA *et al.* 2025. A gnotobiotic system reveals multifunctional effector roles in plant-fungal pathogen dynamics. *BioRxiv*. doi: 10.1101/2025.03.27.645772.

Raaijmakers JM, Weller DM. 1998. Natural plant protection by 2,4-diacetylphloroglucinol-producing Pseudomonas spp. in take-all decline soils. *Molecular Plant–Microbe Interactions* **11**: 144–152.

Raffaele S, Kamoun S. 2012. Genome evolution in filamentous plant pathogens: why bigger can be better. *Nature Reviews Microbiology* **10**: 417–430.

Rolfe SA, Griffiths J, Ton J. 2019. Crying out for help with root exudates: adaptive mechanisms by which stressed plants assemble health-promoting soil microbiomes. *Current Opinion in Microbiology* **49**: 73–82.

Rovenich H, Boshoven JC, Thomma BPHJ. 2014. Filamentous pathogen effector functions: of pathogens, hosts and microbiomes. *Current Opinion in Plant Biology* **20**: 96–103.

Sánchez-Vallet A, Saleem-Batcha R, Kombrink A, Hansen G, Valkenburg DJ, Thomma BPHJ, Mesters JR. 2013. Fungal effector Ecp6 outcompetes host immune receptor for chitin binding through intrachain LysM dimerization. *eLife* **2013**: e00790.

Sato Y, Bex R, van den Berg GCM, Santhanam P, Höfte M, Seidl MF, Thomma BPHJ. 2025. Starship giant transposons dominate plastic genomic regions in a fungal plant pathogen and drive virulence evolution. Nature Communications 16: 6806.

Snelders NC, Boshoven JC, Song Y, Schmitz N, Fiorin GL, Rovenich H, van den Berg GCM, Torres DE, Petti GC, Prockl Z *et al.* 2023. A highly polymorphic effector protein promotes fungal virulence through suppression of plant-associated Actinobacteria. *New Phytologist* **237**: 944–958.

Snelders NC, Petti GC, van den Berg GCM, Seidl MF, Thomma BPHJ. 2021. An ancient antimicrobial protein co-opted by a fungal plant pathogen for *in planta* mycobiome manipulation. *Proceedings of the National Academy of Sciences, USA* **118**: e2110968118.

Snelders NC, Rovenich H, Petti GC, Rocafort M, van den Berg GCM, Vorholt JA, Mesters JR, Seidl MF, Nijland R, Thomma BPHJ. 2020. Microbiome manipulation by a soil-borne fungal plant pathogen using effector proteins. *Nature Plants* **6**: 1365–1374.

Spooren J, van Bentum S, Thomashow LS, Pieterse CMJ, Weller DM, Berendsen RL. 2024. Plant-driven assembly of disease-suppressive soil microbiomes. *Annual Review of Phytopathology* **62**: 1–30.

Torres DE, Kramer HM, Tracanna V, Fiorin GL, Cook DE, Seidl MF, Thomma BPHJ. 2024. Implications of the three-dimensional chromatin organization for genome evolution in a fungal plant pathogen. *Nature Communications* **15**: 1701.

Torres DE, Thomma BPHJ, Seidl MF. 2021. Transposable elements contribute to genome dynamics and gene expression variation in the fungal plant pathogen *Verticillium dahliae*. *Genome Biology and Evolution* **13**: evab135.

Trivedi P, Leach JE, Tringe SG, Sa T, Singh BK. 2020. Plant–microbiome interactions: from community assembly to plant health. *Nature Reviews Microbiology* **18**: 607–621.

Usami T, Momma N, Kikuchi S, Watanabe H, Hayashi A, Mizukawa M, Yoshino K, Ohmori Y. 2017. Race 2 of *Verticillium dahliae* infecting tomato in Japan can be split into two races with differential pathogenicity on resistant rootstocks. *Plant Pathology* **66**: 230–238.

Varadi M, Anyango S, Deshpande M, Nair S, Natassia C, Yordanova G, Yuan D, Stroe O, Wood G, Laydon A *et al.* 2022. AlphaFold Protein Structure Database: massively expanding the structural coverage of protein-sequence space with high-accuracy models. *Nucleic Acids Research* **50**(D1): D439–D444.

Veltri D, Kamath U, Shehu A. 2018. Deep learning improves antimicrobial peptide recognition. *Bioinformatics* **34**: 2740–2747.

Wang Z, Song Y. 2022. Toward understanding the genetic bases underlying plant-mediated "cry for help" to the microbiota. *iMeta* **1**: e8.

Wippel K, Tao K, Niu Y, Zgadzaj R, Kiel N, Guan R, Dahms E, Zhang P, Jensen DB, Logemann E *et al.* 2021. Host preference and invasiveness of commensal bacteria in the Lotus and Arabidopsis root microbiota. *Nature Microbiology* **6**: 1150–1162.

Yuan J, Zhao J, Wen T, Zhao M, Li R, Goossens P, Huang Q, Bai Y, Vivanco JM, Kowalchuk GA *et al.* 2018. Root exudates drive the soil-borne legacy of aboveground pathogen infection. *Microbiome* **6**: 1–12.

Supporting Information

Additional Supporting Information may be found online in the Supporting Information section at the end of the article.

Fig. S1 *Verticillium dahliae Av2* is expressed in soil extract.

Fig. S2 The predicted structure of the antimicrobial effector Av2 shows positively charged surface residues.

Fig. S3 Microbes were successfully reintroduced into sterile flowpot substrate with 10% nonautoclaved soil.

Fig. S4 Growth of a *Verticillium dahliae Av2* deletion strain is selectively impaired when cocultured with *Pseudomonas* spp.

Fig. S5 Differentially abundant bacterial orders between mock and *Verticillium dahliae*-inoculated plants.

Please note: Wiley is not responsible for the content or functionality of any Supporting Information supplied by the authors. Any queries (other than missing material) should be directed to the *New Phytologist* Central Office.

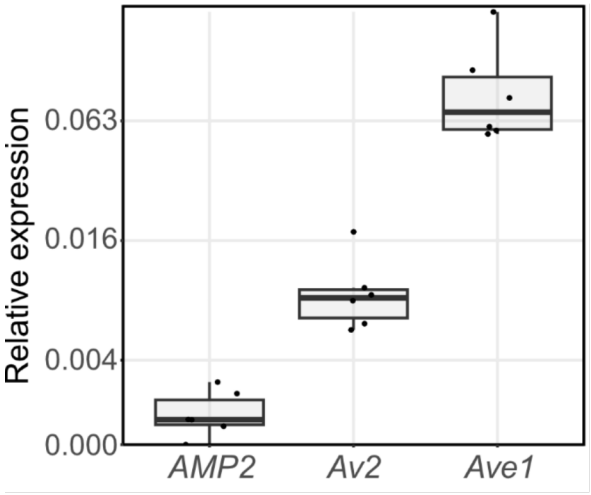

Supplementary Fig. 1. *Verticillium dahliae Av2* is expressed in soil extract. Expression of *V. dahliae* effectors after seven days of growth in soil extract when normalised to glyceraldehyde 3-phosphate dehydrogenase (*VdGAPDH*) expression. Boxes indicate the interquartile range of the values, the median values are indicated by horizontal lines, and the whiskers extend to the minimum and maximum values.

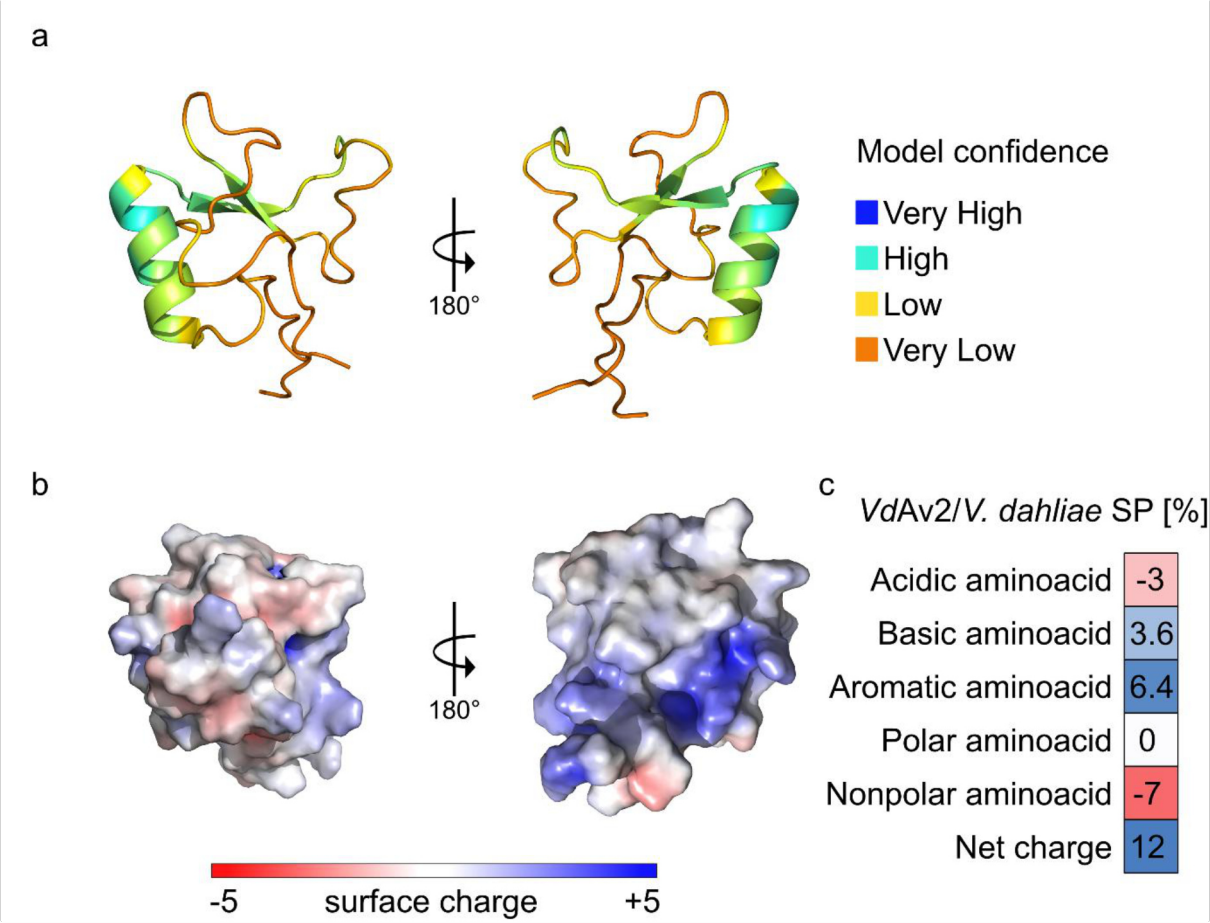

Supplementary Fig. 2. The predicted structure of the antimicrobial effector Av2 shows positively charged surface residues. (a) Structural prediction of Av2 using Alphafold2 resulted in a low confidence structure with an overall pLDDT score of 53.8. Colouring of the individual amino acids in the structure according to the Alphafold Protein Structure Database, where amino acids with a pLDDT score >90 appear in blue, between 90 and 70 in cyan, between 70 and 50 in yellow and <50 in orange. While local stretches have higher pLDDT scores, the majority of Av2 is predicted with a score <50. **(b)** Surface charge of the predicted structure was calculated using the APBS plugin for PyMOL. **(c)** To assess differences in amino acid composition between Av2 and the average *V. dahliae* secreted protein, the proportion of chemically distinct amino acids in Av2 was subtracted from their expected proportions in the overall secretome.

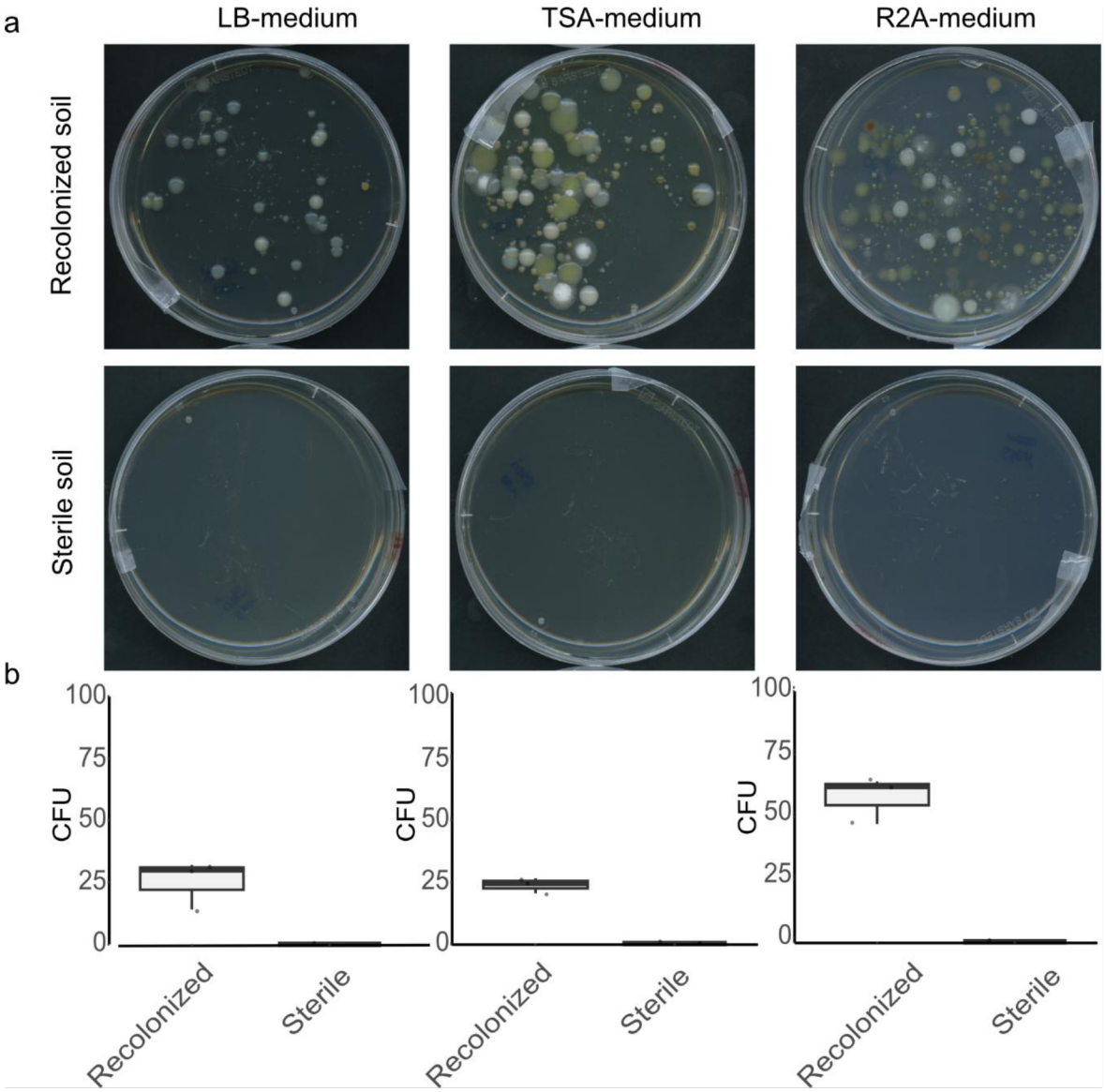

Supplementary Fig. 3. Microbes were successfully reintroduced into sterile flowpot substrate with 10% non-autoclaved soil. (a) Either recolonized or sterile Flowpot substrate were resuspended in $MgCl_2$ and streaked out on three different media, namely Lysogeny broth agar (LB), Tryptic soy agar (TSA) and Reasoner's 2A agar (R2A). There was growth on all plates containing recolonised substrate while no growth was observed on plates with sterile substrate. Photographs display agar plates after the plating of a 100x diluted substrate-$MgCl_2$ suspension and a 4-day incubation in darkness at room temperature. **(b)** Boxplots displaying the number of colony-forming units (CFU) on three different growth media after plating a 100x substrate-$MgCl_2$ suspension and 4 days of incubation in darkness at room temperature. Substrate suspension from recolonized substrate showed significant more colonies compared to sterile substrate (unpaired two-sided student's t-test; $p < 0.05$). Boxes indicate the interquartile range of the values, the median values are indicated by horizontal lines, and the whiskers extend to the minimum and maximum values.

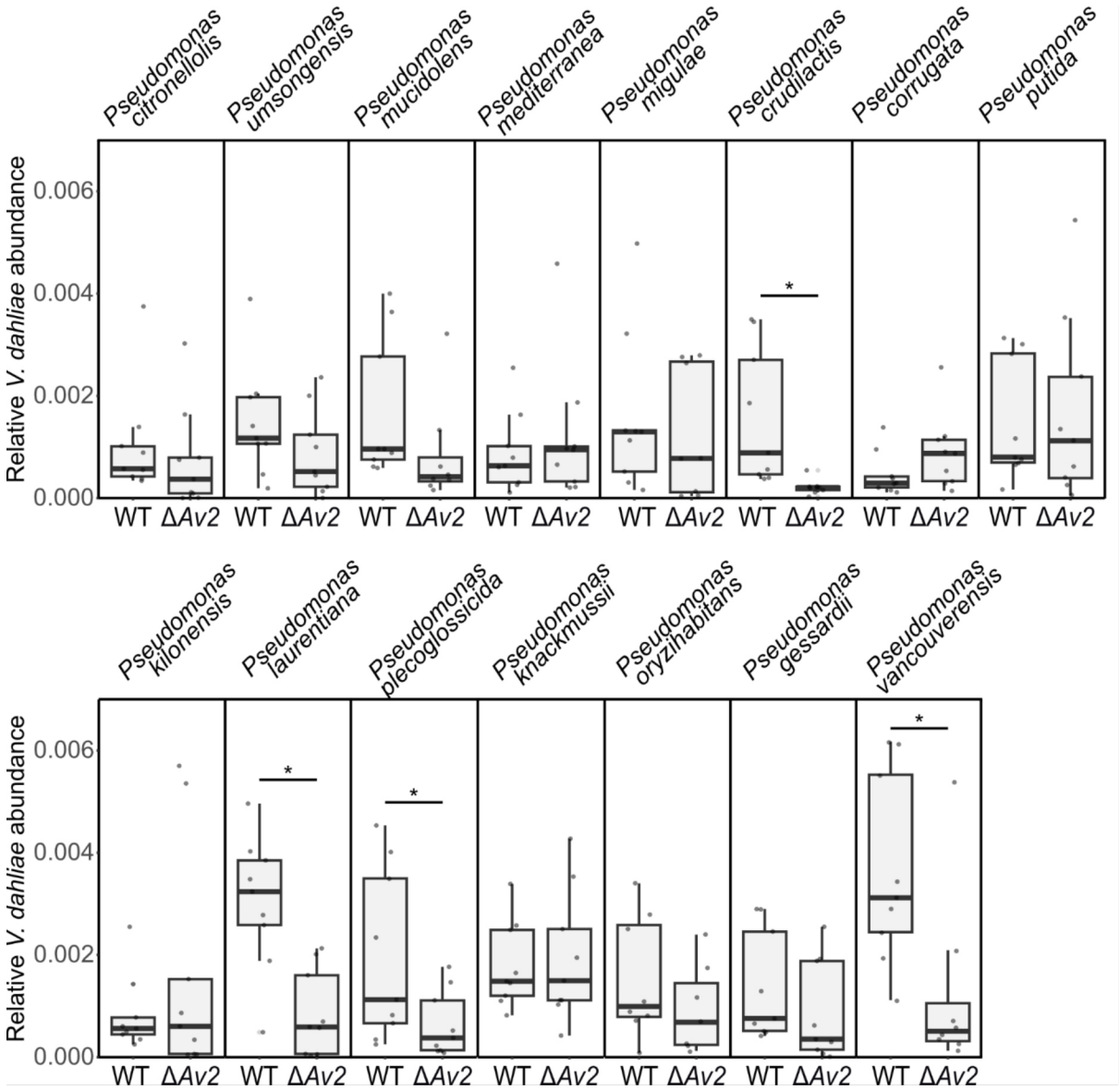

Supplementary Fig. 4. Growth of a *Verticillium dahliae Av2* deletion strain is selectively impaired when co-cultured with *Pseudomonas* spp. Relative biomass of wild-type *V. dahliae* strain TO22 (WT) and the corresponding *VdAv2* deletion strain (Δ*Av2*) was quantified with real-time PCR after co-cultivation with a panel of Pseudomonadales in half-strength Murashige and Skoog medium for 48 h. *V. dahliae* biomass was normalised against abundance of spike-in DNA added during DNA extraction. The asterisks indicate significant difference in *V. dahliae* abundance between the genotypes (unpaired two-sided student's t-test; $p < 0.05$). Boxes indicate the interquartile range of the values, the median values are indicated by horizontal lines, and the whiskers extend to the minimum and maximum values.

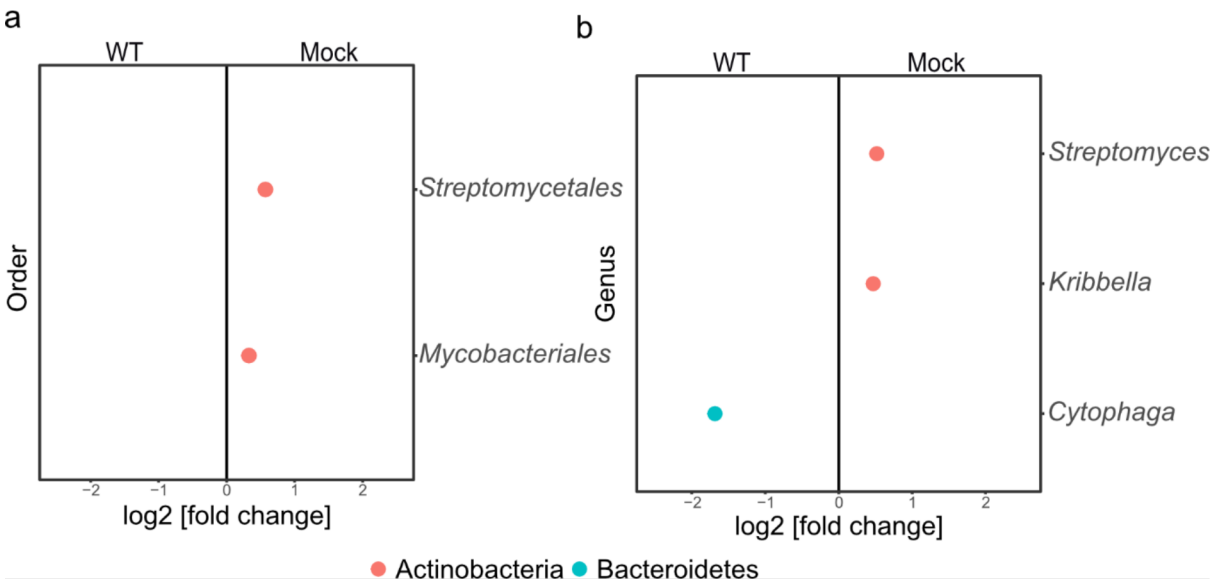

Supplementary Fig. 5. Differentially abundant bacterial orders between mock and *Verticillium dahliae* inoculated plants. (a) Differentially abundant bacterial orders in the stem endosphere of tomato plants upon inoculation with either wild-type *V. dahliae* (WT) or mock treatment (Wald test, adjusted P < 0.05). **(b)** Differential abundance analysis of bacterial genera in the tomato stems upon inoculation with wild-type *V. dahliae* or mock treatment.

Chapter 3

Differential contributions of an antimicrobial effector from *Verticillium dahliae* to virulence and tomato microbiota assembly across natural soils

Wilko Punt[1*], Anton Kraege[1*], Sabine Metzger[1], Natalie Schmitz[1], Jinyi Zhu[1], Stéphane Hacquard[2], Michael Bonkowski[3], Nick C. Snelders[1#] & Bart P.H.J. Thomma[1#§]

[1]University of Cologne, Institute for Plant Sciences, Cluster of Excellence on Plant Sciences (CEPLAS), 50674 Cologne, Germany

[2]Max Planck Institute for Plant Breeding Research, Cluster of Excellence on Plant Sciences (CEPLAS), 50829, Cologne, Germany

[3]University of Cologne, Institute for Zoology, Cluster of Excellence on Plant Sciences (CEPLAS), 50674, Cologne, Germany

*These authors contributed equally

#These authors contributed equally

§Corresponding author: bthomma@uni-koeln.de

This article was published on *BioRxiv* (2025)

doi: doi.org/10.1101/2025.09.30.679524

Abstract

Background

Throughout their life cycle, plants associate with diverse and complex microbial communities collectively known as their microbiota. These microbiota contribute to plant performance and health by enhancing nutrient acquisition, modulating immunity, and providing a microbial barrier against pathogens. To successfully colonize their hosts, pathogens must overcome not only plant immune defenses but also this microbial barrier. For example, the soil-borne fungal pathogen *Verticillium dahliae* secretes the antimicrobial effector Ave1 to suppress antagonistic microbes and facilitate infection. Although many plant pathogens, including *V. dahliae*, inhabit both plant-associated and soil environments, how antimicrobial effectors contribute to pathogen establishment across these diverse ecological contexts remains poorly understood.

Results

To explore this question, we assembled a collection of natural soils differing in physicochemical properties and microbiota composition. Using three host plant species — barley, tomato, and cotton — we found that root-associated bacterial and fungal communities were primarily shaped by soil type, whereas phyllosphere microbiota were mainly determined by plant species identity. On tomato, we further observed that the effector Ave1 differentially contributed to *V. dahliae* virulence depending on the soil of origin. While Ave1 consistently altered tomato-associated microbiota across all soils tested, the specific microbial taxa affected varied between soils.

Conclusions

Our findings demonstrate that the impact of the antimicrobial effector Ave1 on microbiota composition and pathogen virulence is context-dependent, influenced by the specific soil-derived microbial community that assembles on the host. This work highlights the ecological complexity of effector functions and suggests that pathogen success in natural environments depends on dynamic interactions with both the plant host and its microbiota.

Introduction

Plants host diverse microbial communities, known as the plant microbiota, which mainly include bacteria, fungi, and protists (Trivedi et al., 2020). These microorganisms colonize all plant parts, and together with the host plant, form a unified biological entity often referred to as the holobiont (Vandenkoornhuyse et al., 2015). Apart from seed-borne microbes inherited from the mother plant in the previous plant generation, the majority of microbes that make up the plant microbiota are recruited from environmental niches. While some microbes are transmitted through the air, the surrounding soil serves as the primary reservoir from which plants acquire most of their microbiota (Chialva et al., 2022). Soil properties such as pH, nutrient availability, organic carbon content, temperature and redox status shape the pool of microbes available for recruitment into the plant microbiota (Fierer, 2017). Consequently, the physicochemical properties of soil have a strong influence on plant microbiota assembly, as evidenced by the distinct microbial communities found in plants grown on different soils (Bulgarelli et al., 2012; Thiergart et al., 2020). At the same time, host genetics exert selective pressure on which taxa colonize and persist in the plant microbiota (Bulgarelli et al., 2012; Lundberg et al., 2012; Wagner et al., 2016). This is particularly evident in the formation of the core microbiota, which is a consistent subset of microbial taxa that reliably establish within the microbiota of a plant, even when plants are grown in diverse soils (Lundberg et al., 2012; Almario et al., 2022).

To date, numerous studies have separately demonstrated the importance of the bulk soil on the one hand, and of host genetics on the other hand, in structuring plant microbiota (Bulgarelli et al., 2012; Lundberg et al., 2012; Wagner et al., 2016; Fitzpatrick et al., 2018; Walters et al., 2018; Thiergart et al., 2020; Simonin et al., 2020; Tkacz et al., 2020). These studies have examined plant-associated microbes in diverse natural environments, where abiotic factors like local climate and weather can influence microbiota assembly, or have compared microbiota of different plant species grown in the same soil at a single location (Ofek-Lalzar et al., 2014; Wagner et al., 2016; Walters et al., 2018). However, studies that simultaneously evaluate the contribution of plant genetics and differential bulk soil microbiota on plant microbiota assembly, for instance by using various plant species in diverse natural soils while controlling for environmental influences, remain scarce (Tkacz et al., 2020, Dumack et al., 2022).

Microbes that establish in the plant microbiota interact with the host plant in various ways. Many microbes interact with plants as neutral commensals, while other microbes can be beneficial to the plant, or can be pathogenic and cause disease (Hassani et al., 2018). The community balance and composition of the microbiota plays an important role in plant health

and performance, particularly by contributing to defense against pathogens (Du et al., 2025). Notably, plants have the ability to actively recruit beneficial microbes in response to pathogen attack. For instance, cucumber plants infected by the soil-borne pathogen *Fusarium oxysporum* f. sp. *cucumerinum* recruit *Bacillus amyloliquefaciens* to reduce disease severity (Liu et al., 2017). Over longer timescales, such plant-driven recruitment of beneficial microbes can result in the formation of disease-suppressive soils, where susceptible plants can grow in the presence of pathogens without experiencing severe disease symptoms (Du et al., 2025). A well-documented example, is the response of wheat plants to infection by *Gaeumannomyces graminis* var. *tritici*, the causal agent of “take-all” disease. In this case, wheat recruits beneficial *Pseudomonas* species that antagonize the pathogen through the secretion of antimicrobial compounds, ultimately contributing to disease suppression over successive planting cycles in particular fields (Raaijmakers and Weller, 1998; Spooren et al., 2024). Importantly, protection via microbial recruitment is not limited to direct antagonism of pathogens. Some beneficial microbes enhance plant immunity through the induction of systemic defense responses (Pieterse et al., 2014). For example, *Arabidopsis thaliana* plants infected with the foliar pathogen *Hyaloperonospora arabidopsidis* (Hpa) selectively promote the growth of three bacterial species in the rhizosphere. This recruitment boosts systemic resistance to Hpa, improves overall plant growth, and can even benefit subsequent plant generations by fostering a protective microbiome (Berendsen et al., 2018). In this way, the plant microbiota has also often been considered as an additional layer of the immune system against pathogens by both inducing immune responses and directly antagonizing pathogens (Mendes et al., 2011; Carrión et al., 2019; Du et al., 2025; Durán et al., 2018).

While colonizing their hosts, plant pathogens secrete so-called effector molecules to promote host colonization by manipulating host physiology, including immunity (Jones and Dangl, 2006; Cook et al., 2015). Recently, several studies have demonstrated that pathogens exploit effector proteins that possess antimicrobial activity to manipulate the host microbiota, and thus facilitate colonization (Snelders et al., 2020; Chavarro-Carrero et al., 2024; Snelders et al., 2021; Snelders et al., 2023; Ökmen et al., 2023; Kettles et al., 2018; Chang et al., 2021; Gómez-Pérez et al., 2023; Mesny et al., 2024; Kraege et al., 2025). For example, the soil-borne fungal plant pathogen *Verticillium dahliae* exploits the antimicrobial effector protein Ave1 to suppress antagonistic Sphingomonadales bacteria during host colonization of tomato and cotton plants (Snelders et al., 2020). Interestingly, predictions from a machine learning tool suggest that 349 secreted *V. dahliae* effectors possess antimicrobial activity, indicating that *V. dahliae* may devote a substantial proportion of its secreted proteins to microbiota manipulation (Mesny and Thomma, 2024).

Fungal pathogens such as *V. dahliae* occupy a range of ecologically distinct niches throughout their life cycle (Fradin and Thomma, 2006; Guerreiro and Stukenbrock, 2025). While they infect host plants during specific life stages, many also persist outside the host for extended periods, particularly in the soil (Fradin and Thomma 2006; Katan, 2017). Soil microbial communities are generally more diverse than those associated with plants and vary substantially depending on the physicochemical properties of the soil (Fierer, 2017; Sokol et al., 2022). Accordingly, many pathogens are exposed to diverse microbial environments and must interact with a wide range of microbial taxa over time (Snelders et al., 2022). This is particularly relevant for broad host range pathogens like *V. dahliae*, which are adapted to numerous hosts and habitats and are thought to rely on antimicrobial effectors that facilitate interactions with different microbial communities (Trivedi et al., 2020; Snelders et al., 2022). Building on previous studies that explored antimicrobial effector functions using a single type of soil (Snelders et al., 2020), we hypothesize that the virulence contribution of antimicrobial effectors like Ave1, as well as their impact on microbial communities, may vary depending on the host-associated microbiota, which is largely determined by the bulk soil microbial community.

Here we report the establishment of a collection of natural soils that are diverse in both physicochemical characteristics and microbiota composition. We use this resource to simultaneously assess the contributions of the diverse types of soil and the plant genotype to plant microbiota assembly under controlled greenhouse conditions by analyzing fungal and bacterial communities associated with barley, cotton and tomato plants grown on each soil. Additionally, we utilize the soil collection to investigate the impact of the antimicrobial effector protein Ave1 on tomato microbiota composition and its role in *V. dahliae* virulence during infection of tomato plants harboring distinct microbiota.

Materials & methods

Soil collection and storage

Natural soils were collected. Two soil collections were performed, in February 2022 and February 2023 at nine sites in the Netherlands: Makkum (53°05'09.8"N 5°26'20.3"E), Oranjewoud (52°57'11.7"N 5°57'45.6"E), Ginkelse Heide (52°02'10.7"N 5°43'38.9"E), Eckelrade (50°47'57.7"N 5°44'42.5"E) Maasduinen (51°28'34.3"N 6°11'34.9"E), Oostvaardersplassen (52°27'50.0"N 5°25'10.8"E), Reijerscamp (52°00'37.7"N 5°46'25.0"E), Blauwe Kamer (51°56'34.4"N 5°37'12.9"), Aijen (51°34'55.0"N 6°02'27.3"E). For collection, the top 10 cm of soil was removed and the subsequent 30 cm of soil was collected. After collection, soil samples were homogenized and rocks and pieces of plant material were removed before the soil was stored in sealed buckets at 8℃ until further use. Further, Cologne agricultural soil (50°57'27.8"N 6°51'22.4"E; Bai et al., 2015) was included.

Physicochemical soil analysis

For physicochemical analysis, 50 g of each soil was freeze dried and ground to fine powder using a mortar and pestle. To measure soil pH, ground soil powder was suspended with 150 ml of distilled water and incubated for 1 hour. Subsequently the pH was measured using a pH-electrode (Meddler Toledo, Giessen, Germany). Carbon and nitrogen levels were measured using the FLASH2000 CHNS/O analyzer (Thermo Fisher Scientific, Waltham, USA). To measure elemental contents, 100 mg of soil powder was weighed into metal-free centrifugation tubes (VWR, Radnor, USA). Samples were the soaked in 500 µl of 30% nitric acid for 2 hours. Subsequently, the volume was adjusted to 1 ml with 30% nitric acid and the sample was incubated for 14 hours at 65℃. Next, the suspension was incubated at 95℃ for 90 minutes. Samples were cooled to room temperature and 200 µl of hydrogen peroxide were added. Subsequently, the samples were incubated at 95℃ for 30 minutes. Next, the samples were diluted to 10 ml using MQ-water and centrifuged at 13,000 rpm for 1 hour at 4℃. The supernatant was transferred to a clean metal-free 50 ml centrifugation tube and incubated at 4℃ overnight, followed by centrifugation at 13,000 rpm for 1 hour at 4℃. Finally, 600 µl of supernatant were mixed with 2,4 ml of 2% nitric acid. ICP-MS measurements were carried out on an Agilent 7700 ICP-MS (Agilent Technologies, Waldbronn, Germany) in the Biocenter MS-Platform of the University of Cologne. All measurements were performed in technical triplicates and strictly followed the manufacturer`s instructions using He in the collision cell mode to minimize spectral interference.

Plant growth assays

Tomato (*Solanum lycopersicum L.*) cultivar MoneyMaker, barley (*Hordeum vulgare*) cultivar GoldenPromise and cotton (*Gossypium hirsutum*) cultivar DDHY642201-AC were used for all assays. Before sowing, seeds were surface-sterilized using chlorine gas generated by adding 3 mL of hydrochloric acid (HCl) to 100 mL of bleach (sodium hypochlorite) in a 250 mL beaker placed inside a glass container sealed with a lid and parafilm and incubated for 5 hours. After sterilization, the container was vented in a fume hood overnight. Subsequently, surface sterilized seeds were sown on soil and grown for three weeks in a greenhouse chamber with 16 hours of light at 23°C, followed by 8 hours in darkness at 22°C. Plant growth was assessed by calculating canopy areas, for tomato and cotton based on overhead pictures and for barley plants based on side pictures using ImageJ (Schneider *et al.*, 2012). Subsequently, plants were harvested for microbiota analysis. Tomato and cotton phyllosphere samples were collected by harvesting the stem from the soil-line to the cotyledons, while barley phyllosphere samples were collected by harvesting the first 5 cm of plant tissue above the soil line. To collect root microbiota samples, plants were uprooted and loose soil was removed from the root system through gentle shaking.

Microbiota sequencing

Samples were manually ground to fine powder using a mortar and pestle. Subsequently, 400 mg of tissue or soil were used for DNA extraction using the DNeasy PowerSoil Pro Kit (Qiagen, Venlo, The Netherlands). Next, DNA was further purified using the Monarch PCR&DNA Clean Up kit (New England Biolabs, Ipswich, USA). DNA purity and concentration were assessed using the Qubit 4 fluorometer (Thermo Fisher Scientific, Waltham, USA) and the Nanodrop 2000 spectrophotometer (Thermo Fisher Scientific, Waltham, USA). DNA was used for the amplification of the variable regions 3-4 of the 16S region using primers 341f (ACTCCTACGGGAGGCAGCAG) and 806r (GGACTACHVGGGTWTCTAAT) in the presence of the mPNA (GGCAAGTGTTCTTCGGA) and pPNA (GGCTCAACCCTGGACAG) blocking clamps (PNABio, Newbury Park, USA). Additionally, amplification of the ITS2 region was conducted using the primers ITS3 (GCATCGATGAAGAACGCAGC) and ITS4 (TCCTCCGCTTATTGATATGC) in the presence of the ITS2 PNA (CGAGGGCACGTCTGCCTGG) blocking clamp (PNABio, Newbury Park, USA). All amplicons were sequenced on an Illumina MiSeq Platform (BGI-Genomics, Shenzhen, China). For the bulk soil microbiota from the soil collections, the V5-V7 regions were amplified with primers 799F (AACMGGATTAGATACCCKG) and 1139R (ACGTCATCCCCACCTTCC) and amplicons were similarly sequenced on an Illumina Miseq Platform (Cologne Center for Genomics,

Cologne, Germany). Only samples with at least 10.000 reads were considered for the analysis. Data analysis was conducted as described previously (Callahan *et al*., 2016; Snelders *et al*., 2020).

Microbiota analysis

Sequencing data were processed using R v.4.2.0. as described previously (Callahan et al., 2016; Snelders et al., 2020). In brief, reads were demultiplexed with cutadapt (v4.1; Martin, 2011), then trimmed and filtered to an average paired read length of 412 bp with a Phred score of 30. OTUs were inferred from the trimmed reads using the DADA2 method (v 1.24; Callahan et al., 2016). Taxonomy was assigned using the Ribosomal Database Project (RDP,v 18; Cole et al., 2014). The pyloseq package (v1.40.0; McMurdie & Holmes, 2013) was used to calculate α- and β-diversity, while PERMANOVA was conducted with the vegan package (v2.6-4; Oksanen et al., 2004) package. Differential abundance analysis was done using the DESeq2 package (v1.36.0; Love et al., 2014) using a negative binomial Wald test and a significance P adjusted threshold < 0.05.

***Verticillium dahliae* inoculation assays**

Verticillium dahliae Kleb. inoculations were conducted on 10-day-old tomato plants. Inoculum was prepared by harvesting conidiospores of 10-day-old cultures of *V. dahliae* strain JR2 and an *Ave1* deletion mutant (de Jonge et al., 2012; Snelders et al., 2020) on potato dextrose agar (PDA; Carl Roth, Karlsruhe, Germany). The collected conidiospores were washed three times in MQ water, each time followed by centrifugation at 10.000 rpm for 10 minutes. Subsequently, the conidiospores were counted using a Neubauer chamber and the inoculum concentration was adjusted to 10^6 conidiospores/ml. For the inoculations, plants were uprooted and the roots were rinsed with MQ-water before being placed into the conidiospore suspension for 8 minutes. Subsequently, plants were planted back into the soil. Disease symptoms were monitored at 14 dpi by measuring the tomato canopy area based on overhead pictures using ImageJ (Schneider et al., 2012).

Results

Composing a collection of diverse natural soil samples

To study microbiota assemblies and the role of antimicrobial effector proteins of fungal plant pathogens in diverse soils we composed a collection of natural soil samples. We collected our soil samples in the Netherlands given the well-documented types of soil and the opportunity to sample a wide range of distinct types of soil on a relatively short geographical distance (Hartemink and Sonneveld 2013; Figure 1a). In total we collected samples from nine different natural soils which map onto five major conventional soil classes: river clay, sea clay, sand, peat and loam (Suppl. Table 1). Sampling sites were selected to avoid agricultural usage. In order to eliminate weeds and the majority of roots, the top 10 cm of soil was removed and the subsequent 30 cm of soil was collected. Besides the nine Dutch soils, we included the well-characterized and intensively studied Cologne agricultural soil (Bulgarelli et al., 2012).

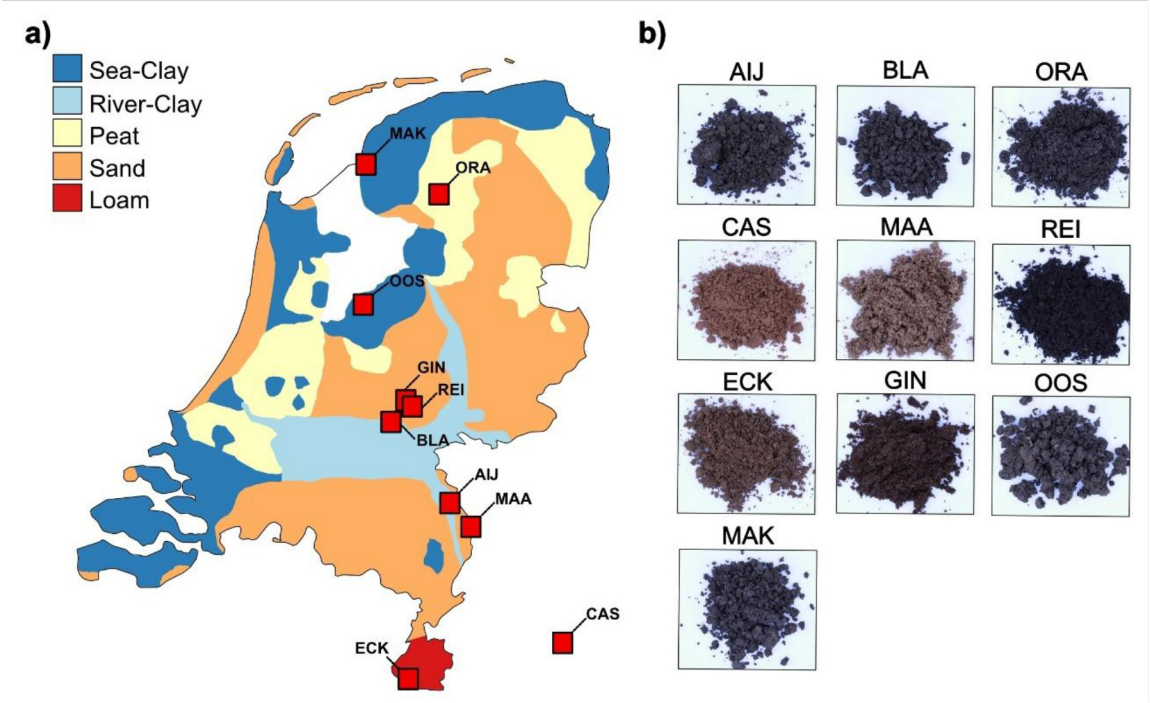

Figure 1. Establishment of a natural soil collection. a) Soil collection sites in the Netherlands. The map is colored according to major types of soil in the Netherlands. Sampling locations are indicated by red squares. **b)** Pictures of each soil from the soil sample collection.

The diversity of our soil sample collection is apparent from visible differences in soil texture and appearance (Figure 1b). To determine differences in physicochemical properties of our soil samples, we measured pH, the amount of total organic carbon and nitrogen, as well as element levels for all soil samples. The sandy soils (sand, peat, loam) displayed relatively low pH values, between 4.0 and 5.6, while the clay soils (river clay, sea clay) displayed higher pH values ranging from 6.2 to 7.7 (Figure 2a). With respect to carbon content, particularly the two river clay soils collected in Aijen (AIJ) and Blauwe Kamer (BLA) stood out with the highest carbon content of 4,83% and 7,01% respectively. The lowest carbon content was measured for the Cologne agricultural soil (CAS) with 0,26% and the sand soil collected in Maasduinen (MAA) with 0,21% (Figure 2b). A similar pattern was observed for the nitrogen content, as the highest value was measured for the river clay BLA with 0,35%, while lowest values were again determined for MAA at 0,006% and CAS at 0,02% (Figure 2C). Further, we also performed a total element analysis by conducting a HNO_3-based element extraction followed by inductively coupled plasma mass spectrometry (ICP-MS) measurement. The elemental profiles of our soil samples were dominated by iron, calcium and aluminum (Figure 2d). Notably, when computing a principal component analysis (PCA) of the ICP-MS elemental raw data we observed separation according to types of soil, as the clay soils separated from the sandy soils and the CAS-soil (Figure 2e).

Many of the physicochemical properties are known to influence soil microbiota composition (Fierer 2017). To determine the bulk soil microbiota, we conducted 16S amplicon sequencing and analyzed the β-diversity by computing a principal coordinate analysis (PCoA) using the weighted Unifrac distance (Figure 2f). As expected, we observed separation of the microbiota according to the type of soil. Notably, we observed that apart from Reijerscamp (REI) the sandy soils collected from de Ginkelse Heide (GIN), Maasduinen (MAA), Oranjewoud (ORA) and ECK separate from the clay soil samples.

To investigate the consistency of the bulk soil microbiota, we compared the bulk soil microbiota of soil samples that were collected in two consecutive years; 2022 and 2023. In the PCoA, soils collected in the different years clustered, demonstrating a high degree of stability of these natural bulk soil microbiota (Figure 2f). Collectively, our data characterize the diversity of our natural soil sample collection with respect to physicochemical properties and bulk soil microbiota.

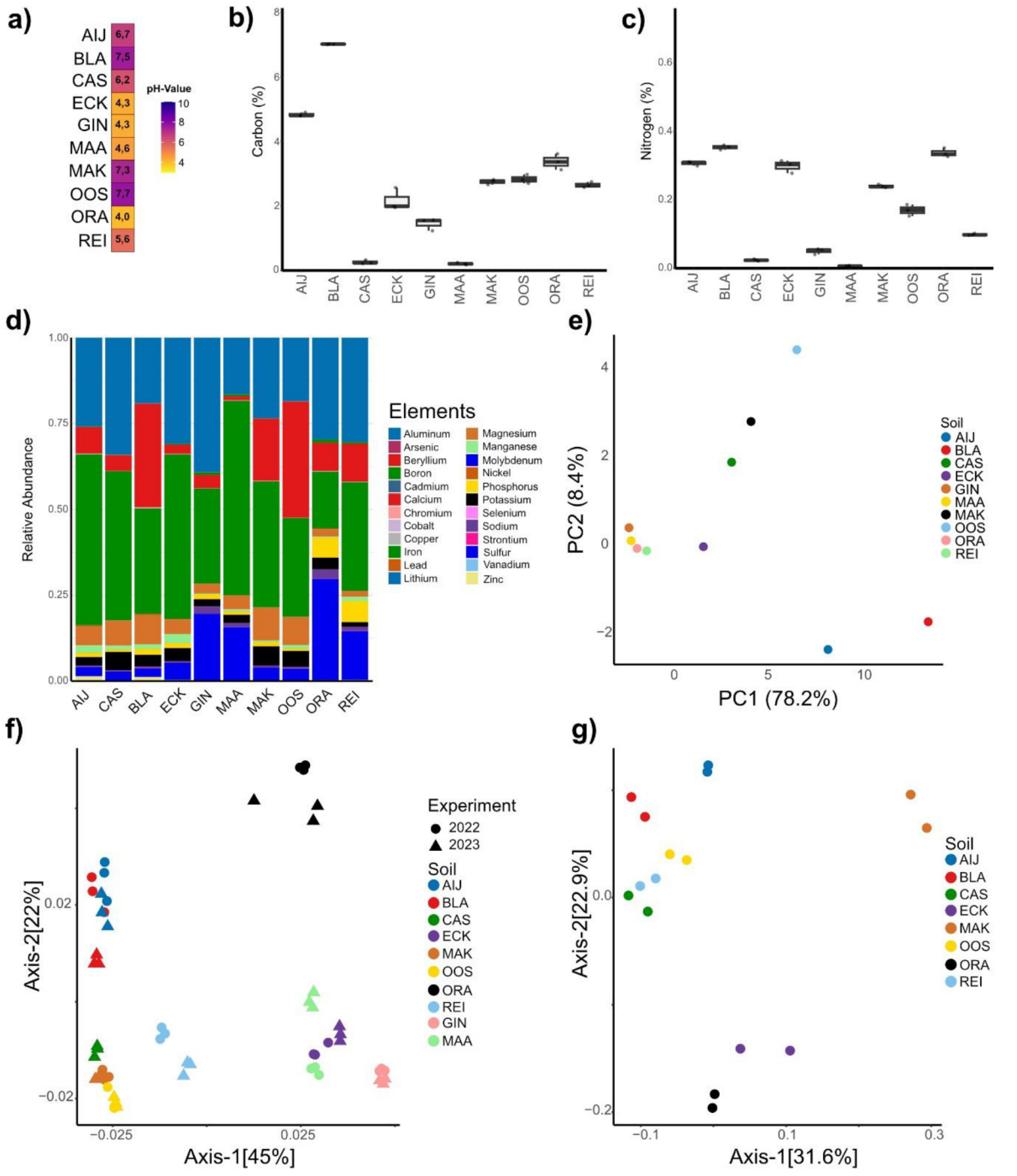

Figure 2. Physicochemical and microbiota analysis of the natural soil collection. a) Heatmap of pH-values. **b)** Boxplots displaying soil carbon contents. Different letters indicate statistical differences based on One-Way-Anova (Tukey HSD-Test pval < 0.05). **c)** Boxplots displaying soil nitrogen contents. Different letters indicate statistical differences based on One-Way-Anova (Tukey HSD-Test pval < 0.05). **d)** Relative abundance barplot for elements measured with ICP-MS. **e)** Principal component analysis (PCA) of the elemental profiles measured with ICP-MS. **f)** Principal coordinate analysis (PCoA) using weighted unifrac distances displaying bacterial bulk soil microbiota. Datapoints are shaped according to collection timepoint. **g)** PCoA using weighted unifrac distances displaying fungal bulk soil microbiota.

Drivers of bacterial community assembly in roots and phyllosphere microbiota

Several studies have demonstrated that the soil as well as plant genetics influence plant microbiota assemblies (Bulgarelli et al., 2012; Lundberg et al., 2012; Wagner et al., 2016; Fitzpatrick et al., 2018; Walters et al., 2018; Thiergart et al., 2020; Simonin et al., 2020; Tkacz et al., 2020). These investigations typically involved plants collected from diverse natural environments, where microbiota assembly may additionally be affected by various abiotic factors, such as local climate and weather conditions, or they involve different plant species grown in the same soil at the same site (Ofek-Lalzar et al., 2014; Wagner et al., 2016; Walters et al., 2018). However, studies that simultaneously assess the contributions of different soils and of the plant genetics to microbiota assembly by examining diverse plant species grown in diverse natural soils while eliminating the impact of environmental factors remain scarce. Thus, we used our soil sample collection to investigate how plant-associated microbiota assemble across different plant species when grown under controlled conditions in a greenhouse. Specifically, we grew tomato (*Solanum lycopersicum*), cotton (*Gossypium hirsutum*), and barley (*Hordeum vulgare*) on the ten soils of our soil sample collection.

We first assessed how the diverse properties of the natural soils influence plant growth, by measuring plant canopy areas at three weeks after sowing. Cotton, tomato and barley plants grew on all soils except on the GIN and MAA soil samples, while tomato additionally failed to grow on ECK. Significant growth differences were observed across soils for each plant species (Suppl. Figure 2). Generally, the highest plant growth was observed on clay soil. For cotton the highest plant growth was determined on the MAK soil samples with an average canopy area of 39,76 cm^2. Barley and tomato plants displayed highest plant growth on the BLA soil with barley plants reaching an average canopy area of 10,89 cm^2 and tomato 22,23 cm^2. Lowest plant growth for all three plants species was observed on the ORA soil, with average canopy areas of 23,44 cm^2 for cotton, 1,8 cm^2 for tomato plants and 1,42 cm^2 for barley plants (Suppl. Figure 2). These results highlight the influence of the different soils on plant growth.

.

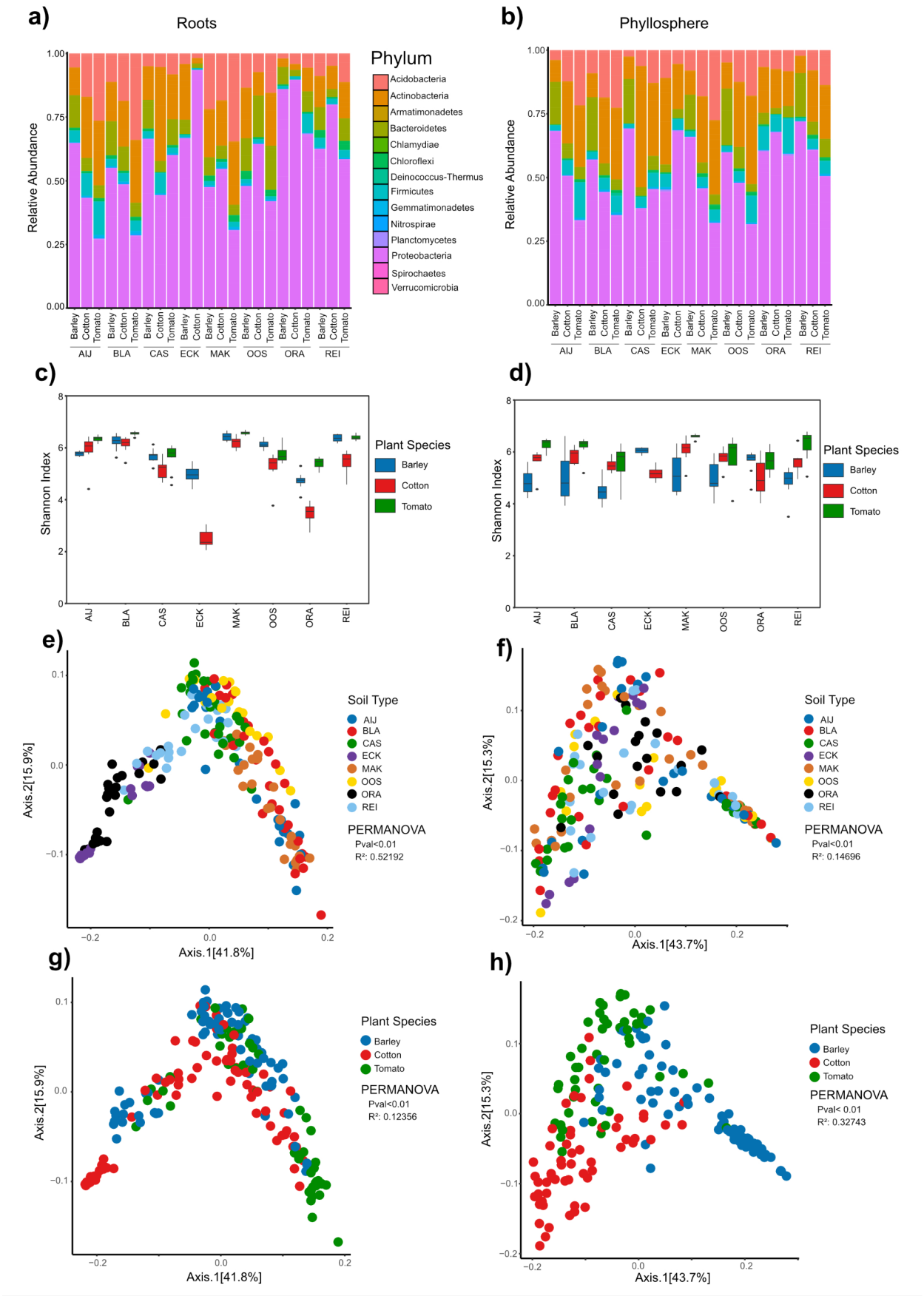
a)
Roots
Relative Abundance
1.00
0.75
0.50
0.25
0.00
Barley
Cotton
Tomato
AIJ
BLA
CAS
ECK
MAK
OOS
ORA
REI
Phylum
Acidobacteria
Actinobacteria
Armatimonadetes
Bacteroidetes
Chlamydiae
Chloroflexi
Deinococcus-Thermus
Firmicutes
Gemmatimonadetes
Nitrospirae
Planctomycetes
Proteobacteria
Spirochaetes
Verrucomicrobia
b)
Phyllosphere
c)
Shannon Index
Plant Species
Barley
Cotton
Tomato
d)
e)
Axis.2[15.9%]
Axis.1[41.8%]
Soil Type
PERMANOVA
Pval<0.01
R²: 0.52192
f)
Axis.2[15.3%]
Axis.1[43.7%]
R²: 0.14696
g)
R²: 0.12356
h)
R²: 0.32743

Figure 3. Bacterial composition of root and phyllosphere associated microbiota of barley, cotton and tomato plants grown on the different natural soils. a) Relative abundance in percentage on phylum level of the bacterial root microbiota. **b)** Relative abundance in percentage on phylum level of the bacterial phyllosphere microbiota. **c)** Shannon index of root microbiota. **d)** Shannon index of phyllosphere microbiota. **e)** Principal coordinate analysis (PCoA) based on weighted Unifrac distance of root microbiota. Datapoints are colored according to type of soil. **f)** PCoA based on weighted Unifrac distance of phyllosphere. Datapoints are colored according to type of soil. **g)** PCoA based on weighted Unifrac distance of root microbiota. Datapoints are colored according to plant species. **h)** PCoA based on weighted Unifrac distance of phyllosphere microbiota. All PERMANOVAs are performed with 9999 permutations. Datapoints are colored according to plant species.

Next, we assessed the bacterial root and phyllosphere microbiota of the diverse plants grown on the soil collection by performing 16S rRNA sequencing. Bacterial communities in the root-associated microbiota were dominated by Proteobacteria, Actinobacteria, Acidobacteria, and Bacteroidetes across all soils and plant species. Notably, we observed considerable variation among individual plants of the same species grown in the same soil, despite prior homogenization. This may result from heterogeneity that persists in the natural soils samples even after mixing (Suppl. Figure 3). Nevertheless, as expected, we observed strong differences in bacterial community composition between plant species grown on the same soils. For instance, on the river clay soil AIJ, over 50% of the bacterial community in the barley root microbiota consisted of Proteobacteria, compared to only 25% of Proteobacteria in the tomato root microbiota. Rather, the tomato root microbiota on AIJ harbored higher proportions of Acidobacteria and Actinobacteria (Figure 3a). To assess the diversity of the root-associated microbial communities, we investigated microbial alpha diversities by calculating the Shannon index for each bacterial community sample. Notably, Shannon indices for the root microbiota varied across plant species and soils, with no plant species consistently exhibiting higher or lower diversity compared to the other species across the soils (Figure 3c). This was also supported by the calculated Hill numbers (Suppl. Figure 7). The lowest Shannon index was measured for cotton plants grown on ECK (2,49), whereas the most diverse communities were assembled by tomato plants grown on MAK (6,57).

To further disentangle the contributions of the type of soil and plant species to microbial diversity in the root microbiota, we analyzed β-diversities by conducting Principal Coordinate Analyses (PCoAs) based on weighted UniFrac distances. In the root-associated microbiota, bacterial communities grouped primarily according to the type of soil, with sandy soils (ORA, ECK, REI) separating from clay soils (AIJ, BLA, OOS, MAK, CAS). The type of soil accounted for 52,2% of the observed variation within the microbiota, suggesting a dominant contribution to shaping root-associated bacterial communities (Figure 3e). We observed a “horseshoe

effect", which is thought to arise when applying linear ordination such as PCoA to gradient data (Morton et al., 2017). Therefore, we additionally calculated nonlinear ordination-based NMDS plots, which show a similar pattern of our data as the PCoA analysis (Suppl. Figure 8). Although also plant species significantly contributed to root-associated microbiota differentiation, it explained only 12,4% of the variation (Figure 3 g; Suppl. Figure 4b). Thus, root-associated microbiota are primarily structured according to the type of soil, and furthermore by plant species.

Next, we assessed if the patterns observed for root microbiota similarly hold true for phyllosphere microbiota. Similar to root microbiota, phyllosphere microbiota were dominated by Proteobacteria, Actinobacteria, Acidobacteria, and Bacteroidetes across all soils and plant species (Figure 3b). Also, for the phyllosphere microbiota we observed considerably variation between individual plants of the same species when grown in the same soil (Suppl. Figure 4). Notably, we observed strong differences between phyllosphere microbiota of different plant species grown in the same soil. Interestingly, these differences were similar across soils. For example, the tomato phyllosphere microbiota consistently exhibiting the lowest levels of Acidobacteria, followed by cotton and then barley in seven of the eight soils tested, with ECK as exception (Figure 3b). Next, we assessed community diversity in the phyllosphere microbiota by calculating Shannon indices (Figure 3d). In the phyllosphere, the lowest Shannon indices were determined for barley plants grown on CAS (4,51) and AIJ (4,84), whereas highest values were again observed for tomato plants grown on MAK (6,59) and REI (6,27). Notably, the alpha diversity of bacterial phyllosphere microbiota displayed a more structured pattern when compared with the alpha diversity in the root microbiota, as barley consistently exhibited the lowest alpha diversity across six out of the eight soil samples, followed by cotton and then tomato (Figure 3d). This suggests that the plant species has a more pronounced influence on community diversity in the phyllosphere microbiota when compared with root-associated microbiota. We also analyzed β-diversities by conducting Principal Coordinate Analyses (PCoAs) based on the weighted UniFrac distances of the phyllosphere microbiota. Like the root-associated microbiota, the phyllosphere microbiota exhibited significant separation based on the type of soil, albeit that this explained substantially less variation (14,7%). Rather, plant species was the strongest determinant of the phyllosphere community composition, accounting for approximately 32,7% of the observed variation (Figure 3f, Suppl. Figure 3).

Collectively, our findings indicate that the soil is the strongest driver of bacterial microbiota diversity in the root microbiota, while plant species plays a more significant role in shaping bacterial phyllosphere communities.

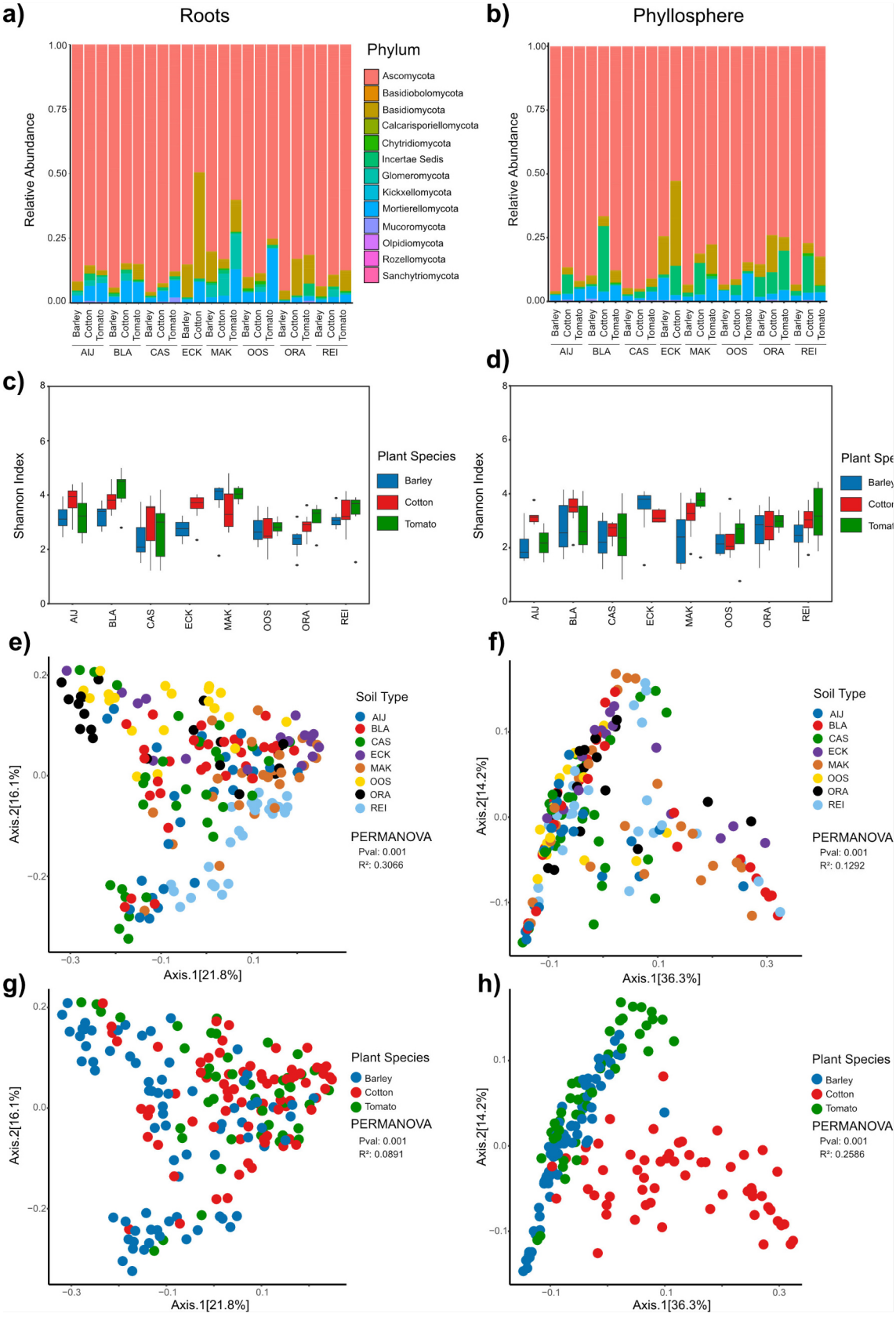
a)
Roots
b)
Phyllosphere
Relative Abundance
Phylum
Ascomycota
Basidiobolomycota
Basidiomycota
Calcarisporiellomycota
Chytridiomycota
Incertae Sedis
Glomeromycota
Kickxellomycota
Mortierellomycota
Mucoromycota
Olpidiomycota
Rozellomycota
Sanchytriomycota
Barley
Cotton
Tomato
AIJ
BLA
CAS
ECK
MAK
OOS
ORA
REI
c)
d)
Shannon Index
Plant Species
e)
f)
Soil Type
Axis.1[21.8%]
Axis.2[16.1%]
Axis.1[36.3%]
Axis.2[14.2%]
PERMANOVA
Pval: 0.001
R²: 0.3066
R²: 0.1292
g)
h)
R²: 0.0891
R²: 0.2586

Figure 4. Composition of the fungal root and phyllosphere associated microbiota of barley, cotton and tomato plants grown on the different natural soils. a) Relative abundance in percentage on phylum level of the fungal root microbiota **b)** Relative abundance in percentage on phylum level of the fungal phyllosphere microbiota **c)** Shannon index of root microbiota. **d)** Shannon index of phyllosphere microbiota. **e)** Principal coordinates analysis based on weighted Unifrac distance of root microbiota. Datapoints are colored according to type of soil. **f)** PCoA based on weighted Unifrac distance of phyllosphere. Datapoints are colored according to type of soil. **g)** PCoA based on weighted Unifrac distance of root microbiota. Datapoints are colored according to plant species. **h)** PCoA based on weighted Unifrac distance of phyllosphere microbiota. Datapoints are colored according to plant species. All PERMANOVAs are performed with 9,999 permutations.

Drivers of fungal community assembly in root-associated and phyllosphere microbiota

To assess whether patterns observed for bacterial microbiota across plant species grown on our soil collection also apply to the fungal component of the microbiota, we conducted ITS sequencing. First, we examined the fungal communities in the bulk soil microbiota of the eight soil samples used for the plant microbiota assembly study. This analysis revealed that the sand-like soils ECK and ORA separate from the clay soil. The REI soil, although also a sandy-soil, grouped with the clays. This indicates that the soil sample collection harbors distinct fungal communities (Figure 2g).

Analysis of the fungal communities in the root-associated microbiota revealed that fungal communities across plant species and type of soil were dominated by fungal species from the phyla Ascomycota, with Basidiomycota and Mortierellomycota (Figure 4a). Notably, the fungal composition of the root microbiota is also influenced by plant species across soil samples. For instance, on ECK, the fungal communities in the barley root microbiota contained more than 80% Ascomycota, while the fungal root microbiota of cotton plants contained only 50% Ascomycota, with a substantially higher abundance of Basidiomycota (Figure 4a; Suppl. Figure 6). Shannon index calculations revealed lower alpha diversities of the root-associated fungal communities when compared with bacterial communities, with no consistent patterns of alpha diversity based on the plant species emerging across soil samples. Analysis of the β-diversity by performing a PCoA using the weighted Unifrac distance matrix revealed that root-associated fungal communities separate based on the soil sample in which the plants were grown, explaining 31% of the variation observed in the fungal microbiota (Figure 4e). Root-associated fungal communities also displayed weak separation according to plant species, which explained 9% of the variation (Figure 4g; Suppl. Figure 6b).

Overall, these findings suggest that fungal communities in the root-associated microbiota are primarily shaped by the type of soil. As expected, also in the phyllosphere microbiota the fungal communities were dominated by Ascomycetes, followed by Basidiomycetes and Mortierellomycetes (Figure 4b; Suppl. Figure 5). Similar as for the alpha diversity in the root-associated fungal microbiome we did not observe any alpha diversity patterns based on plant species or the type of soil in the fungal phyllosphere microbiota (Figure 4d). The β-diversity analysis of the fungal community in the phyllosphere microbiota revealed weak separation based on the type of soil, which explained 13% of the variation (Figure 4f). Notably, similar as for the bacterial phyllosphere microbiota, we observed strong separation of the fungal phyllosphere community based on plant species, which explained 26% of the variation (Figure 4h; Suppl. Figure 5b). Collectively, our dataset reveals that fungal communities in the root-associated microbiota are more strongly influenced by types of soilthan by plant species, while the plant species acts as the primary driving factor for fungal communities in the phyllosphere microbiota.

Differential contribution of antimicrobial effectors to fungal virulence across soil types

The plant microbiota plays an important role in plant health, fitness and defense against plant pathogens (Trivedi et al., 2020). To colonize their hosts, plant pathogens have evolved antimicrobial effector proteins to manipulate host-associated microbiota (Mesny et al., 2024). For instance, *Verticillium dahliae* uses the antimicrobial effector Ave1 to suppress antagonistic microbes during host colonization. Ave1 was demonstrated to facilitate host colonization of cotton and tomato plants grown in potting soil through targeting, amongst others, antagonistic Sphingomonadales bacteria (Snelders et al., 2020). As a globally distributed soil-borne pathogen with a broad host range, *V. dahliae* successfully colonizes host plants across diverse types of soil, which likely harbor distinct microbial communities (Klimes et al., 2015; Singh et al., 2025). We hypothesized that the outcome of effector-mediated microbiota manipulation may vary depending on the host-associated microbiota, which is largely assembled from the surrounding bulk soil microbiota. To address this, we assessed the virulence contribution of the antimicrobial effector Ave1 by growing plants on our soil collection and inoculating them with either wild-type *V. dahliae* or an *Ave1* deletion mutant (Jonge et al., 2012; Snelders et al., 2020). As we have studied the interaction of *V. dahliae* with tomato most intensively, and the Ave1 effectors acts as a major virulence factor on this plant species (de Jonge et al., 2012; Snelders et al., 2020), we focused our experiment on tomato plants (Jonge et al., 2012; Snelders et al., 2020). We observed a significant reduction in biomass of tomato plants inoculated with the wild type strain when compared with plants inoculated with the *Ave1* deletion strain on AIJ, BLA, ORA and MAK, indicating that Ave1 contributes to fungal virulence

on these soils. In contrast, no such difference was observed for plants grown in OOS and REI, suggesting that Ave1 differentially contributes to fungal virulence across soils (Figure 5a). To rule out the possibility that the observed differences between soil types were due to coinfections with naturally occurring *Verticillium* strains, we quantified the relative abundance of *Verticillium* in bulk soil and found only low abundances with no significant differences (Suppl. Figure 9). Previous work demonstrated that Ave1 also negatively impacts the abundance of other taxa, including Verrucomicrobiales, Chitinophagaceae, Flavobacteriales and Burkholderiales during infections of cotton and tomato plants grown on potting soil (Snelders et al., 2020). We then asked whether variation in the abundance of these bacteria in the root-associated microbiota of tomato plants could explain the differences in virulence contribution of Ave1 across soils. To test this, we measured their relative abundance in tomato plants grown in the different natural soil samples. Of the tested taxa, Sphingomonadales, Flavobacteriales, and Burkholderiales showed no significant differences in relative abundances across soils. While significant variation in relative abundance was observed for the Verrucomicrobiales and Chitinophagaceae on several soils, these differences did not correlate with the observed Ave1-related virulence phenotype (Suppl. Figure 10a).

To assess the impact of Ave1 on the tomato root-associated microbiota we investigated the microbiota composition of tomato plants that were mock-inoculated, or inoculated with *V. dahliae* strain JR2 or the *Ave1* deletion mutant. By computing PCoAs based on UniFrac distances, we observe differences in the microbiota composition of tomato plants across treatments on our soil collection (Figure 5b). We further computed a PCoA based on UniFrac distances, focusing only on plants that were inoculated with *V. dahliae* and observed that the tomato microbiota from plants inoculated with the wild type and the deletion mutant consistently separated across all soils, except for the ORA soil (Suppl. Figure 11). Notably, we also observe such separation in the microbiota of plants grown on REI and OOS, even though we did not detect a virulence contribution of Ave1.

To investigate the bacterial taxa affected by Ave1 on the natural soils we conducted differential abundance analysis using DeSeq2 (Love et al., 2014) between the microbiota of plants inoculated with *V. dahliae* strain JR2 or the *Ave1*-deletion mutant. This analysis revealed significant shifts in microbiota composition at the genus level across all soil samples, including OOS and REI, even though no virulence contribution of Ave1 was observed on these soils (Suppl. Figure 10b). Notably, on each of the soils the effector causes distinct shifts in the microbiota (Suppl. Figure 10b). Collectively, our data indicates that the outcome of effector-mediated microbiota manipulation by *V. dahliae* is determined by the composition of the host-associated microbiota which, in turn, is influenced by the surrounding soil.

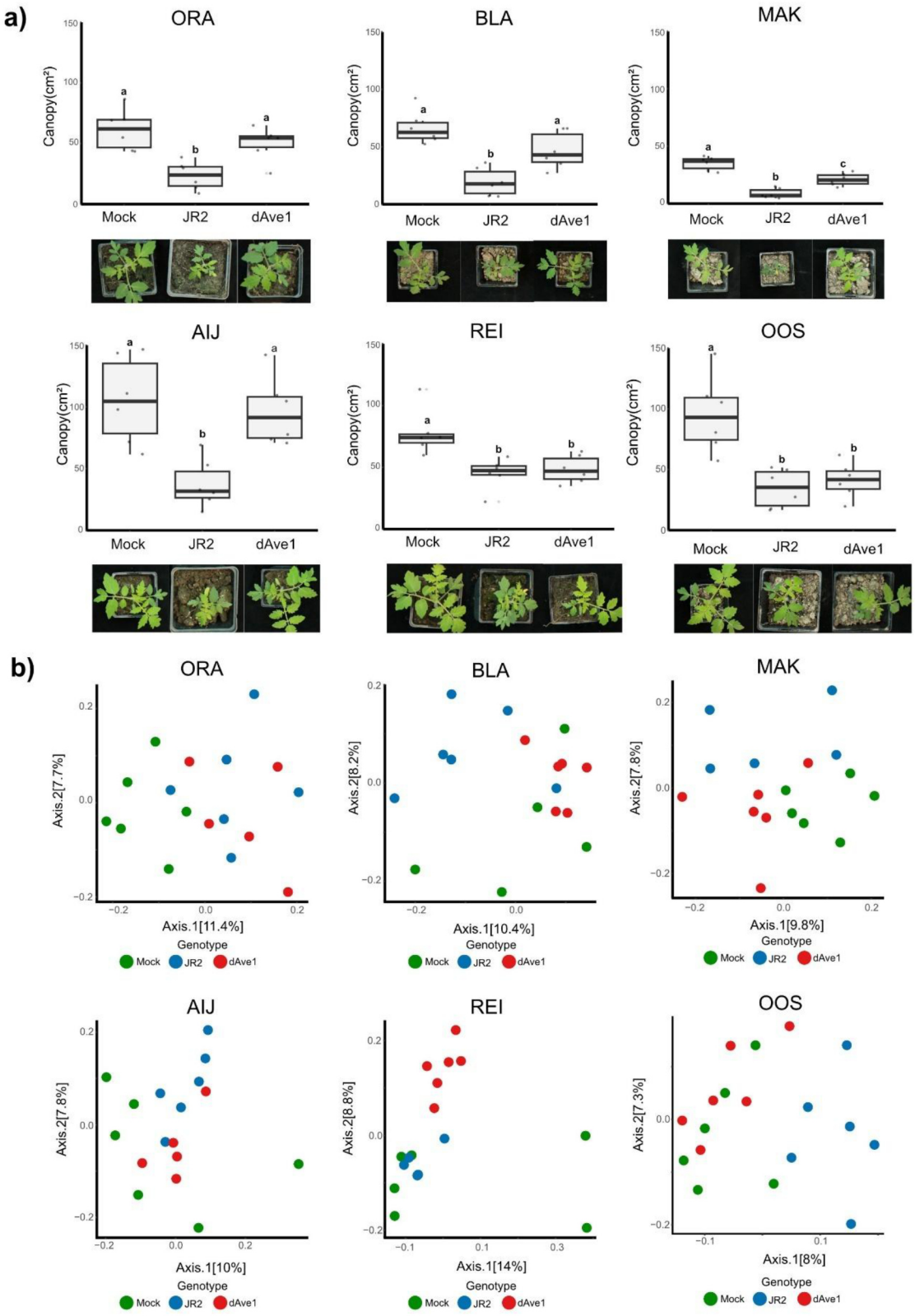
a)
ORA
BLA
MAK
AIJ
REI
OOS
Canopy(cm²)
Mock
JR2
dAve1
b)
Axis.1[11.4%]
Axis.2[7.7%]
Axis.1[10.4%]
Axis.2[8.2%]
Axis.1[9.8%]
Axis.2[7.8%]
Axis.1[10%]
Axis.2[7.8%]
Axis.1[14%]
Axis.2[8.8%]
Axis.1[8%]
Axis.2[7.3%]
Genotype

Figure 5. Antimicrobial effector Ave1 differentially contributes to virulence of *Verticillium dahliae* depending on the soil. a) Canopy area in cm^2 of tomato plants grown on the different natural soils at 14 dpi with mock treatment, wild-type *V. dahliae* (JR2) or an *Ave1* deletion mutant (dAve1). Different letters indicate statistical differences based on One-Way-Anova (Tukey HSD-Test pval < 0.05). Pictures display a representative plant per treatment. **b)** Principal coordinate analysis (PCoA) based on Unifrac distances of the root microbiota of tomato plants grown on different soils at 14 dpi with wild-type *V. dahliae* (JR2) or an *Ave1* deletion mutant (dAve1).

Discussion

Plant microbiota contribute substantially to plant productivity, in part by serving as an additional barrier against invading pathogens (Mesny et al., 2024; Du et al., 2025). Over recent years, it has become evident that plant pathogens manipulate host microbiota through the secretion of antimicrobial effector proteins in turn, thus facilitating niche establishment and host colonization (Snelders et al., 2020; Chavarro-Carrero et al., 2024; Snelders et al., 2021; Snelders et al., 2023; Ökmen et al., 2023; Kettles et al., 2018; Chang et al., 2021; Gómez-Pérez et al., 2023; Mesny et al., 2024; Kraege et al., 2025). Notably, many pathogens spend parts of their life cycles outside their hosts, where they encounter diverse microbial communities. However, how antimicrobial effectors aid fungal establishment across these diverse environments is still poorly understood. Here, we present a collection of natural soils that we thoroughly characterized in terms of their physicochemical properties as well as their microbiota compositions. Using this soil collection, we reveal that the antimicrobial effector protein Ave1 from soil-borne fungal plant pathogen *Verticillium dahliae,* which was previously demonstrated to facilitate host colonization through the suppression of antagonistic Sphingomonadales bacteria (Snelders et al., 2020)*,* contributes to fungal virulence on tomato plants only in a subset of these soils. Our finding suggests that the virulence contribution of this effector is determined by the soil on which the host plant grows. Interestingly, differential virulence contributions have similarly been reported for another antimicrobial effector from *V. dahliae*, called Av2. While initially no contribution to fungal virulence was recorded (Chavarro-Carrero et al., 2021), a subsequent study using a different growth substrate, likely with a distinct microbiota, revealed that Av2 interfered with the host plant's 'cry for help' recruitment of beneficial *Pseudomonas* bacteria, leading to a clear virulence contribution of the effector (Kraege et al., 2025). These differences in virulence contributions of antimicrobial effectors are likely due to variation in soil microbiota, which impacts the composition of plant-associated microbial communities encountered by the pathogen during infection in turn. Interestingly, our microbiota analyses revealed that the Ave1 effector significantly altered the tomato microbiota on all tested soils. This implies that microbiota manipulation by the effector does not necessarily translate into measurable contributions to fungal virulence and thus, that this effector does not solely target antagonists of *V. dahliae* growth. We therefore infer that the presence or absence of antagonistic microbes that can be impacted by an antimicrobial effector will determine whether that effector contributes to fungal virulence during host infection. This hypothesis is supported by observations made for the *V. dahliae* antimicrobial effector protein Ave1L2. A previous study investigating Ave1L2 demonstrated that in communities artificially depleted of antagonistic Actinobacteria, described as a crucial target

of the effector, the protein still impacted community composition albeit without a measurable virulence contribution (Snelders et al., 2023).

Notably, the observed impact that Ave1 caused on the plant microbiota substantially differed across soils. Many antimicrobial effector proteins do not specifically act on a single antagonistic microbe, but rather act on multiple plant microbiota members, thus exerting broader, system-level impacts on microbial communities (Snelders et al., 2020; Snelders et al., 2021; Chavarro-Carrero et al., 2024; Kraege et al., 2025). Since plant microbiota function as networks of interdependent species (van der Heijden and Hartmann, 2016), changes affecting one member can cascade through the community. Thus, removal or suppression of particular microbes by fungal effectors may trigger cascading shifts in community structure and function due to these intermicrobial interactions. This interconnectedness implies that the effects of antimicrobial effector activity on the microbiota can vary substantially between microbial communities, driven by the unique web of intermicrobial interactions in each environment.

Our study additionally provides a controlled comparison of how both types of soil and plant genotype influence microbiota assembly across different plant compartments. While previous studies have independently demonstrated that rhizosphere communities are primarily shaped by soil and phyllosphere communities by host genotype (Bulgarelli et al., 2012; Lundberg et al., 2012; Wagner et al., 2016; Fitzpatrick et al., 2018; Walters et al., 2018; Thiergart et al., 2020; Simonin et al., 2020; Tkacz et al., 2020) these insights were often derived from field studies conducted in divergent natural environments, where additional abiotic factors such as climate and weather may influence microbiota composition, or from experiments that varied either soil or plant species, but rarely both. Tkacz et al. (2020) assessed microbiota assembly across four plant species grown in two distinct soils and demonstrated that soil has a stronger influence than plant species on shaping rhizosphere microbiota. In our study, we extend these findings by using a different set of plant species and a broader collection of ten diverse, well-characterized soils, including the Cologne agricultural soil (Bulgarelli et al., 2012; Yang Bai et al., 2015) and Reijerscamp soil (Berendsen et al., 2018; Poppeliers et al., 2024) under highly controlled greenhouse conditions. We not only confirm that the type of soil plays a dominant role in rhizosphere microbiota assembly, but also show simultaneously that, in contrast, phyllosphere communities are primarily shaped by plant species rather than the type of soil. Notably, this work also demonstrates a stronger degree of plant selection on fungal communities in the phyllosphere when compared to the rhizosphere, highlighting a so-called rhizosphere effect on fungal communities. Such rhizosphere effects are an important aspect of microbiome assembly that remains underexplored when compared with bacterial communities.

Taken together, our findings support the view that antimicrobial effector proteins are context-dependent components of fungal secretomes, rather than universally acting virulence factors with consistent effects across environments. Notably, a recent machine-learning analysis predicted that, for several fungi, at least one-third of effector proteins possess antimicrobial activity (Mesny and Thomma, 2024), suggesting that fungi may deploy large repertoires of such antimicrobial effectors to establish themselves in diverse environments. Deeper insight into their functions and the mechanisms underlying this environmental variability will not only advance our understanding of fungal niche adaptation but may also inform the development of more robust, microbiota-based disease control strategies for agriculture.

Data availability

16S profiling data are available in the NCBI Genbank database under BioProject PRJEB95937.

Funding

B.P.H.J.T. acknowledges funding by the Alexander von Humboldt Foundation in the framework of an Alexander von Humboldt Professorship endowed by the German Federal Ministry of Education and is furthermore supported by the Deutsche Forschungsgemeinschaft (DFG, German Research Foundation) under Germany's Excellence Strategy – EXC 2048/1 – Project ID: 390686111.

Authors' contributions

W.P., A.K., N.C.S and B.P.H.J.T. conceived the project. W.P., A.K., N.C.S and B.P.H.J.T. designed the experiments. S.H. provided biological materials. W.P., A.K., J.Z., S.M., M.B., N.S. and N.C.S. performed the experiments. W.P., A.K., N.C.S and B.P.H.J.T. analyzed the data. W.P., A.K. and B.P.H.J.T. wrote the manuscript. All authors read and approved the final manuscript.

References

Almario, J.; Mahmoudi, M.; Kroll, S.; Agler, M.; Placzek, A.; Mari, A. et al. (2022) The leaf microbiome of Arabidopsis displays reproducible dynamics and patterns throughout the growing season. *mBio* 13 (3), e0282521. DOI: 10.1128/mbio.02825-21.

Bai, Y.; Müller, D.B.; Srinivas, G.; Garrido-Oter, R.; Potthoff, E.; Rott, M. et al. (2015) Functional overlap of the Arabidopsis leaf and root microbiota. *Nature* 528 (7582), pp. 364–369. DOI: 10.1038/NATURE16192.

Berendsen, R.L.; Vismans, G.; Yu, K.; Song, Y.; de Jonge, R.; Burgman, W.P. et al. (2018) Disease-induced assemblage of a plant-beneficial bacterial consortium. *The ISME Journal* 12 (6), pp. 1496–1507. DOI: 10.1038/s41396-018-0093-1.

Bulgarelli, D.; Rott, M.; Schlaeppi, K.; Ver Loren Themaat, E.; Ahmadinejad, N.; Assenza, F. et al. (2012) Revealing structure and assembly cues for Arabidopsis root-inhabiting bacterial microbiota. *Nature* 488 (7409), pp. 91–95. DOI: 10.1038/nature11336.

Carrión, V.J.; Perez-Jaramillo, J.; Cordovez, V.; Tracanna, V.; de Hollander, M.; Ruiz-Buck, D. et al. (2019) Pathogen-induced activation of disease-suppressive functions

in the endophytic root microbiome. *Science* 366 (6465), pp. 606–612. DOI: 10.1126/science.aaw9285.

Callahan, B. J., McMurdie, P. J., Rosen, M. J., Han, A. W., Johnson, A. J. A., & Holmes, S. P. (2016). DADA2: High-resolution sample inference from Illumina amplicon data. *Nature Methods*, 13(7), 581–583. https://doi.org/10.1038/NMETH.3869

Chang, H.; Noel, Z.A.; Chilvers, M.I. (2021) A β-lactamase gene of *Fusarium oxysporum* alters the rhizosphere microbiota of soybean. *The Plant Journal: For Cell and Molecular Biology* 106 (6), pp. 1588–1604. DOI: 10.1111/tpj.15257.

Chavarro-Carrero, E.A.; Snelders, N.C.; Torres, D.E.; Kraege, A.; López-Moral, A.; Petti, G.C. et al. (2024) The soil-borne white root rot pathogen *Rosellinia necatrix* expresses antimicrobial proteins during host colonization. *PLoS Pathogens* 20 (1), e1011866. DOI: 10.1371/journal.ppat.1011866.

Chavarro-Carrero, E.A.; Vermeulen, J.P.; Torres, D.; Usami, T.; Schouten, H.J.; Bai, Y. et al. (2021) Comparative genomics reveals the in planta-secreted *Verticillium dahliae* Av2 effector protein recognized in tomato plants that carry the V2 resistance locus. *Environmental Microbiology* 23 (4), pp. 1941–1958. DOI: 10.1111/1462-2920.15288.

Chialva, M.; Lanfranco, L.; Bonfante, P. (2022) The plant microbiota: composition, functions, and engineering. *Current Opinion in Biotechnology* 73, pp. 135–142. DOI: 10.1016/j.copbio.2021.07.003.

Cole, J. R., Wang, Q., Fish, J. A., Chai, B., McGarrell, D. M., Sun, Y. et al. (2014). Ribosomal Database Project: data and tools for high throughput rRNA analysis. *Nucleic Acids Research*, 42(D1), D633–D642. https://doi.org/10.1093/NAR/GKT1244

Cook, D.E.; Mesarich, C.H.; Thomma, B.P.H.J. (2015) Understanding plant immunity as a surveillance system to detect invasion. *Annual Reviews in Phytopathology*, pp. 541–563. DOI: 10.1146/ANNUREV-PHYTO-080614-120114.

de Jonge, R.; van Esse, H.P.; Maruthachalam, K.; Bolton, M.D.; Santhanam, P.; Saber, M.K. et al. (2012) Tomato immune receptor Ve1 recognizes effector of multiple fungal pathogens uncovered by genome and RNA sequencing. *Proceedings of the National Academy of Sciences of the United States of America* 109 (13), pp. 5110–5115. DOI: 10.1073/pnas.1119623109.

Du, Y.; Han, X.; Tsuda, K. (2025) Microbiome-mediated plant disease resistance: recent advances and future directions. *Journal of General Plant Pathology* 91 (1), pp. 1–17. DOI: 10.1007/s10327-024-01204-1.

Dumack K., Feng K., Flues S., Sapp M., Schreiter S., Grosch R. et al. (2022) What Drives the Assembly of Plant-associated Protist Microbiomes? Investigating the Effects of

Crop Species, Soil Type and Bacterial Microbiomes. *Protist* 173: 125913. DOI: 10.1016/j.protis.2022.125913

Durán P, Thiergart T, Garrido-Oter R, Agler M, Kemen E, Schulze-Lefert P, et al. Microbial Interkingdom Interactions in Roots Promote Arabidopsis Survival. *Cell*. 2018 Nov 1;175(4):973-983.e14. DOI: 10.1016/j.cell.2018.10.020.

Fierer, N. (2017) Embracing the unknown: disentangling the complexities of the soil microbiome. *Nature reviews. Microbiology* 15 (10), pp. 579–590. DOI: 10.1038/nrmicro.2017.87.

Fitzpatrick, C.R.; Copeland, J.; Wang, P.W.; Guttman, D.S.; Kotanen, P.M.; Johnson, Marc T. J. (2018) Assembly and ecological function of the root microbiome across angiosperm plant species. *Proceedings of the National Academy of Sciences of the United States of America* 115 (6), E1157-E1165. DOI: 10.1073/pnas.1717617115.

Fradin, E.F.; Thomma, B.P.H.J. (2006) Physiology and molecular aspects of Verticillium wilt diseases caused by V. dahliae and V. albo-atrum. *Molecular Plant Pathology* 7 (2), pp. 71–86. DOI: 10.1111/j.1364-3703.2006.00323.x.

Gómez-Pérez, D.; Schmid, M.; Chaudhry, V.; Hu, Y.; Velic, A.; Maček, B. et al. (2023) Proteins released into the plant apoplast by the obligate parasitic protist Albugo selectively repress phyllosphere-associated bacteria. *New Phytologist* 239 (6), pp. 2320–2334. DOI: 10.1111/nph.18995.

Guerreiro, M.A.; Stukenbrock, E.H. (2025) Fungal plant pathogens. *Current Biology: CB* 35 (11), R480-R484. DOI: 10.1016/j.cub.2025.02.046.

Hartemink, A.E.; Sonneveld, M.P.W. (2013) Soil maps of The Netherlands. *Geoderma* 204-205, pp. 1–9. DOI: 10.1016/j.geoderma.2013.03.022.

Hassani, M.A.; Durán, P.; Hacquard, S. (2018) Microbial interactions within the plant holobiont. *Microbiome* 6 (1), p. 58. DOI: 10.1186/s40168-018-0445-0.

Jones, J.D.G.; Dangl, J.L. (2006) The plant immune system. *Nature* 444 (7117), pp. 323–329. DOI: 10.1038/nature05286.

Katan, J. (2017) Diseases caused by soilborne pathogens: Biology, management, challenges. *Journal of Plant Pathology* 99 (2), pp. 305-315

Kettles, G.J.; Bayon, C.; Sparks, C.A.; Canning, G.; Kanyuka, K.; Rudd, J.J. (2018) Characterization of an antimicrobial and phytotoxic ribonuclease secreted by the fungal wheat pathogen Zymoseptoria tritici. *New Phytologist* 217 (1), pp. 320–331. DOI: 10.1111/nph.14786.

Klimes, A.; Dobinson, K.F.; Thomma, B.P.H.J.; Klosterman, S.J. (2015) Genomics spurs rapid advances in our understanding of the biology of vascular wilt pathogens in the genus Verticillium. *Annual Review of Phytopathology* 53, pp. 181–198. DOI: 10.1146/annurev-phyto-080614-120224.

Kraege, A.; Punt, W.; Doddi, A.; Zhu, J.; Schmitz, N.; Snelders, N.C. et al. (2025) Undermining the cry for help: The phytopathogenic fungus *Verticillium dahliae* secretes an antimicrobial effector protein to undermine host recruitment of antagonistic *Pseudomonas* bacteria. *bioRxiv* DOI: 10.1101/2025.06.09.658588

Liu, Y.; Chen, L.; Wu, G.; Feng, H.; Zhang, G.; Shen, Q. et al. (2017) Identification of root-secreted compounds involved in the communication between cucumber, the beneficial *Bacillus amyloliquefaciens*, and the soil-borne pathogen *Fusarium oxysporum*. *Molecular Plant-Microbe Interactions* 30 (1), pp. 53–62. DOI: 10.1094/MPMI-07-16-0131-R.

Love, M. I., Huber, W., & Anders, S. (2014). Moderated estimation of fold change and dispersion for RNA-seq data with DESeq2. *Genome Biology,* 15(12), 1–21. https://doi.org/10.1186/S13059-014-0550-8/FIGURES/9

Lundberg, D.S.; Lebeis, S.L.; Herrera Paredes, S.; Yourstone, S.; Gehring, J.; Malfatti, S. et al. (2012) Defining the core Arabidopsis thaliana root microbiome. *Nature* 488 (7409), pp. 86–90. DOI: 10.1038/nature11237.

Martin, M. (2011). Cutadapt removes adapter sequences from high-throughput sequencing reads. *EMBnet.Journal*, 17(1), 10–12. https://doi.org/10.14806/EJ.17.1.200

McMurdie, P. J., & Holmes, S. (2013). phyloseq: An R Package for Reproducible Interactive Analysis and Graphics of Microbiome Census Data. *PLOS ONE*, 8(4), e61217. https://doi.org/10.1371/JOURNAL.PONE.0061217

Mendes, R.; Kruijt, M.; de Bruijn, I.; Dekkers, E.; van der Voort, M.; Schneider, J.H.M. et al. (2011) Deciphering the rhizosphere microbiome for disease-suppressive bacteria. *Science* 332 (6033), pp. 1097–1100. DOI: 10.1126/science.1203980.

Mesny, F.; Bauer, M.; Zhu, J.; Thomma, B.P.H.J. (2024) Meddling with the microbiota: Fungal tricks to infect plant hosts. *Current Opinion in Plant Biology* 82, p. 102622. DOI: 10.1016/j.pbi.2024.102622.

Mesny, F.; Thomma, B.P.H.J. (2024) AMAPEC: accurate antimicrobial activity prediction for fungal effector proteins. *bioRxiv* DOI: 10.1101/2024.01.04.574150

Morton, J.T., Toran, L., Edlund, A., Metcalf, J.L., Lauber, C., Knight, R. (2017) Uncovering the Horseshoe Effect in Microbial Analyses. *mSystems* DOI:10.1128/msystems.00166-16.

Oksanen, J., Simpson, G., Blanchet, F., Kindt, R., Legendre, P., Minchin, P., et al. (2004). vegan: Community Ecology Package (p. https://github.com/vegandevs/vegan).

Ofek-Lalzar, M.; Sela, N.; Goldman-Voronov, M.; Green, S.J.; Hadar, Y.; Minz, D. (2014) Niche and host-associated functional signatures of the root surface microbiome. *Nature Communications* 5, p. 4950. DOI: 10.1038/ncomms5950.

Ökmen, B.; Katzy, P.; Huang, L.; Wemhöner, R.; Doehlemann, G. (2023) A conserved extracellular Ribo1 with broad-spectrum cytotoxic activity enables smut fungi to compete with host-associated bacteria. *New Phytologist* 240 (5), pp. 1976–1989. DOI: 10.1111/nph.19244.

Pieterse, C. M. J.; Zamioudis, C.; Berendsen, R.L.; Weller, D.M.; van Wees, S.C.M.; Bakker, P.A.H.M. (2014) Induced systemic resistance by beneficial microbes. *Annual Review of Phytopathology* 52, pp. 347–375. DOI: 10.1146/annurev-phyto-082712-102340.

Raaijmakers, J.M. and Weller D.M. (1998) Natural plant protection by 2,4-Diacetylphloroglucinol-producing *Pseudomonas* spp. in take-all decline soils. *Molecular Plant-Microbe Interactions* 11(2), pp. 144-152

Simonin, M.; Dasilva, C.; Terzi, V.; Ngonkeu, E.L.M.; Diouf, D.; Kane, A. et al. (2020) Influence of plant genotype and soil on the wheat rhizosphere microbiome: evidences for a core microbiome across eight African and European soils. *FEMS Microbiology Ecology* 96 (6). DOI: 10.1093/femsec/fiaa067.

Singh, B.K.; Jiang, G.; Wei, Z.; Sáez-Sandino, T.; Gao, M.; Liu, H. et al. (2025) Plant pathogens, microbiomes, and soil health. *Trends in Microbiology* 33 (8), pp. 887–902. DOI: 10.1016/j.tim.2025.03.013.

Snelders, N.C.; Boshoven, J.C.; Song, Y.; Schmitz, N.; Fiorin, G.L.; Rovenich, H. et al. (2023) A highly polymorphic effector protein promotes fungal virulence through suppression of plant-associated Actinobacteria. *New Phytologist* 237 (3), pp. 944–958. DOI: 10.1111/nph.18576.

Snelders, N.C.; Petti, G.C.; van den Berg, G.C.M.; Seidl, M.F.; Thomma, B.P.H.J. (2021) An ancient antimicrobial protein co-opted by a fungal plant pathogen for in planta mycobiome manipulation. *Proceedings of the National Academy of Sciences* 118 (49), e2110968118. DOI: 10.1073/PNAS.2110968118/-/DCSUPPLEMENTAL.

Snelders, N.C.; Rovenich, H.; Petti, G.C.; Rocafort, M.; van den Berg, G.C.M.; Vorholt, J.A. et al. (2020) Microbiome manipulation by a soil-borne fungal plant pathogen using effector proteins. *Nature Plants* 6 (11), pp. 1365–1374. DOI: 10.1038/s41477-020-00799-5.

Snelders, N.C.; Rovenich, H.; Thomma, B.P.H.J. (2022) Microbiota manipulation through the secretion of effector proteins is fundamental to the wealth of lifestyles in the fungal kingdom. *FEMS Microbiology Reviews* 46 (5). DOI: 10.1093/femsre/fuac022.

Sokol, N.W.; Slessarev, E.; Marschmann, G.L.; Nicolas, A.; Blazewicz, S.J.; Brodie, E.L. et al. (2022) Life and death in the soil microbiome: how ecological processes influence biogeochemistry. *Nature Reviews. Microbiology* 20 (7), pp. 415–430. DOI: 10.1038/s41579-022-00695-z.

Spooren, J.; van Bentum, S.; Thomashow, L.S.; Pieterse, C.M.J.; Weller, D.M.; Berendsen, R.L. (2024) Plant-driven assembly of disease-suppressive soil microbiomes. *Annual Review of Phytopathology* 62 (1), pp. 1–30. DOI: 10.1146/annurev-phyto-021622-100127.

Thiergart, T.; Durán, P.; Ellis, T.; Vannier, N.; Garrido-Oter, R.; Kemen, E. et al. (2020) Root microbiota assembly and adaptive differentiation among European Arabidopsis populations. *Nature Ecology & Evolution* 4 (1), pp. 122–131. DOI: 10.1038/s41559-019-1063-3.

Tkacz, A.; Bestion, E.; Bo, Z.; Hortala, M.; Poole, P.S. (2020) Influence of plant fraction, soil, and plant species on microbiota: A multikingdom comparison. *mBio* 11 (1). DOI: 10.1128/mBio.02785-19.

Trivedi, P.; Leach, J.E.; Tringe, S.G.; Sa, T.; Singh, B.K. (2020) Plant-microbiome interactions: from community assembly to plant health. *Nature Reviews. Microbiology* 18 (11), pp. 607–621. DOI: 10.1038/s41579-020-0412-1.

van der Heijden, M.G.A.; Hartmann, M. (2016) Networking in the plant microbiome. *PLoS Biology* 14 (2), e1002378. DOI: 10.1371/journal.pbio.1002378.

Vandenkoornhuyse, P.; Quaiser, A.; Duhamel, M.; Le Van, A.; Dufresne, A. (2015) The importance of the microbiome of the plant holobiont. *New Phytologist* 206 (4), pp. 1196–1206. DOI: 10.1111/nph.13312.

Wagner, M.R.; Lundberg, D.S.; Del Rio, T.G.; Tringe, S.G.; Dangl, J.L.; Mitchell-Olds, T. (2016) Host genotype and age shape the leaf and root microbiomes of a wild perennial plant. *Nature Communications* 7, p. 12151. DOI: 10.1038/ncomms12151.

Walters, W.A.; Jin, Z.; Youngblut, N.; Wallace, J.G.; Sutter, J.; Zhang, W. et al. (2018) Large-scale replicated field study of maize rhizosphere identifies heritable microbes. *Proceedings of the National Academy of Sciences of the United States of America* 115 (28), pp. 7368–7373. DOI: 10.1073/pnas.1800918115.

Supplementary Materials

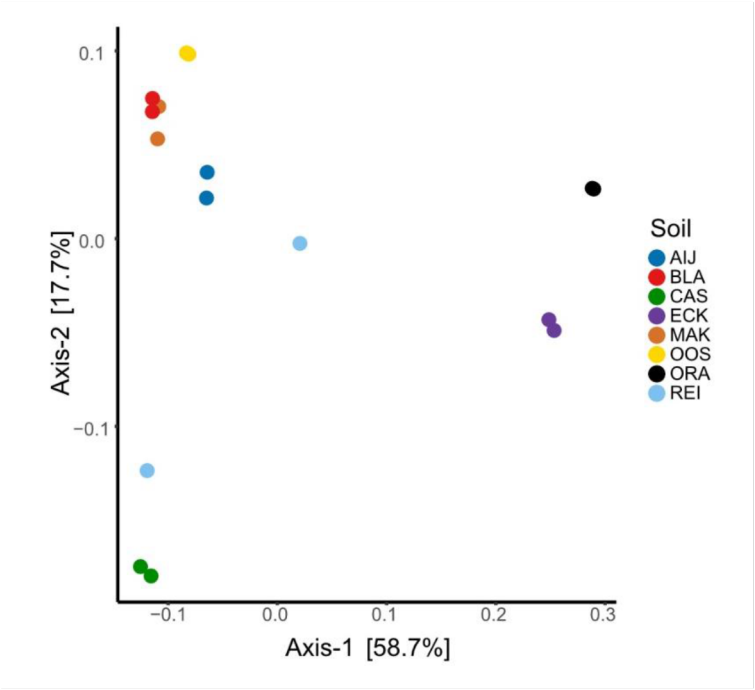

Supplementary Figure 1. Principal coordinate analysis (PCoA) based on weighted unifrac distances of the bacterial bulk soil microbiota from soil samples collected in 2024.

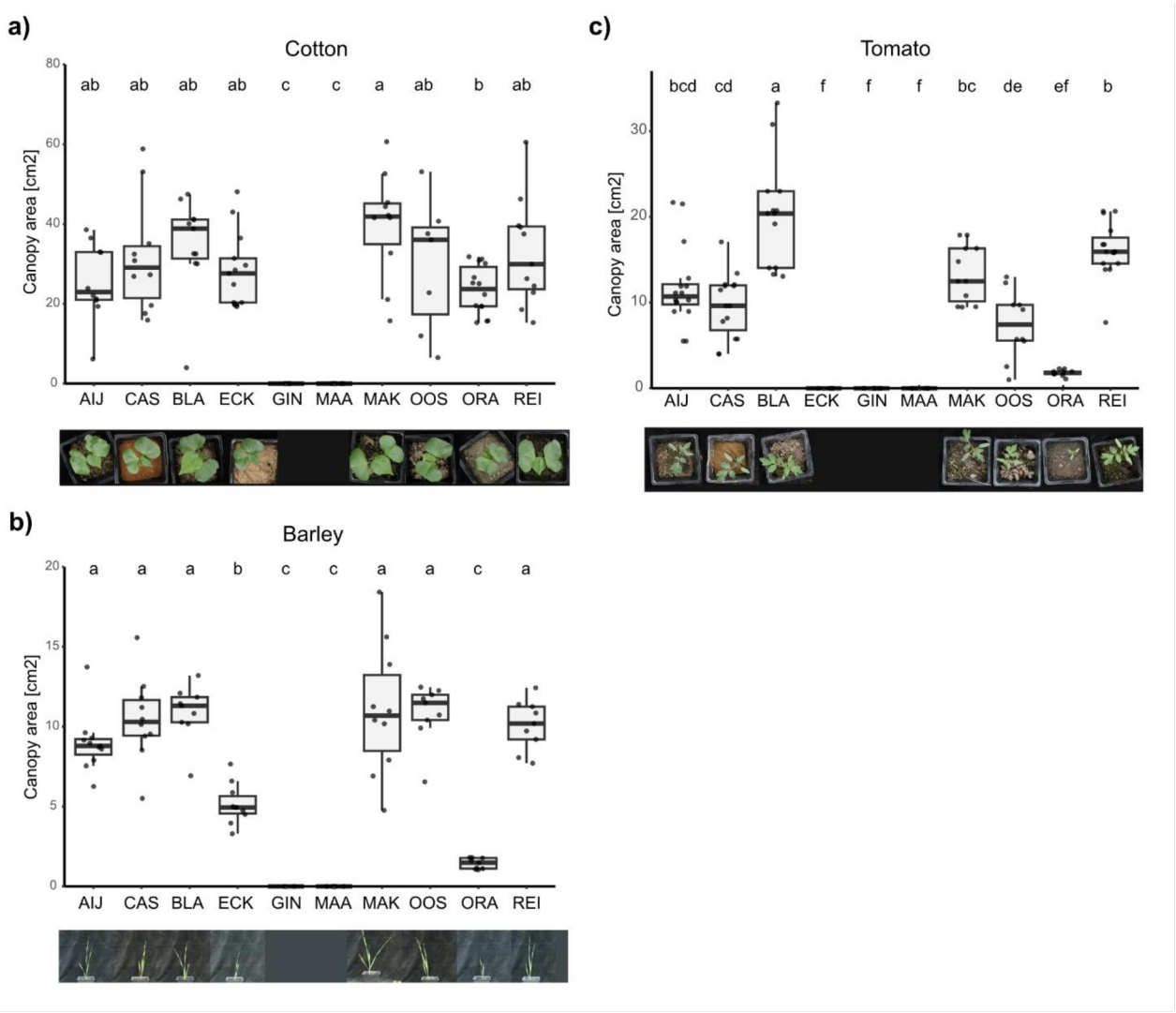

Supplementary Figure 2. Plant growth on natural soils. a) Canopy area of cotton plants grown on natural soils for 21 says. **b)** Canopy area of tomato plants grown on natural soils for 21 says. **c)** Canopy area of barley plants grown on natural soils for 21 says. Different letters indicate statistical differences based on One-Way-Anova (Tukey HSD-Test pval < 0.05) for each panel. Soil where no plant growth was observed were excluded from the statistics and labeled na.

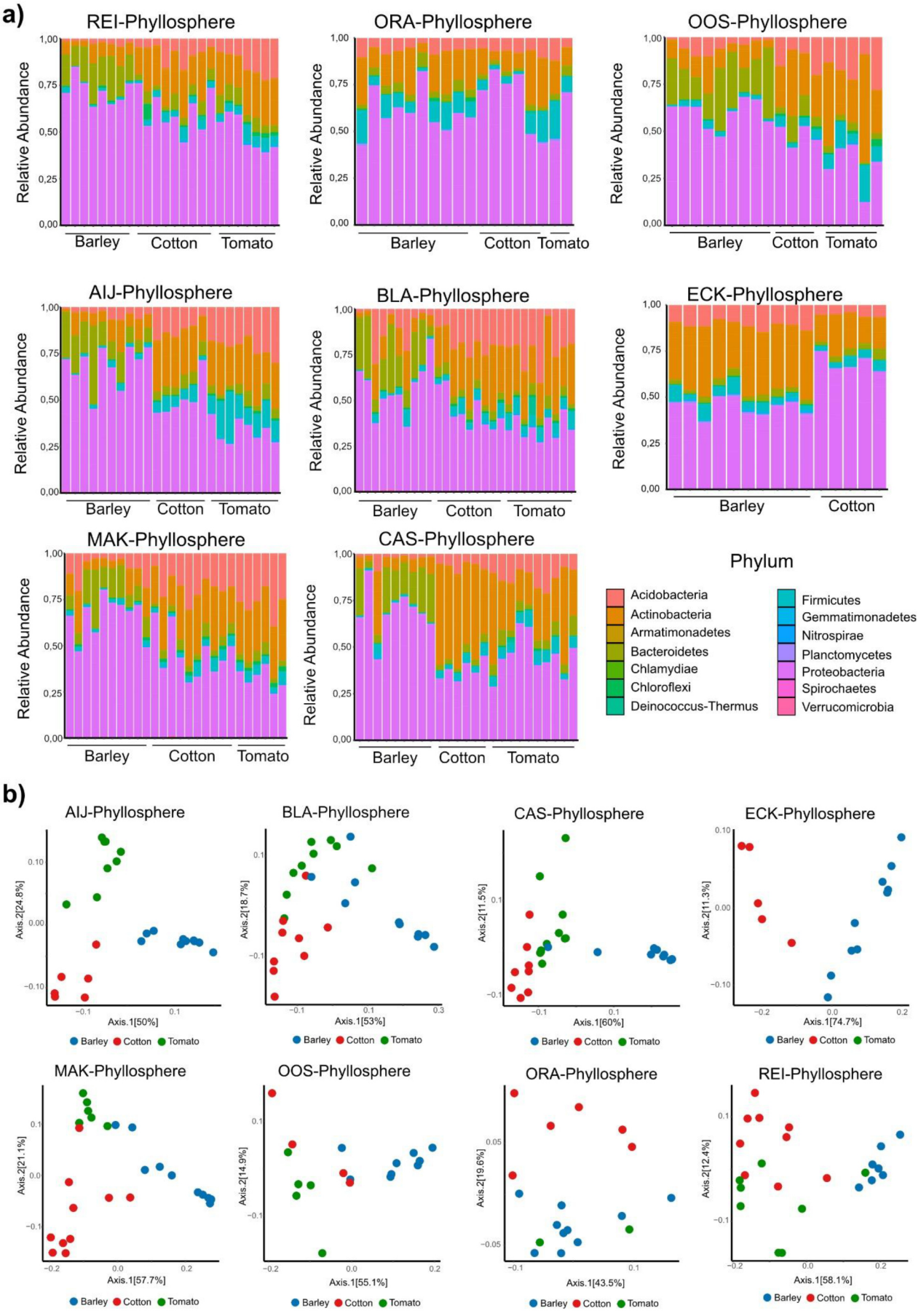
a)
REI-Phyllosphere
ORA-Phyllosphere
OOS-Phyllosphere
AIJ-Phyllosphere
BLA-Phyllosphere
ECK-Phyllosphere
MAK-Phyllosphere
CAS-Phyllosphere
Relative Abundance
1,00
0,75
0,50
0,25
0,00
Barley
Cotton
Tomato
Phylum
Acidobacteria
Actinobacteria
Armatimonadetes
Bacteroidetes
Chlamydiae
Chloroflexi
Deinococcus-Thermus
Firmicutes
Gemmatimonadetes
Nitrospirae
Planctomycetes
Proteobacteria
Spirochaetes
Verrucomicrobia
b)
AIJ-Phyllosphere
BLA-Phyllosphere
CAS-Phyllosphere
ECK-Phyllosphere
MAK-Phyllosphere
OOS-Phyllosphere
ORA-Phyllosphere
REI-Phyllosphere
Axis.1[50%]
Axis.2[24.8%]
Axis.1[53%]
Axis.2[18.7%]
Axis.1[60%]
Axis.2[11.5%]
Axis.1[74.7%]
Axis.2[11.3%]
Axis.1[57.7%]
Axis.2[21.1%]
Axis.1[55.1%]
Axis.2[14.9%]
Axis.1[43.5%]
Axis.2[19.6%]
Axis.1[58.1%]
Axis.2[12.4%]
Barley
Cotton
Tomato

Supplementary Figure 3. Bacterial phyllosphere microbiota. a) Relative abundance in percentage of the bacterial phyllosphere microbiota from barley, cotton and tomato plants grown for three weeks on different natural soils. **b)** Principal coordinate analysis (PCoA) based on weighted Unifrac distances of bacterial phyllosphere microbiota from barley, cotton and tomato plants grown on the different natural soils.

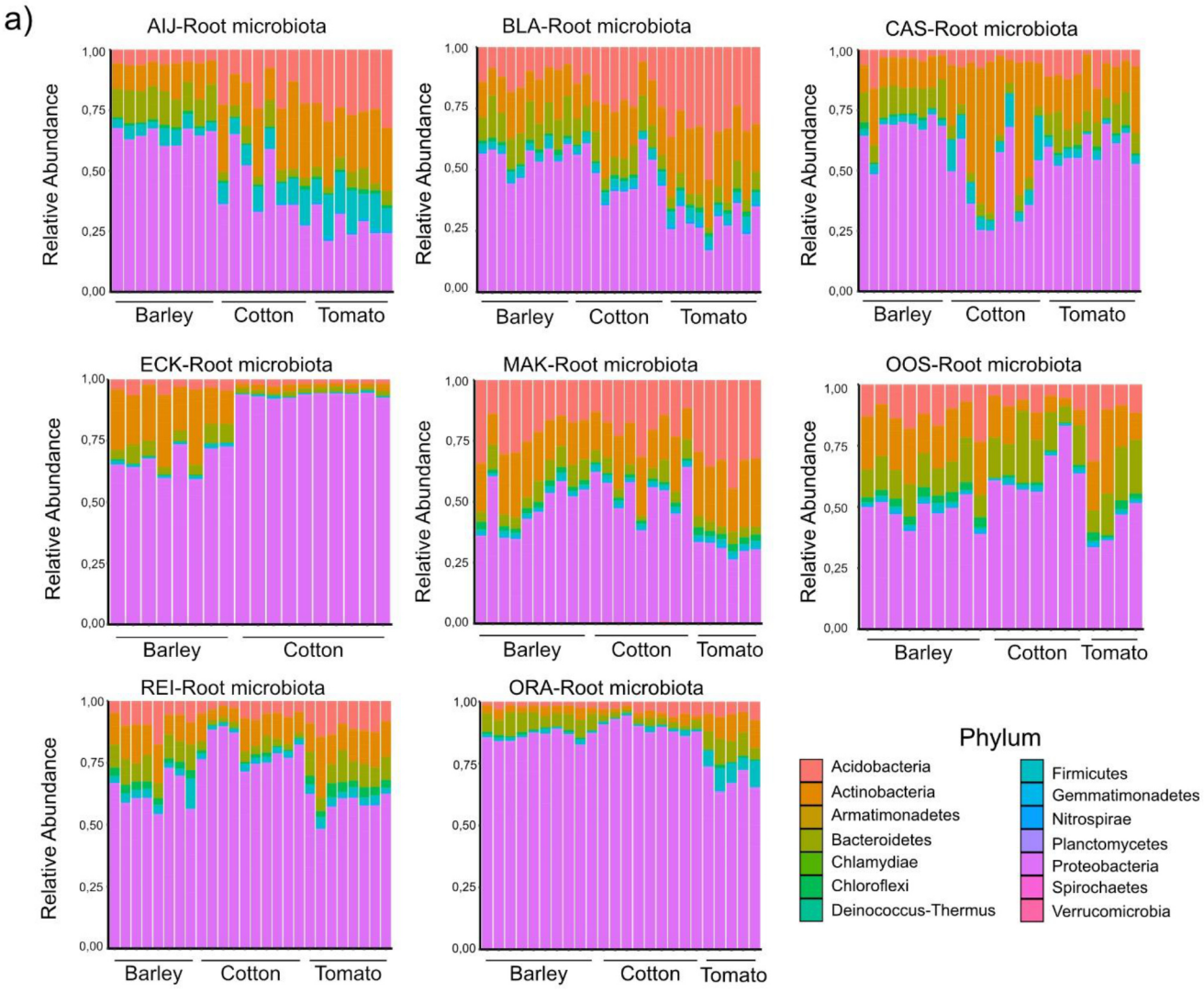
a)
AIJ-Root microbiota
BLA-Root microbiota
CAS-Root microbiota
ECK-Root microbiota
MAK-Root microbiota
OOS-Root microbiota
REI-Root microbiota
ORA-Root microbiota
Relative Abundance
1,00
0,75
0,50
0,25
0,00
Barley
Cotton
Tomato
Phylum
Acidobacteria
Actinobacteria
Armatimonadetes
Bacteroidetes
Chlamydiae
Chloroflexi
Deinococcus-Thermus
Firmicutes
Gemmatimonadetes
Nitrospirae
Planctomycetes
Proteobacteria
Spirochaetes
Verrucomicrobia

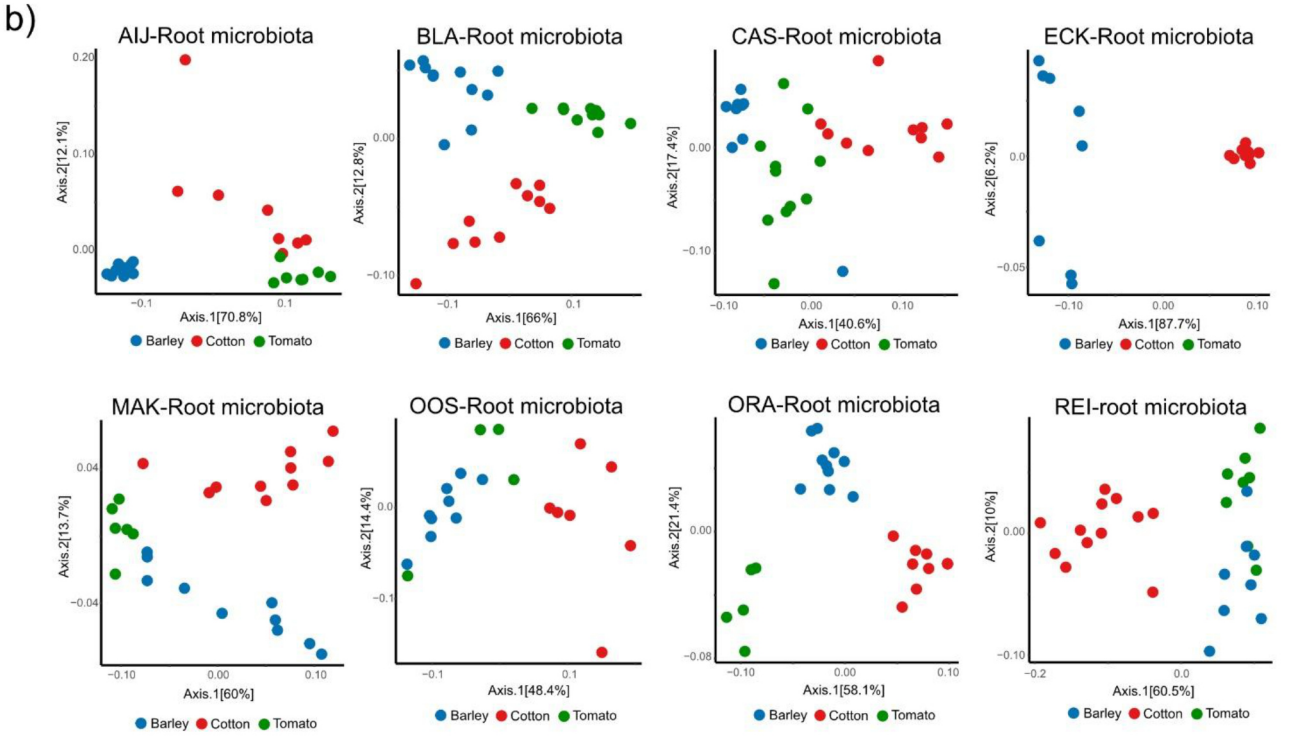
b)
AIJ-Root microbiota
Axis.1[70.8%]
Axis.2[12.1%]
BLA-Root microbiota
Axis.1[66%]
Axis.2[12.8%]
CAS-Root microbiota
Axis.1[40.6%]
Axis.2[17.4%]
ECK-Root microbiota
Axis.1[87.7%]
Axis.2[6.2%]
MAK-Root microbiota
Axis.1[60%]
Axis.2[13.7%]
OOS-Root microbiota
Axis.1[48.4%]
Axis.2[14.4%]
ORA-Root microbiota
Axis.1[58.1%]
Axis.2[21.4%]
REI-root microbiota
Axis.1[60.5%]
Axis.2[10%]
Barley
Cotton
Tomato

Supplementary Figure 4. Bacterial root microbiota. a) Relative abundance in percentage of the bacterial root microbiota of barley, cotton and tomato plants grown for three weeks on different natural soils. **b)** Principal coordinate analysis (PCoA) based on weighted Unifrac distances of the bacterial root microbiota from barley, cotton and tomato plants grown on the different natural soils.

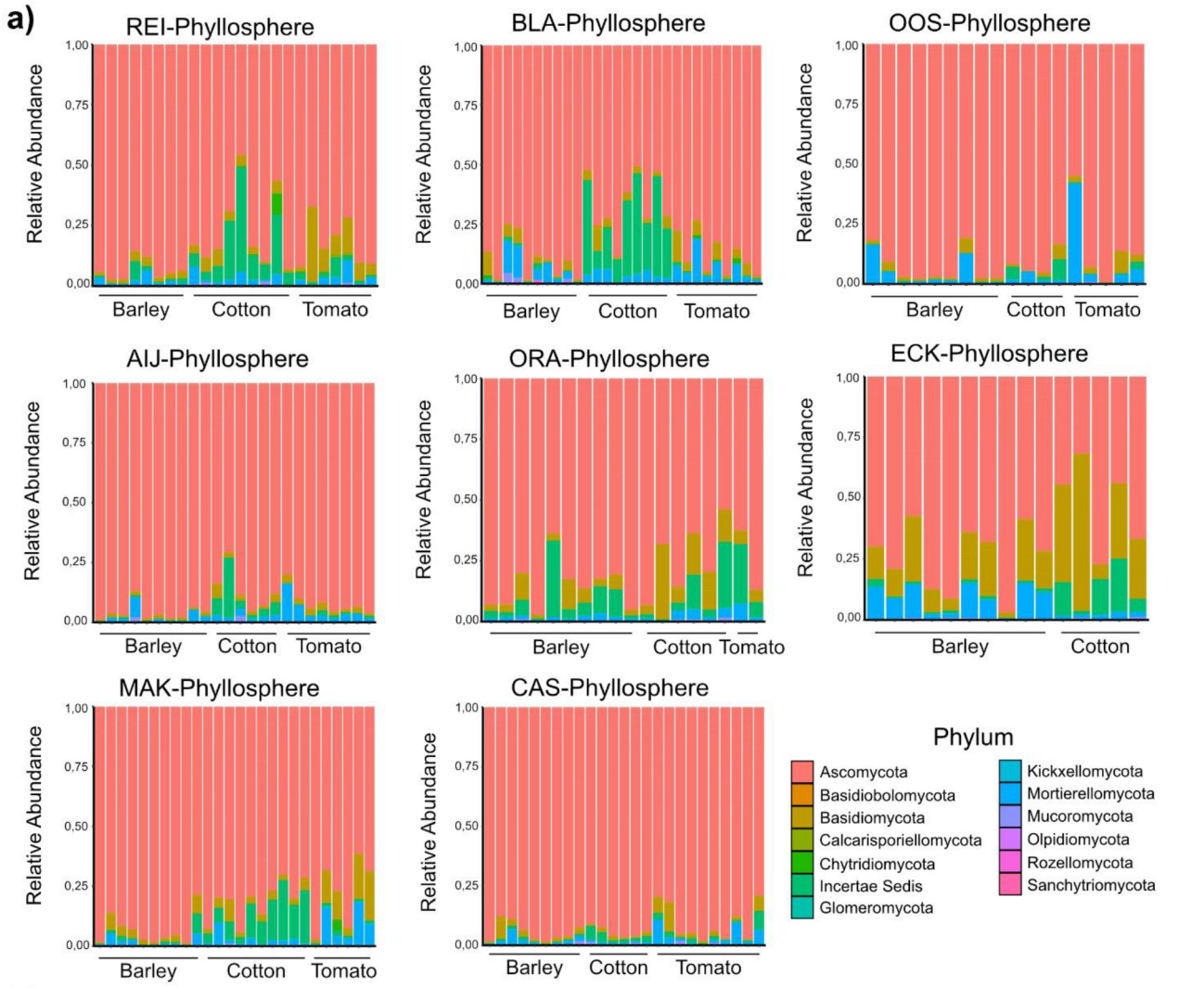
a)
REI-Phyllosphere
BLA-Phyllosphere
OOS-Phyllosphere
AIJ-Phyllosphere
ORA-Phyllosphere
ECK-Phyllosphere
MAK-Phyllosphere
CAS-Phyllosphere
Relative Abundance
1,00
0,75
0,50
0,25
0,00
Barley
Cotton
Tomato
Phylum
Ascomycota
Basidiobolomycota
Basidiomycota
Calcarisporiellomycota
Chytridiomycota
Incertae Sedis
Glomeromycota
Kickxellomycota
Mortierellomycota
Mucoromycota
Olpidiomycota
Rozellomycota
Sanchytriomycota

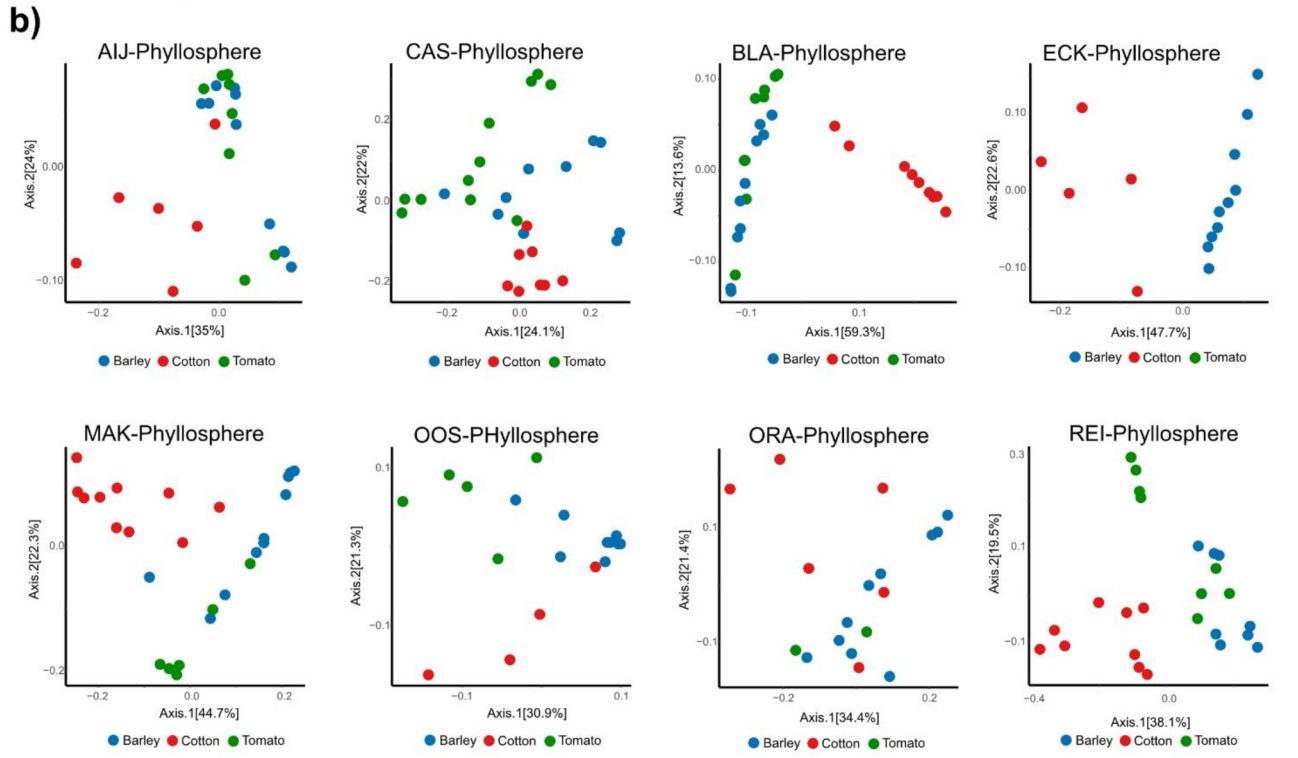
b)
AIJ-Phyllosphere
CAS-Phyllosphere
BLA-Phyllosphere
ECK-Phyllosphere
MAK-Phyllosphere
OOS-PHyllosphere
ORA-Phyllosphere
REI-Phyllosphere
Axis.1[35%]
Axis.2[24%]
Axis.1[24.1%]
Axis.2[22%]
Axis.1[59.3%]
Axis.2[13.6%]
Axis.1[47.7%]
Axis.2[22.6%]
Axis.1[44.7%]
Axis.2[22.3%]
Axis.1[30.9%]
Axis.2[21.3%]
Axis.1[34.4%]
Axis.2[21.4%]
Axis.1[38.1%]
Axis.2[19.5%]
Barley
Cotton
Tomato

Supplementary Figure 5. Fungal phyllosphere microbiota. a) Relative abundance in percentage of the fungal phyllosphere microbiota from barley, cotton and tomato plants grown for three weeks on different natural soils. **b)** Principal coordinate analysis (PCoA) based on weighted Unifrac distances of fungal phyllosphere microbiota from barley, cotton and tomato plants grown on the different natural soils.

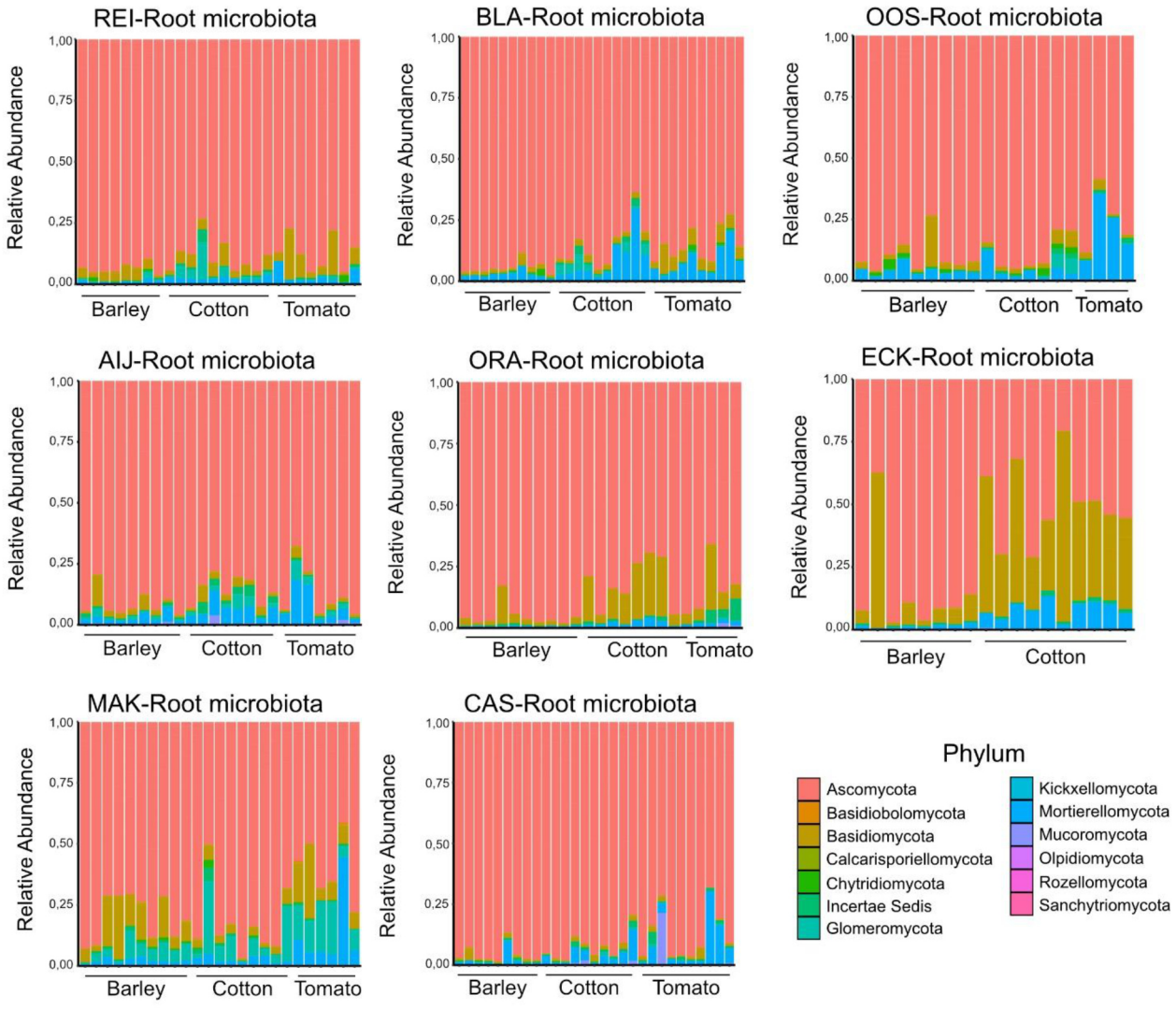
REI-Root microbiota
BLA-Root microbiota
OOS-Root microbiota
AIJ-Root microbiota
ORA-Root microbiota
ECK-Root microbiota
MAK-Root microbiota
CAS-Root microbiota
Relative Abundance
1,00
0,75
0,50
0,25
0,00
Barley
Cotton
Tomato
Phylum
Ascomycota
Basidiobolomycota
Basidiomycota
Calcarisporiellomycota
Chytridiomycota
Incertae Sedis
Glomeromycota
Kickxellomycota
Mortierellomycota
Mucoromycota
Olpidiomycota
Rozellomycota
Sanchytriomycota

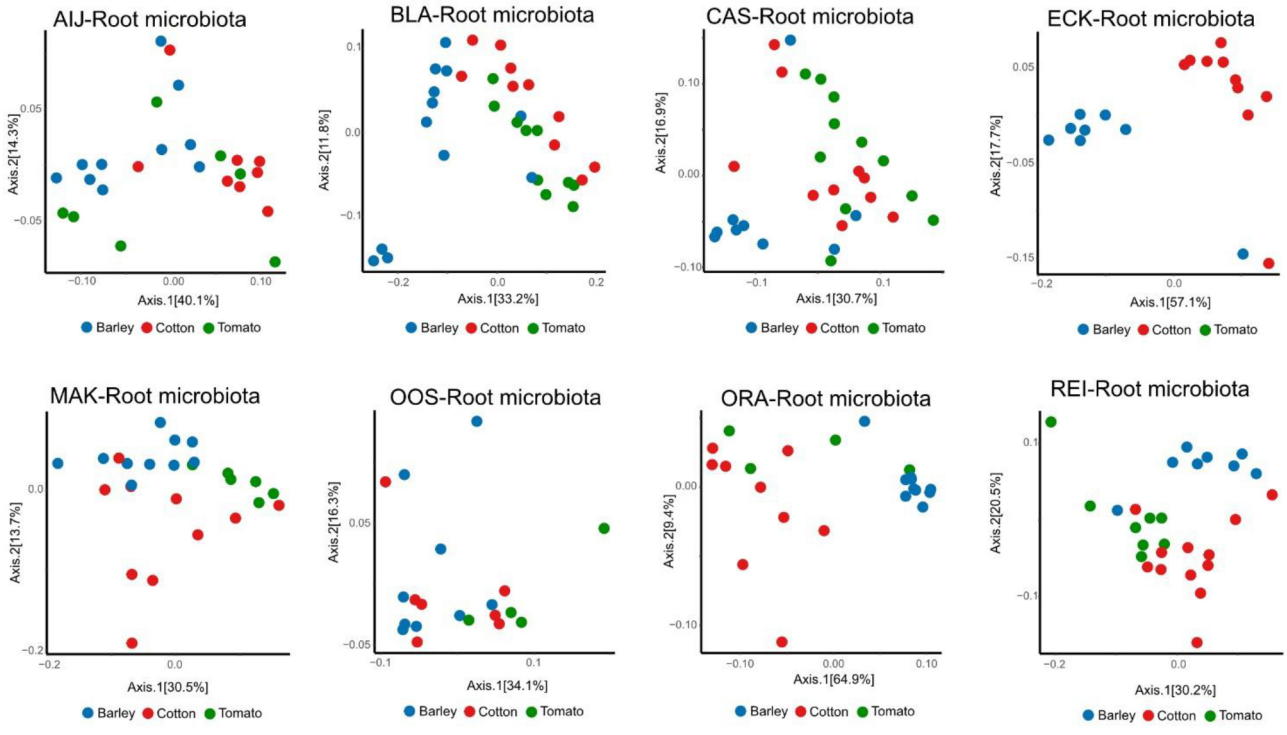
AIJ-Root microbiota
Axis.2[14.3%]
Axis.1[40.1%]
BLA-Root microbiota
Axis.2[11.8%]
Axis.1[33.2%]
CAS-Root microbiota
Axis.2[16.9%]
Axis.1[30.7%]
ECK-Root microbiota
Axis.2[17.7%]
Axis.1[57.1%]
MAK-Root microbiota
Axis.2[13.7%]
Axis.1[30.5%]
OOS-Root microbiota
Axis.2[16.3%]
Axis.1[34.1%]
ORA-Root microbiota
Axis.2[9.4%]
Axis.1[64.9%]
REI-Root microbiota
Axis.2[20.5%]
Axis.1[30.2%]
Barley
Cotton
Tomato

Supplementary Figure 6. Fungal root microbiota. a) Relative abundance in percentage of the fungal root microbiota from barley, cotton and tomato plants grown on different natural soils. **b)** Principal coordinate analysis (PCoA) based on weighted Unifrac distances of the fungal root microbiota from barley, cotton and tomato plants grown on the different natural soils.

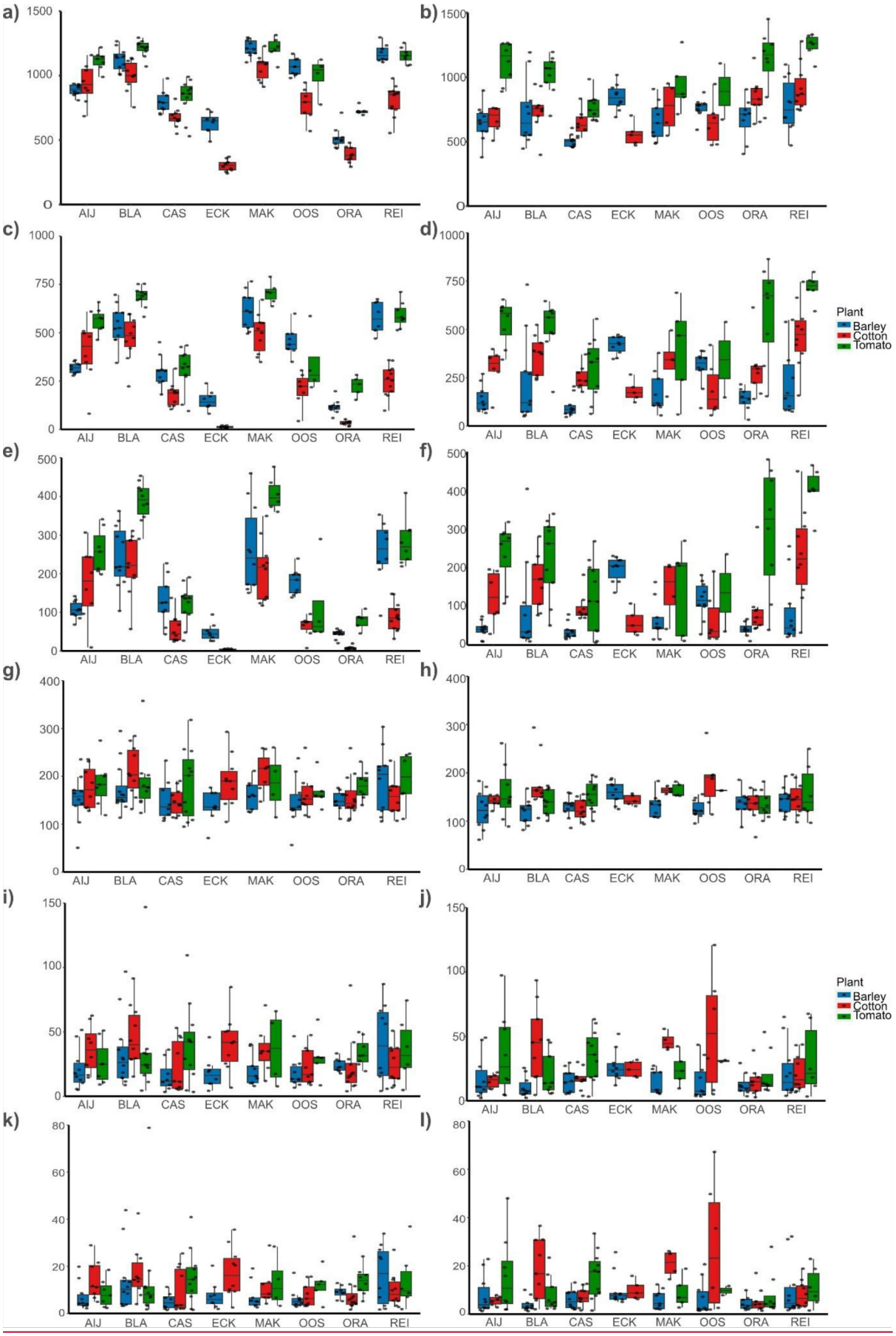
a)
b)
c)
d)
e)
f)
g)
h)
i)
j)
k)
l)
AIJ
BLA
CAS
ECK
MAK
OOS
ORA
REI
Plant
Barley
Cotton
Tomato

Supplementary figure 7. α-diversity measurements for bacterial and fungal communities in both the rhizosphere and the phylosphere of different plant species grown on different natural soils. a) c) e) correspond to the hill#0, hill#1 and hill#2 of the bacterial rhizosphere microbiota. b), d), f) correspond to the hill#0, hill#1 and hill#2 of the bacterial phylosphere microbiota. g) i) k) correspond to the hill#0, hill#1 and hill#2 of the fungal rhizosphere microbiota. h), j), l) correspond to the hill#0, hill#1 and hill#2 of the fungal phylosphere microbiota.

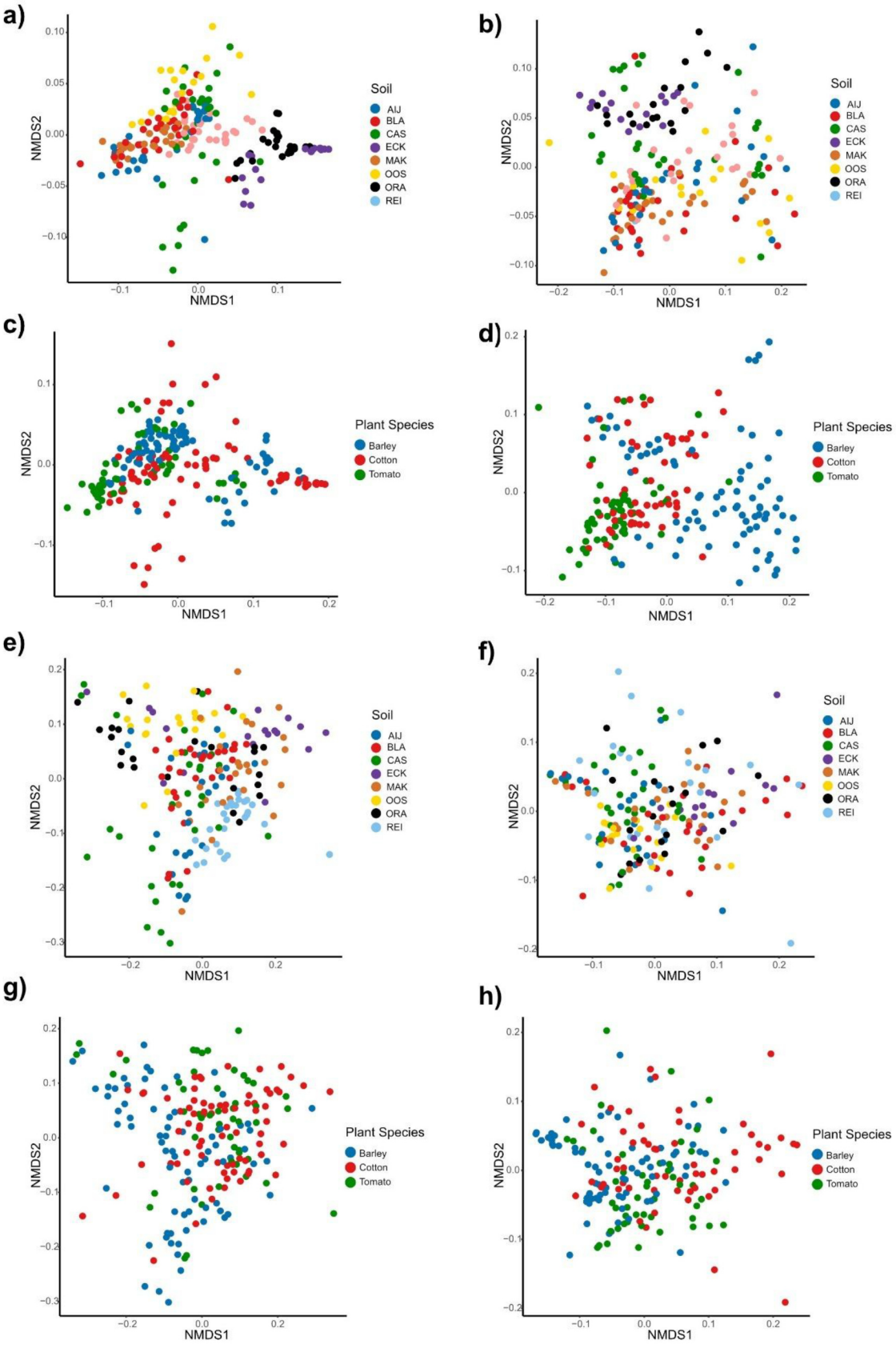
a)
b)
c)
d)
e)
f)
g)
h)
NMDS1
NMDS2
Soil
AIJ
BLA
CAS
ECK
MAK
OOS
ORA
REI
Plant Species
Barley
Cotton
Tomato

Supplementary Figure 8. ComposiČon of the root and phyllosphere associated microbiota of barley, cotton and tomato plants grown on the different natural soils. a) NMDS based on weighted Unifrac distance of root bacteria colored by the type of soil **b)** NMDS based on weighted Unifrac distance of phyllosphere bacteria colored by the type of soil **c)** NMDS based on weighted Unifrac distance of root bacteria colored by plant species **d)** NMDS based on weighted Unifrac distance of phyllosphere bacteria colored by plant species **e)** NMDS based on weighted Unifrac distance of root fungi colored by the type of soil **f)** NMDS based on weighted Unifrac distance of phyllosphere fungi colored by the type of soil **g)** NMDS based on weighted Unifrac distance of root fungi colored by plant species **h)** NMDS based on weighted Unifrac distance of phyllosphere fungi colored by plant species

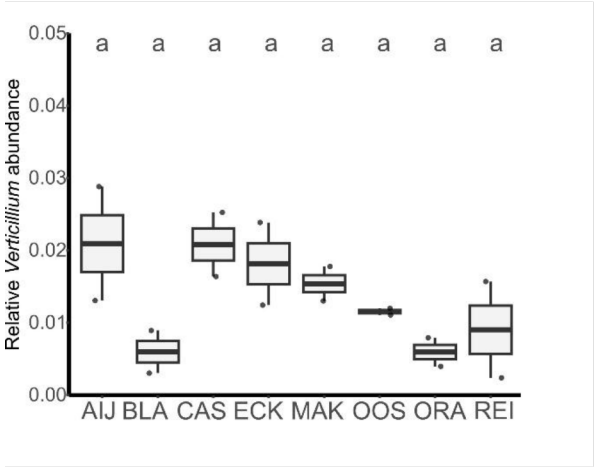

Supplementary figure 9. There is no significant difference in the relative abundance comparison of *Verticillium* in natural soil. Different letters represent significant differences (one-way ANOVA and Tukey's post hoc test; $P < 0.05$).

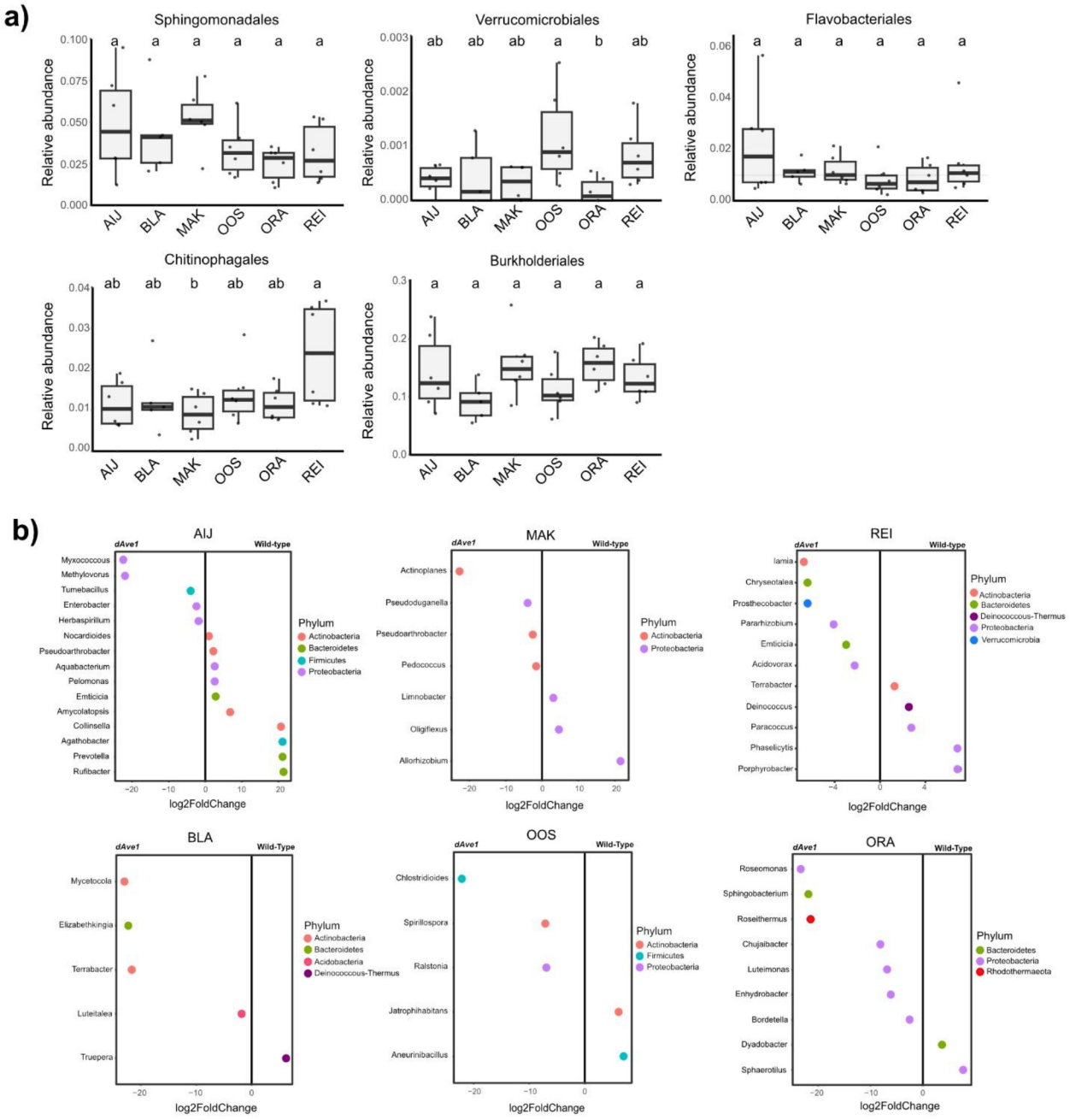

Supplementary Figure 10. Ave1-mediated microbiota manipulation in the different natural soils. **a)** Bacterial families previously reported to be impacted by Ave1 during tomato colonization. Relative abundance of each family in the root microbiota of three-week-old mock-inoculated plants. Different letters indicate statistical differences based on One-Way-Anova (Tukey HSD-Test pval < 0.05). **b)** Differential abundance of bacterial genera between root microbiota of tomato plants inoculated with wild-type *V. dahliae* or an *Ave1* deletion strain (Wald test, adjusted P < 0.05).

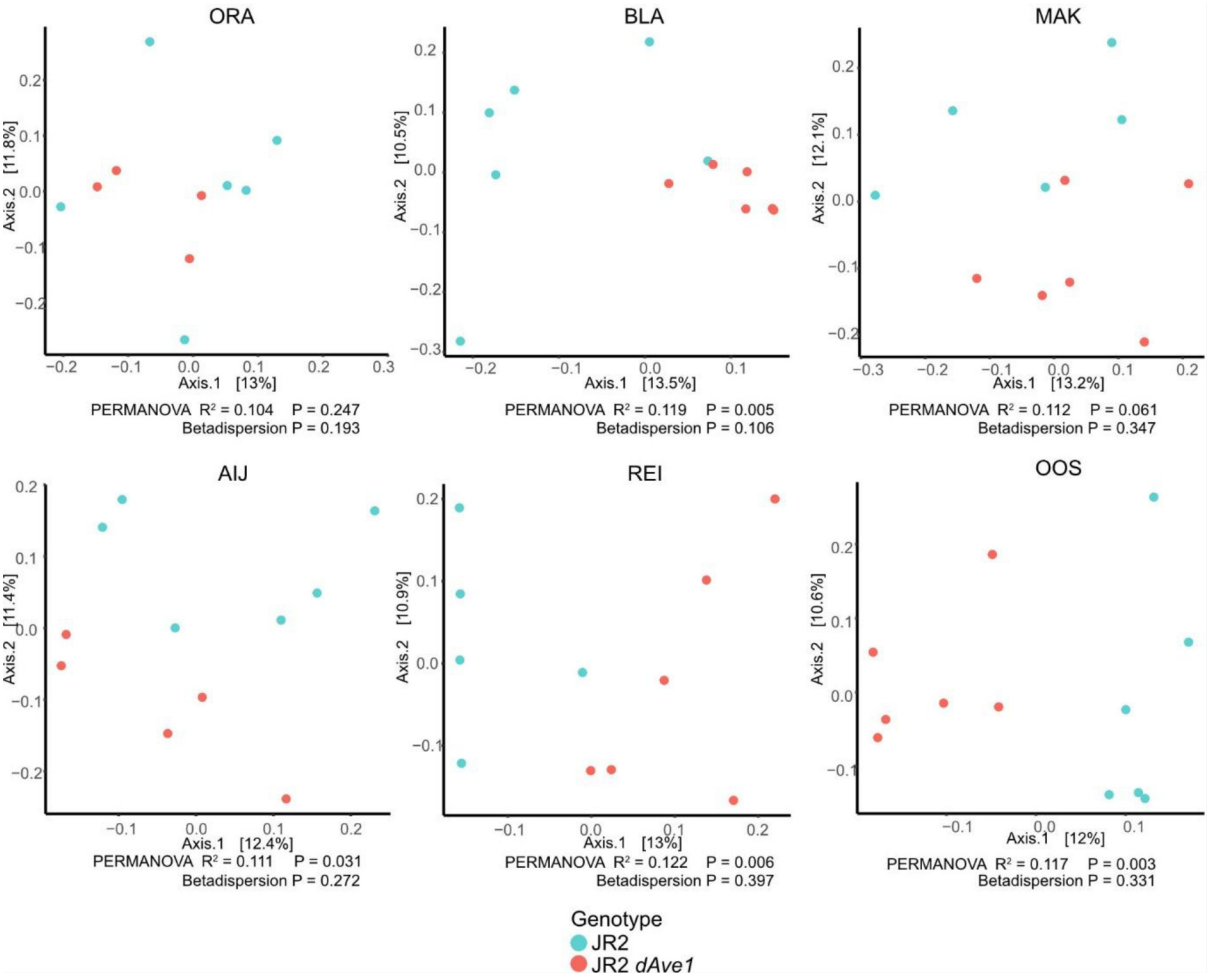

Supplementary figure 11. **Microbiota of plants inoculated with *V. dahliae* wt or the *Ave1* deletion strain (dAve1) significantly differ.** Principal coordinate analysis (PCoA) based on Unifrac distances of the root microbiota of tomato plants grown on different soils at 14 dpi with wild-type *V. dahliae* (JR2) or an *Ave1* deletion mutant (dAve1). All PERMANOVAs are performed with 9999 permutations.

Supplementary Table 1: Locations of the soil collection sites

LOCATION	COORDINATES	TYPE OF SOIL	ABBREVIATION
AIJEN	51°34'55.0"N 6°02'27.3"E	River Clay	AIJ
DE BLAUWE KAMER	51°56'34.4"N 5°37'12.9"	River Clay	BLA
MAKKUM	53°05'09.8"N 5°26'20.3"E	Sea Clay	MAK
OOSTVARDERSPLASSEN	52°27'50.0"N 5°25'10.8"E	Sea Clay	OOS
ECKELRADE	50°47'57.7"N 5°44'42.5"E	Loam	ECK
ORANJEWOUD	52°57'11.7"N 5°57'45.6"E	Peat	ORA
REIJERSCAMP	52°00'37.7"N 5°46'25.0"E	Sand	REI
DE GINKELSE HEIDE	52°02'10.7"N 5°43'38.9"E	Sand	GIN
MAASDUINEN	51°28'34.3"N 6°11'34.9"E	Sand	MAA
COLOGNE	50°57'27.8"N 6°51'22.4"E	Clay	CAS

Chapter 4

Plant-associated fungi co-opt ancient antimicrobials for host manipulation

Fantin Mesny[1†], Valentina Wolf[1‡#], Ana Lòpez-Moral[1 §#], Anton Kraege[1#], Wilko Punt[1#], Saifei Liu[1#,] Jinyi Zhu[1], Jiyeun Park[1], Yukiyo Sato[1], Bart PHJ Thomma[1*].

[1] Institute for Plant Sciences, University of Cologne, Cluster of Excellence on Plant Sciences (CEPLAS), Cologne, 50674, Germany

[†] Present address: Institute of Plant and Microbial Biology, University of Zurich, Switzerland

[‡] Present address: Department of Biology, Lund University, Sweden

[§] Present address: Department of Agronomy, University of Cordoba, Spain

[#] These authors contributed equally

[*]Corresponding author. Email: bthomma@uni-koeln.de

This article was published on *BioRxiv.*

doi: doi.org/10.1101/2024.01.04.574150

Abstract

Evolutionary histories of effector proteins secreted by fungal pathogens to mediate plant colonization remain largely elusive. While most functionally characterized effectors modulate plant immunity, recent discoveries have revealed novel functions in targeting host-associated microbiota. We now developed an Antimicrobial Activity Predictor for Effector Candidates (AMAPEC), and identified a wealth of antimicrobial effectors, including many highly conserved ones — suggesting ancient evolutionary origins. Surprisingly, several plant immunomodulatory effectors display antimicrobial activity. We propose that these evolved from ancestral antimicrobials while perhaps retaining their original functions. In addition to roles in suppressing host immunity, they may manipulate plant microbiota to promote colonization. We show that the *Verticillium dahliae* effector Vd424Y impacts host microbiota during infection, and more recently evolved to target plant cell nuclei to manipulate host immunity. Thus, we argue that microbial antagonism is a fundamental fungal effector function and suggest that fungi repurposed ancient antimicrobials to serve diverse roles during host-pathogen co-evolution.

Introduction

Under continuous threat of microbial parasitism, organisms evolved immune systems to withstand pathogenic encounters (1–4). In turn, pathogens evolved strategies to interfere with immune responses to mediate host colonization, typically through the secretion of molecules of diverse nature that are collectively called “effectors”. These effectors target a wide variety of molecular mechanisms in planta, ultimately resulting in compromised host immunity and resilience. Plant-pathogenic fungi typically secrete effectors apoplastically, several of which may subsequently be taken up by host cells to reach intracellular destinations. Effectors that localize in the apoplast may perturb detection by immune receptors or disarm apoplastic defenses, whereas those that localize intracellularly in the cytoplasm or within particular organelles may modulate immune signaling or particular metabolic pathways (5, 6). In addition to manipulating these well-documented plant targets, effectors may also serve in microbial competition, as revealed by the recent identification of effectors with selective antimicrobial properties that suppress antagonistic plant microbiota members with disease-suppressive functions (7–14). It is generally accepted that effectors are the products of long co-evolutionary “arms races” in which plants and pathogens aim to defend and overcome defenses, respectively (1, 3). Although particular effectors may originate from gene divergent evolution through the accumulation of mutations that ultimately lead to novel gene functions, genome recombination or horizontal gene transfer during host adaptation (15–18), the evolutionary histories and, more particularly, the molecular origins of most effectors remain enigmatic.

Here, we investigate evolutionary histories of effectors in the light of the recent discovery of antimicrobial effectors. As we reveal that many secreted antimicrobial proteins show broad conservation throughout the fungal kingdom, suggesting ancient origins, we hypothesize that effectors with functions in host physiology manipulation evolved from ancient antimicrobials. We validate this hypothesis by demonstrating that effectors with reported functions in host immunomodulation have ancestral antimicrobial properties that may serve in microbial antagonism during plant colonization. Thus, our study provides unprecedented insights into fungal evolution and the origins of key factors required for host colonization.

Results

Accurate prediction of effector antimicrobial activity

We first sought to identify novel fungal effectors with antimicrobial activities. Machine learning classifiers have previously supported the identification of antimicrobial peptides (AMPs) that are shorter than 100 amino acids in length, based on their physicochemical properties (19–21). However, these are not suited to predict antimicrobial activities of effectors, as they are generally longer and form more complex structures (fig. S1). To train an adequate predictor, we curated a dataset of experimentally validated antimicrobial proteins from diverse organisms in the size range of effectors (35–642 amino acids, median = 125.5; Fig. 1, A and B and table S1). Only few carbohydrate-active enzymes (CAZymes) were included since, although several families target microbial structures, it is often unknown whether individual members compromise microbial growth and can thus be classified as genuine antimicrobials. Thus, only few CAZymes could be included as *bona fide* antimicrobials. Additionally, we curated a negative training set of equivalent proteins unlikely to have antimicrobial activity according to their functional annotation (table S2). For each protein in the training sets, we calculated properties from their amino acid sequences and predicted high-confidence protein structures (Fig. 1, C and fig. S2), representing 70 numerical values reflecting diverse physicochemical properties (table S3). Moreover, we queried for the presence/absence of six k-mers that are over- or underrepresented in the sequences of the antimicrobial proteins (see Materials & Methods for details; table S3). All data were used to train a Support Vector Machines classifier and subsequently estimated its quality through leave-one-out cross-validation, revealing that our classifier has high accuracy, recall and specificity, particularly for fungal proteins (Fig. 1, D). Analysis of support vector coefficients, representing the importance of individual properties for the prediction, revealed a role for hydrophobicity, charge, secondary structures, identity of exposed amino acids, disulfide bonds and structural cavities (fig. S3). To confirm that our predictor can reliably identify novel fungal antimicrobial proteins, we tested whether it correctly calls out seven more recently characterized fungal antimicrobials that were not included in the training set (22–26). As all seven proteins were correctly classified as antimicrobials (table S4), we implemented the predictor in the novel software package AMAPEC (**a**nti**m**icrobial **a**ctivity **p**rediction for fungal **e**ffector **c**andidates; Fig. 1, E), available at https://github.com/fantin-mesny/amapec.

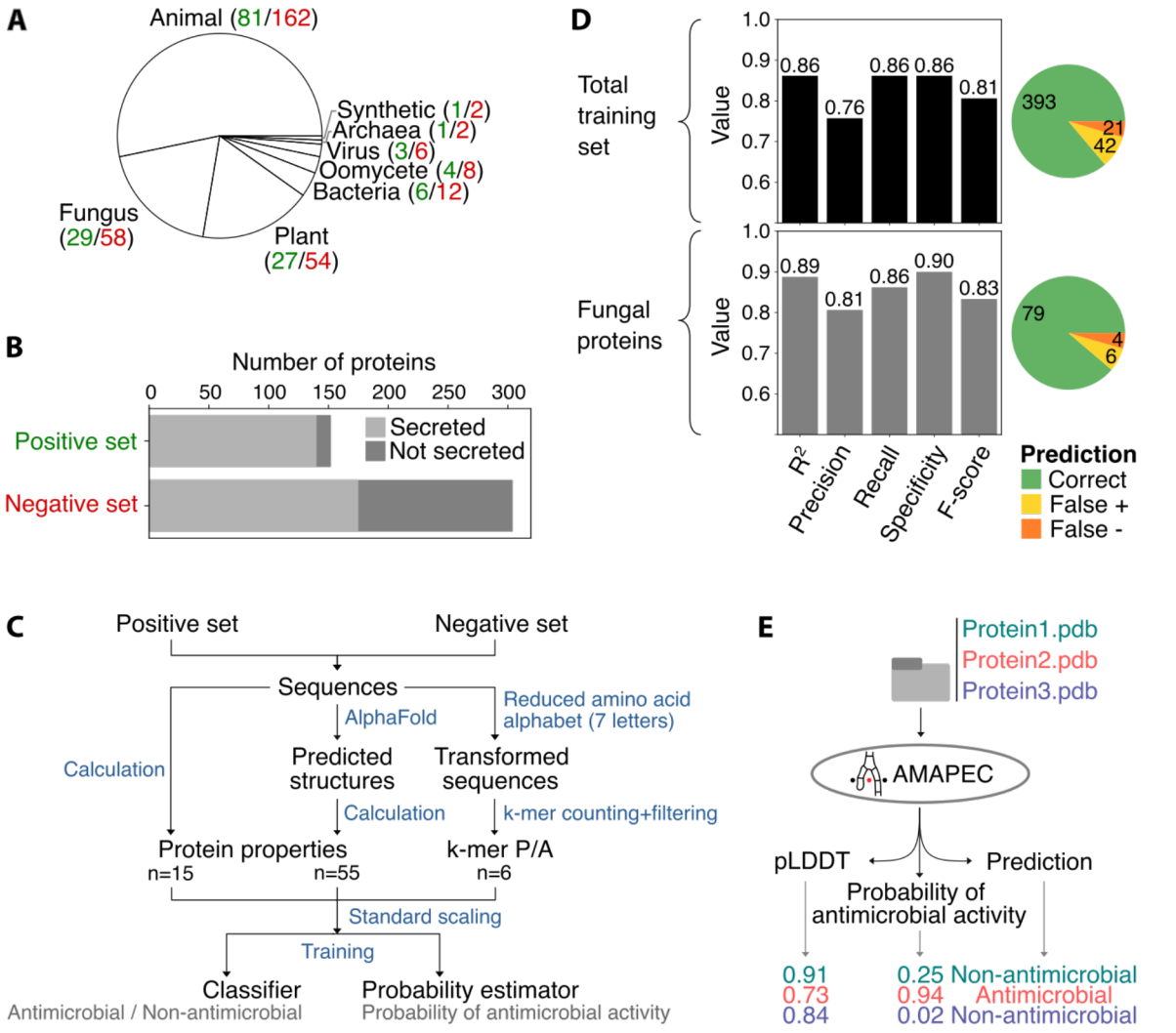

Fig. 1. AMAPEC accurately predicts antimicrobial activities of fungal effector proteins. (**A**) Phylogenetic origin of the proteins in the dataset (green: number of proteins in positive dataset; red: number in negative dataset) used to train the predictor. (**B**) Number of proteins included in the training dataset and proportion of secreted proteins. (**C**) Diagram presenting a schematic overview of the training pipeline. In addition to physicochemical properties retrieved from protein sequences and structures, the pipeline considers the presence/absence (P/A) in protein sequences of six short motifs (k-mers) that are over- or underrepresented in the positive training set. These k-mers are encoded in a reduced amino acid alphabet, which groups amino acids according to their physicochemical properties. (n= number of variables). (**D**) Estimation of the classifier quality, based on "leave-one-out" cross-validation in the training dataset. The top bar plot and pie chart show quality estimates calculated on the total dataset (n=456), while the bottom charts analyze only the classifications of fungal proteins (n=87) during the "leave-one-out" cross validation. (**E**) Schematic overview of AMAPEC v1.0 showing its inputs and outputs with an example of three proteins.

We used AMAPEC to identify candidate antimicrobial proteins in the secretomes of three phylogenetically distant fungi with distinct lifestyles, namely the mycorrhizal glomeromycete *Rhizophagus irregularis*, the saprotrophic basidiomycete *Coprinopsis cinerea* and the ubiquitous plant-pathogenic ascomycete *Verticillium dahliae* that causes vascular wilt disease in a wide diversity of host plants, including many crops (27) (Fig. 2, A to C). Functional compositions of fungal secretomes remain largely elusive, as they comprise a significant proportion of proteins without functional annotations (Fig. 2, A) and proteins for which the assigned annotations are poorly informative (tables S5-S7). Although in principle the AMAPEC predictor can be used on CAZymes, we excluded these enzymes from the analysis given the low number of CAZymes in our training set, which may lead to less robust predictions, but also to be rather conservative in our predictions. Surprisingly, AMAPEC prediction revealed that one third to half of each of the secretomes without CAZymes of the three fungi is composed of putative antimicrobial proteins (Fig. 2, B). Importantly, orthology analysis revealed that some antimicrobials are conserved across the three fungi, despite their wide phylogenetic spread, and thus ancestral to the three phyla (Fig. 2, C). Moreover, antimicrobials show significantly greater conservation across species (i.e. occurrence of orthologs) than non-antimicrobials (Fig. 2, C; Fisher's exact test: odd's ratio = 2.19, P = 3.6×10-4), suggesting that microbial antagonism is relatively ancient among secretome functions.

Secreted antimicrobial proteins are conserved throughout the fungal kingdom

The evolution of antimicrobial proteins was further investigated in 150 genomes of diverse soil- and plant-associated fungi, spanning 3 phyla, 9 classes and 24 orders (fig. S4 and table S8). This dataset encompasses over 700 million years of fungal evolution, whereas pathogenicity towards land plants only evolved after plants colonized land, about 500 million years ago. After classifying secreted proteins into sequence-related families through orthology prediction, antimicrobial activities were predicted for the most representative protein of each family (table S9). Remarkably, many of the most conserved protein families, which occur in fungi with diverse lifestyles, were predicted as antimicrobials (Fig. 2, D). We calculated the percentage of predicted antimicrobial families across different levels of conservation (Fig. 2, E) and identified a significant decrease from 56.9% of multi-phyla families to 49.1% of genus-specific families (Cochran-Armitage test for trend: statistic = 5129.0, P < 2.36×10-5). This overrepresentation of predicted antimicrobials among the most conserved secreted protein families signifies their ancient origins, preceding fungal phyla divergence, and corroborates that fungi have relied on antimicrobials long before establishing symbioses with multicellular eukaryotes such as land plants and animals (28). While the most conserved secreted protein

families expectedly exhibit the most diverse sequences, certain predicted antimicrobial families, including previously characterized ribonuclease-like antimicrobials (11, 29), retained low sequence diversity during evolution, possibly to conserve their ancestral function (i.e. purifying selection; Fig. 2, F). Together, our results demonstrate that microbial antagonism through the secretion of antimicrobial proteins is an ancient and conserved trait that likely supports fungal fitness across a wide diversity of habitats.

Effectors of plant-pathogenic fungi display antimicrobial activities

We recently showed that *V. dahliae* secretes effector proteins with selective antimicrobial activity to manipulate resident microbiota at various life stages, including host colonization (7–9, 14). Intriguingly, we noticed that several *V. dahliae* effectors previously characterized to modulate host immunity have predicted antimicrobial properties (table S10), including VdCP1 (30), Vd424Y (also known as VdXyn4) (31, 32) and Vd2LysM (33), a member of the LysM effector family which represses chitin-triggered plant immunity and has an ancient origin since family members occur throughout the fungal kingdom (34, 35). Based on these findings, we hypothesized that plant-pathogenic fungi have evolved effectors to manipulate plant host physiology from ancestral antimicrobial proteins. In support of this hypothesis, we found that most functionally characterized effectors registered in PHI-base (36) (n=76/133), some of which are broadly conserved throughout our dataset of 150 genomes (Fig. 3, B), have predicted antimicrobial properties (Fig. 3, A and table S11). To validate these predictions, we subsequently selected five effectors for experimental validation: the LysM effector Ecp6 from the tomato leaf mould fungus *Cladosporium fulvum* (37), AGLIP1 from the root rot fungus *Rhizoctonia solani* (38), AVR-Pita from the rice blast fungus *Magnaporthe oryzae* (39) and Vd424Y (31, 32) and VdCP1 (30) from *V. dahliae*. All proteins were heterologously produced in *Escherichia coli* and employed in antimicrobial activity assays using a diverse set of plant-associated microbes including 12 bacteria that were isolated from tomato plants (40), as tomato is a host of three of the four above-mentioned fungi, four yeasts and three filamentous fungi. Interestingly, despite their well-characterized host targets, all five effectors exhibited antimicrobial activities *in vitro* with highly distinct activity spectra at micromolar concentrations (Fig. 3, C and D, and fig. S6-S15). As homologs of all five proteins occur in fungi that do not live in association with plants, and most homologs in their protein families are predicted antimicrobials (fig. S5 and table S12-16), antimicrobial activity is likely ancestral and predates the evolution of host manipulation. Overall, our data suggest that pathogen effectors evolved from ancient antimicrobial proteins that retain their ancestral functions while acquiring the ability to manipulate host physiology.

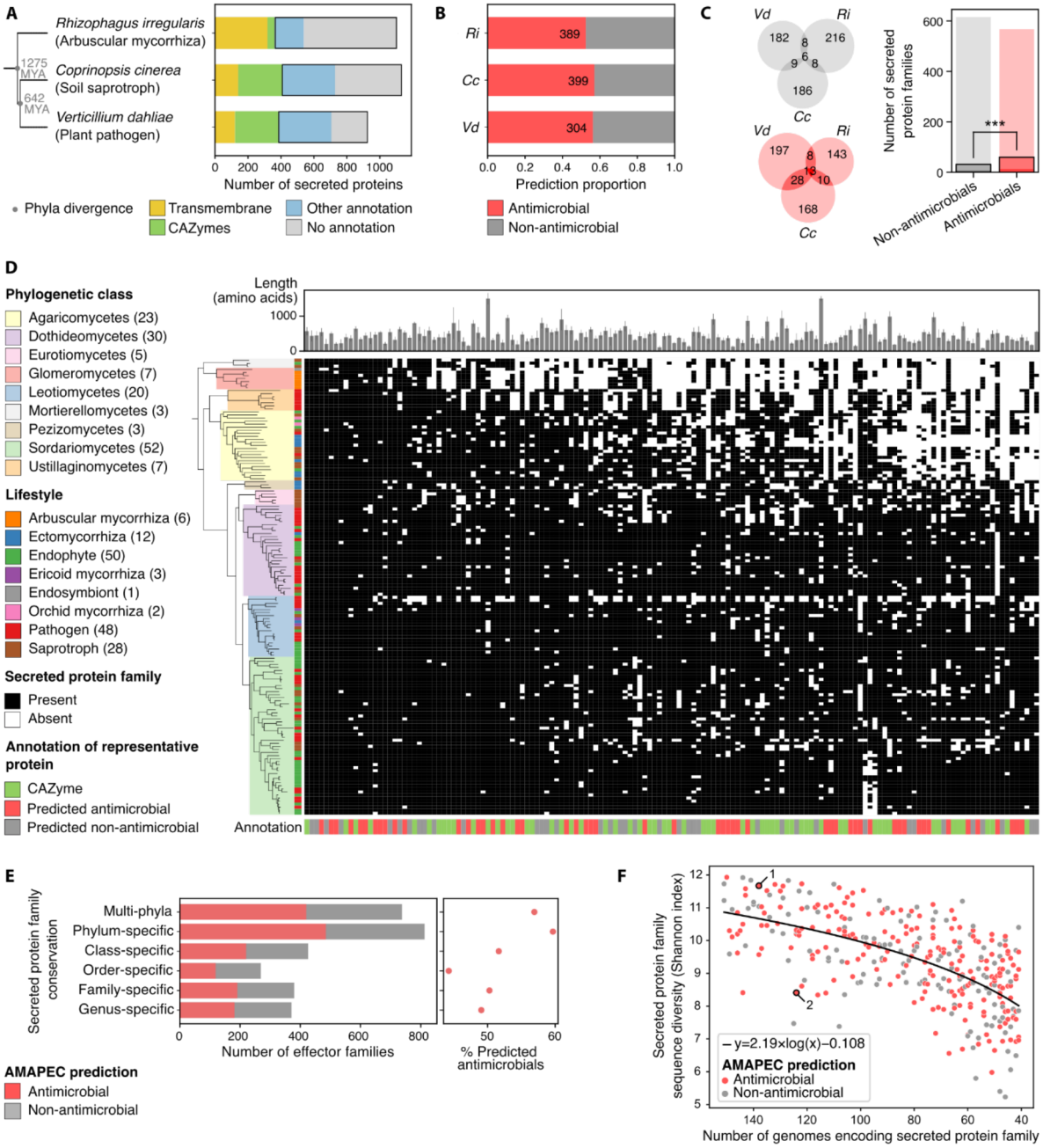

Fig. 2. Predicted antimicrobials are abundant in fungal secretomes and exhibit high conservation. (**A**) Selected set of three fungi with broad phylogenetic diversity and distinct lifestyles, together with the functional annotation of their predicted secretomes. Parts of the secretomes framed with black rectangles were used for antimicrobial effector prediction with AMAPEC. The species-level phylogenetic tree was generated with phyloT (phylot.biobyte.de) based on NCBI taxonomy data (114). It is annotated with median taxa divergence times registered in the database TimeTree (41).

(**B**) Results of AMAPEC antimicrobial activity prediction, highlighting proportions and numbers of predicted antimicrobials in the secretomes (excluding transmembrane proteins and CAZymes) of the arbuscular mycorrhizal Glomeromycota *Rhizophagus irregularis* (Ri), the saprophytic basidiomycete *Coprinopsis cinerea* (Cc) and the plant-pathogenic ascomycete *Verticillium dahliae* (Vd). (**C**) Orthology prediction analysis revealing the numbers of conserved predicted antimicrobial effectors (red Venn diagram) and non-antimicrobials (grey Venn diagram) across the three secretomes. On the right, a barplot shows numbers of secreted protein families and highlights with darker colors and a dash line the proportions of conserved antimicrobials and non-antimicrobials across the three secretomes. Fisher's exact test (odd's ratio = 2.19, P = 3.6×10-4) revealed an overrepresentation of conserved effectors among predicted antimicrobials. (**D**) Analysis of the 150 most conserved secreted protein families (according to orthology prediction) in a diverse dataset of 150 fungal genomes. On the left, a phylogeny describes the genomic dataset composition, with phylogenetic classes and lifestyles annotated in colors. In the central heatmap, each column corresponds to a secreted protein family with black and white squares highlighting the presence/absence of these families in each genome. Protein family conservation decreases from left to right. On top, a barplot shows average protein sequence lengths. At the bottom, colored bars highlight the CAZyme annotation or results of AMAPEC antimicrobial activity prediction performed on a representative member of each protein family. As only few CAZymes were available for the positive AMAPEC training set, we consider predictions for such proteins less robust, and hence they were excluded here. (**E**) On the left, a barplot depicts numbers of predicted antimicrobial and non-antimicrobial families (prediction performed on one representative protein per family, excluding families which representative protein was annotated as transmembrane protein or CAZyme) across effector family conservation levels in the 150-genome dataset. On the right, a scatterplot presents proportions of predicted antimicrobials along the same effector family conservation levels. These proportions follow a significantly descending trend according to Cochran-Armitage test (statistic = 5129.0, P < 2.36×10-5). (**F**) A sequence diversity index (Shannon alpha-diversity calculated from k-mer composition of amino acid sequences) of protein families is plotted as a function of decreasing family conservation across the dataset of 150 fungal genomes. A logarithm function was fitted to these data to highlight a general trend linking protein family sequence diversity to family conservation. While outlier datapoints located above the curve may be under diversifying selection (i.e. accumulating mutations), outliers located below the curve may be under purifying selection (i.e. preventing protein sequences to change extensively to conserve ancestral functions). Datapoint colors correspond to antimicrobial activity prediction on a representative member of each family. Two protein families labeled 1 and 2 include previously experimentally validated fungal antimicrobial proteins (11, 29, 115).

Effectors of plant-pathogenic fungi display antimicrobial activities

We recently showed that *V. dahliae* secretes effector proteins with selective antimicrobial activity to manipulate resident microbiota at various life stages, including host colonization (7–9, 14). Intriguingly, we noticed that several *V. dahliae* effectors previously characterized to modulate host immunity have predicted antimicrobial properties (table S10), including VdCP1 (30), Vd424Y (also known as VdXyn4) (31, 32) and Vd2LysM (33), a member of the LysM effector family which represses chitin-triggered plant immunity and has an ancient origin since family members occur throughout the fungal kingdom (34, 35). Based on these findings, we hypothesized that plant-pathogenic fungi have evolved effectors to manipulate plant host physiology from ancestral antimicrobial proteins. In support of this hypothesis, we found that most functionally characterized effectors registered in PHI-base (36) (n=76/133), some of which are broadly conserved throughout our dataset of 150 genomes (Fig. 3, B), have predicted antimicrobial properties (Fig. 3, A and table S11). To validate these predictions, we subsequently selected five effectors for experimental validation: the LysM effector Ecp6 from the tomato leaf mould fungus *Cladosporium fulvum* (37), AGLIP1 from the root rot fungus *Rhizoctonia solani* (38), AVR-Pita from the rice blast fungus *Magnaporthe oryzae* (39) and Vd424Y (31, 32) and VdCP1 (30) from *V. dahliae*. All proteins were heterologously produced in *Escherichia coli* and employed in antimicrobial activity assays using a diverse set of plant-associated microbes including 12 bacteria that were isolated from tomato plants (40), as tomato is a host of three of the four above-mentioned fungi, four yeasts and three filamentous fungi. Interestingly, despite their well-characterized host targets, all five effectors exhibited antimicrobial activities *in vitro* with highly distinct activity spectra at micromolar concentrations (Fig. 3, C and D, and fig. S6-S15). As homologs of all five proteins occur in fungi that do not live in association with plants, and most homologs in their protein families are predicted antimicrobials (fig. S5 and table S12-16), antimicrobial activity is likely ancestral and predates the evolution of host manipulation. Overall, our data suggest that pathogen effectors evolved from ancient antimicrobial proteins that retain their ancestral functions while acquiring the ability to manipulate host physiology.

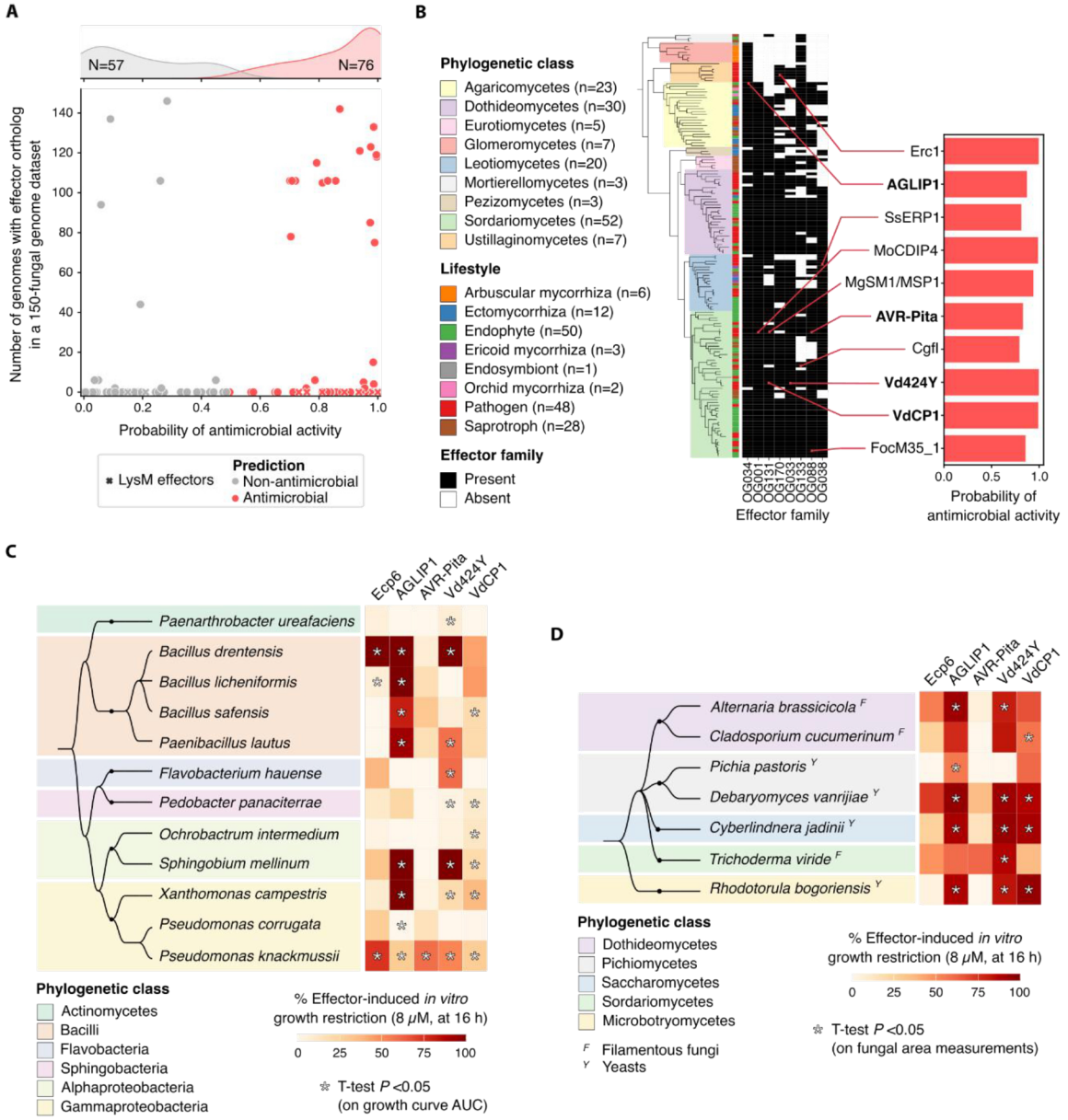

Fig. 3. Immunomodulatory effectors also possess antimicrobial properties. (**A**) Scatterplot showing the antimicrobial activity prediction for fungal effectors from the curated PHI-base database (36) together with their number of orthologs in our dataset of 150 fungal genomes as a proxy for their conservation across the fungal kingdom. (**B**) Presence/absence patterns in the dataset of 150 fungal genomes of eight secreted protein families, including effectors that were previously demonstrated to act on plant hosts. On the right, a barplot shows the name of the previously studied effectors together with their AMAPEC-predicted antimicrobial activity. The eight families were selected because they include a highly similar protein to the PHI-base reference effectors (≥80% amino acid sequence identity), they show high conservation across the fungal kingdom (family represented in ≥100 genomes in the 150-genome dataset) and because the associated reference effectors are predicted antimicrobials with highly confident structure prediction (mean pLDDT ≥ 70).

Effector names in bold indicate effectors selected for experimental validation of predicted antimicrobial activities. (**C**) Heatmap highlighting bacterial growth restriction induced by the presence of 8 µM of effector protein in the growth medium. A phylogenetically diverse set of 12 bacteria was used and is described with a species phylogeny on the left (generated with Taxallnomy (116)). Each heatmap column corresponds to a different fungal effector. Percentages of effector-induced growth restriction were calculated after 16 hours of growth. Asterisks highlight significant differences between from bacterial growth in presence and in absence of effector protein, identified with Student's T-tests on area under curve (AUC) values. (**D**) Heatmap highlighting fungal growth restriction induced by the presence of 8 µM of effector protein in the growth medium. A phylogenetically diverse set of 7 fungi (4 yeasts and 3 filamentous fungi) was used and is described with species phylogeny on the left (tree generated with Taxallnomy (116)). Each heatmap column corresponds to a different fungal effector. Percentages of effector-induced growth restriction were calculated after 16 hours of growth. Asterisks highlight significant differences between from fungal growth in presence and in absence of effector protein, identified with Student's T-tests. More details on the results of in vitro assays depicted on panels **C** and **D** can be found in fig. S6-S15.

A dual role of the effector Vd424Y in host manipulation and microbial antagonism

Since many fungal effectors have evolutionary conserved ancestral antimicrobial properties (Fig. 3), we hypothesize that, in addition to manipulation of host physiology, they antagonize microbial competitors during infection. To address this hypothesis, we focused on the *V. dahliae* effector Vd424Y, which is known to exert xylanolytic and cytotoxic activities *in planta* (31, 32). To investigate whether this effector also functions in microbial competition, we first measured effector gene expression in a diverse set of ten soils, in absence of a plant host (fig. S16). We found that *V. dahliae* expresses the *Vd424Y* gene in these soils, suggesting functions beyond host physiology manipulation. Next, we tested if the antimicrobial activity of Vd424Y plays a role during plant colonization, by performing tomato inoculation experiments in a gnotobiotic system, allowing to study virulence contributions of effector genes in the presence and absence of host-associated microbiota (40). We identified a significant microbiota-dependent contribution of Vd424Y to *V. dahliae* virulence, as disease development was compromised upon Vd424Y deletion in the presence, but not in the absence of host-associated microbes (Fig. 4, A and B). This finding suggests that Vd424Y plays a role in microbiota manipulation during tomato plant infection, and thus that it retained its ancestral antimicrobial property throughout co-evolution with plant hosts. To investigate this hypothesis further, we profiled the bacterial microbiota of the *V. dahliae* WT- and ∆*424Y*-infected tomato plants and found that their compositions differed significantly (PERMANOVA, $P < 0.05$; Fig. 4, C). A differential abundance analysis enabled to identify several bacterial genera, including

Pseudoxanthomonas, Comamonas, Brachybacterium and *Sphingobium*, whose relative abundance is reduced in presence of the Vd424Y gene (fig. S17, A). Since the Vd424Y protein restricted the growth of a *Sphingobium* isolate *in vitro* (fig. S9), these bacterial genera may represent microbial targets of the effector in planta. We assessed whether the growth of *Pseudoxanthomonas* bacteria, whose abundance *in planta* was significantly reduced in presence of Vd424Y (fig. S17, A), is similarly restricted by Vd424Y *in vitro*. Although our results revealed notable intra-genus variation, we indeed found that Vd424Y is able to inhibit particular *Pseudoxanthomonas* strains (fig. S17, B). Thus, we conclude that Vd424Y plays a role in microbiota manipulation through direct antimicrobial activity.

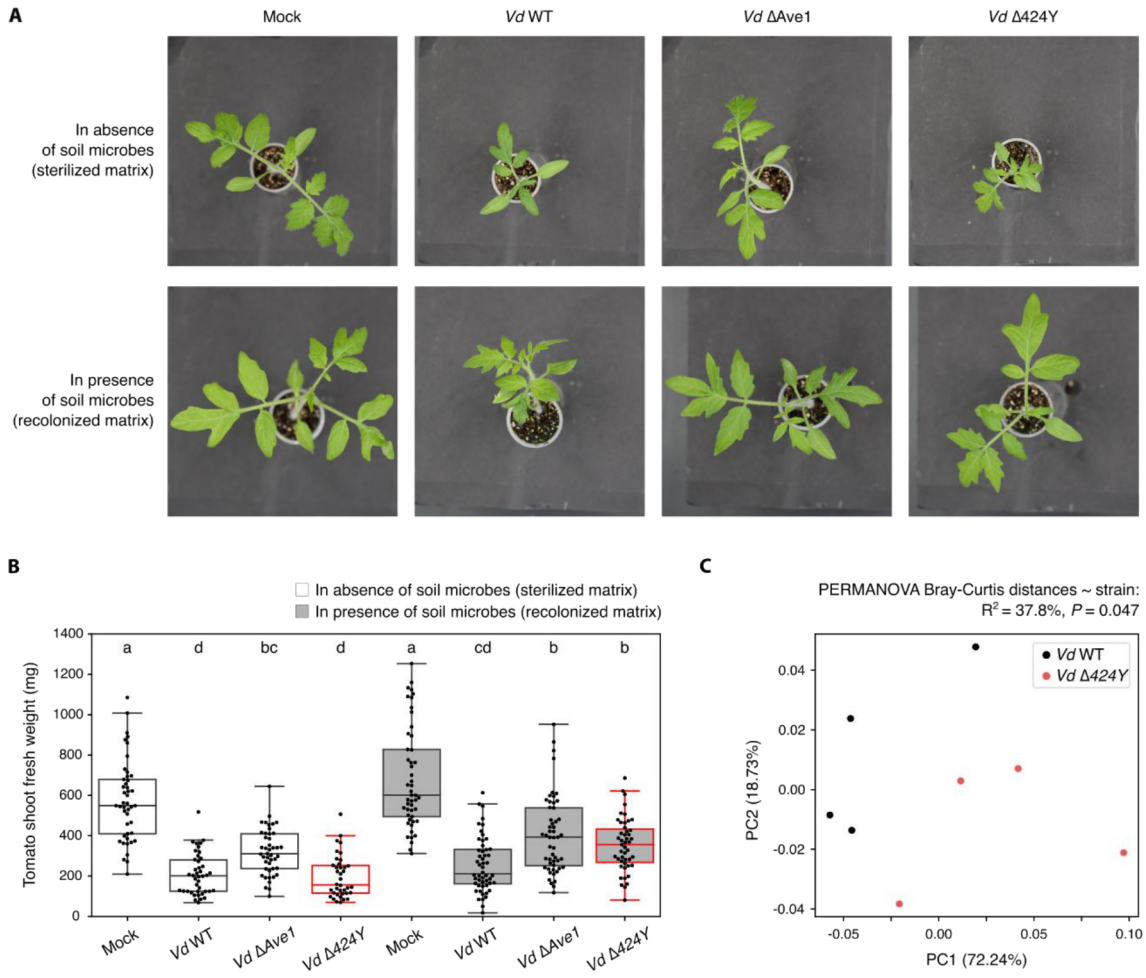

Fig. 4. The effector Vd424Y acts in *Verticillium dahliae* antagonism towards plant microbiota members. (**A**) Representative photographs of tomato plants upon mock or fungal inoculation in a gnotobiotic system in absence (sterilized soil; top) or presence (sterilized soil recolonized with microbes derived from non-sterilized soil; bottom) of a soil microbiota. Fungal strains used for plant infections include wild-type *V. dahliae* (Vd WT), *Vd424Y* deletion mutant (Vd Δ*424Y*), and as a control, an *Ave1* deletion mutant lacking the Ave1 effector previously demonstrated to contribute to *V. dahliae* virulence through both an antimicrobial activity targeting plant microbiota members and the manipulation of plant physiology (7, 40). (**B**) Tomato shoot fresh weight values reflecting plant health after mock or fungal inoculation in a gnotobiotic system. Plants were grown axenically (sterilized matrix; white boxes) or in presence of microbes (recolonized matrix; grey boxes). The *Vd424Y* deletion mutant (Vd Δ*424Y*) is highlighted with red box edges. Between 38 and 52 tomato plants were grown per condition, over three independent biological replicates. Letters on the boxplot highlight significant differences between treatments identified by ANOVA test (P<0.05) followed by Tukey HSD post-hoc test (adjusted P<0.05). (**C**) Principal coordinates analysis (PCoA) of Bray-Curtis dissimilarities between bacterial microbiota compositions of tomato plants inoculated with *Vd* WT or Vd Δ*424Y*. Results of a PERMANOVA test revealing the significant difference of tomato microbiota compositions between *Vd* WT- and Vd Δ*424Y*-inoculated conditions are displayed above the PCoA.

Vd424Y evolved to manipulate plant physiology by locating to host cell nuclei

Vd424Y was previously demonstrated to localize into chloroplasts and nuclei of host cells and, accordingly, carries a chloroplast transit peptide (cTP) and a nuclear localization signal (NLS) (31, 32). While the cTP is sparsely detected throughout the Vd424Y family (fig. S18, A) and shows a high degree of sequence variation (fig. S18, B), the occurrence of the NLS is restricted to a single clade that is exclusively composed of proteins secreted by plant pathogens and endophytes from the Sordariomycete genera *Verticillium, Fusarium* and *Cylindrocarpon* (Fig. 5, A and fig. S18, A), which diverged about 250 million years ago (41). This observation suggests that, contrary to antimicrobial properties, the plant cell nuclear localization that is required for immunomodulation and cytotoxicity *in planta* (31) is a trait that emerged recently in the family of Vd424Y homologs. We hypothesized that homologs of Vd424Y from saprotrophic fungi do not exert immunomodulatory and cytotoxic effects *in planta*, given that these fungi do not typically live in association with plants and that these traits are mediated by the NLS. To address this hypothesis, we selected two orthologs of Vd424Y, secreted by the basidiomycete *C. cinerea* and the ascomycete *Penicillium restrictum*, that we named Cc424Y and Pr424Y, respectively. Following *Agrobacterium*-mediated transient effector gene expression in *Nicotiana benthamiana* leaves, we observed that Vd424Y caused cell death, in line with previous reports (31, 32). Importantly, the Cc424Y and Pr424Y homologs did not cause cell death in *N. benthamiana* (Fig. 5, B and fig. S19). This finding corroborates the recent evolution of plant immunomodulatory functions in the 424Y effector family, as it highlights that (a relatively recent ancestor of) *V. dahliae* repurposed this ancient antimicrobial protein for host manipulation. We furthermore tested whether the acquisition of the NLS is sufficient for such neofunctionalization by engineering a chimeric Pr424Y variant that comprises the NLS of *Vd424Y* (Pr424Y-NLS). Strikingly, *Agrobacterium*-mediated expression of this variant in *N. benthamiana* leaves resulted in clearly visible cell death, showing that the *P. restrictum* 424Y homolog gained the capability to manipulate host physiology (Fig. 5, B). Through fluorescent confocal microscopy, we observed that Vd424Y localized to the nuclei of *N. benthamiana* leaf cells upon transient gene expression, in contrast to Cc424Y and Pr424Y. However, like Vd424Y, also the artificially engineered Pr424Y variant that contains the NLS of Vd424Y could be found in the nucleus, confirming that cell death induction depends on the nuclear localization of the effector (Fig. 5, C). Together, these results suggest that the recent evolution of an NLS underlies the host immunomodulatory functions of Vd424Y by mediating its localization in host nuclei.

We finally hypothesized that in absence of an NLS, Vd424Y homologs support diverse fungal lifestyles by serving functions in microbial antagonism. We tested whether Pr424Y contributes to fungal niche colonization by comparing the capacity of *P. restrictum* wild-type and a Pr∆*424Y* gene deletion mutant to colonize soil in presence and absence of a resident microbiota. Concordant with a role in microbial competition, no significant difference in colonization was observed following inoculation of *P. restrictum* in sterilized soil. However, although fungal colonization in natural soil was greatly reduced when compared with growth in sterilized soil due to the presence of microbial competitors, in presence of a soil-associated microbiota, Pr∆*424Y* mutants displayed a significantly reduced soil colonization when compared with wild-type *P. restrictum*. This finding suggests that ancient antimicrobial properties of 424Y proteins underly diverse fungal lifestyles by supporting the colonization of various niches through microbial antagonism.

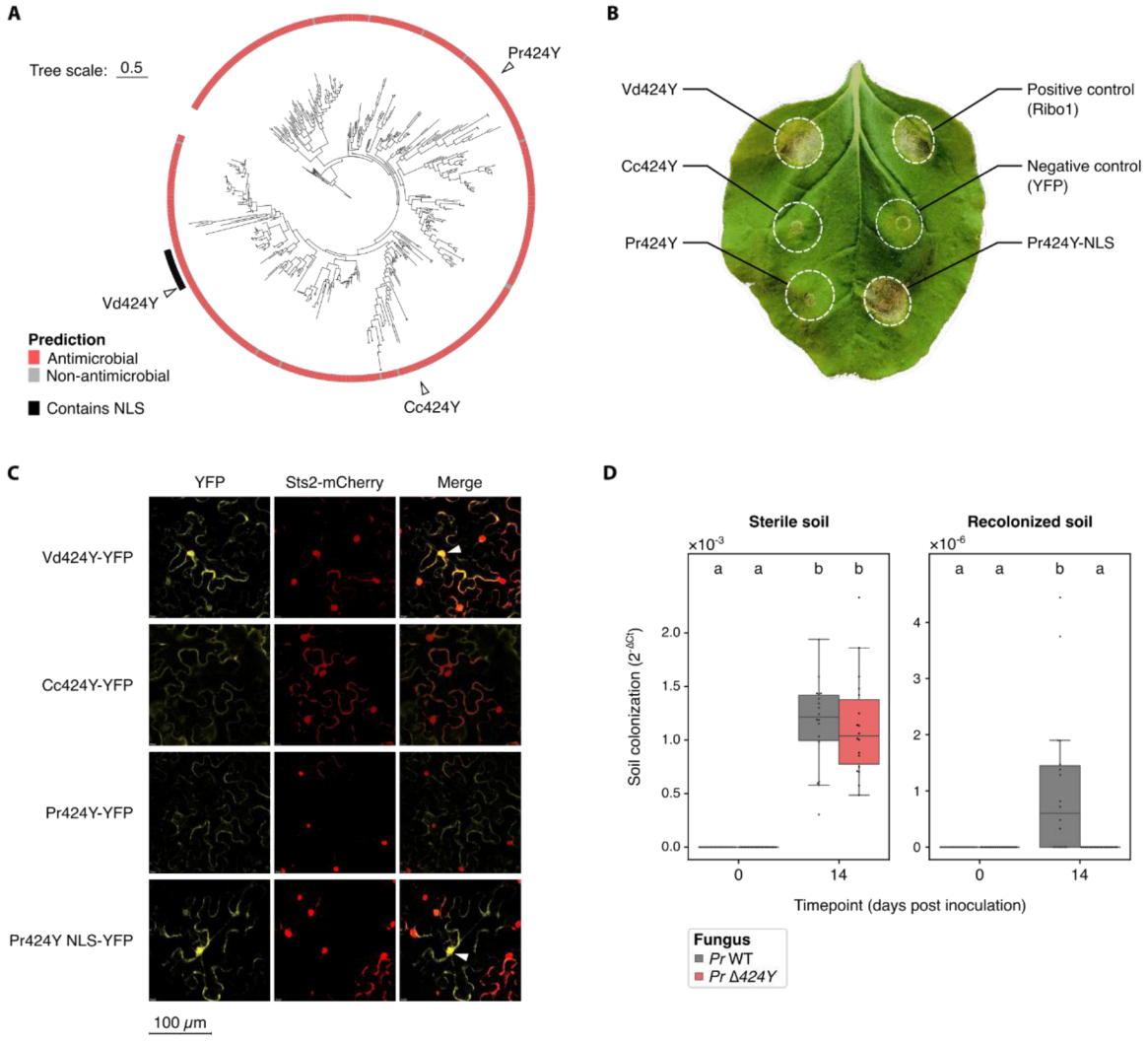

Fig. 5. Evolutionary and functional analysis of the Vd424Y family. (**A**) Maximum-likelihood phylogenetic tree (computed with IQ-TREE (88), model 'LG') of Vd424Y homologs in a dataset of 150 fungal genomes (as in fig. S5), supplemented with the orthologs of Vd424Y identified in the genomes of *Coprinopsis cinerea* (Cc424Y) and *Penicillium restrictum* (Pr424Y). The tree is annotated with the results of antimicrobial activity prediction as well as the occurrence of a nuclear localization signal (NLS), annotated using cNLS Mapper (93). The annotated NLS sequences in the effector family are all identical (fig. S17, B). (**B**) Photograph of a representative *Nicotiana benthamiana* leaf in which proteins were transiently expressed by *Agrobacterium*-mediated transformation. Leaf areas that were infiltrated are circled by dotted white lines and annotated with the names of the genes that were transiently expressed. In addition to Vd424Y, Cc424Y, Pr424Y, the positive control Ribo1 (11) and the negative control YFP, a chimeric variant corresponding to Pr424Y that carries the NLS of Vd424Y ("Pr424Y-NLS") was transiently expressed. Photographs showing experimental replicates are displayed in fig. S19. (**C**) Fluorescent confocal microscopy photographs displaying the localization of effector proteins fused to yellow fluorescent protein "YFP". in *N. benthamiana* cells following *Agrobacterium*-mediated transient gene expression. From top to bottom: Vd424Y, Cc424Y, Pr424Y and Pr424Y-NLS. The first column shows the localization of effectors, detected by YFP fluorescence signal. The second column shows localization of the mCherry-tagged nuclear localized effector protein Sts2 as a positive control (110). The third column shows merged YFP and mCherry signals; white arrowheads point to plant cell nuclei in which both effector proteins were detected. (**D**) Soil colonization by wild-type *P. restrictum* (Pr WT) and a deletion mutant lacking the Pr424Y gene (PrΔ*424Y*), in sterilized soil (left) and sterilized soil that was recolonized with soil microbes (right). Colonization was quantified with real-time PCR with species-specific primers and normalized to an artificial spike-in plasmid added before DNA extraction ($2^{-\Delta Ct}$). Letters on the boxplots indicate significant differences according to Kruskal-Wallis ($P < 0.05$) and post-hoc Dunn test (adjusted $P < 0.05$).

Discussion

Before plants colonized land about 500 million years ago, fungi lived as saprotrophs and/or parasites of bacteria and primitive algae in (semi)aquatic environments (42). The study of a 600 million years-old fossil found evidence of a symbiosis between a fungus and an auxotrophic organism, highlighting the ancient origins of fungi-plant interactions (43). However, pathogenicity towards land plants represents a relatively recent trait in the 1.5 billion year-long fungal evolutionary history, which evolved multiple times independently across the fungal tree of life (44). Effector-based strategies to manipulate host physiology are essential for the pathogenic lifestyle (5, 6), yet their evolutionary origins remained elusive. The broad conservation of certain effector families throughout the fungal kingdom (Fig. 3, B), together with their occurrence in fungi that do not colonize plants, demonstrates ancient origins of these effectors and suggests their primary roles beyond plant host manipulation. Since antimicrobial effectors are likely secreted upon encountering plant microbiota epiphytically and in the apoplast of host tissues, they may be particularly prone to evolve functions to manipulate host physiology through interactions with host surface and apoplastic proteins. However, our findings that underpin an evolutionary history of Vd424Y through the acquisition of a NLS (Fig. 5) demonstrates that some antimicrobial effectors acquired *in planta* functions by evolving intracellular localization. Thus, many effector proteins with diverse *in planta* modes of action have ancestral antimicrobial properties, indicating that microbial antagonism is a fundamental effector role that likely supported fungal fitness in (semi)aquatic environments prior to the evolution of fungal pathogenicity towards land plants (28). In line with this discovery, previous studies identified peptides with dual functions in microbial antagonism and immunity modulation, suggesting these two protein activities may often co-occur given their functional complementarity (45, 46). Moreover, a recent study identified that changes in protein domain organization may have repurposed an effector from antimicrobial to immunomodulator, thereby mediating a recent fungal lifestyle transition from saprotroph to plant symbiont (47). Hypothetically, the co-option of antimicrobial proteins for host manipulation mediated the compatibility of the first fungal symbioses with land plants and predates the evolution of a plethora of other molecular mechanisms that underly more specific pathogenic interactions. Indeed, some fungal effectors represent recent innovations, as evidenced by their lineage-specificity, and likely result from fungal adaptation to specific plant lineages (15, 48). Such effectors are generally thought of as products of co-evolutionary “arms races” in which plant immune systems and fungi aim to detect and overcome detection, respectively (1, 3). While this study focuses on the occurrence of antimicrobial properties among the most conserved effector families, it paves the way for further research on effector evolution, particularly to

investigate how recently evolved antimicrobial effectors may mediate host and niche adaptation (49). More generally, this study, and more particularly the AMAPEC software, will support the discovery of novel fungal antimicrobial proteins and assist studies on their modes-of-action, which currently remain largely unknown. Furthermore, the broad variety of fungal secreted antimicrobials and their crucial role in supporting host colonization are important factors to consider when designing novel biocontrol strategies to protect crops efficiently from pathogenic fungi. Finally, the evolutionary trajectories identified in this study are likely to be relevant beyond plant colonization, given the need for human- and animal-pathogenic fungi to manipulate immune responses of their hosts during infection too (50).

Materials & Methods

Curation of a training dataset for antimicrobial activity prediction

To develop the AMAPEC predictor, a positive training set of antimicrobial proteins (table S1) was curated from literature. Only proteins for which antimicrobial activity has been experimentally demonstrated in vitro (i.e. restricting the growth of bacteria and/or fungi in culture medium) were selected. While not restraining the dataset to proteins encoded by any phylogenetic group, we paid particular attention to include all the fungal antimicrobial proteins reported in scientific literature. Importantly, secretion signal peptides were removed from sequences (SignalP v6.0 (51)), since the antimicrobial function of proteins occurs after secretion. Considering sequence lengths of fungal secreted proteins, peptide with mature sequence lengths below 40 amino acids were excluded (fig. S1), not to enrich the protein set in AMPs, for which dedicated predictors exist (19, 52–56). By largely spanning the size range of typical effector proteins, this protein set should support the prediction of effector antimicrobial activity without bias towards the recognition of short AMPs, that are the most described antimicrobial proteins in the literature.

A negative training dataset was assembled by gathering presumable non-antimicrobial proteins (table S2). As previously suggested (19, 53), this negative set was curated by retrieving proteins which functional annotation does not suggest any antimicrobial activity from the UniProt database (57). To do so, Gene Ontology (GO) terms associated to antimicrobial activity were filtered out (i.e. GO:0090729, GO:0001878, GO:0045087, GO:0050830, GO:0050829, GO:0042742, GO:0071222, GO:0071224, GO:0001530, GO:0031640, GO:0050832). Additionally, only well-annotated proteins without any known function in microbial antagonism or immunity were selected. To prevent strong effects of potential misjudgment during the curation process, the negative training dataset includes twice as many non-antimicrobial proteins as there are antimicrobials in the positive set. For each antimicrobial in the positive set, two presumably non-antimicrobial proteins encoded by the same organism (or a close relative) and with similar sizes (+/- 4 amino acids) were included in the negative set. We paid attention to include at least as many secreted proteins (signal peptide detected and removed with SignalP (51)) in the negative set as in the positive set, not to bias the prediction towards apoplastically released proteins. Finally, since 11 proteins in the positive training set were annotated or described as ribonucleases, 11 ribonucleases, unlikely to exert antimicrobial functions according to their annotation (for instance, involved in transfer RNA maturation) were included in the negative set.

Classifier training and quality estimation

Numerical variables reflecting properties of our 456 proteins were standardized using function preprocessing.StandardScaler() of Python library scikit-learn v1.2.1 (69). Then, a Support Vector Machines (SVM) classifier with a linear kernel was trained using function svm.SVC() from scikit-learn. The correct the imbalance of the training set (152 proteins in the positive set and 304 in the negative set), the weight of antimicrobials was set to 2 and the weight of non-antimicrobials to 1. A second model was trained to predict the probability of antimicrobial activity, by computing Platt scaling over the SVM binary classifier. To do so, the function calibration.CalibratedClassifierCV(method='sigmoid', cv='prefit') from sci-kit learn was used. Both models were exported using function dump() from Python library joblib v1.2.0.

Due to the small size of the training dataset (n=456), classifier quality testing was performed through leave-one-out cross-validation. As implemented in function cross_val_score(cv=KFold(n_splits=456)) of scikit-learn, 456 SVM classifiers were trained with a train/test split of 455/1 to classify individual proteins using as a basis, protein properties in the rest of the dataset. Protein classifications into "antimicrobial" or "non-antimicrobial" were then analyzed by counting numbers of true positives, false positives, true negatives and false negatives. These counts allowed the estimation of the overall classifier accuracy (R2) but also its precision, recall, specificity and F-score. Such quality estimates were also calculated by exclusively taking the classification correctness of fungal proteins into account, to identify if the predictor is suited for the annotation of fungal proteins. Finally, the predictor was tested on seven recently characterized fungal proteins demonstrated to have antimicrobial activities (22–26), after structure prediction with ESMFold v1.0.3 (70) (table S4).

A bash pipeline allowing both the calculation of protein properties and antimicrobial activity prediction using the trained predictors was written, resulting in the software AMAPEC v1.0 (https://github.com/fantin-mesny/amapec), (developed and tested on operating system GNU/Linux Ubuntu v20.04.3 LTS).

Secretome analysis on three phylogenetically distant fungi

Sets of proteins associated to the published genomes of three phylogenetically distant fungi with distinct lifestyles were downloaded: Verticillium dahliae JR2 (71) (annotation VDAG_JR2 v.4.0 downloaded from the database Ensembl Fungi (72)), Coprinopsis cinerea AmutBmut pab1-1 (73) (annotation Copci_AmutBmut1 v1.0 downloaded from the database JGI Mycocosm (74)) and Rhizophagus irregularis DAOM197198 (75). SignalP v6.0 (51) was then used to predict secretion signal peptides in protein sequences and thereby define the

secretomes of these fungi. Sequences with removed signal peptides were used in all subsequent analyses. Functional annotation of proteins in these secretomes was carried out using emapper v2.0 (76) and the database EggNog v5 (77). CAZymes and transmembrane proteins were specifically annotated in these secretomes using dbCAN v4.0 and TMBed v1.0.0 respectively (78, 79). Structure predictions were computed with ESMFold v1.0.3 (70), using default parameters, of all secreted proteins besides CAZymes. The structures of two proteins from V. dahliae (VDAG_JR2_Chr4g10970 and VDAG_JR2_Chr1g22375) could not be predicted due to high computational requirements linked to their size (>2500 amino acids) and were excluded from our analyses. To validate that the quality of protein structures predicted by ESMFold is sufficient, structure prediction for 626/635 non-CAZyme secreted proteins of V. dahliae was also performed with AlphaFold v2.0 (59) with parameters --max_template_date=2021-05-14 --preset=casp14, with nine predictions failing due to high computational requirements. Average structure pLDDT values were compared between AlphaFold and ESMFold (fig. S20). Then, AMAPEC v1.0 was used to predict the antimicrobial activity of proteins secreted by *V. dahliae*, *C. cinerea* and *R. irregularis*, while excluding CAZymes and transmembrane proteins. ESMFold (70)-predicted structures, which pLDDT confidence scores are in tables S5-7, were used as an input. To analyze the conservation of predicted antimicrobials and non-antimicrobials, an orthology prediction was computed on the three fungal secretomes with OrthoFinder v2.5.5 (80). The conservation of antimicrobials and non-antimicrobials was studied independently, after subsetting the OrthoFinder-generated ‘orthogroups’ tables to only contain proteins from each group.

Comparative genomics in a dataset of 150 fungal genomes

A set of 150 fungal genomes was assembled, based on a previously published dataset of 120 fungal genomes for which fungal lifestyles had been manually curated (81). This dataset was supplemented with 23 genomes of plant-pathogenic fungi and 7 genomes of Glomeromycetes (see details in table S8). An orthology prediction was performed on total sets of annotated proteins with OrthoFinder v2.5.5 (80) to generate a phylogenomic tree with the implemented method ‘STAG’ (82). This genome-scale phylogeny is displayed on Fig. 2D and fig. S4. In all 150 genomes, sets of proteins carrying SignalP v6.0 (51)-annotated signal peptides were considered to form secretomes. A second orthology prediction with OrthoFinder v2.5.5 was performed on these 150 secretomes. In each secreted protein family (i.e. ‘orthogroup’) defined by this orthology prediction, the most central and representative protein was identified with phylorep v0.1 (83) using OrthoFinder-generated gene trees (relying on method FastTree (84)) as inputs. CAZymes and transmembrane proteins among these family representatives were

annotated using dbCAN v4.0 and TMBed v.1.0.0, respectively (78, 79). The structures of other representative proteins were predicted with ESMFold v1.0.3 (70) then submitted to antimicrobial activity prediction with AMAPEC v1.0. Protein family conservation analyses were performed considering the presence/absence of families in each genome (i.e. considering the occurrence of orthologs but not the numbers of paralogs). Specifically, each family was assigned a conservation level according to the clade (phylum, class, order, family or genus) its occurrence is restricted to, in the 150 genome dataset. Proportions of protein families which representative members are predicted antimicrobials/non-antimicrobials were analyzed, excluding CAZyme- and transmembrane protein-encoding families. Then, sequence diversity within the 600 most conserved secreted protein families (excluding CAZymes) was estimated through k-mer based Shannon index calculation with MerCat2 v1.0 (68) using a k-mer size of 3 amino acids.

Analysis of predicted antimicrobials in PHI-base

Sequences of proteins that have been studied for their contribution to host-pathogen interactions were downloaded from the PHI-base database (36) (accessed in January 2024). To identify proteins previously studied for their contribution to fungal virulence in the *V. dahliae* JR2 secretome, SignalP v6.0 (51)-predicted secreted proteins in the *V. dahliae* genome were blasted against the downloaded PHI-base sequences using blastp v2.5.0 with parameters -evalue 0.0001 -max_target_seqs 1 and additional filtering to only keep hits with more than 95% sequence identity to query proteins (table S10). To investigate more generally if previously characterized fungal effectors have antimicrobial activities, the PHI-base dataset was subsetted to only retain proteins from fungi that have secretion signal peptides according to SignalP v6.0 (51) and that were classified as “effectors (plant avirulence determinants)” in the database. After structure prediction with ESMFold v1.0.3 (70), the antimicrobial activity of these proteins was predicted with AMAPEC v1.0. To estimate the conservation of these effectors across the fungal kingdom, the protein family of the most similar protein in the 150-genome dataset was considered and the number of genomes in which it occurs was used as a proxy for effector conservation (Fig. 3, A). To identify previously characterized fungal effectors with confidently predicted antimicrobial activity and broad conservation across the fungal kingdom (Fig. 3, B), the following filtering criteria were used: highly confident effector structure prediction with an average pLDDT>70, predicted antimicrobial activity, presence of an effector homolog with more than 80% sequence identity in the 150-genome dataset and representation of the associated family in more than 100/150 genomes.

Effector protein production and purification

For heterologous production of the AGLIP1, AVR-Pita, Ecp6, Vd424Y and VdCP1 effectors, protein sequences were retrieved from PHI-base (36), then codon-optimized nucleotide sequences encoding for mature proteins were subcloned into pET-15b (AVR-Pita, Vd424Y, AGLIP1), pET-28a(+) (VdCP1) or pETSUMO (Ecp6) expression vectors. All the constructs with an N-terminal His6 tag (Gene Universal, Newark, DE, USA) were transformed into *Escherichia coli* BL21 or Shuffle cells by heat shock (45 s at 42 °C, 5 min on ice). The transformed BL21 cells (AGLIP1, AVR-Pita, Vd424Y and VdCP1) were grown at 37 °C with constant shaking at 180 rpm in 2x YT medium (16 g/l tryptone, 10 g/l yeast extract, 5 g/l NaCl) containing 100 µg/ml ampicillin. Protein production was induced with 1 mM isopropyl-ß-d-thiogalactoside (IPTG) when cultures reached an optical density (OD600) of 2.0. Induction was performed for 2 h at 37 °C for AVR-Pita and Vd424Y, 4 h at 37 °C for AGLIP1, and 2 h at 42 °C for VdCP1, all with constant shaking at 180 rpm. For protein extraction, the bacterial cells were pelleted and then resuspended in denaturing 6 M guanidinium chloride (GdmCl), 10 mM β-mercaptoethanol and 10 mM Tris, pH 8.0, and incubated overnight at 4 °C with continuous rotation. The lysate was centrifuged at 16,000 × g for 1 h and the resulting cleared supernatant was collected for protein purification by metal affinity chromatography using a nickel His60 Ni Superflow Resin (Takara, San Jose, CA, USA) column in the ÄKTA go™ protein purification system (Cytiva, Marlborough, MA, USA). After column equilibration with 6 M GdmCl, 10 mM Tris at pH 8.0, denatured protein was loaded onto the column and weakly bound protein was washed off with 6 M GdmCl, 10 mM Tris, 20 mM Imidazole at pH 8.0 before the His6-tagged protein was eluted with 6 M GdmCl, 10 mM Tris, 200 mM Imidazole at pH 8.0. Purified proteins were dialyzed (Spectra/Por™ 3 RC Dialysis Membrane Tubing 3500 Dalton molecular weight cut-off; Spectrum Laboratories – Rancho Dominguez, CA, USA) sequentially against 20 volumes of buffers with decreasing GdmCl concentrations (table S17) to promote refolding. Each dialysis step lasted a minimum of 24 h. Finally, depending on their isoelectric point, the proteins were dialyzed twice against 200 volumes of 30 mM sodium phosphate buffer (pH 7.0 for Vd424Y, pH 5.8 for AGLIP1) or 30 mM potassium phosphate buffer (pH 7.5 for AVR-Pita, pH 6.5 for VdCP1). Final concentrations were determined with a Qubit 4 Fluorometer (Invitrogen – Waltham, MA, USA). For the heterologous protein production of Ecp6 (85, 86), *E. coli* Shuffle cells carrying pETSUMO-Ecp6 were grown at 37°C in lysogeny broth (LB) containing 50 µg/mL kanamycin until an OD600 of 0.8. Protein expression was induced with 0.2 mM IPTG, followed by incubating at 18°C overnight. Cells were pelleted and resuspended in cell lysis buffer (50 mM Tris-HCl pH 7.5, 150 mM NaCl, 10% glycerol, 6 mg/ml lysozyme, 2 mg/ml deoxycholic acid, 60 µg/ml DNase I (Roche – Basel, Switzerland; ref. 04536282001) and one protease inhibitor cocktail pill (Roche; ref. 11836170001)), then

incubated either at room temperature for 3 h or at 4 °C overnight with stirring. The lysate was centrifuged at 20,000 × g for 1 h, and the cleared supernatant was collected for protein purification. His6-tagged SUMO-Ecp6 was purified using His60 Ni Superflow Resin, pre-equilibrated with 20 mM Tris, 150 mM NaCl, 5 mM imidazole, pH 8.0. Bound protein was eluted with 20 mM Tris, 150 mM NaCl, 300 mM imidazole, pH 8.0. The His6-SUMO affinity tag was removed by incubation overnight with ULP-1 protease (Sigma-Aldrich – St. Louis, MO, USA; ref. SAE0067) in dialysis buffer (20 mM Tris, 100 mM NaCl, 2% glycerol, pH 8.0). Non-cleaved fusion protein was removed by a second round of affinity purification using His60 Ni Superflow resin, and the flow-through containing cleaved Ecp6 was dialyzed overnight. The final protein concentration was determined spectrophotometrically at 280 nm.

In vitro microbial growth inhibition assays

A diverse set of twelve bacteria previously isolated from tomato plants (40) were grown on LB agar plates at room temperature in the dark, then transferred into low-salt tryptic soy broth (ls-TSB; 17 g/l tryptone, 3 g/l soy peptone, 0.5 g/l sodium chloride, 2.5 g/l dipotassium phosphate, and 2.5 g/l glucose) and grown overnight at 28 °C while shaking at 180 rpm. Overnight cultures were resuspended to the final OD600 = 0.025 in equal parts of fresh ls-TSB and AVR-Pita, Vd424Y, AGLIP1, VdCP1 or Ecp6 in phosphate buffer of the corresponding pH (see above; final protein concentration: 8 µM) or in the respective phosphate buffer only as a control. Total volumes of 100 µl were incubated in clear 96-well flat-bottom polystyrene tissue culture plates in a CLARIOstar plate reader (BMG Labtech – Ortenberg, Germany) at 25 °C with double orbital shaking every 15 minutes (10 seconds at 300 rpm). The optical density was measured every 15 minutes at 600 nm. After OD600 normalization, areas under curves in presence and absence of effector proteins were calculated using the trapezoidal method.

Four yeasts, i.e. *Pichia pastoris* GS115, *Cyberlindnera jadinii* (DSM 70167), *Debaryomyces vanrijiae* (DSM 70252) and *Rhodotorula bogoriensis* (DSM 70872), were grown on potato dextrose agar (PDA; ROTH – Karlsruhe, Germany, ref. X931) at room temperature in the dark then transferred into 0.05X potato dextrose broth (PDB) and grown overnight at 25 °C while shaking at 180 rpm. Overnight cultures were resuspended to the final OD600 = 0.025 in equal parts of fresh 0.05X PDB and AVR-Pita, Vd424Y or AGLIP1 in phosphate buffer of the corresponding pH (see above; final protein concentration: 8 µM) or in the phosphate buffer only as a control. Additionally, spores from filamentous fungal strains of *Alternaria brassicicola*, *Cladosporium cucumerinum, Trichoderma viride* (from our in-house culture collection) were harvested from PDA plates after culture at room temperature in the dark, then separated from the mycelium with a sterile 40 µm nylon filter (VWR – Radnor, PA, USA) and suspended in

equal parts of 0.05X PDB and AVR-Pita, Vd424Y or AGLIP1 in phosphate buffer of the corresponding pH (see above; final protein concentration: 8 µM) or in the respective phosphate buffer only as a control to a final concentration of 104 spores/ml. Total volumes of 100 µl were incubated in clear 96-well flat-bottom polystyrene tissue culture plates at 25 °C overnight. For both filamentous fungi and yeasts, fungal growth was imaged using an CKX41 inverted microscope (Olympus – Shinjuku City, Japan) with DP20 camera (Olympus). Images were analyzed with ImageJ (87): Each image was first subjected to binarization and next to particle analysis to measure total particle area.

Analysis of the evolutionary histories of effectors with validated antimicrobial activities

The evolutionary histories of effectors AGLIP1, AVR-Pita, Vd424Y and VdCP1 were analyzed by reconstructing the protein family phylogenies. All sequences in the protein families (defined through orthology prediction in the 150-genome dataset) including these effectors were used to reconstruct maximum-likelihood phylogenetic trees using IQ-TREE v2.0.3 (model 'LG', default settings) (88) after multiple sequence alignment with MAFFT v7.310 (default parameters) (89). Since fungal LysM effectors are thought to represent a single effector family but exhibit large sequence diversity and therefore occur in multiple protein families defined by orthology prediction, the LysM effector family was identified through functional annotation, following a previously introduced procedure (34). In the 150-fungal genome dataset, and additionally in the genome of the fungus *Cladosporium fulvum* which secretes the well-characterized Ecp6 LysM effector (37), functional domains were annotated using InterProScan v5.65-97.0 (90). Secreted proteins containing LysM domains (IPR036779, IPR018392, IPR045030), but not any other functional domains (e.g. chitinase domains), were considered as LysM effectors. All annotated LysM effectors were used to reconstruct a protein phylogenetic tree with IQ-TREE (model 'LG') after sequence alignment with MAFFT, as performed for the four other effector families. In all five effector families, antimicrobial activities were predicted using AMAPEC v1.0 after structure prediction with ESMFold v1.0.3 (70). Protein family phylogenetic trees were visualized and annotated with antimicrobial activity prediction results using iTOL (91).

The recent evolution of the Vd424Y effector family was further studied focusing on the subfamily (clade identified on the total protein family tree, fig. S5) containing Vd424Y. As previously (32), chloroplastic transit peptides and nuclear localization signals were annotated using ChloroP v1.1 (92) and cNLS Mapper (93) (used online with default parameters in May 2025: https://nls-mapper.iab.keio.ac.jp/), respectively. To analyze sequence variations in the

Vd424Y subfamily, subfamily-members were aligned using MAFFT and a figure was generated with iTOL (91), referring to a previously published domain annotation of Vd424Y to highlight the domain organization of the proteins (32).

Measurements of *V. dahliae* effector gene expression in soils

Soil extracts were prepared from 10 previously sampled soils with distinct properties and microbial communities (94). To do so, 20 g of soil (stored at 4 °C) were mixed with 100 ml of sterile water (1:5, w/v) followed by incubation at room temperature for 2 days. Soil particles were removed by centrifugation at 4,000 × g for 30 min, and the resulting supernatant was used as soil extract.

Conidiospores of *V. dahliae* JR2 were harvested from mycelium cultured on PDA plates for 7 days. The spores were washed once with sterile water and collected by centrifugation at 10,000 × g for 2 min. Spore concentration was determined by counting with a hemocytometer, and 1×10^6 spores were inoculated into 10 ml of PDB in 50 ml flasks. Cultures were incubated at 22 °C with shaking at 130 rpm for 2 days. Mycelia were then collected, rinsed with sterile water, and transferred into 10 ml of prepared soil extracts in new 50 ml flasks. After 2 days of incubation, the mycelia were collected using Miracloth, rinsed with sterile water, and blotted dry with tissue paper. The samples were transferred to 2 ml tubes containing two 2.3 mm iron beads, flash-frozen in liquid nitrogen, and ground using a tissue lyser. Total RNA was extracted using TRIzol reagent (Thermo Fisher Scientific – Waltham, MA, USA). For each sample, 500 ng of RNA was reverse transcribed using the HiScript® III RT SuperMix for qPCR (+gDNA Wiper) (Vazyme Biotech Co., Ltd. - Nanjing, China; ref. R323-01). The resulting cDNA was diluted 10 fold with nuclease-free water. Quantitative real-time PCR was performed using SsoAdvanced™ Universal SYBR® Green Supermix (Bio-Rad, Hercules, CA, USA). Primers 5'-TGTTACCAAAGCAGCACACAAGG-3' and 5'-CCTTATGCCTCGTTCCCTTCCAC-3' were used to amplify the Ave1-encoding gene (positive control, (7)), primers 5'-GCAAGCGAGGACTGACAAGATC-3' and 5'-CGACGGAATGGACGGCGTG-3' were used to amplify the Tom1-enconding gene (negative control, (95)), newly designed primers 5'-TCGGGCGGTTTCTACTACTC-3' and 5'-TGTTGTTCTTCCAGCTGACG-3' were used to amplify the Vd424Y-encoding gene (VDAG_JR2_Chr5g00880), and the primers 5'-CGAGTCCACTGGTGTCTTCA-3' and 5'-CCTCAACGATGGTGAACTT-3' were used to amplify the glyceraldehyde 3-phosphate dehydrogenase gene (GAPDH, house-keeping gene). The PCR cycling conditions were as follows: initial denaturation at 95 °C for 3 mins, followed by 40 cycles of denaturation at 95 °C for 10 s and annealing/extension at 60 °C for 30 s with fluorescence signal collection. After amplification, a melt curve analysis was

performed from 65 °C to 95 °C, increasing by 0.5 °C every 5 seconds, to verify the specificity of the PCR products. Gene expression levels of effector genes were normalized to the *V. dahliae GAPDH* using the ΔCt method.

Vd424Y gene deletion in *Verticillium dahliae*

Gene deletion was performed following previously published protocols for *V. dahliae* protoplast transformation (96) and CRISPR-Cas9-based fungal genome editing (97). After culturing on PDA plates at room temperature for 7-15 days in the dark, 3×107 spores of *V. dahliae* JR2 were harvested from the mycelium surface and inoculated into 100 ml of liquid Complete Medium (CM) composed of 0.6% yeast extract (Duchefa – Haarlem, The Netherlands; ref. Y1333), 0.6% casein hydrolysate (ROTH; ref. AE41) and 1% sucrose (VWR; ref. 0335) in milli-Q water. After 20 hours in culture at 28 °C with agitation, mycelium was harvested on a Falcon® 40µm nylon filter (ref. 352340) and washed with a sterile 0.7 M NaCl solution. Then, the harvested mycelium was incubated in 10 ml of sterile-filtered driselase solution (0.2% of enzyme in 0.7 M NaCl, Sigma-Aldrich – St. Louis, MO, USA; ref. D9515) for 2.5 hours at 33 °C with agitation. The resulting solution was passed through a 40 µm nylon filter, then centrifugated at 3000 × g for 5min. After supernatant removal, the protoplast pellet was resuspended in 1 ml of sterile STC (20% Sucrose, 10 mM Tris-HCl pH 8.0 and 50 mM CaCl2 in milli-Q water) and centrifuged at 3000 × g for 5 min. This last step was repeated twice to thoroughly wash the protoplasts. Protoplasts were counted under a microscope, and their concentration was adapted to 5 × 106 protoplasts/ml in STC. After adding 1% of DMSO, protoplast solutions were kept at -80 °C.

To delete the gene of interest, two single guide RNA (sgRNA) were designed using CRISPick (https://portals.broadinstitute.org/gppx/crispick/public) to target the upstream and downstream regions of the Vd424Y-encoding gene (VDAG_JR2_Chr5g00880): CATACGTCCTGTTCAGCCGG (upstream) and GCCATCCGACCAGCATTCAG (downstream). A blastn was performed (with parameter --word_size 11) to check that these sgRNA protospacer sequences only occur near the targeted gene in the V. dahliae JR2 genome. Oligonucleotides with sequences corresponding to the designed sgRNA protospacer in between sequences 5'-AAGCTAATACGACTCACTATA-3' and 5'-GTTTTAGAGCTAGAAATAGCAAG-3' were ordered. To synthesize sgRNA from these oligonucleotides, 1 µl of oligonucleotide (100 µM) was mixed with 1 µl of oligonucleotide 5'-AAAAGCACCGACTCGGTGCCACTTTTTCAAGTTGATAACGGACTAGCCTTATTTTAACTT GCTATTTCTAGCTCTAAAAC-3' (100 µM) and 8 µl of nuclease-free water. This mixture was incubated in a thermocycler for annealing with the following program: 95 °C for 5 min, 95 °C

to 85 °C at 2 °C/sec, 85 °C to 25 °C at -0.1 °C/sec. Then, 2.5 µl of dNTPs (10 mM each), 2 µl of NEBuffer™ r2.1 (10X, New England Biolabs – Ipswich, MA, USA; ref. B6002S), 0.5 µl T4 DNA polymerase (New England Biolabs; ref. M0203S) and 5 µl nuclease-free water were added to the mixture, followed by an incubation at 12 °C for 20 min. Products of this reaction were purified with a Monarch® PCR & DNA Cleanup Kit (New England Biolabs; ref. T1030L). Concentration in DNA was then measured with a NanoDrop device. To transcribe the DNA molecules into sgRNA, 2 µg of DNA was mixed with 6µl of RNA NTPs (25 mM each), 1.5 µl of T7 buffer (10X), 1.5µl of HiScribe® T7 polymerase (New England Biolabs; ref. E2040S), 1 µl of DTT (0.1 M) and nuclease-free water up to 20 µl total volume. After incubation overnight at 37 °C, 14 µl of nuclease-free water, 4 µl of RQ1 DNase buffer (10X, Promega – Walldorf, Germany; ref. M198A) and 2 µl of RQ1 DNAse (Promega; ref. M610A) were added in the reaction tube. An incubation of 30 min at 37 °C followed to digest remaining DNA. sgRNA molecules were then purified using RNA Clean & Concentrator (Zymo Research – Irvine, CA, USA; ref. R1017 & R1018) kit. Purified sgRNA were stored at -80 °C until transformation.

Double-stranded donor DNA corresponding to the 50 bp-sequence upstream of the expected Cas9-mediated cut in the fungal genome, followed by the 50 bp-sequence downstream of the second expected cut was synthesized. Through homologous recombination, this donor DNA promoted genome repair excluding our target gene upon double-stranded cuts by Cas9.

The commercial enzyme EnGen® Spy Cas9 HF1 (New England Biolabs; ref. M0667M) was used for protoplast transformation. First, 4 µM of this Cas9 enzyme was mixed to 2X of NEBuffer™ r3.1 (New England Biolabs; ref. B6003S) and 0.3 µg/µl of sgRNA. The mixture was incubated at 25 °C for 30 min to bind sgRNA and enzyme. Both prebound Cas9-sgRNA complexes were then mixed with 200 µl of fungal protoplasts (5 × 106 protoplasts/ml), 20 pmol of double-stranded donor DNA and 6 µg of telomeric vector pTEL-Hyg (97) containing a hygromycin resistance gene. After 30min of incubation on ice, 1.5 ml of PEG-STC (60% polyethylene glycol 4000, 20% of sucrose, 10 mM of Tris-HCl pH 8.0 and 50 mM CaCl2 in milli-Q water) was added to the mixture and gently mixed by tube rotation. This tube was incubated at room temperature for 15 min. Then, 5 ml of TB3 medium (3% yeast extract, 3% casein hydrolysate and 20% sucrose in water) were added to the mixture, stimulating protoplast regeneration over an 18 hour-incubation in the dark at room temperature.

Regeneration medium was centrifuged at 3000 × g for 5 min. The supernatant was removed and pelleted fungi were resuspended in sterile water to be plated on PDA medium containing 50 µg/ml of hygromycin. Plates were incubated at room temperature for 5 days. Then, visible colonies were screened by PCR using a pair of primers targeting ~500 bp upstream and downstream of the gene of interest (forward: 5'-ACATATCGCGACGAGTTCCC-3', reverse: 5'-

CTCTTCTTCTCGAGCGACCC-3'). One colony for which the amplicon size was the one expected upon successful gene deletion was identified. Sanger sequencing of the amplicon confirmed the successful gene deletion. After cultivation of this mutant on PDA+hygromycin plate, spores were harvested and inoculated on hygromycin-free PDA medium. A colony that successfully grew in absence of hygromycin and that was confirmed to have lost the pTEL-Hyg vector was used as *Vd424Y* deletion line (Δ*424Y*).

Before to be used in plant recolonization experiments, the newly generated mutant line was tested to verify it is not impaired in growth. *V. dahliae* JR2 wild-type and the Δ*424Y* mutant were cultured on PDA plates for 10 days. Conidiospores were harvested and washed twice with sterile milli-Q water. The final concentration was adjusted to 1×10^6 spores/ml in 1 ml of PDB medium. This spore solution was incubated horizontally at 25 °C with shaking for 48 hours. Following incubation, fungal cells were collected by centrifugation at 13,000 rpm for 5 minutes, and 900 µl of the supernatant was carefully removed to avoid disturbing the pellet. As an internal control, 1 ng of synthetic spike-in plasmid (98) was added to each sample, and genomic DNA was extracted from the resulting pellets using the DNeasy PowerSoil Pro Kit (Qiagen – Hilden, Germany; ref. 47014), following the manufacturer's protocol. *V. dahliae* biomass was quantified by real-time PCR using species-specific primers VdITS1-F (5'-AAAGTTTTAATGGTTCGCTAAGA-3') and STVe1-R (5'-CTTGGTCATTTAGAGGAAGTAA-3') targeting the internal transcribed spacer (ITS) region. The spike-in plasmid was amplified in the same solutions using primers qRT-Spike-F (5'-TTTCTTTTCCAAGGTTTGTGC-3') and qRT-Spike-R (5'-AACATTTACCCTGCTTGTAGCTCT-3'). A fungal growth index was calculated from both amplifications' Ct values: index = 2-(CtITS/CtSpike). The growth index values of *V. dahliae* wild-type and Δ*424Y* mutant were then compared to check that the Δ*424Y* mutant line is not impaired in growth (fig. S21).

Tomato plant inoculation assays in a gnotobiotic system

The protocol applied here follows an adaptation of the FlowPot gnotobiotic system (99) to tomato plant inoculations with V. dahliae strains (40). FlowPot substrate, a 1:1 mixture of peat and vermiculite (Balster Einheitserde – Frödenberg, Germany; LIMERA Gartenbauservice – Geldern-Walbeck, Germany) was sterilized by two consecutive autoclaving rounds. Following substrate sterilization, FlowPot units were created by filling truncated 50 ml Luer lock syringes (Terumo Europe, Leuven, Belgium) with sterilized substrate and autoclaving for a third time on a liquid cycle. Additionally, a recolonized condition was created, by mixing sterilized substrate with non-sterile substrate in a 9:1 ratio, followed by an incubation at room temperature overnight. To remove toxic compounds, that may accumulate during autoclaving,

the substrate was flushed using 30 ml of sterile Milli-Q water using a vacuum system. Further, substrate was enriched using 30 ml of half-strength Murashige & Skoog medium (Duchefa; ref. M0222). Following FlowPot preparation, tomato seeds (*Solanum lycopersium* L.; cultivar "MoneyMaker") were surface sterilized as described previously (100), stratified at 8 ℃ for 24 hours and sown into each FlowPot unit. Subsequently, up to 5 FlowPot units were placed into Microbox containers with 4 air filters (SacO2; Deinze, Belgium) and kept in a greenhouse (17 hours of light at 23 ℃ followed by 7 hours of darkness at 22 ℃). After 14 days of growth, tomato plants were inoculated using *V. dahliae* wild-type and Δ*424Y* strains as well as ΔAve1 (7) a control. To this end, Microboxes were opened in a sterile hood, and plants were carefully uprooted from the substrate. Roots were rinsed using sterile milliQ-water and subsequently placed into a V. dahliae spore suspension, containing 106 spores/ml. After 8 minutes of incubation, plants were placed back into the FlowPots and Microboxes were placed back into the greenhouse chamber. Symptom development was assessed at 14 days-post inoculation by measuring tomato shoot fresh weight.

Microbiota profiling and analysis

Tomato plants inoculated with *V. dahliae* wild-type and Δ*424Y* strains grown in recolonized substrate were harvested. Stem samples were collected by cutting the region between the soil surface and the lowest leaf and were manually ground with a mortar and a pestle. Total DNA was extracted following a phenol-chloroform-based extraction method (101). The bacterial 16S rRNA gene was PCR amplified using the universal primer pair 27F (5′-AGAGTTTGATCCTGGCTCAG-3′) and 1492R (5′-GGWTACCTTGTTACGACT-3′). To suppress co-amplification of host-derived mitochondrial and chloroplast DNA, peptide nucleic acid (PNA) blocking clamps mPNA (GGCAAGTGTTCTTCGGA) and pPNA (GGCTCAACCCTGGACAG) (PNABio, Newbury Park, USA) were included in the PCR reactions, each at a final concentration of 0.25 μM. PCR products were purified using the Monarch PCR & DNA cleanup kit (New England Biolabs, Ipswich, USA). Sequencing libraries were prepared using the Native Barcoding Kit 96 v14 (SQK-NBD114.96) according to the manufacturer's protocol (Oxford Nanopore Technologies, Oxford, UK). Barcoded libraries were pooled and sequenced on a MinION sequencing device (Oxford Nanopore Technologies, Oxford, UK). Sequenced reads were processed using porechop v0.2.4 to remove Nanopore adapters, then using cutadapt v5.2 to exclude reads shorter than 1,000 nucleotides in length (parameter -m 1000). The filtered sets of 16S reads were assigned to bacterial taxa using the method EMU v3.4.6 and its default database (102). To profile differences in bacterial microbiota compositions between samples, Bray-Curtis distances were calculated using the

function spatial.distance.pdist(metric="braycurtis") of the Python library SciPy v1.13.1 (103), and a principal coordinate analysis (PCoA) was computed on these distances. A PERMANOVA test was computed with the function adonis2(perm=999) of the R package vegan v2.6.4 to assess whether *V. dahliae* wild-type- and ∆*424Y*-inoculated plants have significantly different microbiota compositions (formula BrayCurtis~InoculatedFungus). To identify bacteria that may be suppressed by the Vd424Y effector, numbers of reads assigned to each bacterial taxa were summed up at genus level. Then, a differential abundance analysis was computed using DESeq v1.40.2 with default parameters (104). Since a single genus was found significantly differentially abundant between *V. dahliae* wild-type- and ∆*424Y*-inoculated plants (adjusted $P < 0.05$) due to the small number of sequenced samples and the inherent variability of the microbiota that limits the statistical power of the analysis, the 10 bacterial genera showing the lowest log-transformed fold-change values were considered as candidate targets of the Vd424Y effector.

Agrobacterium-mediated transient effector gene expressions in *Nicotiana benthamiana*

Orthologs of Vd424Y were identified in two phylogenetically distant saprotrophic fungi: *Coprinopsis cinerea* AmutBmut1 (basidiomycete) and *Penicillium restrictum* MPI-SP2-AT-0405 (ascomycete). While the genome assembly and annotation of *C. cinerea* were available through JGI mycocosm (ID: Copci_AmutBmut1) (74, 105), no genome assembly was available for P. restrictum MPI-SP2-AT-0405. Therefore, previously sequenced raw reads (106) were downloaded from ENA (project PRJEB50298, sample SAMEA12383883, run ERR8084596), assembled with Flye v2.9.2 (default parameters) and annotated with BRAKER v3.0.8 (mode --fungus) (107, 108). Orthologs of *Vd424Y* were identified in these two genomes using blastp v2.5.0+ on their set of annotated proteins. The ortholog of *Vd424Y* in *C. cinerea* was named *Cc424Y* (protein ID: 491702, gene locus: scaffold_317:14532-15602) and the ortholog in *P. restrictum* was named *Pr424Y* (protein ID: g8033.t1, gene locus: contig_7:133414-134175).

Total RNA was isolated from *V. dahliae, C. cinerea* and *P. restrictum* cultured on PDA medium and the coding sequences of the 424Y homologs were amplified using the primer pairs 35S:Vd424Y-F (5'-TTACGAACGATAGCATCTAGAATGGTCTCGTTCACTTCTCTCCT-3') and 35S:Vd424Y-R (5'-GTAGTCCATCCCGGGGGTACCAGACACAGTCATGGTGGCGC-3'), 35S:Cc424Y-F (5'-TTACGAACGATAGCATCTAGAATGAAGTTCTCTTCTCTCTTCGTTG-3') and 35S:Cc424Y-R (5'-GTAGTCCATCCCGGGGGTACCGGAGACGGTGATGGTAGCG-3'), and 35S:Pr424Y-F (5'-TTACGAACGATAGCATCTAGAATGGTTTCTTTCACTTCTTTGATCGC-3') and 35S:Pr424Y-R (5'-GTAGTCCATCCCGGGGGTACCGCTGACTGTGATAGTCGAGGA-3'), respectively, and

cloned into the pCNF3 vector (109) by homologous recombination. Pr424Y carrying the Vd424Y nuclear localization signal (Pr424Y-NLS) was synthesized by BioCat GmbH (Heidelberg, Germany) and cloned into the same vector. The 424Y homologs were C-terminally fused to YFP using the primer pair YFP-F (5'-GGGGTACCATGGTGAGCAAGGGCGAGG-3') and YFP-R (5'-TCCCCCGGGCTTGTACAGCTCGTCCATGC-3') in the pCNF3-424Y recombinant vectors, so their subcellular localization can be assessed. Then, the recombinant vectors 35Spro:Vd424Y-Flag/YFP, 35Spro:Cc424Y-Flag/YFP, 35Spro:Pr424Y-Flag/YFP, and 35Spro:Pr424YNLS-Flag/YFP were transformed into *A. tumefaciens* strain GV3101. The p19 silencing suppressor from *tomato bushy stunt virus* was used to enhance transient expression. *A. tumefaciens* cultures carrying the expression constructs (Kanamycin + Rifampicin) or p19 (Ampicillin, Rifampicin + Gentamicin) were grown overnight at 28°C in Luria–Bertani (LB) medium. Bacterial cells were collected by centrifugation at 4,000 × g for 10 min and resuspended in infiltration buffer (10 mM MgCl2, 10 mM MES, pH 5.6, and 150 μM acetosyringone). The suspensions were adjusted to OD600 = 1, and incubated at room temperature for 2-3 h before infiltration. Next, *A. tumefaciens* suspensions carrying the expression construct and p19 were mixed in 1:1 ratio and infiltrated into the leaves of 3- to 4-week-old *N. benthamiana* plants using a needle-less syringe. After infiltration, the plants were kept under high humidity in the dark overnight, after which the plants were grown under normal conditions (22-24 °C, 16 hours light/8 hours dark). After 7 days, the occurrence of cell death was recorded.

For western blotting, leaf tissue was ground into a fine powder, mixed with extraction buffer (150 mM NaCl, 1.0 NP-40, 50 mM Tris, pH 8.0), and incubated on ice for 20-30 minutes. The mixture was then centrifuged at 12,000 rpm for 15 minutes at 4 °C. After collecting the supernatant, anti-Flag magnetic beads (MedChemExpress, Monmouth Junction, USA) were added and the mixture was incubated overnight at 4 °C. Next, the beads were washed three times with PBS buffer (0.137 M NaCl, 2.7 mM KCl, 1.8 mM KH2PO4, 10 mM Na2HPO4), resuspended in 60 μL of water with 20 μL of loading buffer, incubated at 98 °C for 10 minutes, and subjected to conventional sodium dodecyl sulfate - polyacrylamide gel electrophoresis (SDS-PAGE). The resulting protein blot was hybridized with α-Flag antibody (Sigma, St. Louis, USA) and developed with SuperSignal™ West Pico PLUS Chemiluminescence-Substrate (ref. 34577, Thermo Fisher Scientific, Waltham, MA, USA).

To assess subcellular localization, *A. tumefaciens* suspensions encoding YFP-tagged 424Y homologs and Sts2-mCherry (110) were co-infiltrated into the leaves of 3- to 4-week-old *N. benthamiana* plants. After 2-3 days, fluorescence signals were observed using a confocal laser scanning microscope (SP8, Leica, Wetzlar, Germany). YFP was excited at 514 nm and detected at 527 nm, while mCherry was excited at 587 nm and detected at 610 nm.

Pr424Y gene deletion in *Penicillium restrictum* and soil colonization assays

A *P. restrictum* gene deletion mutant lacking the *Pr424Y* gene (g8033.t1) was generated essentially following the protocol used to generate the *V. dahliae* Δ*424Y* mutant, while using GAGATCGGCAGAAATCCACA (upstream) and GCCCAGGGACAAAGCCCCAG (downstream) as sgRNA. Following protoplast transformation and regeneration, gene deletion mutants were screened for with PCR using primers 5'-AAGCGATGGCTGGTTTCAGA-3' and 5'-TGTTCTTCGCACCATACCCC-3'.

Cologne agricultural soil (CAS) (111) was autoclaved twice to obtain sterile soil. Briefly, after initial autoclaving, the soil was thoroughly mixed using a sterile spoon in a laminar flow cabinet and autoclaved once more. For sterile soil treatment, 1 g of autoclaved soil was weighed into a 15 mL sterile tube. For the recolonized soil treatment, 10% (w/w) non-autoclaved CAS was mixed with 90% autoclaved CAS, and 1 g of the mixture was transferred into a 15 mL sterile tube. All soil samples were incubated at room temperature in the dark for 2 days prior to inoculation.

Wild-type and *424Y* deletion strains of *P. restrictum* were grown on medium at room temperature for 7 days. Conidiospores were harvested by adding 5 mL of sterile Milli-Q water, gently scraping the surface, and filtering through a cell strainer to remove mycelial fragments. After centrifugation at 10,000 × g for 2 min the conidiospores were washed twice with sterile water. A spore suspension of 10^3 conidiospores mL-1 was prepared in a 50 mL tube containing 20 mL of PDB medium and incubated overnight at room temperature while shaking at 60 rpm. Next, cultures were pelleted by centrifugation at 4,000 rpm for 15 min, washed twice with sterile Milli-Q water, and resuspended in 20 mL of sterile Milli-Q water. A total of 100 µL fungal suspension was added to 1 g of the soil samples and incubated at room temperature in the dark. Soil samples were collected at 0 and 14 days after inoculation, thoroughly homogenized using a sterile spatula, and 250 mg of soil was transferred into PowerBead tubes for DNA extraction using the DNeasy PowerSoil Pro Kit (Qiagen, Hilden, Germany). One ng of spike-in plasmid was added to the CD1 lysis buffer of each sample for calibration (98). Finally, DNA was eluted in 50 µL sterile Milli-Q.

Quantitative real-time PCR (qPCR) was performed using SsoAdvanced™ Universal SYBR® Green Supermix (Bio-Rad, Hercules, CA, USA) with primers 5′-TTTCTTTTCCAAGGTTTGTGC-3′ and 5′-AACATTTACCCTGCTTGTAGCTCT-3′ for the spike-in, and 5′-GGAGGCATCAGCAAGTACCA-3′ and 5′-GGCTGGTTCCACCCATACTC-3′ for *P. restrictum* (designed for specifically targetting the *RPB1* gene of this species). The qPCR cycling conditions consisted of 95 °C for 3 min, followed by 40 2-step cycles of denaturation at 95 °C for 10 s and annealing/extension at 60 °C for 30 s, with fluorescence signal acquisition

at the end of each cycle. Melt curve analysis was performed from 65 °C to 95 °C, with temperature increments of 0.5 °C every 5 s, to verify the specificity of the amplification products. Fungal relative biomass was calculated by $2^{Ct(P.\ restrictum) - Ct(Spike\text{-}in)}$.

Statistics

Fisher's exact tests were computed using the function stats.fisher_exact in SciPy v1.13.0 (103). Mann-Whitney U tests were performed using the function stats.mannwhitneyu of SciPy v1.13.0. Cochrane-Armitage tests for trend were calculated with the function stats.contingency_tables.Table.test_ordinal_association of statsmodels v0.14.0 (112). In case of multiple testing, p-values from the tests mentioned above were adjusted using Benjamini-Hochberg correction with the function stats.multitest.multipletests(method='fdr_bh') of statsmodels v0.14.0. Measurements from in vitro microbial growth restriction assays were analyzed in R v4.4.1, first by using the shapiro.test function and Q-Q plots to assess normality of the datasets (Shapiro-Wilk test $P>0.05$) then since all data was normally distributed, pairwise one-sided Student's t-tests comparing microbial growth in presence and absence of protein were performed using the function t.test(alternative='less'). To analyze the tomato shoot fresh weight measurements, a square-root transformation (in R: lm(sqrt(ShootFreshWeight)~Condition)) was applied to reach normal distribution of the data (Shapiro-Wilk test $P>0.05$), then statistical comparison between treatments was performed using an ANOVA test and a post-hoc Tukey HSD test (functions aov and TukeyHSD of R v4.2.0). Letters reflecting the significant differences between treatments were obtained with function multcompLetters4 from R package multcompView v0.1-1 (113). Significant differences between conditions of the P. restrictum soil colonization assays were assessed with a Kruskal-Wallis test, since data were not normally distributed (Shapiro-Wilk test $P<0.05$), using the function kruskal.test in R v4.2.0. Post-hoc testing was performed with a Dunn test using the function DunnTest of the R package DescTools v0.99.50.

Acknowledgments

We thank Stéphane Hacquard and his group for providing the Penicillium restrictum strain and a Pseudoxanthomonas isolate used in this study. We thank Gunther Doehlemann and his group for providing control A. tumefaciens vectors used in this study. We thank Michael F. Seidl for his helpful suggestions and for proofreading this manuscript.

Funding

This work was supported by the Deutsche Forschungsgemeinschaft (DFG, German Research Foundation), through the funding of F.M.'s Walter Benjamin position (Project ID: ME 6064/1-1, Project number: 508411006). S.L. acknowledges funding from the China Scholarship Council, while Y.S. acknowledges funding through an Overseas Research Fellowship from the Japan Society for the Promotion of Science while ALM acknowledges receipt of a postdoctoral research fellowship funded by the 'Fundación Ramón Areces'. B.P.H.J.T. acknowledges funding by the Alexander von Humboldt Foundation in the framework of an Alexander von Humboldt Professorship endowed by the German Federal Ministry of Education and Research and is furthermore supported by DFG under Germany's Excellence Strategy – EXC 2048/1 – Project ID: 390686111 and by the DFG – Project ID 458090666 / CRC1535/1.

Competing Interests

All authors declare they have no competing interests.

Author Contributions

Conceptualization: FM, ALM, AK, BPHJT

Methodology: FM, VW, ALM, AK, WP, SL, JZ, YS

Software: FM

Validation: FM, VW, ALM, AK, WP, SL, JZ

Formal analysis: FM, VW, ALM, AK, WP, SL, JZ

Investigation: FM, VW, ALM, AK, WP, SL, JZ, JP

Resources: YS

Data curation: FM, VW, ALM, AK, WP, SL, JZ

Writing—original draft: FM, VW, BPHJT

Writing—review & editing: FM, VW, ALM, AK, WP, SL, JZ, YS, BPHJT

Visualization: FM, VW

Supervision: FM, BPHJT

Project administration: BPHJT

Funding acquisition: FM, ALM, YS, BPHJT

Data Availability

The AMAPEC software and training pipelines are available at https://github.com/fantin-mesny/amapec. The *Verticillium*-infected tomato plant microbiota amplicon sequencing data were deposited at ENA in study ERP187384 (PRJEB106306) . The *de novo* genome assembly of *Pencillium restrictum* MPI-SP2-AT-0405 has been deposited on GenBank in BioProject PRJEB105285. Other data and analysis scripts are available at https://github.com/fantin-mesny/Scripts_analysis_ancient_fungal_antimicrobials.

References

1. D. E. Cook, C. H. Mesarich, B. P. H. J. Thomma, Understanding plant immunity as a surveillance system to detect invasion. *Annu. Rev. Phytopathol.* **53**, 541–563 (2015).

2. G. Z. Han, Origin and evolution of the plant immune system. *New Phytol.* **222**, 70–83 (2019).

3. J. D. G. Jones, B. J. Staskawicz, J. L. Dangl, The plant immune system: From discovery to deployment. *Cell* **187**, 2095–2116 (2024).

4. V. Müller, R. J. de Boer, S. Bonhoeffer, E. Szathmáry, An evolutionary perspective on the systems of adaptive immunity. *Biol. Rev.* **93**, 505–528 (2018).

5. I. Stergiopoulos, P. J. G. M. De Wit, Fungal effector proteins. *Annu. Rev. Phytopathol.* **47**, 233–263 (2009).

6. G. Doehlemann, B. Ökmen, W. Zhu, A. Sharon, Plant pathogenic fungi. *Microbiol. Spectr.* **5** (2017).

7. N. C. Snelders, H. Rovenich, G. C. Petti, M. Rocafort, G. C. M. van den Berg, J. A. Vorholt, J. R. Mesters, M. F. Seidl, R. Nijland, B. P. H. J. Thomma, Microbiome manipulation by a soil-borne fungal plant pathogen using effector proteins. *Nat. Plants* **6**, 1365–1374 (2020).

8. N. C. Snelders, G. C. Petti, G. C. M. van den Berg, M. F. Seidl, B. P. H. J. Thomma, An ancient antimicrobial protein co-opted by a fungal plant pathogen for in planta mycobiome manipulation. *Proc. Natl. Acad. Sci.* **118**, e2110968118 (2021).

9. N. C. Snelders, J. C. Boshoven, Y. Song, N. Schmitz, G. L. Fiorin, H. Rovenich, G. C. M. van den Berg, D. E. Torres, G. C. Petti, Z. Prockl, L. Faino, M. F. Seidl, B. P. H. J. Thomma, A highly polymorphic effector protein promotes fungal virulence through suppression of plant-associated Actinobacteria. *New Phytol.* **237**, 944–958 (2023).

10. E. A. Chavarro-Carrero, N. C. Snelders, D. E. Torres, A. Kraege, A. López-Moral, G. C. Petti, W. Punt, J. Wieneke, R. García-Velasco, C. J. López-Herrera, M. F. Seidl, B. P. H. J. Thomma, The soil-borne white root rot pathogen Rosellinia necatrix expresses antimicrobial proteins during host colonization. *PLOS Pathog.* **20**, e1011866 (2024).

11. B. Ökmen, P. Katzy, L. Huang, R. Wemhöner, G. Doehlemann, A conserved extracellular Ribo1 with broad-spectrum cytotoxic activity enables smut fungi to compete with host-associated bacteria. *New Phytol.* **240**, 1976–1989 (2023).

12. D. Gómez-Pérez, M. Schmid, V. Chaudhry, Y. Hu, A. Velic, B. Maček, J. Ruhe, A. Kemen, E. Kemen, Proteins released into the plant apoplast by the obligate parasitic protist Albugo selectively repress phyllosphere-associated bacteria. *New Phytol.* **239**, 2320–2334 (2023).

13. H. X. Chang, Z. A. Noel, M. I. Chilvers, A β-lactamase gene of Fusarium oxysporum alters the rhizosphere microbiota of soybean. *Plant J.* **106**, 1588–1604 (2021).

14. A. Kraege, W. Punt, A. Doddi, J. Zhu, N. Schmitz, N. C. Snelders, B. P. H. J. Thomma, Undermining the cry for help: The phytopathogenic fungus Verticillium dahliae secretes an antimicrobial effector protein to undermine host recruitment of antagonistic Pseudomonas bacteria. *bioRxiv*, 2025.06.09.658588 (2025).

15. M. Möller, E. H. Stukenbrock, Evolution and genome architecture in fungal plant pathogens. *Nat. Rev. Microbiol.* **15**, 756–771 (2017).

16. L. J. Ma, H. C. Van Der Does, K. A. Borkovich, J. J. Coleman, M. J. Daboussi, A. Di Pietro, M. Dufresne, M. Freitag, M. Grabherr, B. Henrissat, P. M. Houterman, S. Kang, W. B. Shim, C. Woloshuk, X. Xie, J. R. Xu, J. Antoniw, S. E. Baker, B. H. Bluhm, A. Breakspear, D. W. Brown, R. A. E. Butchko, S. Chapman, R. Coulson, P. M. Coutinho, E. G. J. Danchin, A. Diener, L. R. Gale, D. M. Gardiner, S. Goff, K. E. Hammond-Kosack, K. Hilburn, A. Hua-Van, W. Jonkers, K. Kazan, C. D. Kodira, M. Koehrsen, L. Kumar, Y. H. Lee, L. Li, J. M. Manners, D. Miranda-Saavedra, M. Mukherjee, G. Park, J. Park, S. Y. Park, R. H. Proctor, A. Regev, M. C. Ruiz-Roldan, D. Sain, S. Sakthikumar, S. Sykes, D. C. Schwartz, B. G. Turgeon, I. Wapinski, O. Yoder, S. Young, Q. Zeng, S. Zhou, J. Galagan, C. A. Cuomo, H. C. Kistler, M. Rep, Comparative genomics reveals mobile pathogenicity chromosomes in Fusarium. *Nature* **464**, 367–373 (2010).

17. R. de Jonge, M. D. Bolton, A. Kombrink, G. C. M. Van Den Berg, K. A. Yadeta, B. P. H. J. Thomma, Extensive chromosomal reshuffling drives evolution of virulence in an asexual pathogen. *Genome Res.* **23**, 1271–1282 (2013).

18. Y. Sato, R. Bex, G. C. M. van den Berg, P. Santhanam, M. Höfte, M. F. Seidl, B. P. H. J. Thomma, Starship giant transposons dominate plastic genomic regions in a fungal plant pathogen and drive virulence evolution. *Nat. Commun.* **16**, 1–17 (2025).

19. M. Torrent, D. Andreu, V. M. Nogués, E. Boix, Connecting peptide physicochemical and antimicrobial properties by a rational prediction model. *PLoS One* **6**, e16968 (2011).

20. G. Wang, The antimicrobial peptide database is 20 years old: Recent developments and future directions. *Protein Sci.* **32**, e4778 (2023).

21. F. Wan, F. Wong, J. J. Collins, C. de la Fuente-Nunez, Machine learning for antimicrobial peptide identification and design. *Nat. Rev. Bioeng.* **2**, 392–407 (2024).

22. R. Eichfeld, L. K. Mahdi, C. De Quattro, L. Armbruster, A. B. Endeshaw, S. Miyauchi, M. J. Hellmann, S. Cord-Landwehr, D. Peterson, V. Singan, K. Lail, E. Savage, V. Ng, I. V. Grigoriev, G. Langen, B. M. Moerschbacher, A. Zuccaro, Transcriptomics reveal a mechanism of niche defense: two beneficial root endophytes deploy an antimicrobial GH18-CBM5 chitinase to protect their hosts. *New Phytol.* **244** (2024).

23. F. Chen, L. Ou, H. Wu, L. Huang, Y.-P. Chen, Expression and characterization of the antifungal protein PtAFP from Pyrenophora tritci-repentis by synonymous codon bias in Escherichia coli. *Proc. SPIE 13208, Third Int. Conf. Biomed. Intell. Syst. (IC-BIS 2024)* **13208**, 13–19 (2024).

24. K. de Guillen, L. Mammri, J. Gracy, A. Padilla, P. Barthe, F. Hoh, M. Lahfa, J. Rouffet, Y. Petit-Houdenot, T. Kroj, M.-H. Lebrun, Zymoseptoria tritici effectors structurally related to killer proteins UmV-KP4 and UmV-KP6 are toxic to fungi, and define extended protein families in fungi. *bioRxiv*, 2024.10.14.618152 (2024).

25. Z. Sorger, P. Sengupta, K. Beier-Heuchert, J. Bautor, J. E. Parker, E. Kemen, G. Doehlemann, GH25 lysozyme mediates tripartite interkingdom interactions and microbial competition on the plant leaf surface. *bioRxiv*, 2025.04.04.647216 (2025).

26. L. Florez, V. M. Flores-Núñez, C. S. Francisco, E. Holtgrewe Stukenbrock, The fungal effector AvrStb6 regulates the wheat pathobiome. *Zenodo*, doi: 10.5281/ZENODO.15852925 (2025).

27. E. F. Fradin, B. P. H. J. Thomma, Physiology and molecular aspects of Verticillium wilt diseases caused by V. dahliae and V. albo-atrum. *Mol. Plant Pathol.* **7**, 71–86 (2006).

28. N. C. Snelders, H. Rovenich, B. P. H. J. Thomma, Microbiota manipulation through the secretion of effector proteins is fundamental to the wealth of lifestyles in the fungal kingdom. *FEMS Microbiol. Rev.* **46**, fuac022 (2022).

29. G. J. Kettles, C. Bayon, C. A. Sparks, G. Canning, K. Kanyuka, J. J. Rudd, Characterization of an antimicrobial and phytotoxic ribonuclease secreted by the fungal wheat pathogen Zymoseptoria tritici. *New Phytol.* **217**, 320–331 (2018).

30. Y. Zhang, Y. Gao, Y. Liang, Y. Dong, X. Yang, J. Yuan, D. Qiu, The Verticillium dahliae SnodProt1-like protein VdCP1 contributes to virulence and triggers the plant immune system. *Front. Plant Sci.* **8**, 289292 (2017).

31. L. Liu, Z. Wang, J. Li, Y. Wang, J. Yuan, J. Zhan, P. Wang, Y. Lin, F. Li, X. Ge, Verticillium dahliae secreted protein Vd424Y is required for full virulence, targets the nucleus of plant cells, and induces cell death. *Mol. Plant Pathol.* **22**, 1109–1120 (2021).

32. D. Wang, J. Y. Chen, J. Song, J. J. Li, S. J. Klosterman, R. Li, Z. Q. Kong, K. V. Subbarao, X. F. Dai, D. D. Zhang, Cytotoxic function of xylanase VdXyn4 in the plant vascular wilt pathogen Verticillium dahliae. *Plant Physiol.* **187**, 409–429 (2021).

33. A. Kombrink, H. Rovenich, X. Shi-Kunne, E. Rojas-Padilla, G. C. M. van den Berg, E. Domazakis, R. de Jonge, D. J. Valkenburg, A. Sánchez-Vallet, M. F. Seidl, B. P. H. J. Thomma, Verticillium dahliae LysM effectors differentially contribute to virulence on plant hosts. *Mol. Plant Pathol.* **18**, 596–608 (2017).

34. R. de Jonge, B. P. H. J. Thomma, Fungal LysM effectors: extinguishers of host immunity? *Trends Microbiol.* **17**, 151–157 (2009).

35. A. Kombrink, B. P. H. J. Thomma, LysM effectors: Secreted proteins supporting fungal life. *PLOS Pathog.* **9**, e1003769 (2013).

36. M. Urban, A. Cuzick, J. Seager, V. Wood, K. Rutherford, S. Y. Venkatesh, J. Sahu, S. Vijaylakshmi Iyer, L. Khamari, N. De Silva, M. C. Martinez, H. Pedro, A. D. Yates, K. E. Hammond-Kosack, PHI-base in 2022: A multi-species phenotype database for pathogen–host Interactions. *Nucleic Acids Res.* **50**, D837–D847 (2022).

37. R. de Jonge, H. P. Van Esse, A. Kombrink, T. Shinya, Y. Desaki, R. Bours, S. Van Der Krol, N. Shibuya, M. H. A. J. Joosten, B. P. H. J. Thomma, Conserved fungal LysM effector Ecp6 prevents chitin-triggered immunity in plants. *Science (80-.).* **329**, 953–955 (2010).

38. S. Li, X. Peng, Y. Wang, K. Hua, F. Xing, Y. Zheng, W. Liu, W. Sun, S. Wei, The effector AGLIP1 in Rhizoctonia solani AG1 IA triggers cell death in plants and promotes disease development through inhibiting PAMP-triggered immunity in Arabidopsis thaliana. *Front. Microbiol.* **10**, 483550 (2019).

39. G. Xiao, N. Laksanavilat, S. Cesari, K. Lambou, M. Baudin, A. Jalilian, M. J. Telebanco-Yanoria, V. Chalvon, I. Meusnier, E. Fournier, D. Tharreau, B. Zhou, J. Wu, T. Kroj, The unconventional resistance protein PTR recognizes the Magnaporthe

oryzae effector AVR-Pita in an allele-specific manner. *Nat. Plants* **10**, 994–1004 (2024).

40. W. Punt, J. Park, H. Roevenich, A. Kraege, N. Schmitz, J. Wieneke, N. C. Snelders, G. L. Fiorin, A. López-Moral, E. A. Chavarro-Carrero, G. C. Petti, K. Wippel, B. P. H. J. Thomma, A gnotobiotic system reveals multifunctional effector roles in plant-fungal pathogen dynamics. *bioRxiv*, 2025.03.27.645772 (2025).

41. S. Kumar, G. Stecher, M. Suleski, S. B. Hedges, TimeTree: a resource for timelines, timetrees, and divergence times. *Mol. Biol. Evol.* **34**, 1812–1819 (2017).

42. T. Y. James, F. Kauff, C. L. Schoch, P. B. Matheny, V. Hofstetter, C. J. Cox, G. Celio, C. Gueidan, E. Fraker, J. Miadlikowska, H. T. Lumbsch, A. Rauhut, V. Reeb, A. E. Arnold, A. Amtoft, J. E. Stajich, K. Hosaka, G. H. Sung, D. Johnson, B. O'Rourke, M. Crockett, M. Binder, J. M. Curtis, J. C. Slot, Z. Wang, A. W. Wilson, A. Schüßler, J. E. Longcore, K. O'Donnell, S. Mozley-Standridge, D. Porter, P. M. Letcher, M. J. Powell, J. W. Taylor, M. M. White, G. W. Griffith, D. R. Davies, R. A. Humber, J. B. Morton, J. Sugiyama, A. Y. Rossman, J. D. Rogers, D. H. Pfister, D. Hewitt, K. Hansen, S. Hambleton, R. A. Shoemaker, J. Kohlmeyer, B. Volkmann-Kohlmeyer, R. A. Spotts, M. Serdani, P. W. Crous, K. W. Hughes, K. Matsuura, E. Langer, G. Langer, W. A. Untereiner, R. Lücking, B. Büdel, D. M. Geiser, A. Aptroot, P. Diederich, I. Schmitt, M. Schultz, R. Yahr, D. S. Hibbett, F. Lutzoni, D. J. McLaughlin, J. W. Spatafora, R. Vilgalys, Reconstructing the early evolution of Fungi using a six-gene phylogeny. *Nature* **443**, 818–822 (2006).

43. X. Yuan, S. Xiao, T. N. Taylor, Lichen-like symbiosis 600 million years ago. *Science (80-.).* **308**, 1017–1020 (2005).

44. M. A. Guerreiro, E. H. Stukenbrock, Fungal plant pathogens. *Curr. Biol.* **35**, R480–R484 (2025).

45. C. Y. Huang, K. Araujo, J. N. Sánchez, G. Kund, J. Trumble, C. Roper, K. E. Godfrey, H. Jin, A stable antimicrobial peptide with dual functions of treating and preventing citrus Huanglongbing. *Proc. Natl. Acad. Sci. U. S. A.* **118**, e2019628118 (2021).

46. D. Wu, L. Fu, W. Wen, N. Dong, The dual antimicrobial and immunomodulatory roles of host defense peptides and their applications in animal production. *J. Anim. Sci. Biotechnol.* **13**, 141 (2022).

47. R. Eichfeld, A. B. Endeshaw, M. J. Hellmann, B. M. Moerschbacher, A. Zuccaro, Domain gain or loss in fungal chitinases drives ecological specialization toward antagonism or immune suppression. *bioRxiv*, 2025.06.16.659886 (2025).

48. P. van Dam, L. Fokkens, S. M. Schmidt, J. H. J. Linmans, H. Corby Kistler, L. J. Ma, M. Rep, Effector profiles distinguish formae speciales of Fusarium oxysporum. *Environ. Microbiol.* **18**, 4087–4102 (2016).

49. F. Mesny, M. Bauer, J. Zhu, B. P. H. J. Thomma, Meddling with the microbiota: Fungal tricks to infect plant hosts. *Curr. Opin. Plant Biol.* **82**, 102622 (2024).

50. A. C. Sexton, B. J. Howlett, Parallels in fungal pathogenesis on plant and animal hosts. *Eukaryot. Cell* **5**, 1941–1949 (2006).

51. F. Teufel, J. J. Almagro Armenteros, A. R. Johansen, M. H. Gíslason, S. I. Pihl, K. D. Tsirigos, O. Winther, S. Brunak, G. von Heijne, H. Nielsen, SignalP 6.0 predicts all five types of signal peptides using protein language models. *Nat. Biotechnol.* **40**, 1023–1025 (2022).

52. P. K. Meher, T. K. Sahu, V. Saini, A. R. Rao, Predicting antimicrobial peptides with improved accuracy by incorporating the compositional, physico-chemical and structural features into Chou's general PseAAC. *Sci. Rep.* **7**, 1–12 (2017).

53. D. Veltri, U. Kamath, A. Shehu, Deep learning improves antimicrobial peptide recognition. *Bioinformatics* **34**, 2740–2747 (2018).

54. T.-T. Lin, L.-Y. Yang, I.-H. Lu, W.-C. Cheng, Z.-R. Hsu, S.-H. Chen, C.-Y. Lin, AI4AMP: an antimicrobial peptide predictor using physicochemical property-based encoding method and deep learning. *mSystems* **6** (2021).

55. H. Lee, S. Lee, I. Lee, H. Nam, AMP-BERT: Prediction of antimicrobial peptide function based on a BERT model. *Protein Sci.* **32**, e4529 (2023).

56. J. Yan, P. Bhadra, A. Li, P. Sethiya, L. Qin, H. K. Tai, K. H. Wong, S. W. I. Siu, Deep-AmPEP30: Improve short antimicrobial peptides prediction with deep learning. *Mol. Ther. - Nucleic Acids* **20**, 882–894 (2020).

57. A. Bateman, M. J. Martin, S. Orchard, M. Magrane, R. Agivetova, S. Ahmad, E. Alpi, E. H. Bowler-Barnett, R. Britto, B. Bursteinas, H. Bye-A-Jee, R. Coetzee, A. Cukura, A. Da Silva, P. Denny, T. Dogan, T. G. Ebenezer, J. Fan, L. G. Castro, P. Garmiri, G. Georghiou, L. Gonzales, E. Hatton-Ellis, A. Hussein, A. Ignatchenko, G. Insana, R. Ishtiaq, P. Jokinen, V. Joshi, D. Jyothi, A. Lock, R. Lopez, A. Luciani, J. Luo, Y. Lussi, A. MacDougall, F. Madeira, M. Mahmoudy, M. Menchi, A. Mishra, K. Moulang, A. Nightingale, C. S. Oliveira, S. Pundir, G. Qi, S. Raj, D. Rice, M. R. Lopez, R. Saidi, J. Sampson, T. Sawford, E. Speretta, E. Turner, N. Tyagi, P. Vasudev, V. Volynkin, K. Warner, X. Watkins, R. Zaru, H. Zellner, A. Bridge, S. Poux, N. Redaschi, L. Aimo, G.

Argoud-Puy, A. Auchincloss, K. Axelsen, P. Bansal, D. Baratin, M. C. Blatter, J. Bolleman, E. Boutet, L. Breuza, C. Casals-Casas, E. de Castro, K. C. Echioukh, E. Coudert, B. Cuche, M. Doche, D. Dornevil, A. Estreicher, M. L. Famiglietti, M. Feuermann, E. Gasteiger, S. Gehant, V. Gerritsen, A. Gos, N. Gruaz-Gumowski, U. Hinz, C. Hulo, N. Hyka-Nouspikel, F. Jungo, G. Keller, A. Kerhornou, V. Lara, P. Le Mercier, D. Lieberherr, T. Lombardot, X. Martin, P. Masson, A. Morgat, T. B. Neto, S. Paesano, I. Pedruzzi, S. Pilbout, L. Pourcel, M. Pozzato, M. Pruess, C. Rivoire, C. Sigrist, K. Sonesson, A. Stutz, S. Sundaram, M. Tognolli, L. Verbregue, C. H. Wu, C. N. Arighi, L. Arminski, C. Chen, Y. Chen, J. S. Garavelli, H. Huang, K. Laiho, P. McGarvey, D. A. Natale, K. Ross, C. R. Vinayaka, Q. Wang, Y. Wang, L. S. Yeh, J. Zhang, UniProt: the universal protein knowledgebase in 2021. *Nucleic Acids Res.* **49**, D480–D489 (2021).

58. D. Osorio, P. Rondón-Villarreal, R. Torres, Peptides: A package for data mining of antimicrobial peptides. *R J.* **7**, 4–14 (2015).

59. J. Jumper, R. Evans, A. Pritzel, T. Green, M. Figurnov, O. Ronneberger, K. Tunyasuvunakool, R. Bates, A. Žídek, A. Potapenko, A. Bridgland, C. Meyer, S. A. A. Kohl, A. J. Ballard, A. Cowie, B. Romera-Paredes, S. Nikolov, R. Jain, J. Adler, T. Back, S. Petersen, D. Reiman, E. Clancy, M. Zielinski, M. Steinegger, M. Pacholska, T. Berghammer, S. Bodenstein, D. Silver, O. Vinyals, A. W. Senior, K. Kavukcuoglu, P. Kohli, D. Hassabis, Highly accurate protein structure prediction with AlphaFold. *Nature* **596**, 583–589 (2021).

60. P. J. A. Cock, T. Antao, J. T. Chang, B. A. Chapman, C. J. Cox, A. Dalke, I. Friedberg, T. Hamelryck, F. Kauff, B. Wilczynski, M. J. L. de Hoon, Biopython: freely available Python tools for computational molecular biology and bioinformatics. *Bioinformatics* **25**, 1422–1423 (2009).

61. N. Mih, E. Brunk, K. Chen, E. Catoiu, A. Sastry, E. Kavvas, J. M. Monk, Z. Zhang, B. O. Palsson, ssbio: a Python framework for structural systems biology. *Bioinformatics* **34**, 2155–2157 (2018).

62. H. Chen, F. Gu, Z. Huang, Improved Chou-Fasman method for protein secondary structure prediction. *BMC Bioinformatics* **7**, 1–11 (2006).

63. R. Nagarajan, A. Archana, A. M. Thangakani, S. Jemimah, D. Velmurugan, M. M. Gromiha, PDBparam: online resource for computing structural parameters of proteins. *Bioinform. Biol. Insights* **10**, 73–80 (2016).

64. W. Kabsch, C. Sander, Dictionary of protein secondary structure: pattern recognition of hydrogen-bonded and geometrical features. *Biopolym. Orig. Res. Biomol.* **22**, 2577–2637 (1983).

65. W. G. Touw, C. Baakman, J. Black, T. A. H. Te Beek, E. Krieger, R. P. Joosten, G. Vriend, A series of PDB-related databanks for everyday needs. *Nucleic Acids Res.* **43**, D364--D368 (2015).

66. V. Le Guilloux, P. Schmidtke, P. Tuffery, Fpocket: an open source platform for ligand pocket detection. *BMC Bioinformatics* **10**, 1–11 (2009).

67. Y. Liang, S. Yang, L. Zheng, H. Wang, J. Zhou, S. Huang, L. Yang, Y. Zuo, Research progress of reduced amino acid alphabets in protein analysis and prediction. *Comput. Struct. Biotechnol. J.* (2022).

68. J. L. Figueroa, A. Redinbo, A. Panyala, S. Colby, M. L. Friesen, L. Tiemann, R. A. White, MerCat2: a versatile k-mer counter and diversity estimator for database-independent property analysis obtained from omics data. *Bioinforma. Adv.* **4** (2024).

69. F. Pedregosa, G. Varoquaux, A. Gramfort, M. Vincent, B. Thirion, O. Grisel, M. Blondel, P. Prettenhofer, R. Weiss, V. Dubourg, J. Vanderplas, A. Passos, D. Cournapeau, M. Brucher, M. Perrot, É. Duchesnay, Scikit-learn: machine learning in Python. *J. Mach. Learn. Res.* **12**, 2825–2830 (2011).

70. Z. Lin, H. Akin, R. Rao, B. Hie, Z. Zhu, W. Lu, N. Smetanin, R. Verkuil, O. Kabeli, Y. Shmueli, others, Evolutionary-scale prediction of atomic-level protein structure with a language model. *Science (80-.).* **379**, 1123–1130 (2023).

71. R. de Jonge, H. P. Van Esse, K. Maruthachalam, M. D. Bolton, P. Santhanam, M. K. Saber, Z. Zhang, T. Usami, B. Lievens, K. V. Subbarao, B. P. H. J. Thomma, Tomato immune receptor Ve1 recognizes effector of multiple fungal pathogens uncovered by genome and RNA sequencing. *Proc. Natl. Acad. Sci. U. S. A.* **109**, 5110–5115 (2012).

72. P. J. Kersey, J. E. Allen, I. Armean, S. Boddu, B. J. Bolt, D. Carvalho-Silva, M. Christensen, P. Davis, L. J. Falin, C. Grabmueller, others, Ensembl Genomes 2016: more genomes, more complexity. *Nucleic Acids Res.* **44**, D574--D580 (2016).

73. H. Muraguchi, K. Umezawa, M. Niikura, M. Yoshida, T. Kozaki, K. Ishii, K. Sakai, M. Shimizu, K. Nakahori, Y. Sakamoto, C. Choi, C. Y. Ngan, E. Lindquist, A. Lipzen, A. Tritt, S. Haridas, K. Barry, I. V Grigoriev, P. J. Pukkila, Strand-specific RNA-Seq analyses of fruiting body development in Coprinopsis cinerea. *PLoS One* **10**, e0141586 (2015).

74. I. V. Grigoriev, R. Nikitin, S. Haridas, A. Kuo, R. Ohm, R. Otillar, R. Riley, A. Salamov, X. Zhao, F. Korzeniewski, T. Smirnova, H. Nordberg, I. Dubchak, I. Shabalov, MycoCosm portal: Gearing up for 1000 fungal genomes. *Nucleic Acids Res.* **42**, D699–D704 (2014).

75. G. Yildirir, J. Sperschneider, M. Malar C, E. C. H. Chen, W. Iwasaki, C. Cornell, N. Corradi, Long reads and Hi-C sequencing illuminate the two-compartment genome of the model arbuscular mycorrhizal symbiont Rhizophagus irregularis. *New Phytol.* **233**, 1097–1107 (2022).

76. C. P. Cantalapiedra, A. Herṇandez-Plaza, I. Letunic, P. Bork, J. Huerta-Cepas, eggNOG-mapper v2: functional annotation, orthology assignments, and domain prediction at the metagenomic scale. *Mol. Biol. Evol.* **38**, 5825–5829 (2021).

77. J. Huerta-Cepas, D. Szklarczyk, D. Heller, A. Hernández-Plaza, S. K. Forslund, H. Cook, D. R. Mende, I. Letunic, T. Rattei, L. J. Jensen, C. Von Mering, P. Bork, eggNOG 5.0: a hierarchical, functionally and phylogenetically annotated orthology resource based on 5090 organisms and 2502 viruses. *Nucleic Acids Res.* **47**, D309–D314 (2019).

78. J. Zheng, Q. Ge, Y. Yan, X. Zhang, L. Huang, Y. Yin, dbCAN3: automated carbohydrate-active enzyme and substrate annotation. *Nucleic Acids Res.*, gkad328 (2023).

79. M. Bernhofer, B. Rost, TMbed: transmembrane proteins predicted through language model embeddings. *BMC Bioinformatics* **23**, 1–19 (2022).

80. D. M. Emms, S. Kelly, OrthoFinder: Phylogenetic orthology inference for comparative genomics. *Genome Biol.* **20**, 1–14 (2019).

81. F. Mesny, S. Miyauchi, T. Thiergart, B. Pickel, L. Atanasova, M. Karlsson, B. Hüttel, K. W. Barry, S. Haridas, C. Chen, D. Bauer, W. Andreopoulos, J. Pangilinan, K. LaButti, R. Riley, A. Lipzen, A. Clum, E. Drula, B. Henrissat, A. Kohler, I. V. Grigoriev, F. M. Martin, S. Hacquard, Genetic determinants of endophytism in the Arabidopsis root mycobiome. *Nat. Commun.* **12**, 1–15 (2021).

82. D. M. Emms, S. Kelly, STAG: Species tree inference from all genes. *bioRxiv*, 267914 (2018).

83. F. Mesny, phylorep v0.1. (2023). https://doi.org/10.5281/ZENODO.10142123.

84. M. N. Price, P. S. Dehal, A. P. Arkin, FastTree 2 – Approximately maximum-likelihood trees for large alignments. *PLoS One* **5**, e9490 (2010).

85. G. L. Fiorin, A. Sanchéz-Vallet, D. P. de T. Thomazella, P. F. V. do Prado, L. C. do Nascimento, A. V. de O. Figueira, B. P. H. J. Thomma, G. A. G. Pereira, P. J. P. L. Teixeira, Suppression of plant immunity by fungal chitinase-like effectors. *Curr. Biol.* **28**, 3023-3030.e5 (2018).

86. H. Tian, C. I. MacKenzie, L. Rodriguez-Moreno, G. C. M. van den Berg, H. Chen, J. J. Rudd, J. R. Mesters, B. P. H. J. Thomma, Three LysM effectors of Zymoseptoria tritici collectively disarm chitin-triggered plant immunity. *Mol. Plant Pathol.* **22**, 683–693 (2021).

87. C. A. Schneider, W. S. Rasband, K. W. Eliceiri, NIH Image to ImageJ: 25 years of image analysis. *Nat. Methods* **9**, 671–675 (2012).

88. B. Q. Minh, H. A. Schmidt, O. Chernomor, D. Schrempf, M. D. Woodhams, A. Von Haeseler, R. Lanfear, E. Teeling, IQ-TREE 2: New models and efficient methods for phylogenetic inference in the genomic era. *Mol. Biol. Evol.* **37**, 1530–1534 (2020).

89. K. Katoh, D. M. Standley, MAFFT multiple sequence alignment software version 7: Improvements in performance and usability. *Mol. Biol. Evol.* **30**, 772–780 (2013).

90. P. Jones, D. Binns, H. Y. Chang, M. Fraser, W. Li, C. McAnulla, H. McWilliam, J. Maslen, A. Mitchell, G. Nuka, S. Pesseat, A. F. Quinn, A. Sangrador-Vegas, M. Scheremetjew, S. Y. Yong, R. Lopez, S. Hunter, InterProScan 5: genome-scale protein function classification. *Bioinformatics* **30**, 1236–1240 (2014).

91. I. Letunic, P. Bork, Interactive Tree of Life (iTOL) v6: recent updates to the phylogenetic tree display and annotation tool. *Nucleic Acids Res.* **52**, W78–W82 (2024).

92. O. Emanuelsson, H. Nielsen, G. Von Heijne, ChloroP, a neural network-based method for predicting chloroplast transit peptides and their cleavage sites. *Protein Sci.* **8**, 978–984 (1999).

93. S. Kosugi, M. Hasebe, M. Tomita, H. Yanagawa, Systematic identification of cell cycle-dependent yeast nucleocytoplasmic shuttling proteins by prediction of composite motifs. *Proc. Natl. Acad. Sci. U. S. A.* **106**, 10171–10176 (2009).

94. W. Punt, A. Kraege, B. P. H. J. Thomma, Dutch soils. *Prep.*

95. J. Li, L. Faino, G. L. Fiorin, S. Bashyal, A. Schaveling, C. van den Berg, M. F. Seidl, B. PHJ Thomma, B. Thomma, A single Verticillium dahliae effector determines pathogenicity on tomato by targeting auxin response factors. *bioRxiv*, 2022.11.22.517554 (2022).

96. L. Rehman, X. Su, H. Guo, X. Qi, H. Cheng, Protoplast transformation as a potential platform for exploring gene function in Verticillium dahliae. *BMC Biotechnol.* **16**, 1–9 (2016).

97. T. Leisen, F. Bietz, J. Werner, A. Wegner, U. Schaffrath, D. Scheuring, F. Willmund, A. Mosbach, G. Scalliet, M. Hahn, CRISPR/Cas with ribonucleoprotein complexes and transiently selected telomere vectors allows highly efficient marker-free and multiple genome editing in Botrytis cinerea. *PLOS Pathog.* **16**, e1008326 (2020).

98. X. Guo, X. Zhang, Y. Qin, Y. X. Liu, J. Zhang, N. Zhang, K. Wu, B. Qu, Z. He, X. Wang, X. Zhang, S. Hacquard, X. Fu, Y. Bai, Host-associated quantitative abundance profiling reveals the microbial load variation of root microbiome. *Plant Commun.* **1** (2020).

99. J. M. Kremer, B. C. Paasch, D. Rhodes, C. Thireault, J. E. Froehlich, P. Schulze-Lefert, J. M. Tiedje, S. Y. He, FlowPot axenic plant growth system for microbiota research. *bioRxiv*, 254953 (2018).

100. B. Schlesier, F. Bréton, H. P. Mock, A hydroponic culture system for growing Arabidopsis thaliana plantlets under sterile conditions. *Plant Mol. Biol. Report.* **21**, 449–456 (2003).

101. E. A. Chavarro-Carrero, J. P. Vermeulen, D. E. Torres, T. Usami, H. J. Schouten, Y. Bai, M. F. Seidl, B. P. H. J. Thomma, Comparative genomics reveals the in planta-secreted Verticillium dahliae Av2 effector protein recognized in tomato plants that carry the V2 resistance locus. *Environ. Microbiol.* **23**, 1941–1958 (2021).

102. K. D. Curry, Q. Wang, M. G. Nute, A. Tyshaieva, E. Reeves, S. Soriano, Q. Wu, E. Graeber, P. Finzer, W. Mendling, T. Savidge, S. Villapol, A. Dilthey, T. J. Treangen, Emu: species-level microbial community profiling of full-length 16S rRNA Oxford Nanopore sequencing data. *Nat. Methods* **19**, 845–853 (2022).

103. P. Virtanen, R. Gommers, T. E. Oliphant, M. Haberland, T. Reddy, D. Cournapeau, E. Burovski, P. Peterson, W. Weckesser, J. Bright, S. J. van der Walt, M. Brett, J. Wilson, K. J. Millman, N. Mayorov, A. R. J. Nelson, E. Jones, R. Kern, E. Larson, C. J. Carey, İ. Polat, Y. Feng, E. W. Moore, J. VanderPlas, D. Laxalde, J. Perktold, R. Cimrman, I. Henriksen, E. A. Quintero, C. R. Harris, A. M. Archibald, A. H. Ribeiro, F. Pedregosa, P. van Mulbregt, A. Vijaykumar, A. Pietro Bardelli, A. Rothberg, A. Hilboll, A. Kloeckner, A. Scopatz, A. Lee, A. Rokem, C. N. Woods, C. Fulton, C. Masson, C. Häggström, C. Fitzgerald, D. A. Nicholson, D. R. Hagen, D. V. Pasechnik, E. Olivetti, E. Martin, E. Wieser, F. Silva, F. Lenders, F. Wilhelm, G. Young, G. A. Price, G. L. Ingold, G. E.

Allen, G. R. Lee, H. Audren, I. Probst, J. P. Dietrich, J. Silterra, J. T. Webber, J. Slavič, J. Nothman, J. Buchner, J. Kulick, J. L. Schönberger, J. V. de Miranda Cardoso, J. Reimer, J. Harrington, J. L. C. Rodríguez, J. Nunez-Iglesias, J. Kuczynski, K. Tritz, M. Thoma, M. Newville, M. Kümmerer, M. Bolingbroke, M. Tartre, M. Pak, N. J. Smith, N. Nowaczyk, N. Shebanov, O. Pavlyk, P. A. Brodtkorb, P. Lee, R. T. McGibbon, R. Feldbauer, S. Lewis, S. Tygier, S. Sievert, S. Vigna, S. Peterson, S. More, T. Pudlik, T. Oshima, T. J. Pingel, T. P. Robitaille, T. Spura, T. R. Jones, T. Cera, T. Leslie, T. Zito, T. Krauss, U. Upadhyay, Y. O. Halchenko, Y. Vázquez-Baeza, SciPy 1.0: fundamental algorithms for scientific computing in Python. *Nat. Methods 2020 173* **17**, 261–272 (2020).

104. M. I. Love, W. Huber, S. Anders, Moderated estimation of fold change and dispersion for RNA-seq data with DESeq2. *Genome Biol.* **15**, 550 (2014).

105. H. Muraguchi, K. Umezawa, M. Niikura, M. Yoshida, T. Kozaki, K. Ishii, K. Sakai, M. Shimizu, K. Nakahori, Y. Sakamoto, C. Choi, C. Y. Ngan, E. Lindquist, A. Lipzen, A. Tritt, S. Haridas, K. Barry, I. V. Grigoriev, P. J. Pukkila, Strand-Specific RNA-Seq Analyses of Fruiting Body Development in Coprinopsis cinerea. *PLoS One* **10** (2015).

106. F. Meyer, A. Fritz, Z.-L. Deng, D. Koslicki, T. R. Lesker, A. Gurevich, G. Robertson, M. Alser, D. Antipov, F. Beghini, D. Bertrand, J. J. Brito, C. T. Brown, J. Buchmann, A. Buluç, B. Chen, R. Chikhi, P. T. L. C. Clausen, A. Cristian, P. W. Dabrowski, A. E. Darling, R. Egan, E. Eskin, E. Georganas, E. Goltsman, M. A. Gray, L. H. Hansen, S. Hofmeyr, P. Huang, L. Irber, H. Jia, T. S. Jørgensen, S. D. Kieser, T. Klemetsen, A. Kola, M. Kolmogorov, A. Korobeynikov, J. Kwan, N. LaPierre, C. Lemaitre, C. Li, A. Limasset, F. Malcher-Miranda, S. Mangul, V. R. Marcelino, C. Marchet, P. Marijon, D. Meleshko, D. R. Mende, A. Milanese, N. Nagarajan, J. Nissen, S. Nurk, L. Oliker, L. Paoli, P. Peterlongo, V. C. Piro, J. S. Porter, S. Rasmussen, E. R. Rees, K. Reinert, B. Renard, E. M. Robertsen, G. L. Rosen, H.-J. Ruscheweyh, V. Sarwal, N. Segata, E. Seiler, L. Shi, F. Sun, S. Sunagawa, S. J. Sørensen, A. Thomas, C. Tong, M. Trajkovski, J. Tremblay, G. Uritskiy, R. Vicedomini, Z. Wang, Z. Wang, Z. Wang, A. Warren, N. P. Willassen, K. Yelick, R. You, G. Zeller, Z. Zhao, S. Zhu, J. Zhu, R. Garrido-Oter, P. Gastmeier, S. Hacquard, S. Häußler, A. Khaledi, F. Maechler, F. Mesny, S. Radutoiu, P. Schulze-Lefert, N. Smit, T. Strowig, A. Bremges, A. Sczyrba, A. C. McHardy, Critical Assessment of Metagenome Interpretation: the second round of challenges. *Nat. Methods* **19**, 429–440 (2022).

107. M. Kolmogorov, J. Yuan, Y. Lin, P. A. Pevzner, Assembly of long, error-prone reads using repeat graphs. *Nat. Biotechnol.* **37**, 540–546 (2019).

108. L. Gabriel, T. Brůna, K. J. Hoff, M. Ebel, A. Lomsadze, M. Borodovsky, M. Stanke, BRAKER3: Fully automated genome annotation using RNA-seq and protein evidence with GeneMark-ETP, AUGUSTUS, and TSEBRA. *Genome Res.* **34**, 769–777 (2024).

109. G. Yang, L. Tang, Y. Gong, J. Xie, Y. Fu, D. Jiang, G. Li, D. B. Collinge, W. Chen, J. Cheng, A cerato-platanin protein SsCP1 targets plant PR1 and contributes to virulence of Sclerotinia sclerotiorum. *New Phytol.* **217**, 739–755 (2018).

110. W. Zuo, J. R. L. Depotter, S. C. Stolze, H. Nakagami, G. Doehlemann, A transcriptional activator effector of Ustilago maydis regulates hyperplasia in maize during pathogen-induced tumor formation. *Nat. Commun.* **14**, 6722 (2023).

111. Y. Bai, D. B. Müller, G. Srinivas, R. Garrido-Oter, E. Potthoff, M. Rott, N. Dombrowski, P. C. Münch, S. Spaepen, M. Remus-Emsermann, B. Hüttel, A. C. McHardy, J. A. Vorholt, P. Schulze-Lefert, Functional overlap of the Arabidopsis leaf and root microbiota. *Nature* **528**, 364–369 (2015).

112. S. Seabold, J. Perktold, “statsmodels: Econometric and statistical modeling with python” in *9th {Python} in {Science} {Conference}* (2010).

113. S. Graves, H.-P. Piepho, L. Selzer, multcompView: Visualizations of paired comparisons. (2024). https://github.com/lselzer/multcompview.

114. C. L. Schoch, S. Ciufo, M. Domrachev, C. L. Hotton, S. Kannan, R. Khovanskaya, D. Leipe, R. McVeigh, K. O’Neill, B. Robbertse, S. Sharma, V. Soussov, J. P. Sullivan, L. Sun, S. Turner, I. Karsch-Mizrachi, NCBI Taxonomy: a comprehensive update on curation, resources and tools. *Database* **2020** (2020).

115. N. Istifadah, J. A. Saleeba, P. A. McGee, Isolates of endophytic Chaetomium spp. inhibit the fungal pathogen Pyrenophora tritici-repentis in vitro. *Can. J. Bot.* **84**, 1148–1155 (2006).

116. T. Sakamoto, J. M. Ortega, Taxallnomy: an extension of NCBI Taxonomy that produces a hierarchically complete taxonomic tree. *BMC Bioinformatics* **22**, 1–23 (2021).

117. G. Wang, X. Li, Z. Wang, APD3: the antimicrobial peptide database as a tool for research and education. *Nucleic Acids Res.* **44**, D1087–D1093 (2016).

118. L. V. Hedges, Distribution theory for Glass’s estimator of effect size and related estimators. *J. Educ. Stat.* **6**, 107–128 (1981).

Supplementary Materials

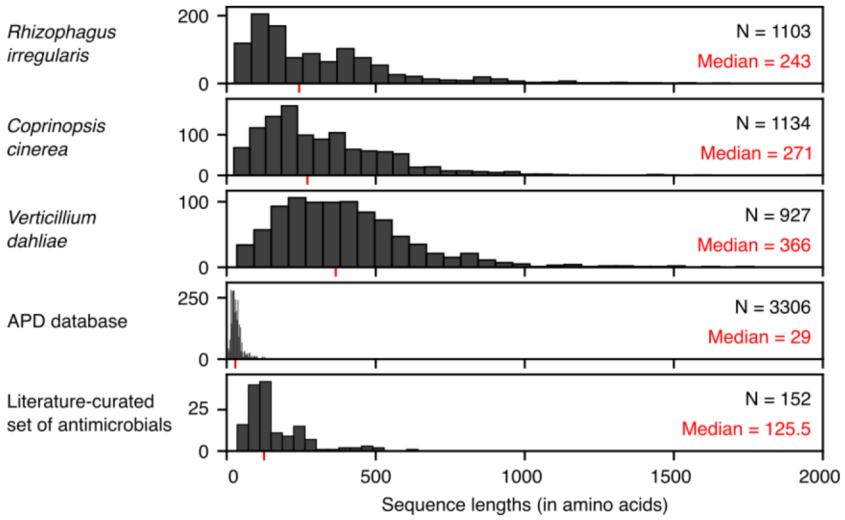

Fig. S1. Protein sequence lengths in three fungal secretomes, the AMP database APD and a literature-curated set of antimicrobials. The top three histograms show mature sequence lengths (in number of amino acids) of secreted proteins predicted with SignalP (51) in three fungi selected based on their distance in the tree of life and their distinct lifestyles: the Glomeromycota mycorrhizal fungus *Rhizophagus irregularis*, the Basidiomycete saprophyte *Coprinopsis cinerea*, and the Ascomycete plant pathogen *Verticillium dahliae*. The fourth histogram shows the length of AMPs in the APD database (117), which was previously used to train published antimicrobial peptide predictors. The bottom histogram shows sequence lengths in our newly curated set of antimicrobial proteins, used as a positive training set to develop AMAPEC.

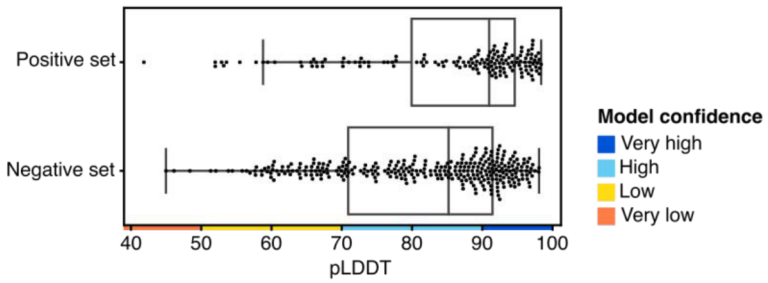

Fig. S2. Confidence of predicted structures in the training datasets. Boxplots showing the distribution of mean pLDDT confidence scores of AlphaFold-predicted protein structures in the positive and negative training sets. The color code depicting model confidence originates from the AlphaFold documentation (59).

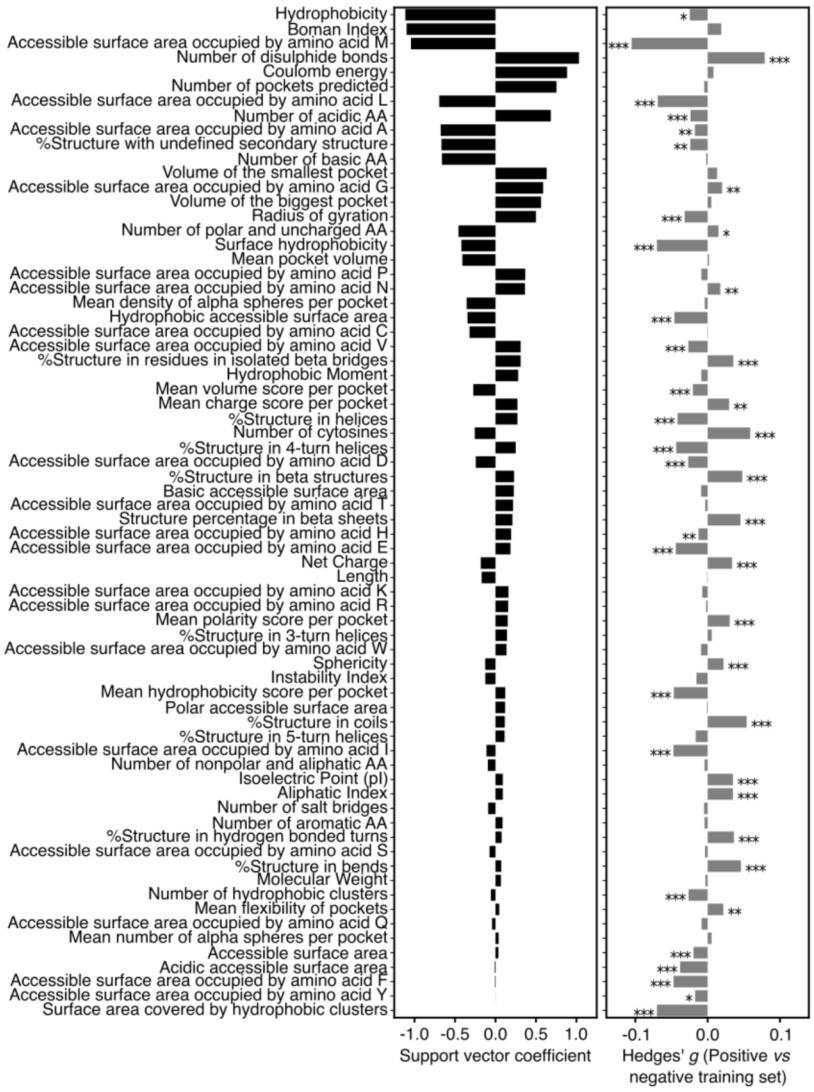

Fig. S3. Physicochemical properties of proteins and their importance for antimicrobial activity prediction. Physicochemical properties implemented in the AMAPEC training pipeline (Fig. 1, C) are listed and ranked according to their importance for our Support Vector Machines (SVM) classifier (vector weights). The left barplot (black) shows support vector coefficients, representing vector weights and orientation. The right barplot (grey) shows the results of an enrichment analysis testing for significant differences between values in the positive and in the negative training set. This analysis was conducted by Mann-Whitney U test and Benjamini-Hochberg correction (FDR values depicted with asterisks: *: ≤0.05; **≤0.01; ***≤0.001) and we additionally calculated standard effect sizes (Hedges' g, (118).

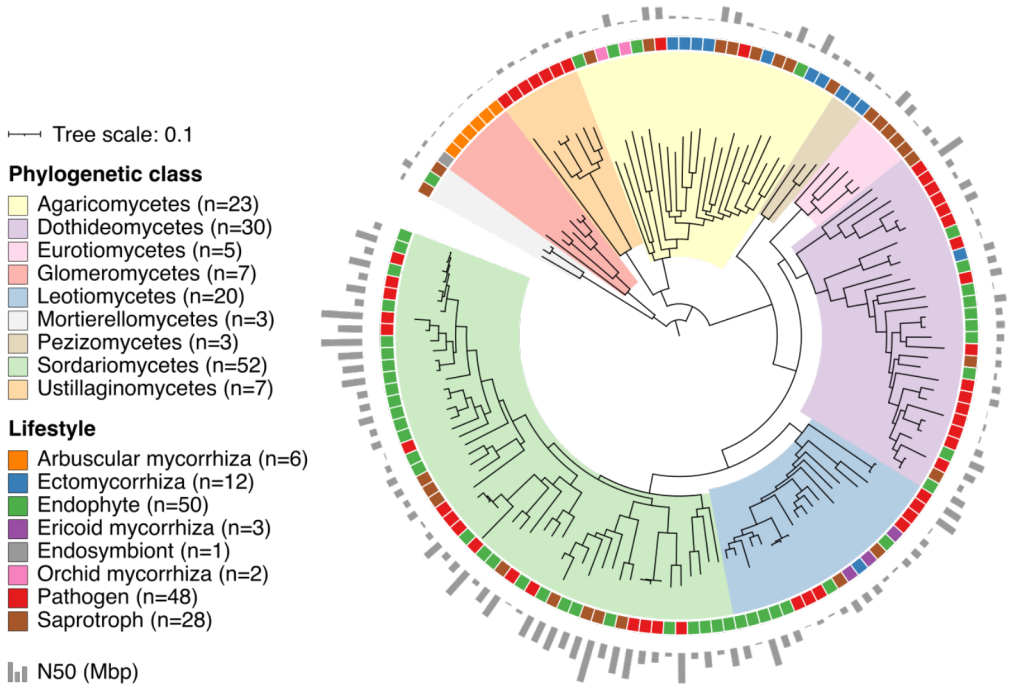

Fig. S4. Description of the dataset of 150 fungal genomes used for comparative genomics. Phylogenomic tree calculated on total sets of proteins from the selected 150 fungi (STAG method (82) implemented in OrthoFinder (80)). Color ranges on the phylogenomic tree highlight phylogenetic classes and fungal lifestyles are indicated. A barplot shows the N50 values, reflecting overall genome quality and fragmentation.

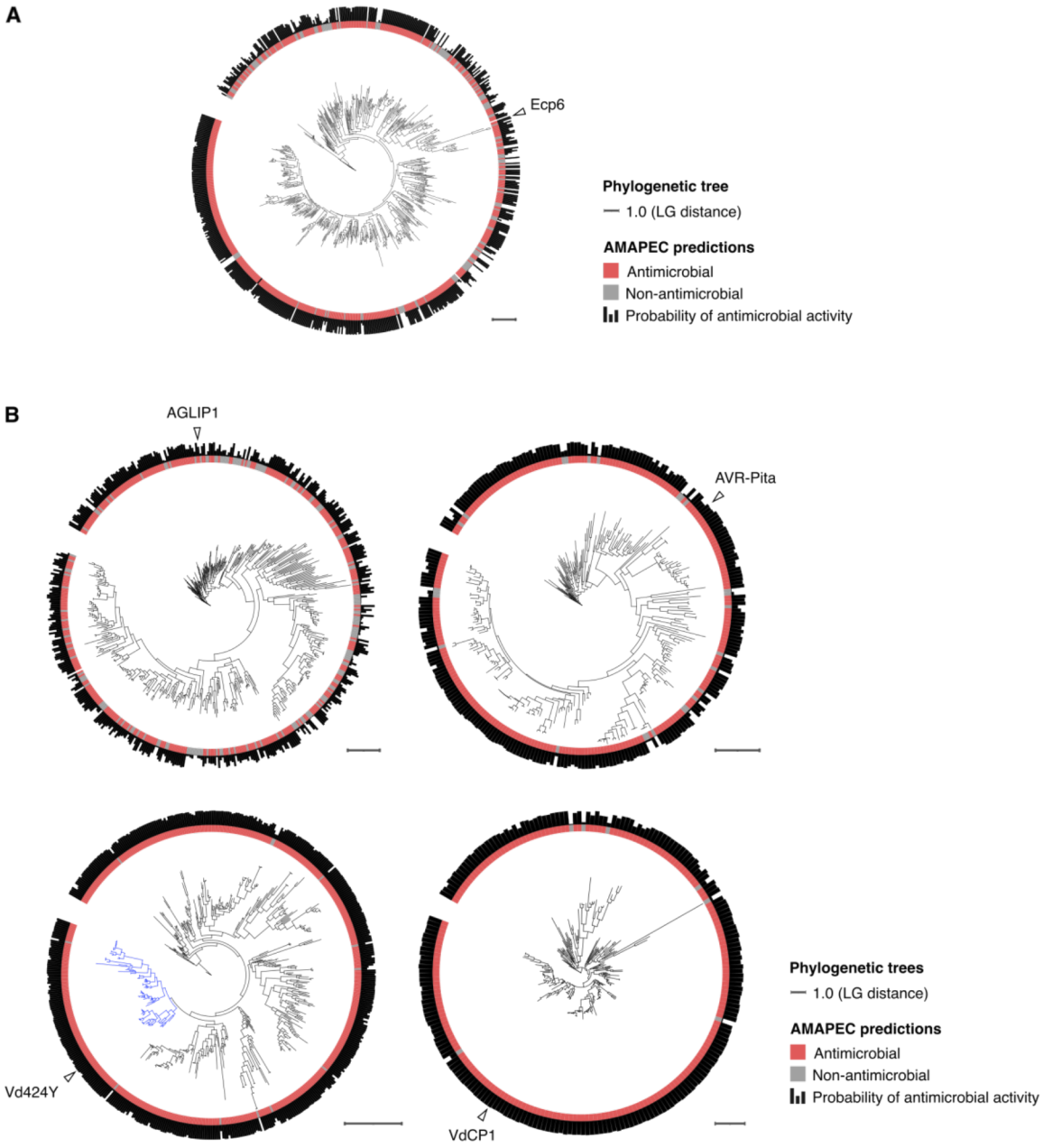

Fig. S5. Phylogenies of five secreted protein families, including reference effectors, with antimicrobial activity prediction for each family member. (A) Phylogeny and antimicrobial activity prediction calculated on LysM effectors annotated in the fungal dataset of 150 genomes and additionally in *Cladosporium fulvum*, which encodes the reference Ecp6 effector (37). (B) Phylogenies of the families of AGLIP1, AVR-Pita, Vd424Y and VdCP1 as defined by orthology prediction in the dataset of 150 fungal genomes. All five phylogenies were calculated by sequence alignment of mature sequence proteins with MAFFT (89), and phylogenetic reconstruction with IQ-TREE (88) with maximum-likelihood model 'LG'. In the family tree of Vd424Y, the clade depicted in blue was considered as the Vd424Y subfamily and was further analyzed in Fig. 4, A and fig. S17.

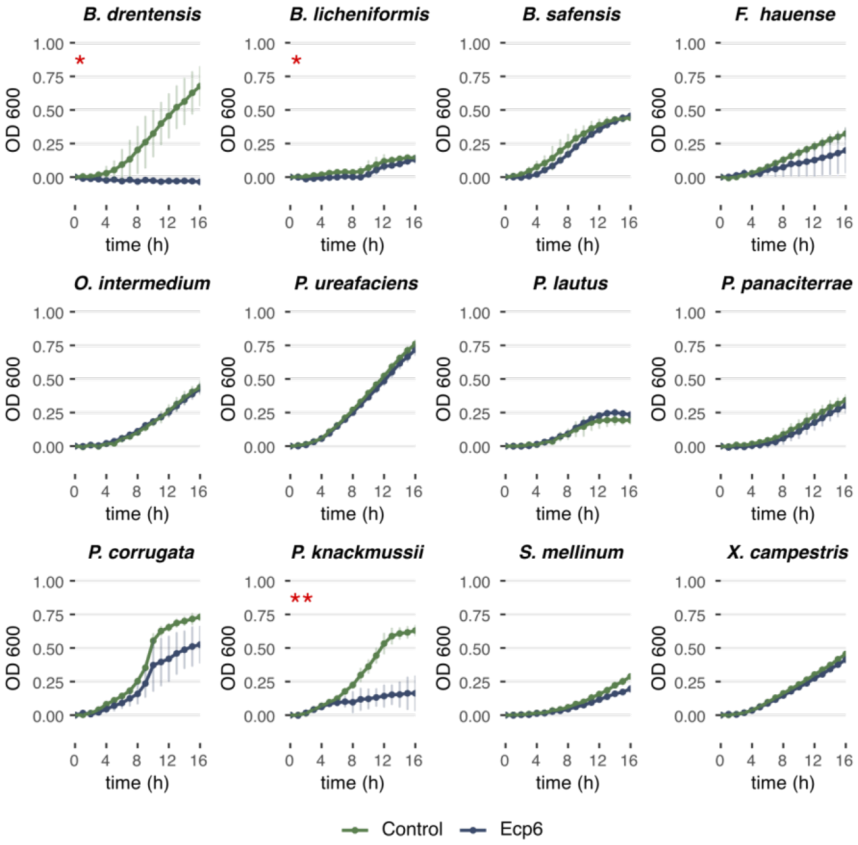

Fig. S6. Selective antibacterial activity displayed in vitro by the Ecp6 effector protein of the tomato leaf mold pathogen *Cladosporium fulvum*. Absorbance measurements (at wavelength 600 nm) over 16 hours of bacterial cultivation in presence and absence of 8 µM of heterologously produced effector protein. Each growth curve represents to the mean OD_{600} over 3 independent replicates and error bars correspond to the standard deviation. The assay was performed on a phylogenetically diverse set of 12 bacterial isolates, which species-level phylogeny can be seen on Fig. 3, C. Asterisks highlight significance (p-value < 0.05) of a Student's T-tests computed on area-under-curve values comparing bacterial growth in presence and absence of effector protein: ***: P < 0.001, **: P < 0.01, *: P < 0.05.

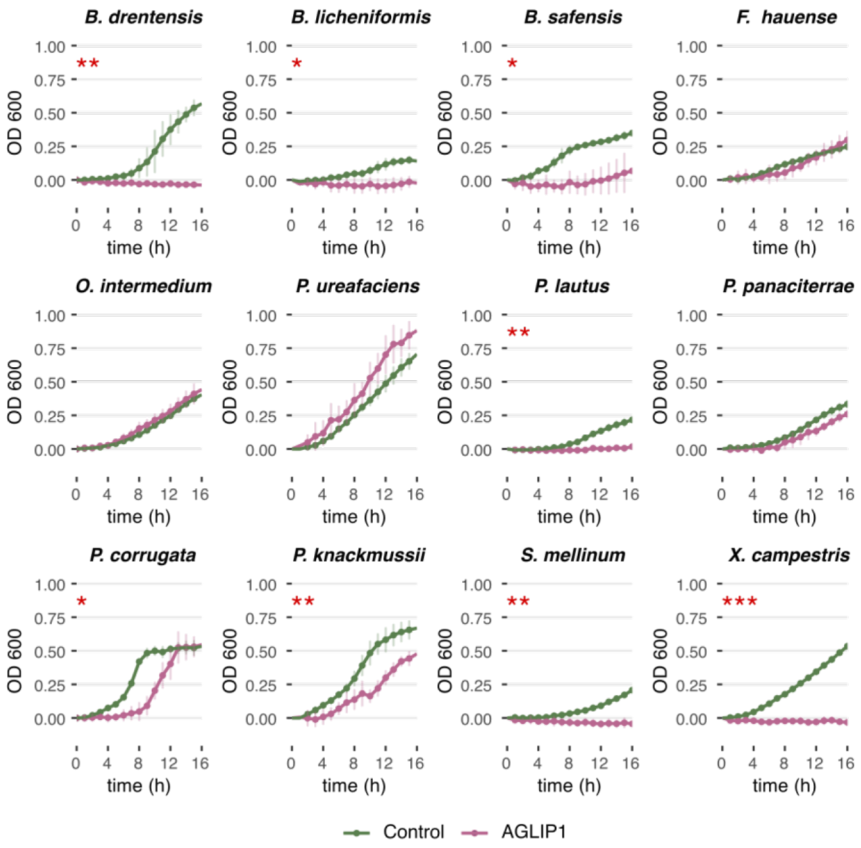

Fig. S7. Selective antibacterial activity displayed in vitro displayed by the AGLIP1 effector protein of the root rot pathogen *Rhizoctonia solani*. Absorbance measurements (at wavelength 600 nm) over 16 hours of bacterial cultivation in presence and absence of 8 µM of heterologously produced effector protein. Each growth curve represents to the mean OD_{600} over 3 independent replicates and error bars correspond to the standard deviation. The assay was performed on a phylogenetically diverse set of 12 bacterial isolates, which species-level phylogeny can be seen on Fig. 3, C. Asterisks highlight significance (p-value < 0.05) of a Student's T-tests computed on area-under-curve values comparing bacterial growth in presence and absence of effector protein: ***: P < 0.001, **: P < 0.01, *: P < 0.05.

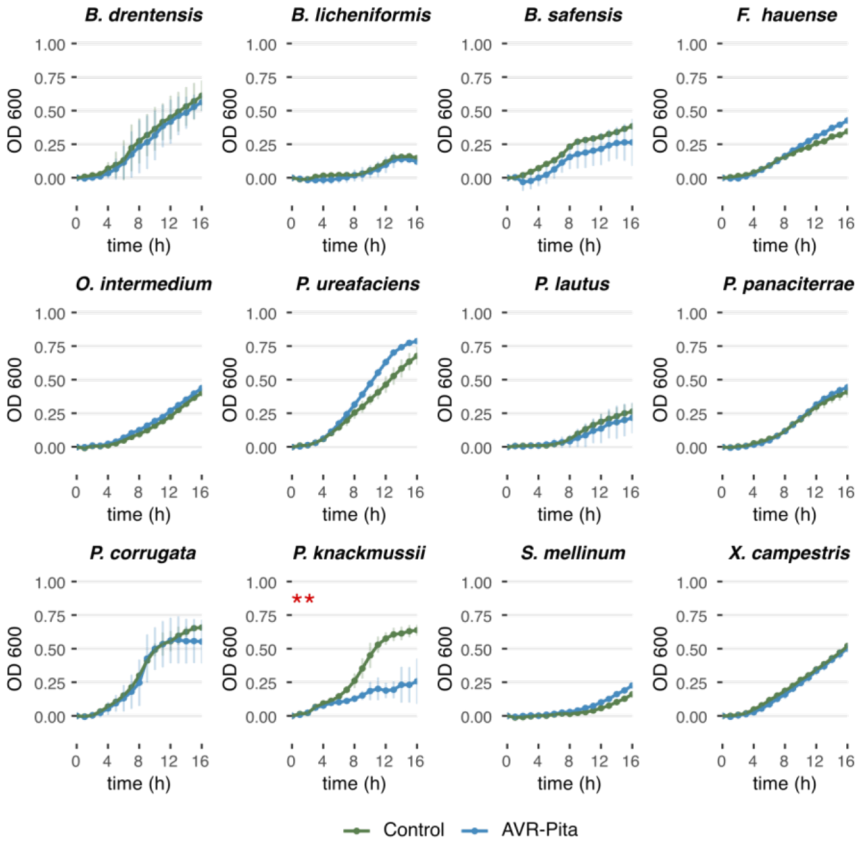

Fig. S8. Selective antibacterial activity displayed in vitro by the AVR-Pita effector protein of the rice blast pathogen *Magnaporthe oryzae*. Absorbance measurements (at wavelength 600 nm) over 16 hours of bacterial cultivation in presence and absence of 8 µM of heterologously produced effector protein. Each growth curve represents to the mean OD_{600} over 3 independent replicates and error bars correspond to the standard deviation. The assay was performed on a phylogenetically diverse set of 12 bacterial isolates, which species-level phylogeny can be seen on Fig. 3, C. Asterisks highlight significance (p-value < 0.05) of a Student's T-tests computed on area-under-curve values comparing bacterial growth in presence and absence of effector protein: ***: P < 0.001, **: P < 0.01, *: P < 0.05.

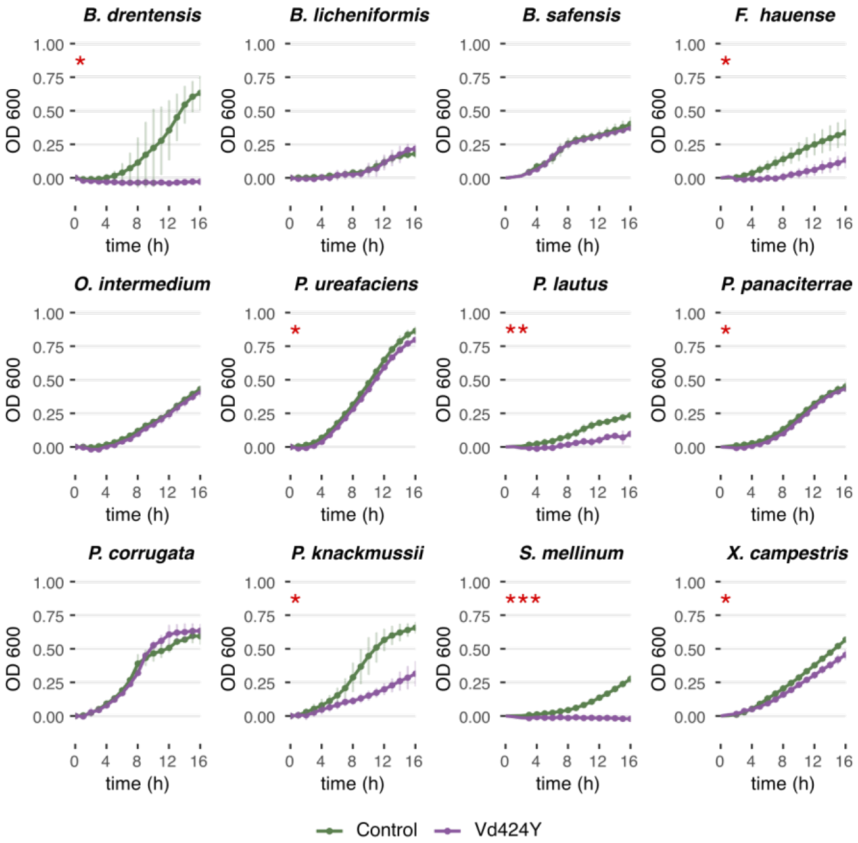

Fig. S9. Selective antibacterial activity displayed in vitro by the Vd424Y effector protein of the vascular wilt pathogen *Verticillium dahliae*. Absorbance measurements (at wavelength 600 nm) over 16 hours of bacterial cultivation in presence and absence of 8 µM of heterologously produced effector protein. Each growth curve represents to the mean OD_{600} over 3 independent replicates and error bars correspond to the standard deviation. The assay was performed on a phylogenetically diverse set of 12 bacterial isolates, which species-level phylogeny can be seen on Fig. 3, C. Asterisks highlight significance (p-value < 0.05) of a Student's T-tests computed on area-under-curve values comparing bacterial growth in presence and absence of effector protein: ***: P < 0.001, **: P < 0.01, *: P < 0.05.

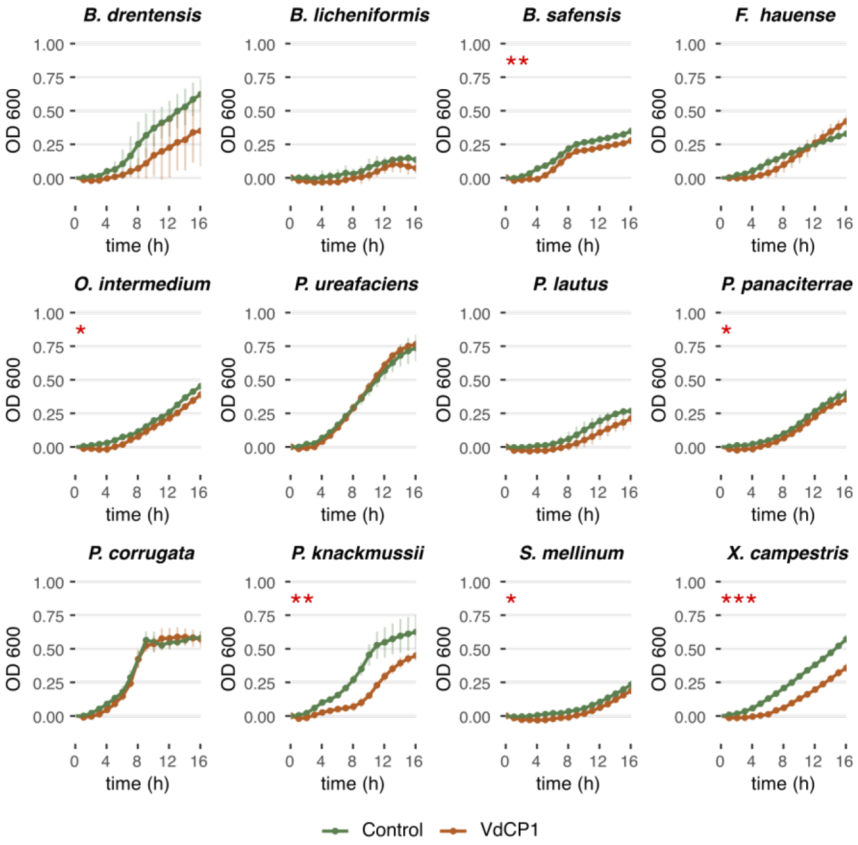

Fig. S10. Selective antibacterial activity displayed in vitro by the VdCP1 effector protein of the vascular wilt pathogen *Verticillium dahliae*. Absorbance measurements (at wavelength 600 nm) over 16 hours of bacterial cultivation in presence and absence of 8 µM of heterologously produced effector protein. Each growth curve represents to the mean OD_{600} over 3 independent replicates and error bars correspond to the standard deviation. The assay was performed on a phylogenetically diverse set of 12 bacterial isolates, which species-level phylogeny can be seen on Fig. 3, C. Asterisks highlight significance (p-value < 0.05) of a Student's T-tests computed on area-under-curve values comparing bacterial growth in presence and absence of effector protein: ***: P < 0.001, **: P < 0.01, *: P < 0.05.

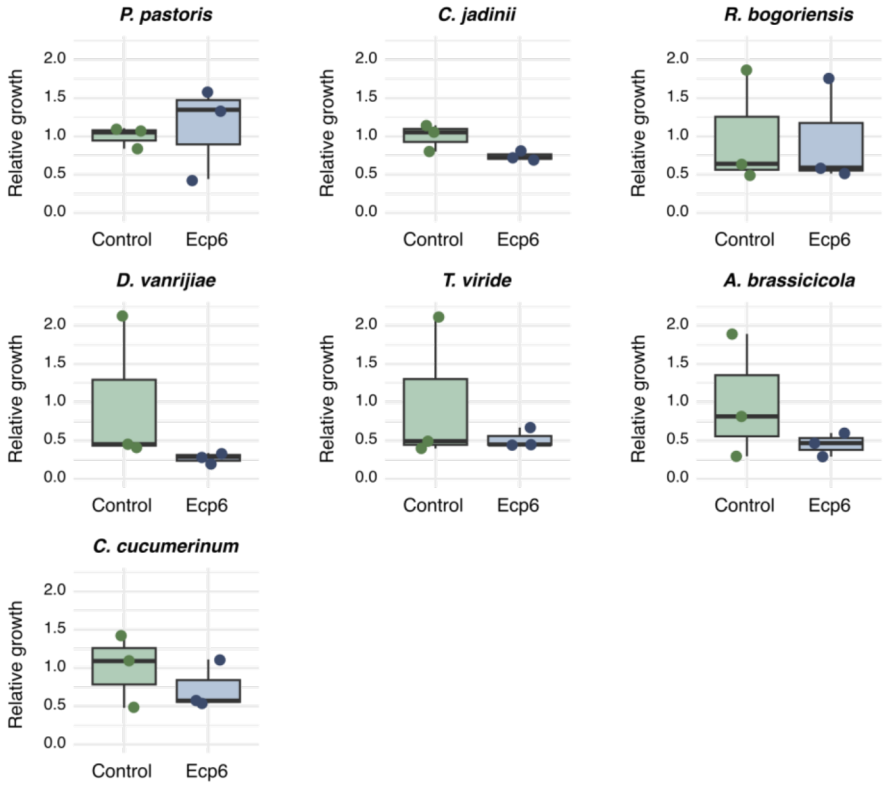

Fig. S11. Absence of antifungal activity displayed in vitro by the Ecp6 effector protein of the tomato leaf mold pathogen *Cladosporium fulvum*. Normalized fungal areas measured on microscopy photographs of growth medium, after 16 hours of fungal culture in presence and absence of 8 µM of heterologously produced effector protein. The assay was performed on a phylogenetically diverse set of seven fungal isolates, which species-level phylogeny can be seen on Fig. 3, D. Asterisks highlight significance (p-value < 0.05) of a Student's T-tests computed comparing fungal growth in presence and absence of effector protein: ***: P < 0.001, **: P < 0.01, *: P < 0.05.

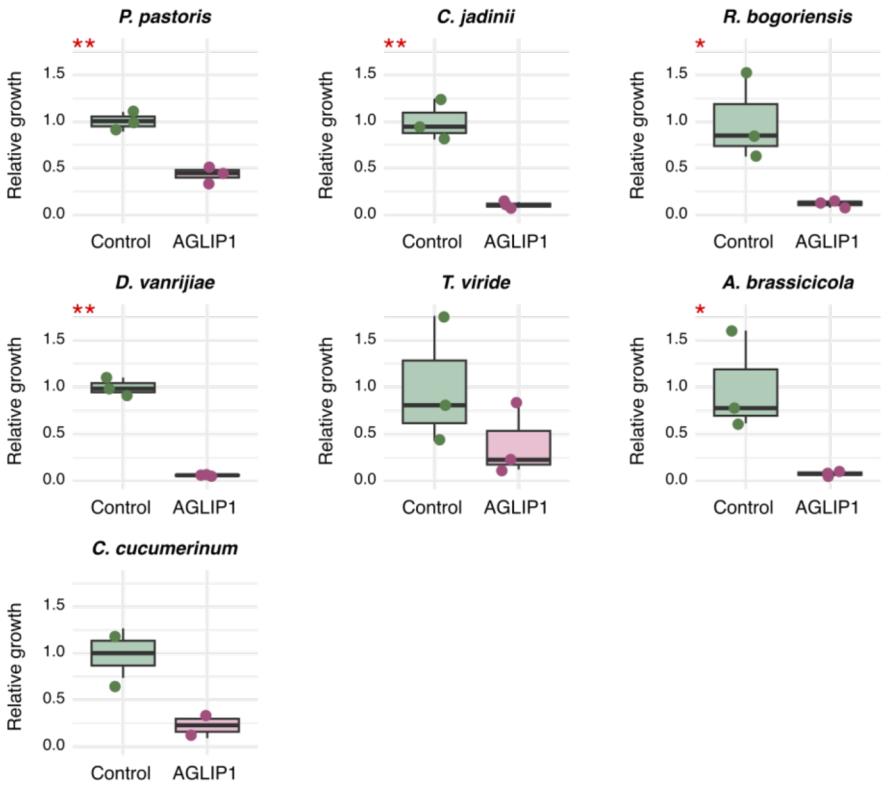

Fig. S12. Antifungal activity displayed in vitro by the AGLIP1 effector protein of the root rot pathogen *Rhizoctonia solani*. Normalized fungal areas measured on microscopy photographs of growth medium, after 16 hours of fungal culture in presence and absence of 8 µM of heterologously produced effector protein. The assay was performed on a phylogenetically diverse set of seven fungal isolates, which species-level phylogeny can be seen on Fig. 3, D. Asterisks highlight significance (p-value < 0.05) of a Student's T-tests computed comparing fungal growth in presence and absence of effector protein: ***: P < 0.001, **: P < 0.01, *: P < 0.05.

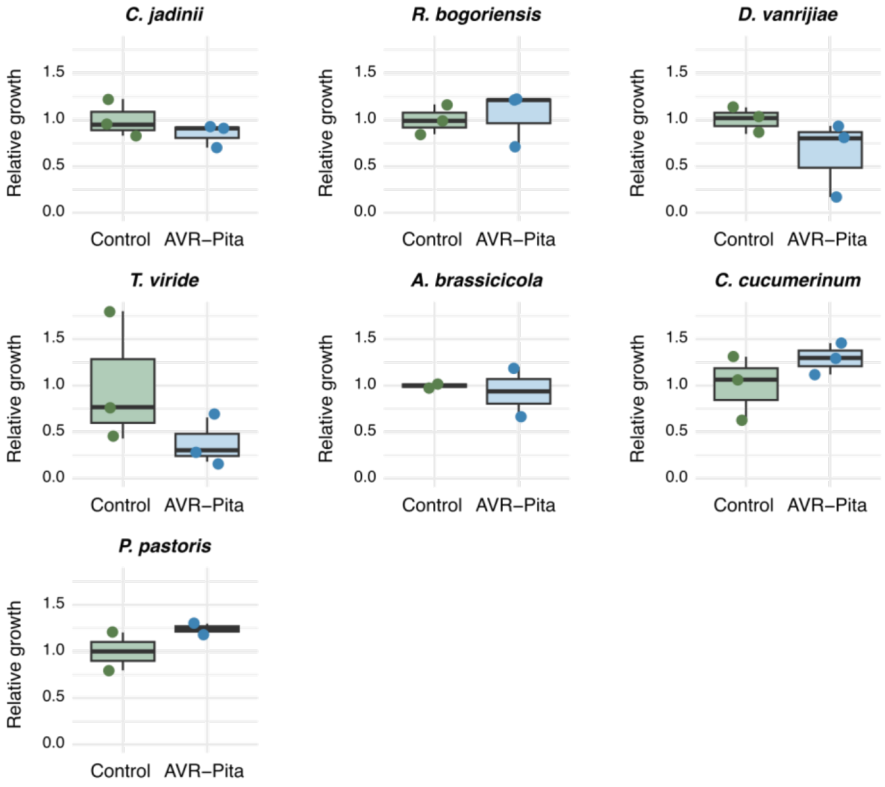

Fig. S13. Absence of antifungal activity displayed in vitro by the AVR-Pita effector protein of the rice blast pathogen *Magnaporthe oryzae*. Normalized fungal areas measured on microscopy photographs of growth medium, after 16 hours of fungal culture in presence and absence of 8 µM of heterologously produced effector protein. The assay was performed on a phylogenetically diverse set of seven fungal isolates, which species-level phylogeny can be seen on Fig. 3, D. Asterisks highlight significance (p-value < 0.05) of a Student's T-tests computed comparing fungal growth in presence and absence of effector protein: ***: P < 0.001, **: P < 0.01, *: P < 0.05.

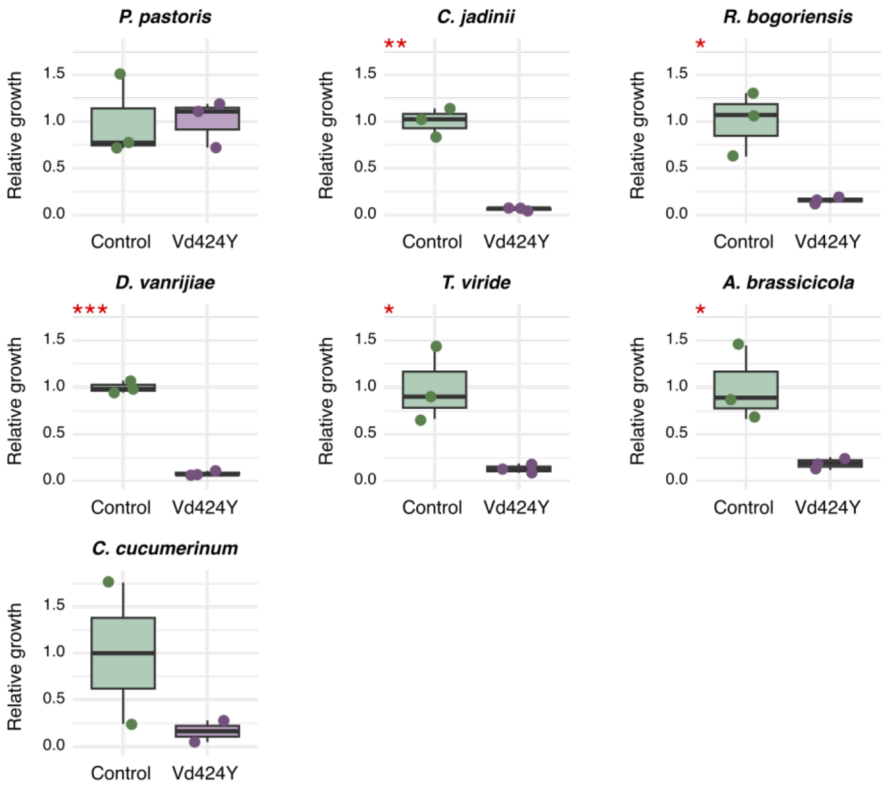

Fig. S14. Antifungal activity displayed in vitro by the Vd424Y effector protein of the vascular wilt pathogen *Verticillium dahliae*. Normalized fungal areas measured on microscopy photographs of growth medium, after 16 hours of fungal culture in presence and absence of 8 µM of heterologously produced effector protein. The assay was performed on a phylogenetically diverse set of seven fungal isolates, which species-level phylogeny can be seen on Fig. 3, D. Asterisks highlight significance (p-value < 0.05) of a Student's T-tests computed comparing fungal growth in presence and absence of effector protein: ***: P < 0.001, **: P < 0.01, *: P < 0.05.

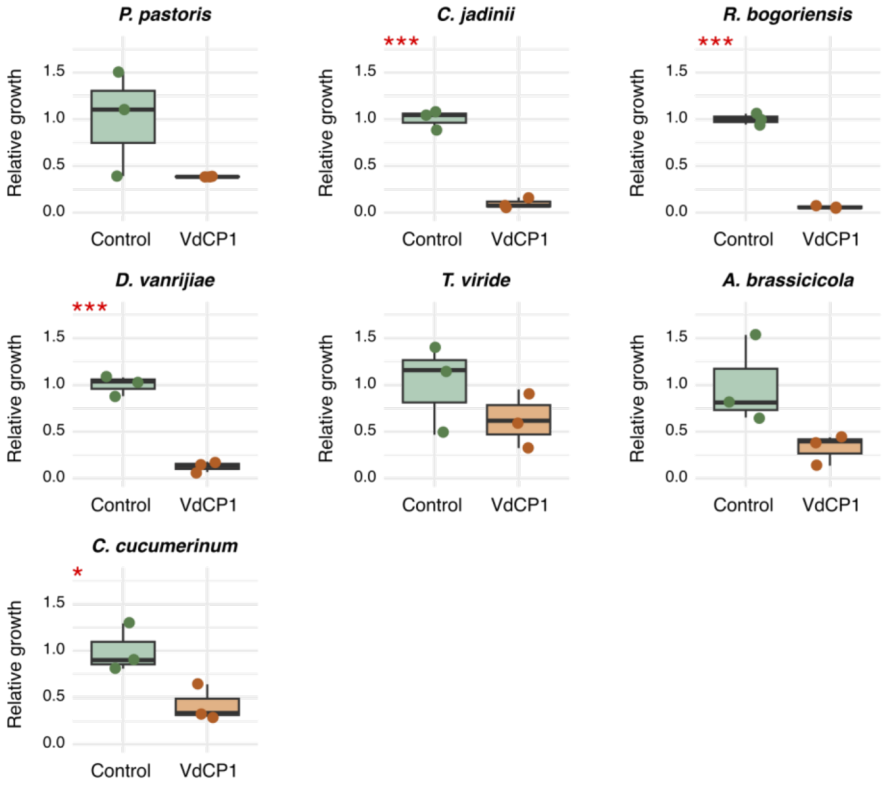

Fig. S15. Antifungal activity displayed in vitro by the VdCP1 effector protein of the vascular wilt pathogen *Verticillium dahliae*. Normalized fungal areas measured on microscopy photographs of growth medium, after 16 hours of fungal culture in presence and absence of 8 µM of heterologously produced effector protein. The assay was performed on a phylogenetically diverse set of seven fungal isolates, which species-level phylogeny can be seen on Fig. 3, D. Asterisks highlight significance (p-value < 0.05) of a Student's T-tests computed comparing fungal growth in presence and absence of effector protein: ***: P < 0.001, **: P < 0.01, *: P < 0.05.

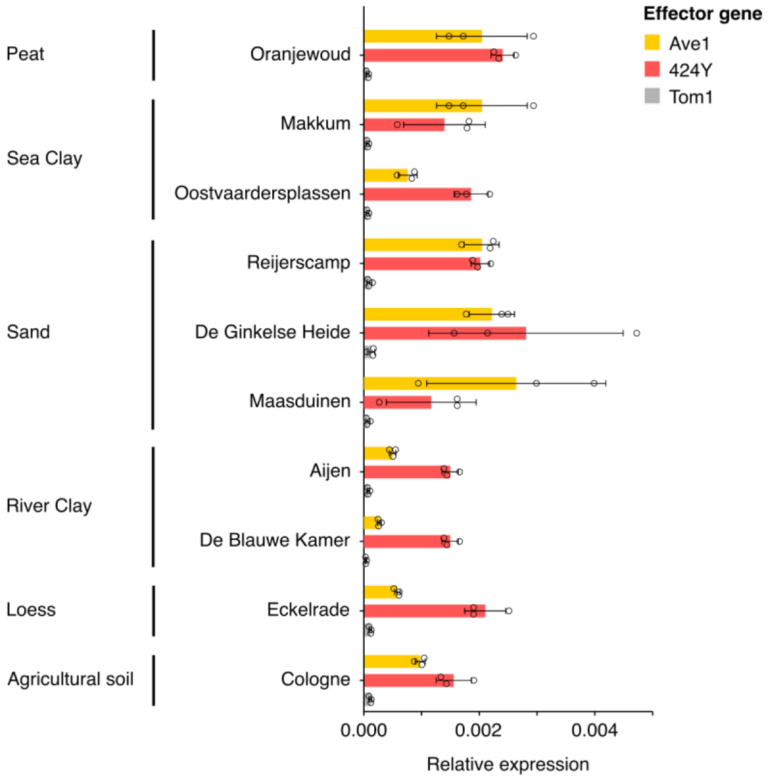

Fig. S16. Expression of the *Verticillium dahliae* 424Y-encoding gene in a diverse set of soils. Real-time PCR measurements of effector gene expression in a diverse set of 10 soils (94), classified by soil type (left). In addition to the 424Y-encoding gene, effector genes Ave1 (7) and Tom1 (95) were studied and serve as positive and negative controls, respectively.

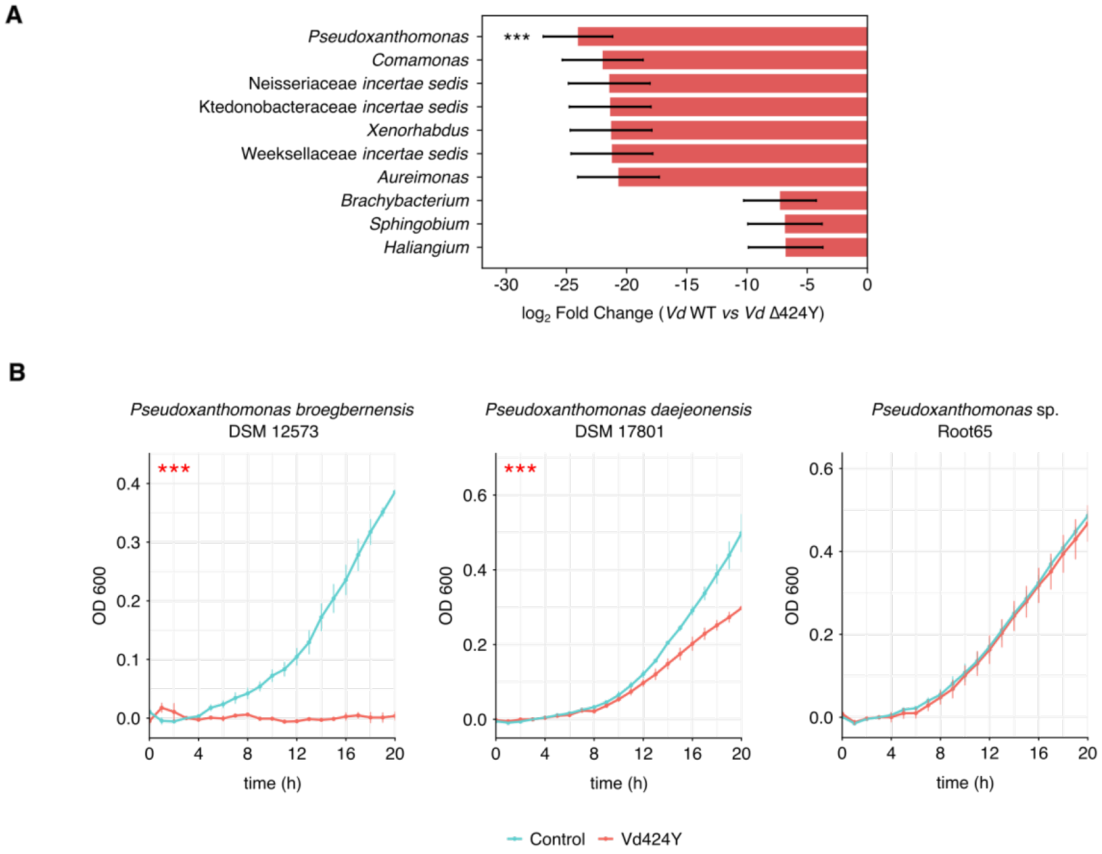

Fig. S17. Candidate bacterial targets of Vd424Y in tomato plant microbiota. (**A**) Barplot showing the log2-transformed fold change values and standard errors of the 10 bacterial genera that are the most depleted in presence of the *Vd424Y* gene in *Verticillium dahliae*-infected plant tissues. These data were obtained by applying the method DESeq2 on the number of reads assigned to each bacterial genus in three plant samples per condition. (**B**) Absorbance measurements (at wavelength 600 nm) over 20 hours of bacterial cultivation in presence and absence of 8 µM of heterologously produced Vd424Y protein. Each growth curve represents to the mean OD_{600} over 3 replicates and error bars correspond to the standard deviation. This assay was performed on three bacterial isolates from genus *Pseudoxanthomonas*. Asterisks highlight significance (p-value < 0.05) of a Student's T-tests computed on area-under-curve values comparing bacterial growth in presence and absence of effector protein: ***: P < 0.001, **: P < 0.01, *: P < 0.05.

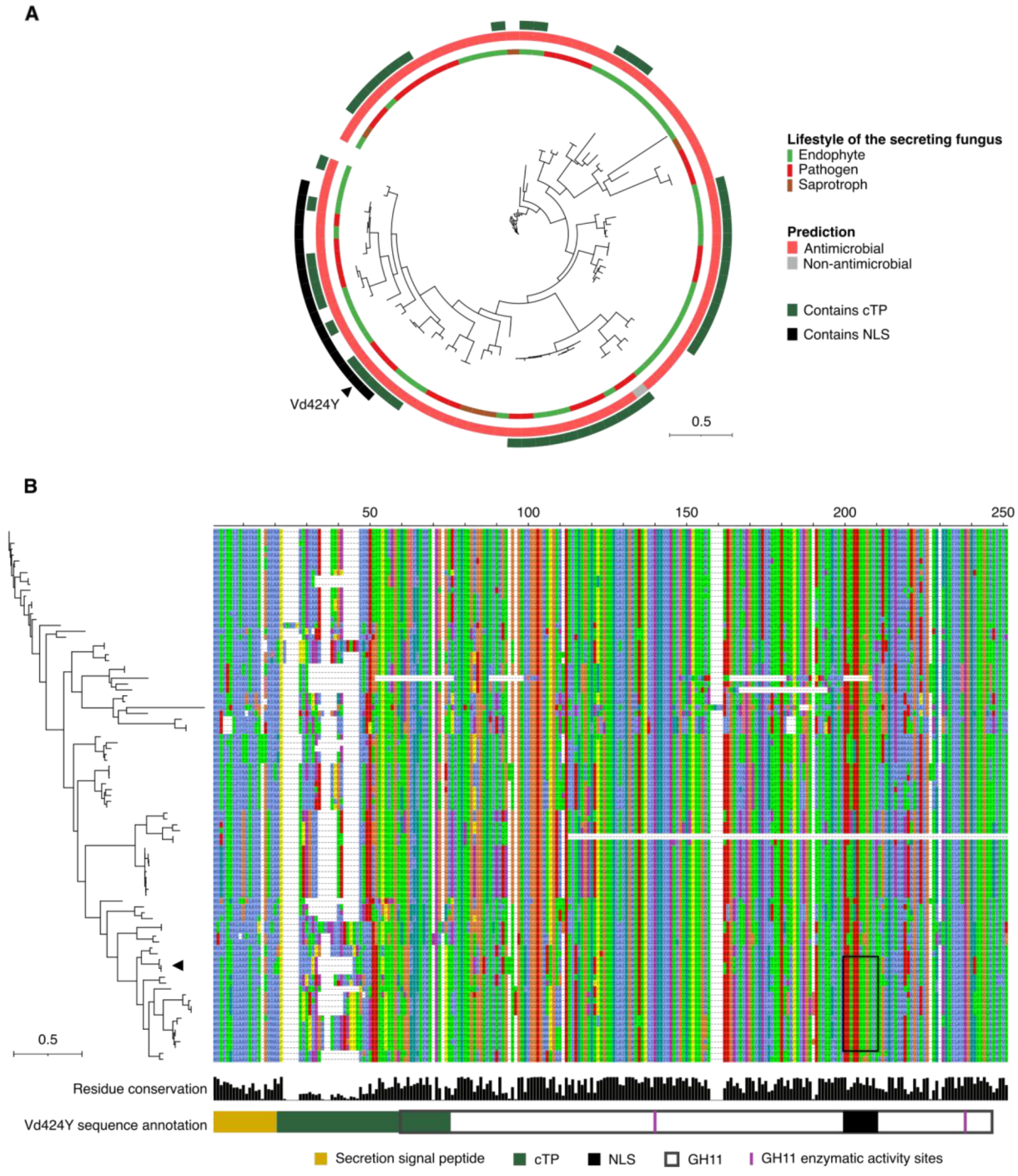

Fig. S18. Evolution of Vd424Y sequence features. (**A**) Maximum-likelihood phylogenetic tree (computed with IQ-TREE (88), model 'LG') of Vd424Y homologs in a dataset of 150 fungal genomes. The set of proteins represent those occurring in the same subfamily (large clade) as Vd424Y, as identified in the total family phylogenetic tree (fig. S5). The tree was manually rooted at the protein identified as an optimal outgroup by IQ-TREE and annotated with the lifestyles of the fungus secreting each protein, the results of antimicrobial activity as well as the occurrence of a chloroplast transit peptide

(cTP) and nuclear localization signal (NLS) annotated using ChloroP (92) and cNLS Mapper (93), respectively. (**B**) The same phylogenetic tree as on panel A is displayed on the left, with a black triangle indicating the location of Vd424Y. On the right, the protein sequence alignment (generated with MAFFT (89)) presents sequence variation in the Vd424Y subfamily. A black rectangle circumscribes annotated NLS motifs in the sequences. At the bottom, a barplot presents the conservation of amino acids at each position in the protein sequence. Below, a diagram shows the organization in functional domains of the Vd424Y sequence, as characterized previously (32).

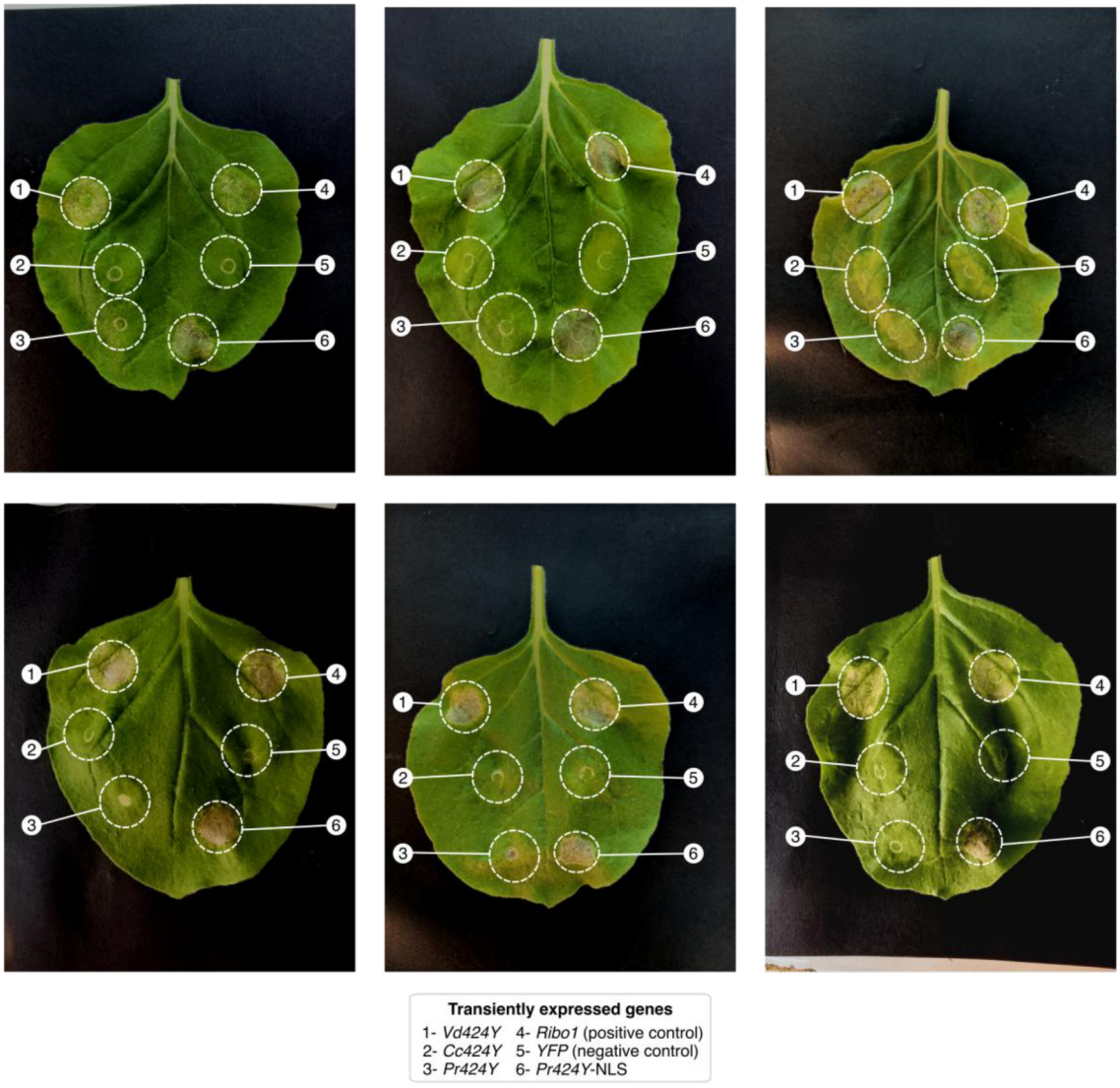

Fig. S19. *Nicotiana benthamiana* leaves transiently expressing Vd424Y and its homologs. Photographs showing the phenotypes of *N. benthamiana* leaves infiltrated with engineered *Agrobacterium tumefaciens* strains to mediate the transient expression of effector genes Vd424Y from *Verticillium dahliae* (1), Cc424Y from *Coprinopsis cinerea* (2), Pr424Y from *Penicillium restrictum* (3), Ribo1 from *Ustilago maydis* (11) as a positive control (4), YFP as a negative control (5) and a chimeric gene corresponding to Pr424Y that carries the NLS of Vd424Y (6). Leaf areas that were infiltrated are circled by dotted white lines and annotated with the names of the genes that were transiently expressed. These six photos present replicates of the experiment shown in Fig. 5, B.

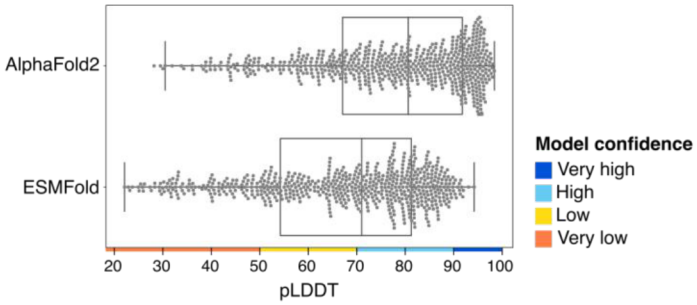

Fig. S20. Confidence of AlphaFold2- and ESMFold-predicted structures for secreted proteins of *Verticillium dahliae*. Boxplots showing the distribution of mean pLDDT confidence scores of AlphaFold2 (59)- and ESMFold (70)-predicted structures for 626 non-CAZyme secreted proteins of *Verticillium dahliae*. While the secretome of *V. dahliae* includes 635 non-CAZyme proteins, AlphaFold2 failed at predicting the structures of nine of these proteins, which were therefore excluding from this analysis. The color code depicting model confidence originates from the documentation of AlphaFold2.

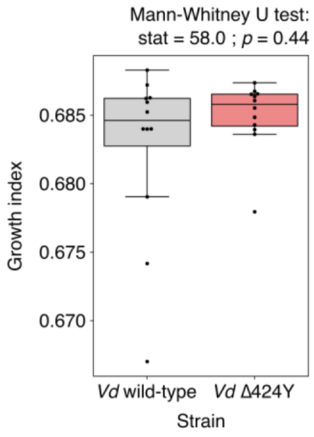

Fig. S21. Growth of *Verticillium dahliae* wild-type and Δ*424Y* mutant in vitro. Boxplot showing growth indices of *Verticillium dahliae* JR2 wild-type and Δ*424Y* calculated from quantitative PCR Ct values (see Material and methods for details) after 48 hours in growth medium. In total, 12 samples per condition corresponding to 12 independent fungal cultures over 3 biological replicates were analyzed. Results of a Mann-Whitney U test revealing no significant difference between the wild-type and the mutant strain are written on top of the figure.

Chapter 5

Conserved antimicrobial activity of the fungal cerato-platanin protein family uncovered through structural clustering of *Verticillium dahliae* effectors

Anton Kraege, Valentina Wolf[#], Fantin Mesny[#], Gabriella C. Petti, Jinyi Zhu, Ole Nielsen, Noah Busch, Bart P.H.J. Thomma*

University of Cologne, Institute for Plant Sciences, Cluster of Excellence on Plant Sciences (CEPLAS), 50674 Cologne, Germany;

[#]These authors contributed equally

*To whom correspondence should be addressed. E-mail: bthomma@uni-koeln.de

Abstract

Pathogens deploy secreted effector proteins to manipulate host biology and promote disease. Beyond direct host targeting, increasing evidence shows that effectors can also shape host-associated microbiota through antimicrobial activity. Despite their functional importance, the evolutionary origins of most effectors remain poorly understood. Recent advances in protein structure prediction have revealed that effector proteins with little or no sequence similarity can nonetheless share highly conserved structural folds across diverse fungal pathogens. Here, we applied structure-based clustering to the *Verticillium dahliae* secretome and unexpectedly identified a group of effectors comprising the known antimicrobial protein Ave1 together with three sequence-unrelated cerato-platanins (CPs), a widespread fungal protein family previously linked to cell wall interactions and host immune activation. Functional assays showed that all three CPs, like Ave1, exhibit selective antimicrobial activity *in vitro*. To assess the evolutionary conservation of this function, we analyzed CPs from 150 fungal species spanning broad phylogenetic distances and ecological lifestyles. Nearly all CPs were predicted to possess antimicrobial properties, and we experimentally confirmed antimicrobial activity in CPs from both pathogenic and non-pathogenic fungi. Together, these results indicate that cerato-platanins represent an ancient and conserved class of antimicrobial proteins that have been recurrently co-opted as effectors during the evolution of fungal pathogenicity. More broadly, our findings support the emerging view that pathogen effectors that target host physiology often derive from ancestral antimicrobial proteins, highlighting an evolutionary link between microbial competition and host manipulation.

Introduction

Throughout all their organs, plants associate with a plethora of microbes, collectively called the plant microbiota, which mainly comprises bacteria, fungi and protists (Trivedi et al., 2020). The composition of the plant microbiota is organ-specific and determined through an interplay of biotic and abiotic factors such as traits encoded by the plant genotype and environmental conditions (Bulgarelli et al., 2012; Punt et al., 2025; Wagner et al., 2016). Plants are able to enrich mutualistic and beneficial microbes in their microbiota, thereby allowing them to alleviate both biotic and abiotic stresses (Berendsen et al., 2012; Harbort et al., 2020). Notably, when under pathogen attack, plants can recruit specific microbes into their microbiota in order to diminish disease progression (Liu et al., 2017; Pieterse et al., 2014; Spooren et al., 2024). Consequently, the plant microbiota has been referred to as an additional layer of the plant immune system (Du et al., 2024; Hacquard et al., 2017). Overall, together with their host, these microbial communities form a complex biological unit that functions together to maintain health and fitness, also referred to as a holobiont (Mesny et al., 2023; Vandenkoornhuyse et al., 2015).

To withstand pathogen attacks, plants have evolved an innate immune system capable to detect invading microbes through the recognition of conserved microbial molecules such as flagellin or chitin, activating so-called pattern-triggered immunity (PTI) (Cook et al., 2015; Jones & Dangl, 2006). While PTI is generally sufficient to restrict non-adapted microbes, host-adapted pathogens have evolved to overcome PTI responses through the secretion of so-called effectors; molecules that are secreted during host invasion to support colonization, often through the manipulation of host physiology (Cook et al., 2015; Lo Presti et al., 2015; Rovenich et al., 2014). In turn, resistant host plants evolved to recognize such effectors or their activities and activate effector-triggered immunity (ETI), aiming to reinstall immunity and halting pathogen ingress (Jones & Dangl, 2006). Pathogens can evade such recognition by losing or altering existing effectors, or by evolving new ones that are capable of interfering with host recognition or downstream immune responses. This continuous molecular coevolution is widely described as an evolutionary arms race in which pathogens aim to colonize their hosts while plants try to prevent or halt such colonization (Cook et al., 2015; Jones et al., 2024; Jones & Dangl, 2006).

Recently, several studies have demonstrated that, in addition to modulating host physiology, pathogens exploit effector proteins with antimicrobial activity to manipulate host-associated microbiota to facilitate colonization (Chang et al., 2021; Chavarro-Carrero et al., 2024; Gómez-Pérez et al., 2023; Kettles et al., 2018; Kraege et al., 2026; Mesny et al., 2024, 2025; Ökmen et al., 2023; Snelders et al., 2020, 2021, 2023). Several antimicrobial effectors have been

identified and characterized in *Verticillium dahliae*, a soilborne fungus that causes vascular wilt disease in a wide range of plant species (Fradin & Thomma, 2006). The antimicrobial effectors Ave1, Ave1L2 and Av2 were shown to display selective antibacterial activity and contribute to fungal virulence by targeting antagonistic Sphingomonadales, Actinobacteria, and Pseudomonadales bacteria, respectively (Kraege et al., 2026; Snelders et al., 2020, 2023). Notably, Ave1 is homologous to plant natriuretic peptides (PNPs) and is believed to have been acquired by *V. dahliae* from plants via horizontal gene transfer (de Jonge et al., 2012). However, *V. dahliae* effectors do not only target bacteria, as the defensin-like effector AMP3 was shown to target fungal microbiota members to support microsclerotia production (Snelders et al., 2021) and Ave1 was recently shown to target fungi too (Petti et al., 2026).

In order to identify novel fungal effectors with antimicrobial activity, we recently developed the machine learning-based predictor for antimicrobial activity AMAPEC (Mesny et al., 2025). Interestingly, a total of 304 out of 909 presumably secreted *V. dahliae* proteins have been predicted to possess antimicrobial activity, suggesting that a substantial proportion of the *V. dahliae* secretome is dedicated to microbial manipulation (Mesny et al., 2025). Intriguingly, also for the arbuscular mycorrhizal fungus *Rhizosphagus irregularis* and the saprotrophic fungus *Coprinopsis cinerea*, which does not associate with plants, more than one third of the secreted proteins have predicted antimicrobial activity, suggesting that antimicrobial effectors play crucial roles in the biology of fungi across life styles (Mesny et al., 2025). Moreover, when analyzing the secretomes of 150 fungi spanning a wide range of phylogeny and lifestyles, predicted antimicrobials were abundant among the most conserved proteins (Mesny et al., 2025), suggesting that intermicrobial competition is an ancient trait that developed in the earliest ancestors of fungi, and thus originates from before the emergence of land plants (Mesny et al., 2024, 2025; Snelders et al., 2022). In line with this hypothesis, homologues of pathogen effectors with reported functions in host immunomodulation occur in non-pathogenic species as well, suggesting that immunomodulating effectors evolved from ancient antimicrobial proteins (Mesny et al., 2025).

Although many effector proteins are lineage-specific, some effectors are widely conserved. For example, LysM effectors occur widely in fungi (Kombrink & Thomma, 2013), and necrosis- and ethylene-inducing-like proteins (NLPs) occur even beyond (Seidl & Van den Ackerveken, 2019). Another widely conserved effector family comprises cerato-platanins (CPs), small cysteine-rich proteins of ~120 amino acids (~12 kDa), the first member of which was identified in the fungus *Ceratocystis platani*, the causal agent of canker stain disease of plane trees (*Platanus* spp.) (De Oliveira et al., 2011; Luti et al., 2020; Pazzagli et al., 1999). CPs lack known enzymatic domains and are structurally related to expansins, a class of plant proteins involved in cell wall loosening (Baccelli et al., 2014). Many CPs have a high surface

hydrophobicity, and have been proposed to act as surfactants (Bonazza et al., 2015). For various plant pathogens, including *V. dahliae*, CPs were shown to contribute to virulence (Luti et al., 2020; Zhang et al., 2017). This has been attributed to carbohydrate-binding properties that may modify host cell walls or sequester chitin oligosaccharides to limit recognition by plant immune receptors (Baccelli et al., 2014; Quarantin et al., 2019; Weiland et al., 2023; Zhang et al., 2017). Despite their widespread occurrence, the roles of CPs in non-pathogenic fungi remain unclear (Gaderer et al., 2014).

Recent advances in structural prediction have reshaped our understanding of fungal effector evolution as structurally conserved yet sequence-unrelated effector families have been identified in several fungal pathogens (Derbyshire & Raffaele, 2023; Seong & Krasileva, 2023). For example, MAX and KP6 folds, initially described in *Magnaporthe oryzae* and *Zymoseptoria tritici*, respectively, are conserved across diverse plant-pathogenic fungi, despite low sequence similarity (de Guillen et al., 2015, 2025; Derbyshire & Raffaele, 2023; Seong & Krasileva, 2023). Interestingly, some folds are more abundant in particular plant pathogens suggesting lineage-specific expansions (Derbyshire & Raffaele, 2023; Seong & Krasileva, 2023). For instance, around 70% of all effectors of the wheat powdery mildew fungus *Blumeria graminis* displays an RNase-like fold (Cao et al., 2023; Pennington et al., 2019). Here, we applied structure-based clustering to the *Verticillium dahliae* secretome to query for novel effector clusters.

Materials and Methods

Structural clustering of secreted proteins

SignalP6 was used to predict secreted proteins encoded in the 4.0 version of the *V. dahliae* strain JR2 genome annotation and mature amino acid sequences were used for the structural predictions (Faino et al., 2015; Teufel et al., 2021). The structural predictions were generated for each secreted protein using AlphaFold2 (casp14 preset; Jumper et al., 2021). For each protein, five models were produced, and the model with the highest predicted local distance difference test (pLDDT) score was selected for further analysis. To generate a structural similarity network, an all-versus-all structural alignment was performed using TM-align (Zhang & Skolnick, 2005), and structural similarity was called for average TM-scores in reciprocal pairwise alignments >0.5 (0–1 scale). The resulting network was visualized using Gephi (Bastian et al., 2009). Clusters containing five or more proteins were annotated using PANNZER (Törönen & Holm, 2022) based on at least three centrally positioned proteins per cluster. Proportionally more proteins were used for annotations with increasing cluster size. When no annotation could be obtained via PANNZER, at least three centrally positioned protein sequences were subjected to BLASTP (Altschul et al., 1990) to identify functionally annotated homologues. Alphafold-generated protein structures were visualized with PyMOL (The PyMOL Molecular Graphics System, Version 2.0 Schrödinger, LLC, DeLano Scientific, Palo Alto, CA, USA) and 3D Mol* viewer (Berman et al., 2000). Sequence similarity was determined using the multiple sequence alignment tool MAFFT in the EBI platform (Katoh, 2002; Madeira et al., 2024).

Protein production and purification

Escherichia coli BL21 cells were transformed by heat shock with a pET-28a(+) expression vector encoding the mature CP1 sequence or pET-15b expression vectors containing the sequences encoding mature Ave1, CP2, CP3, $CP3^{\Delta 132\text{-}262}$, CtCP1, FrCP1, AcCP1, all as fusion proteins with an N-terminal His^6 tag. For heterologous protein production, the transformed BL21 cells were grown at 37°C with constant shaking at 180 rpm in 2x Yeast Extract Tryptone (YT) medium containing 100 µg/mL ampicillin. When cultures reached an optical density (OD_{600}) of 2, protein production was induced with a final concentration of 1 mM isopropyl-ß-d-thiogalactoside (IPTG) and the culture was incubated for 2 h at 42°C with constant shaking at 180 rpm. For protein extraction, the bacterial cells were pelleted at 13,000 g for 30 min and resuspended in 6 M guanidinium chloride (GdmCl), 10 mM β-mercaptoethanol and 10 mM Tris, pH 8.0 at 4°C overnight. Insoluble debris was pelleted at 13,000 g for 30 min and

discarded. Protein purification was performed under denaturing conditions by metal affinity chromatography using a nickel His^{60} Ni Superflow Resin (Takara, San Jose, CA, USA) column on the ÄKTA go protein purification system (Cytiva Marlborough, MA, USA). The column was equilibrated with 6 M GdmCl, 10 mM Tris at pH 8.0 and denatured protein was loaded onto the column after which weakly bound protein was washed off with 6 M GdmCl, 10 mM Tris, 20 mM Imidazole at pH 8.0. The specifically bound, His-tagged protein was eluted with 6 M GdmCl, 10 mM Tris, 200 mM Imidazole at pH 8.0.

Purified proteins were dialyzed step-wise (Spectra/Por 3 Dialysis Membrane, molecular weight cut off of 3.5 kDa, Repligen, Waltham, MA, USA) against 20 volumes of buffers with decreasing GdmCl concentrations for refolding. Dialysis 1: 4 M GdmCl, 50 mM BisTris, 10 mM reduced glutathione (GSH), 2 mM oxidized glutathione (GSSG); dialysis 2: 3 M GdmCl, 50 mM BisTris, 10 mM GSH, 2 mM GSSG; dialysis 3: 2 M GdmCl, 100 mM BisTris, 250 mM ammonium sulfate, 10 mM GSH, 2 mM GSSG; dialysis 4: 1 M GdmCl, 100 mM BisTris, 250 mM ammonium sulfate, 10 mM GSH, 2 mM GSSG; dialysis 5: 100 mM BisTris, 250 mM ammonium sulfate, 10 mM GSH, 2 mM GSSG. Each dialysis step was carried out for at least 24 h. Finally, the proteins were dialyzed two times against 200 volumes of 30 mM potassium phosphate buffer (including 15 mM KCl and 5 mM NaCl) at pH 6.5. Final protein concentrations were determined with a Qubit 4 Fluorometer (Invitrogen, Waltham, Massachusetts, USA).

In vitro microbial growth inhibition assays

Bacterial strains were previously described (Punt et al., 2025) and grown on lysogeny broth (LB) agar at RT in the dark. Bacterial isolates grown on LB agar plates were inoculated into low-salt tryptic soy broth (ls-TSB; 17 g/L tryptone, 3 g/L soy peptone, 0.5 g/L sodium chloride, 2.5 g/L dipotassium phosphate, and 2.5 g/L glucose) and grown overnight at 28°C while shaking at 180 rpm. Overnight cultures were resuspended to the final OD_{600} of 0.025 in equal parts of low-salt TSB and protein in phosphate buffer with a final protein concentration of 8 µM. Phosphate buffer was used as control. Total volumes of 100 µL were incubated in clear 96-well flat-bottom polystyrene tissue culture plates in a CLARIOstar plate reader (BMG Labtech, Ortenberg, Germany) at 25°C where optical density was measured every 15 minutes at 600 nm with double orbital shaking before each measurement (10 seconds at 300 rpm).

The filamentous fungi *Alternaria brassicicola*, *Cladosporium cucumerinum*, *Trichoderma viride*, and the yeasts *Saccharomyces cerevisiae*, *Pichia pastoris* (GS115), *Cyberlindnera jadinii* (DSM 70167*), Debaryomyces vanrijiae* (DSM 70252) and *Rhodotorula bogoriensis* (DSM 70872) were grown on potato dextrose agar (PDA) at room temperature (RT) in the dark. Fungal spores were harvested from PDA plates, separated from mycelium with a sterile

40 µm nylon filter (VWR) and diluted in 0.05 x potato dextrose broth (PDB). Yeast isolates were inoculated into 0.05x PDB and grown overnight at 25°C while shaking at 180 rpm. Overnight cultures were harvested by centrifuging at 10,000 g for 10 min and resuspended to the final OD_{600} of 0.025 in 0.05 x PDB and protein in 30 mM potassium phosphate buffer at pH 6.5, while spores of filamentous fungi were diluted to a final concentration of 10^4 spores/mL in 0.05 x PDB and protein 30 mM in potassium phosphate buffer at pH 6.5. The final protein concentration was 8 µM and phosphate buffer was used as control. The total volume was 100 µL was incubated in clear 96-well flat-bottom polystyrene tissue culture plates (BRAND SCIENTIFIC GMBH, Wertheim, Germany) at 25°C overnight. Fungal growth was imaged using an CKX41 inverted microscope with DP20 camera (Olympus, Shinjuku City, Japan). For image analysis with ImageJ (Schneider et al., 2012), each image was first binarized and subsequently subjected to particle analysis to quantify the total particle area. Statistical analysis was performed with R v4.4.1 (R Core Team, 2023).

Comparative genomics and identification of CP1 homologues

The comparative genomics analysis of 150 fungi was described by Mesny et al. (2025). In brief: orthology prediction was performed on total sets of annotated proteins with OrthoFinder v2.5.5 (Emms & Kelly, 2019). to generate a phylogenomic tree with the implemented method ‘STAG’ (Emms & Kelly, 2018). In all 150 genomes, sets of proteins carrying signal peptides annotated with SignalP v6.0 (Teufel et al., 2021) were considered to form secretomes. A second orthology prediction with OrthoFinder v2.5.5 was performed on these 150 secretomes. Orthogroup trees were created with the FastTree method (Price et al., 2009). The structures of proteins were predicted with ESMFold v1.0.3 (Lin et al., 2023) then submitted to antimicrobial activity prediction with AMAPEC v1.0. PFAM domain (PF07249) annotation within the cerato-platanin trees was performed with InterProScan (Jones et al., 2014).

Computational analysis of CP1 structure and conserved features

To identify positively charged regions in CP1, the protein sequence was divided into 20-amino-acid overlapping segments and the net charge of the CP1 amino acid stretches was calculated as the sum of the charges of every ionizable group in the peptide with the BACHEM peptide calculator (https://www.bachem.com/knowledge-center/peptide-calculator/). To identify conserved structural elements between Ave1 and CP1, the predicted CP1 structure was superimposed onto the Ave1 structure (Petti et al., 2026), which was visualized in 3D Mol* viewer (Berman et al., 2000). A consensus sequence of the CP1 protein family was created in Jalview (Troshin et al., 2011) based on a CLUSTAL W (Thompson et al., 1994) alignment of all sequences in the protein family.

Results

Limited structural clustering within the *Verticillium dahliae* secretome

To determine whether clustering of structural effector families occurs in *V. dahliae*, we predicted structures of all 909 predicted secreted proteins encoded in the genome of *V. dahliae* strain JR2 with Alphafold2 (Jumper 2021, Faino et al., 2015; Figure 1a). While 6.3% of the predicted structures had a pLDDT score below 50 and 14.3% scored between 50 and 70, nearly 80% of the predicted structures were of reliable quality (i.e. pLDDT score >70). Next, the predicted structures were clustered based on structural similarity, identifying 23 clusters containing at least five members (Figure 1b), the largest of which contains 64 members. Of these 23 clusters, 20 correspond to well-known types of hydrolases, including peptidases and carbohydrate-active enzymes. One cluster contains seven members (Figure 1b, cluster number 14) that belong to the widely conserved necrosis- and ethylene-inducing-like proteins (NLPs; Seidl & van den Ackerveken, 2019), and that show high sequence similarity in *V. dahliae* (Santhanam et al., 2013). Due to lack of significant homology to known proteins, two of the 23 clusters could not be annotated (Figure 1b, clusters 16 and 17).

To determine whether the structural clusters, including smaller four-member clusters, contained known effectors or proteins with substantial homology to them, we searched each cluster accordingly. Rather surprisingly, we found one cluster containing the previously described Ave1 effector (de Jonge et al., 2012) together with the previously described CP1 effector (Zhang et al., 2017a) that shares no sequence or functional homology to Ave1, and two further proteins that we tentatively named CP2 and CP3 (Figure 1b red circle, 1c). Structurally, Ave1 and CP1 show a template modelling-score (TM-score) of 0.65 despite sharing only 21.7% sequence identity (Figure 1c). Ave1 displays lower similarity to CP2 and CP3, with TM-scores of 0.51 and 0.47 and sequence identities of 15% and 14%, respectively. CP1 is structurally as similar to CP2 and CP3 as Ave1 (TM-scores of 0.55 and 0.51), but shares higher sequence identity with them (34% and 27%). The closest relationship within the cluster is between CP2 and CP3, which show the highest structural similarity (TM-score 0.89) and highest sequence identity (56%). Superposition of the predicted structures revealed that all four proteins share a conserved fold consisting of a conserved double-ψβ-barrel fold surrounded by several similar α-helices that is typical for cerato-platanins (Figure 1e). Additionally, CP2 and CP3 contain an extended C-terminal region. Previously, Ave1 sequence homologues were identified in the *V. dahliae* population that we termed Ave1L, for Ave1-like proteins (Snelders et al., 2022). However, *V. dahliae* strain JR2 carries variant Ave1L1 that carries a premature stop codon after only 24 amino acids (Snelders et al., 2022), and therefore does not appear in this cluster. However, the full-length homologues Ave1L2, Ave1L5 that

occur in other *V. dahliae* strains share clear structural homology with Ave1 as well as with the CP homologues.

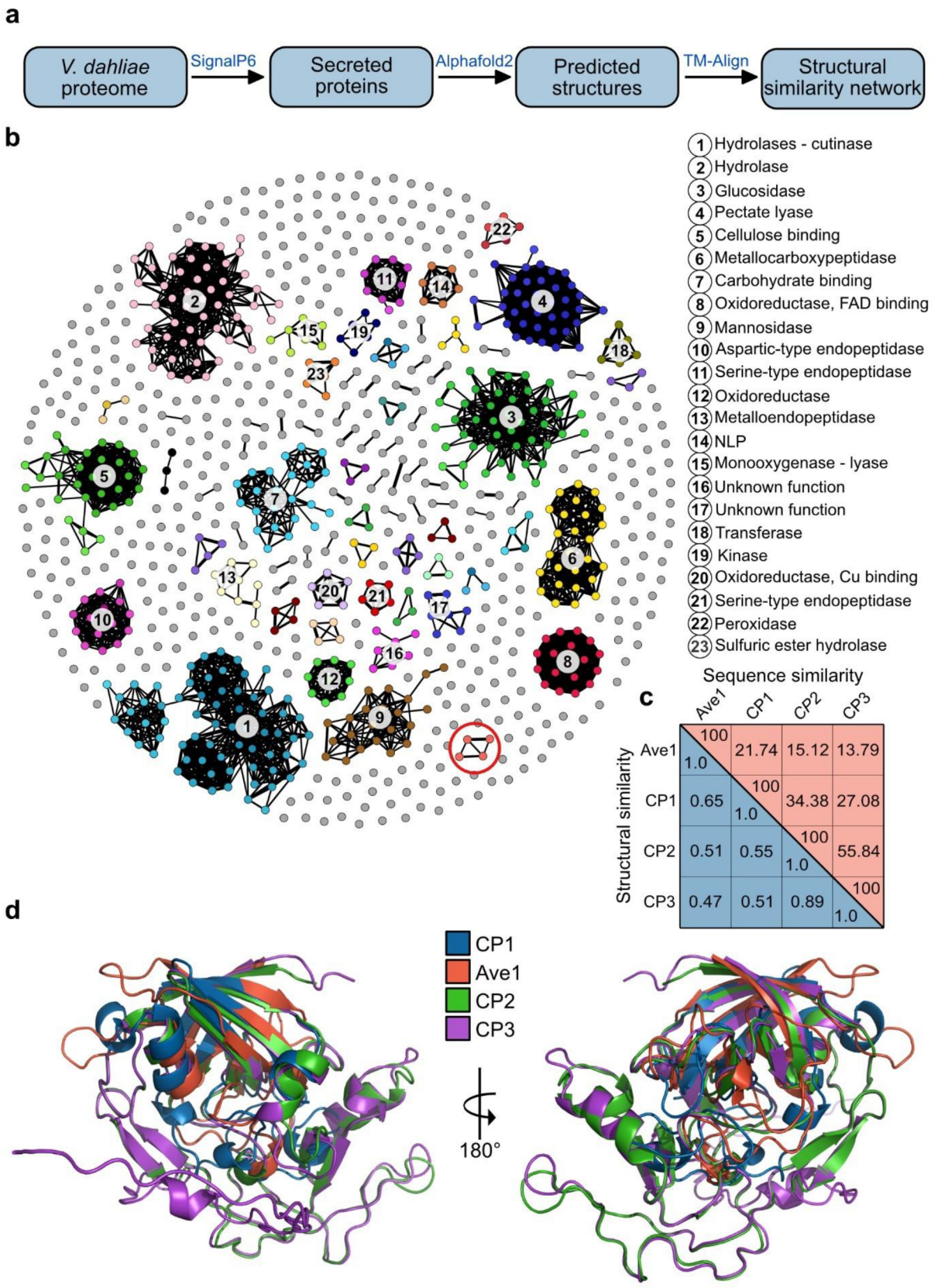

Figure 1. *Verticillium dahliae* effectors show limited structural clustering. (a) Flowchart of the computational pipeline used to cluster secreted proteins encoded in the genome of *V. dahliae* strain JR2 **(b)** The structural clusters that can be identified among the secreted proteins of *V. dahliae* mostly concern hydrolases. Cluster annotation is based on GO-term annotations for representative proteins from each cluster. If no appropriate GO term was identified, annotation was inferred from proteins with significant sequence similarity to the representative proteins. A cluster of four proteins containing the two previously characterized effectors Ave1 (de Jonge et al., 2012) and CP1 (Zhang et al., 2017a) as well as two further proteins that we named CP2 and CP3 is indicated with a red circle. **(c)** Structural similarities within the cluster containing Ave and CP1 were quantified using template modeling (TM)-scores, while sequence similarity is shown as percent identity. **(d)** Superposition of the predicted structures of Ave1, CP1, CP2 and CP3 revealed that all four proteins share a conserved double-ψβ-barrel fold surrounded by several α-helices. Additionally, CP2 and CP3 contain an extended C-terminal region.

The cerato-platanin CP1 displays selective antimicrobial activity *in vitro*

We recently characterized Ave1 and Ave1L2 as effectors with antimicrobial activity that are secreted by *V. dahliae* to selectively manipulate host microbiota compositions (Snelders et al., 2020; 2023). Given the structural similarities between Ave1, Ave1L2 and CP1, we assessed whether CP1 possesses antimicrobial activity as well. To this end, we tested the effect of heterologously produced CP1 protein on five phylogenetically diverse plant-associated bacteria. Interestingly, purified CP1 inhibited the growth of *Sphingomonas* sp., *Bacillus drentensis*, and *Pseudoxanthomonas suwonensis* in a concentration-dependent manner, whereas growth of *Pseudomonas corrugata* and *Sphingomonas mellinum* remained unaffected by protein treatment (Figure 2a). Thus, given that CP1 displays selective antimicrobial activity, we compared its antimicrobial activity spectrum with that of Ave1 on a panel of 23 phylogenetically diverse plant-associated bacteria of seven different bacterial classes that were previously isolated from tomato plants (Punt et al., 2025) (Figure 2b). Interestingly, CP1 and Ave1 exhibited only partially overlapping antimicrobial activity profiles. Whereas the growth of eight bacteria was significantly inhibited by both proteins, and eight others remained unaffected by either protein, four were inhibited exclusively by CP1 and three only by Ave1. Recently it was shown that Ave1 also displays antifungal activity against the yeast *Cyberlindnera jadinii*, completely inhibiting growth at a concentration of 8 μM (Petti et al., 2026). Interestingly, similar to Ave1, also CP1 strongly inhibited yeast growth, with significant inhibition at 4 μM and nearly complete inhibition at 8 μM.

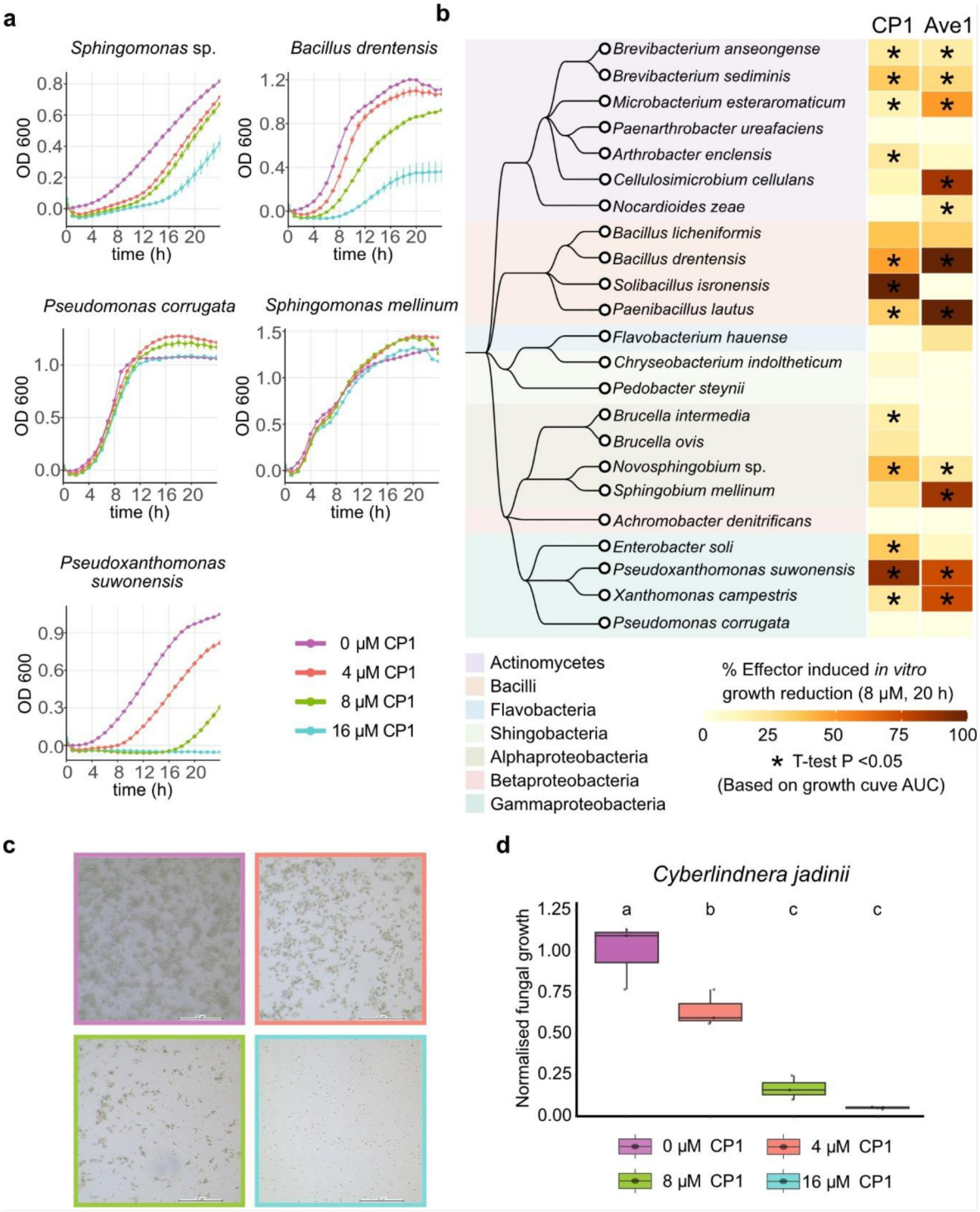

Figure 2. *Verticillium dahliae* cerato-platanin effector CP1 displays selective antimicrobial activity. (a) CP1 selectively inhibits growth of phylogenetically diverse tomato-associated bacteria in a concentration-dependent manner. Graphs display time-course measurements of bacterial densities in the presence or absence of effector proteins with 15 min intervals over 24 h and display the average OD_{600} of three biological replicates ± SD.

(b) The antimicrobial activity profile of CP1 partially overlaps with that of its structural homologue Ave1 across a panel of 23 plant-associated bacteria. The heatmap shows bacterial growth restriction induced by the presence of 8 µM effector protein. The species phylogeny on the left was generated with Taxallnomy (Sakamoto & Ortega, 2021). Each heatmap column corresponds to a different fungal effector. Percentages of effector-induced growth restriction were calculated after 20 hours of growth. Asterisks indicate significant differences in bacterial growth in presence and in absence of effector protein, identified with Student's T-tests on area under curve (AUC) values (Bonferroni corrected, $P < 0.05$). **(c)** CP1 displays selective, dose-dependent antifungal activity against the yeast *Cyberlindnera jadinii*. **(d)** Boxplots indicate fungal growth after incubation with increasing concentrations of CP1. Fungal growth was quantified by measuring the colony area after 18 h of incubation. Different letter labels represent significant differences (one-way ANOVA and Tukey's *post hoc* test; $P < 0.05$).

Cerato-platanins show differential antimicrobial activity profiles

Given the clear antimicrobial activity of CP1, we investigated whether CP2 and CP3 similarly exhibit antimicrobial activity. Therefore, both proteins were heterologously produced and tested on a panel of 13 tomato-associated bacteria. Overall, CP1, CP2, and CP3 exhibited overlapping activity spectra, inhibiting the growth of the same three bacteria while not affecting the growth of seven other bacteria (Figure 3a). In addition, CP1 inhibited three further bacteria, including *Pseudomonas knackmussii*, which was similarly inhibited by CP3 but not by CP2, indicating functional divergence between CP2 and CP3. The remaining two bacteria inhibited by CP1 were not affected by either CP2 or CP3. Furthermore, the antifungal activity of CP1, CP2 and CP3 was tested on eight fungi. Whereas CP1 affected all eight fungi, CP2 and CP3 only significantly affected the growth of three fungi, revealing that the latter two proteins display reduced activity when compared with CP1 (Figure 3b).

To assess the potential contribution of the extended region to the antimicrobial activity, CP3 was C-terminally truncated such that its size and predicted fold matched that of CP1. Antimicrobial activity assays using *Pseudomonas knackmussii*, which is strongly inhibited by full-length CP3, and *P. suwonensis*, which is only weakly affected, revealed that truncation of CP3 did not alter its antibacterial activity (Figure 4d). Thus, the C-terminal extension does not seem to contribute to the antimicrobial activity of CP3.

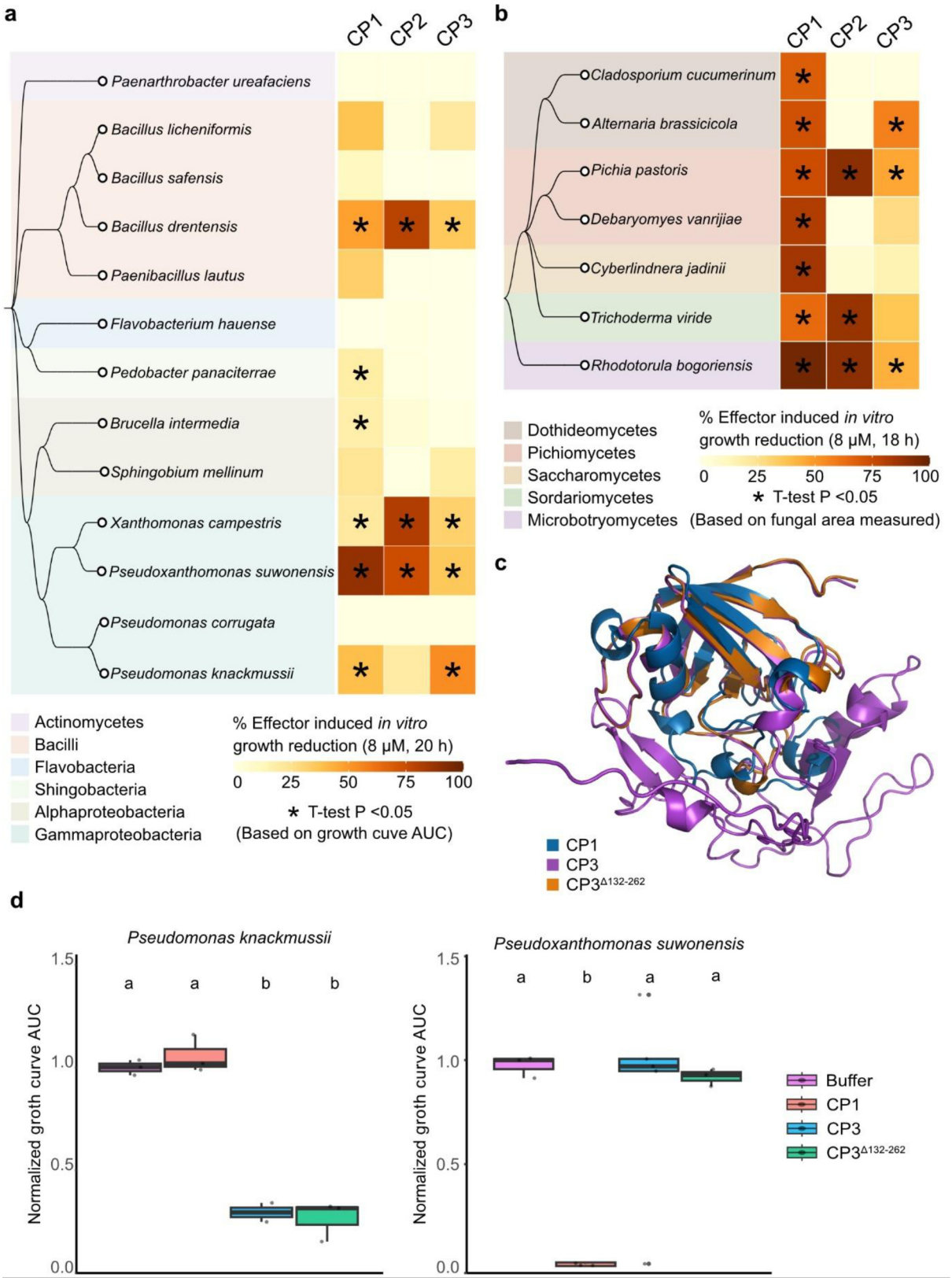

Figure 3. *Verticillium dahliae* cerato-platanin (CP) homologues display antimicrobial activity. (a,b) The heatmap shows bacterial growth restriction (a) or fungal growth restriction (b) induced by the presence of 8 µM effector protein. The species phylogeny on the left was generated with Taxallnomy (Sakamoto & Ortega, 2021). Each heatmap column corresponds to a different fungal effector.

Percentages of effector-induced growth restriction were calculated after 20 (a) or 18 (b) hours of growth. Asterisks indicate significant differences in growth when compared with buffer controls, identified with Student's T-tests on area under curve (AUC) values (Bonferroni corrected, P < 0.05) (a) or with Bonferroni corrected Student's t-test fungal area values ($P < 0.05$) (b). **(c)** Structural superposition of CP1, CP3, and the truncated CP3 variant (CP3$\Delta^{132\text{-}262}$). **(d)** Truncation of CP3 does not affect antibacterial activity against *Pseudomonas knackmussii* and *Pseudoxanthomonas suwonensis*. Bacterial growth was quantified by calculating AUC values normalized to buffer controls. Different letters indicate statistically significant differences (one-way ANOVA followed by Tukey's post hoc test; $P < 0.05$).

Cerato-platanins of phylogenetically divergent fungi exhibit antimicrobial activity

We previously composed a comparative genomics dataset comprising 150 fungi with diverse lifestyles spanning the fungal tree of life (Mesny et al., 2025b; Figure 4a). Based on this dataset, all secreted proteins predicted to be encoded by the 150 fungi were clustered into protein families based on sequence similarity (Mesny et al., 2025a). CP1 is found in a protein family comprising 218 proteins encoded in 116 fungal genomes, many of which do not belong to (plant) pathogens (Mesny et al., 2025a); Figure 4b). Among the 34 genomes that lack CP1 homologues, 21 belong to fungi from the phyla Basidiomycetes and Mucoromycetes, which are phylogenetically the most distant to *V. dahliae* (Figure 4b). Within the 111 Ascomycetes, 13 genomes lacked CP1 homologues. Notably, all three ericoid mycorrhizal fungi in our dataset do not contain a CP1 homologue, two of which cluster with an ectomycorrhizal fungus and a saprotroph that similarly lack a CP1 homologue, indicating a shared loss event. The remaining ericoid mycorrhizal fungus is separated by two fungi that encode a CP1 homologue, suggesting independent losses of the CP1 homologues across the ericoid mycorrhiza (Figure 4a). Additionally, eight pathogenic ascomycetes from the Sordariomycetes and Dothideomycetes lack CP1 homologues (Figure 4b).

All but six of the 218 CP1 orthologs are predicted to display antimicrobial activity (Figure 4c). Four of these six members share the conserved double-ψβ-barrel fold found in CP1, while two are folded differently and are potentially misclassified as CP homologues (Figure S1). Furthermore, all four proteins show additional regions that are not found in CP1, significantly changing the overall fold. This change in structure is likely responsible for the lack of predicted antimicrobial activity by AMAPEC and could suggest functional diversification from other CP1 homologues.

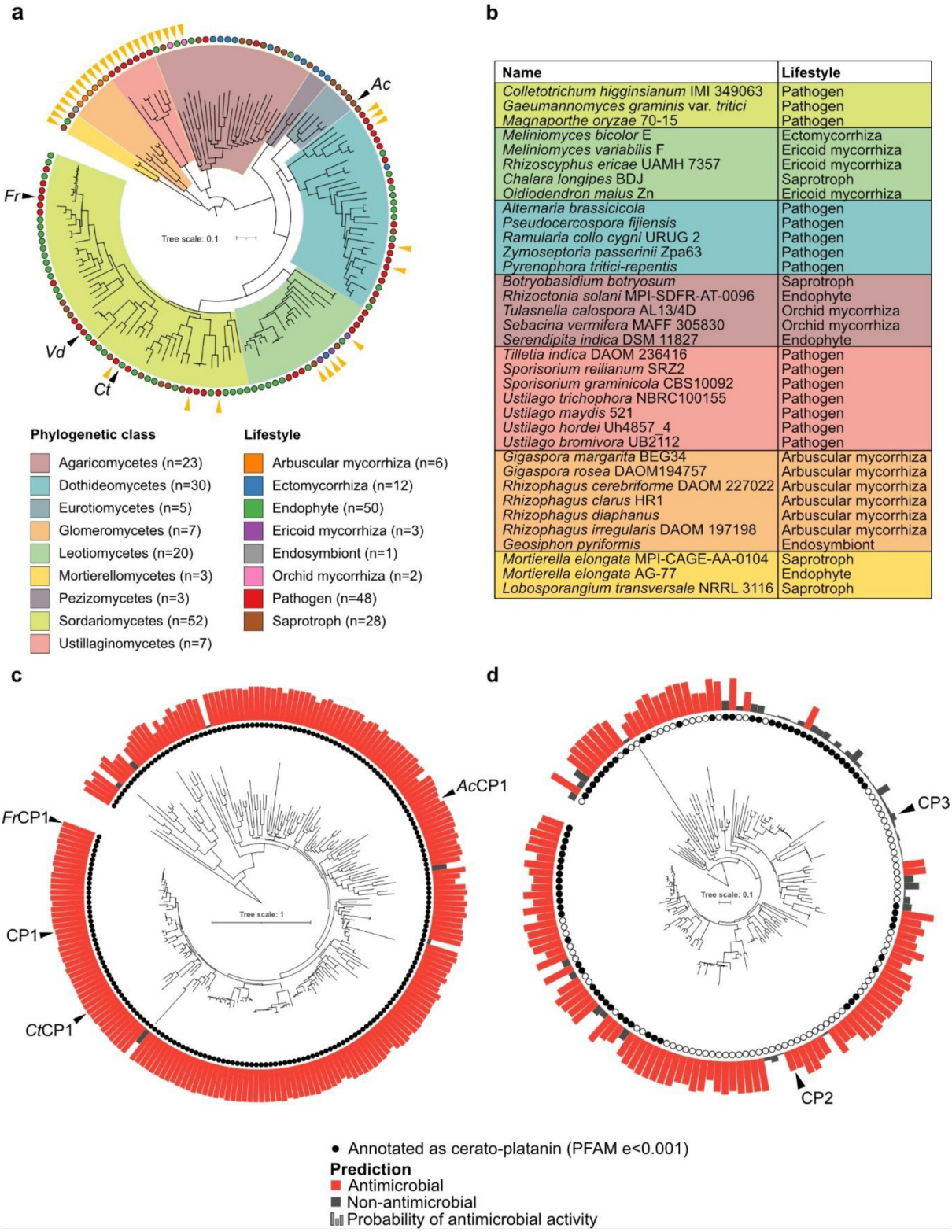

Figure 4. Cerato-platanins are conserved in diverse fungal species. (a) Phylogenetic tree calculated on secreted proteins from a comparative genomics dataset comprising 150 fungal species with diverse lifestyles (Mesny et al., 2025). Color ranges on the phylogenomic tree highlight phylogenetic classes and fungal lifestyles are indicated. The secreted proteins of all fungi were grouped into families according to sequence similarity. Fungal species of which CP1 homologues were tested for antimicrobial activity are annotated with a black arrow: *Verticillium dahliae* (*Vd*), *Fusarium redolens*

(*Fr*), *Colletotrichum tofieldiae* (*Ct*) and *Aspergillus campestris* (*Ac*). Fungal species which lack a CP1 homologue are indicated with a yellow arrow **(b)** Table of genomes that lack a CP1 homologue with life style annotations. **(c,d)** Phylogeny and antimicrobial activity prediction of the orthogroup containing CP1 **(c)** and CP2 and CP3 **(d)**. Proteins containing a cerato-platanin PFAM domain (PF07249) are indicated with a black circle. Highlighting proteins selected for antimicrobial assays: *Ct*CP1 from *C. tofieldiae*; CP1 from *V. dahliae*, *Fr*CP1 from *F. redolens*; and *Ac*CP1 from *A. campestris*.

Since CP1 shares only 34% and 27% sequence identity with CP2 and CP3, respectively (Figure 1c), these proteins do not occur in the same orthogroup. Instead, CP2 and CP3 that share 56% sequence identity occur together in a separate orthogroup (Figure 4d) that is slightly smaller than the one to which CP1 belongs, comprising 155 proteins encoded across 59 Ascomycete genomes, 52 of which belong to the Sodariomycetes. The 155 proteins are similarly sized as CP2 and CP3, as they have the C-terminal extension that is missing in CP1. Of the 155 proteins, 104 are predicted antimicrobials (Figure 4d).

To assess whether antimicrobial activity indeed occurs widely across the cerato-platanin protein family, we selected three CP1 homologues from fungi with different lifestyles: *Ct*CP1 from the endophyte *Colletotrichum tofieldiae*, *Fr*CP1 from the plant pathogen *Fusarium redolens* and *Ac*CP1 from the saprophyte *Aspergillus campestris* (Figure 4a). Although all three homologues displayed high similarity among their predicted structures, with TM-scores ranging from 0.904 to 0.991, their sequence identity was rather low (55-73%, Figure 5a). CtCP1 was first screened against 13 phylogenetically diverse bacteria and, unlike CP1, showed only limited antibacterial activity, inhibiting only *P. knackmussii* (Figure 5b). *Fr*CP1 and *Ac*CP1 were tested on three bacteria: *B. drentensis*, *P. suwonensis* and *P. corrugata*. Both *Fr*CP1 and *Ac*CP1 inhibited *B. drentensis*, demonstrating overlapping antibacterial activity with CP1 (Figure 5b). *Fr*CP1 additionally inhibited *P. suwonensis*, which was not affected by *Ac*CP1. Neither *Fr*CP1 nor *Ac*CP1 inhibited *P. corrugata,* in contrast to CP1. Antifungal assays against seven fungi revealed that *Ct*CP1 inhibited only *Pichia pastoris*, showing little overlap with the activity spectrum of CP1 (Figure 5c). FrCP1 displayed a broader spectrum that overlapped substantially with that of CP1, inhibiting most fungi tested. In contrast, *Ac*CP1 showed no antifungal activity. Altogether, these results show that the CP family has conserved antimicrobial properties.

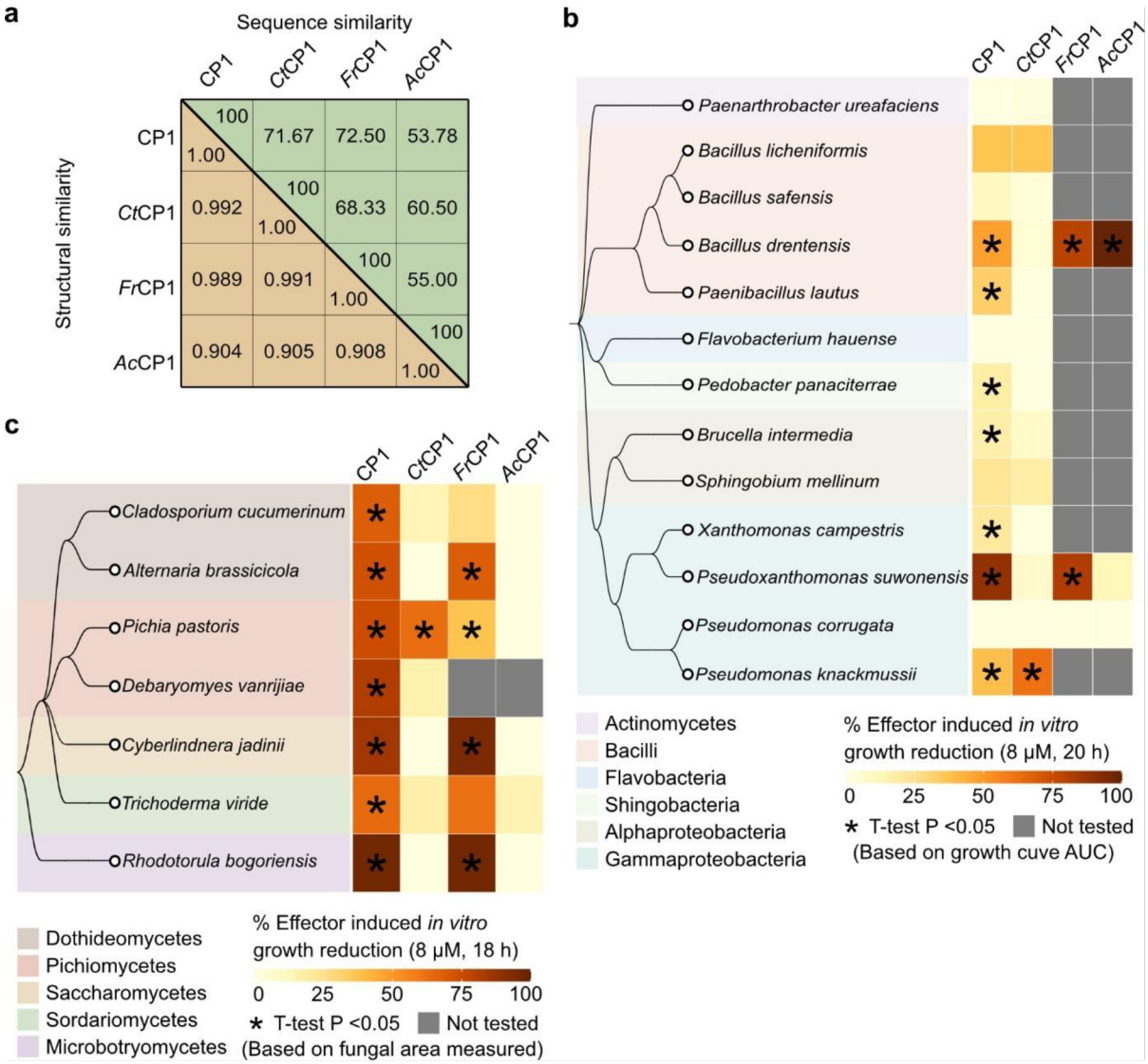

Figure 5. CP1 homologues from diverse fungal species display antimicrobial activity. (a) Structural similarities among CP1 homologues were quantified using template modeling (TM)-scores, while sequence similarity is shown as percent identity. **(b,c)** The heatmap shows bacterial growth restriction (b) or fungal growth restriction (c) induced by the presence of 8 µM effector protein. The species phylogeny on the left was generated with Taxallnomy (Sakamoto & Ortega, 2021). Each heatmap column corresponds to a different fungal effector. Percentages of effector-induced growth restriction were calculated after 20 (b) or 18 (c) hours of growth. If a microbial growth inhibition was not tested, the square was filled grey. Asterisks indicate significant growth differences when compared with buffer controls, identified with Student's T-tests on area under curve (AUC) values (Bonferroni corrected, $P < 0.05$) (b) or with Bonferroni corrected Student's t-test fungal area values ($P < 0.05$) (c).

Positively charged regions may mediate antimicrobial activity of CP1

Recently, the three-dimensional structure of Ave1 was resolved. Together with functional data, this has led to the hypothesis that Ave1 binds lipoteichoic acid (LTA) in the bacterial cell wall, possibly serving as a docking platform that facilitates its accumulation at the bacterial surface to mediate membrane destabilization through positively charged protein regions (Petti et al., 2026). Since CP1 and Ave1 share significant structural similarity and overlap in their antibacterial activity spectrum, we queried CP1 for homology in the positively charged regions and the LTA-binding regions to explore a potential mode of action. Intriguingly, two positively charged regions similar to those in Ave1 were identified (Figure 6a). Superimposition of the two protein structures showed that whereas the first region (aa 31–50) does not occupy the same structural position as in Ave1, the second region (aa 101–120) is structurally conserved at the C-terminal end, comprising one of the beta sheets in the double-ψβ-barrel fold (Figure 6b). To assess conservation of positively charged regions in CP1, we generated a consensus sequence from 218 homologues, defining residues as conserved if present in all sequences (Figures 4c, 6d). In the first positively charged region (N-terminal, aa 31–50), we identified a buried “FPYIGG” motif, likely contributing to fold stability. In the second positively charged region (C-terminal, aa 101–120), we identified surface-exposed “LGR” and “CGL” motifs, which, together with neighboring positively charged residues, form two separate amphipathic surface regions (Figure 6c). None of the amino acid motifs are conserved between Ave1 and CP1. Superimposition of Ave1 (Figure 6e, red) and CP1 (Figure 6e, blue) revealed that the LTA-interacting regions present in Ave1 (Petti et al., 2026; Figure 6e, green), which facilitate accumulation at bacterial surfaces, are absent in CP1 (Figure 6e, yellow). This suggests that CP1 may not bind LTA, but if it does, it is likely to do so through residues distinct from those used by Ave1. Together, these findings indicate that the antimicrobial activity of CP1 may be mediated by the positively charged C-terminal region, but its accumulation at the bacterial surface may not be LTA-dependent and may involve alternative carbohydrate-binding interactions.

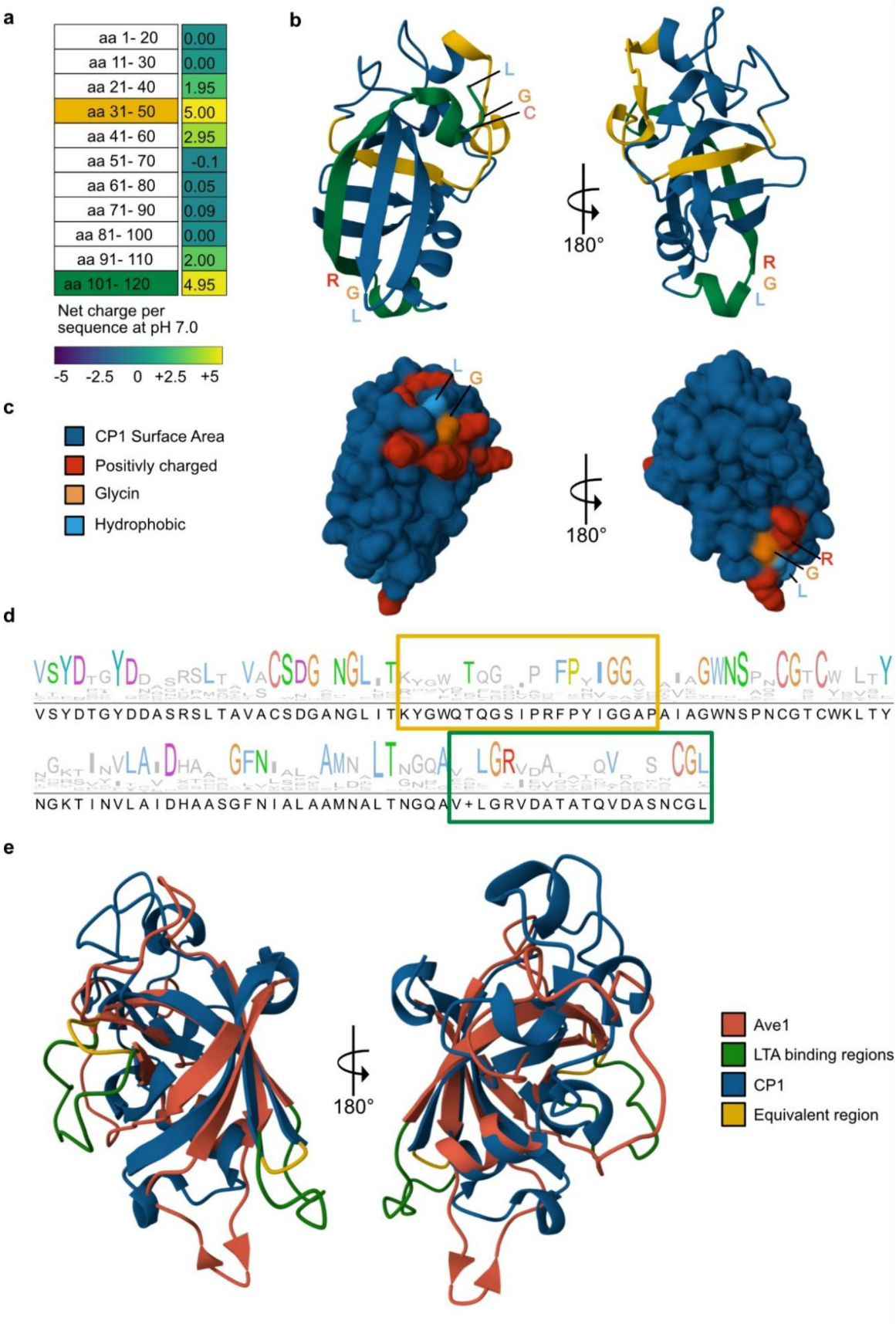

Figure 6. Charge distribution and structural conservation of CP1 (a) Charge distribution analysis of CP1, assessed in overlapping 20-amino-acid windows. **(b)** CP1 three-dimensional structure with

positively charged regions highlighted: residues 31–51 are shown in yellow and residues 101–121 in green. The conserved LGR motif among CP1 homologues is indicated. Positively charged residues are colored red, cysteines pink, and glycines orange. **(c)** Gaussian surface representation of the CP1 structure. Residues that are positively charged within the two regions highlighted in (b) are colored red, while conserved glycine and leucine residues are additionally colored orange and yellow, respectively, to indicate their position on the protein surface. **(d)** Consensus sequence of all 218 CP1 homologues found in the genomes of 116 fungi. The lower sequence shows the consensus amino acid sequence, whereas the upper sequence depicts the conservation at each position. Larger letters indicate higher conservation, and residues that are conserved in more than 75% of the homologues are colored according to their chemical properties: hydrophobic charged residues are colored blue, positively charged red, negatively charged magenta, polar green, aromatic cyan, cysteines pink, glycines orange, and prolines yellow. **(e)** Structural superposition of CP1 and Ave1, with Ave1 regions known to interact with lipoteichoic acid (LTA) shown in green and the regions in CP1 that occupy the same spatial positions shown in yellow.

Discussion

While it has been shown that pathogenic fungi use effector proteins to facilitate successful host colonization, the evolutionary origins of effectors remain central questions in host–microbe biology (Lo Presti et al., 2015; Rovenich et al., 2014; Sperschneider et al., 2015). By applying structure-based clustering to the *Verticillium dahliae* secretome, we uncover a previously unrecognized relationship between fungal cerato-platanins (CPs), the antimicrobial effector Ave1 and the sequence-related Ave1-like proteins, and plant natriuretic peptides (PNPs). Our findings reveal that these proteins share a conserved three-dimensional fold that has been maintained across kingdoms and is associated with antimicrobial activity, suggesting that this fold represents an evolutionarily ancient antimicrobial protein architecture that has been repeatedly repurposed during host–pathogen co-evolution.

A key outcome of this work is the demonstration that structural clustering can uncover deep evolutionary relationships between proteins that are undetectable at the sequence level, as has also been highlighted in recent large-scale analyses of effector proteins (Derbyshire & Raffaele, 2023; Seong & Krasileva, 2023). While many of the structural clusters identified in the *V. dahliae* secretome corresponded to well-characterized enzyme classes or known effector families that share significant sequence homology and thus would have been identifiable based on sequence alone, the grouping of Ave1 with CP1, CP2, and CP3 was unexpected. Previous sequence-based analyses failed to identify any similarity between Ave1 and other *V. dahliae* proteins, leading to the conclusion that Ave1 was acquired via horizontal gene transfer from plants (de Jonge et al., 2012). Our results do not contradict this evolutionary scenario but instead reveal that, despite distinct evolutionary histories and annotations, Ave1 and CPs share a structural fold. This underscores the importance of structure-based approaches for understanding effector effector function and evolution, especially given their rapid sequence divergence.

The identification of a conserved fold linking fungal CPs, fungal Ave1, and PNPs establishes a structural bridge between proteins previously considered unrelated. This finding is striking given that CPs have so far been regarded as fungal-specific proteins (Gaderer et al., 2014), whereas PNPs are plant proteins and Ave1 has been classified as PNP-like (de Jonge et al., 2012). The persistence of a shared fold across plants and fungi implies strong selective pressure to maintain this structure, suggesting that it confers a fundamental and advantageous biological activity. Importantly, this structural conservation cannot be explained by shared function in plant physiology or fungal development alone (Gaderer et al., 2014; Gehring & Irving, 2003), pointing instead to a more ancient and broadly relevant role.

Functional analyses provide critical insight into the nature of this conserved fold. We show that CPs from fungi with diverse ecological lifestyles exhibit broadly conserved antimicrobial activity, while Ave1 and Ave1L2 were previously shown to have selective antimicrobial activity (Snelders et al., 2020; Petti et al., 2026). Moreover, PNPs, which share this fold, can also inhibit microbial growth (Snelders et al., 2020), further supporting the notion that antimicrobial function is a fundamental property of this structure. Together, these observations strongly suggest that antimicrobial activity represents its ancestral role. The maintenance of antimicrobial activity across such phylogenetically distant lineages implies that this fold emerged early in eukaryotic evolution as an effective antimicrobial scaffold that was retained due to its capacity to inhibit microbial growth. This pattern closely parallels that of defensins, which also display remarkable structural conservation and antimicrobial activity across multiple kingdoms (Thomma et al., 2002), reinforcing the idea that certain protein folds are particularly well suited for antimicrobial function.

While antimicrobial activity appears to be ancestral, our findings also highlight extensive functional diversification of this fold. In fungi, CPs are widely conserved and some members from pathogenic fungi have been implicated in virulence through diverse functions, involving immune modulation and host cell wall interactions (Baccelli et al., 2014; Luti et al., 2020; Zhang et al., 2017). Similarly, Ave1 was shown to contribute to virulence not only through antimicrobial activity but also through modulation of host physiology (Punt et al., 2025). Together, these observations suggest that ancestral antimicrobial proteins have been repeatedly co-opted to acquire additional roles in host–pathogen interactions. Such repurposing may reflect intrinsic properties of antimicrobial proteins, including their secretion and extracellular stability in the plant apoplast, which may facilitate the evolution of additional functions (Snelders et al., 2022). The acquisition of additional domains in CP2 and CP3 further supports this model, as domain accretion is a common mechanism by which proteins expand their functional repertoire (Eichfeld et al., 2025; Todd et al., 1999).

Notably, CP homologues are absent from two lineages containing the three ericoid mycorrhizal fungi present in our dataset, suggesting that this effector family has repeatedly been independently lost in lineages engaged in this type of mutualism. This loss cannot be interpreted as a general reduction in antimicrobial capacity, as these fungi encode numerous other AMP families, but rather suggests that CP-mediated functions may be dispensable—or functionally replaced—in this particular ecological context. However, given the low number of ericoid mycorrhizal fungi in our dataset, this finding needs to be confirmed by querying additional species that share this life style.

Beyond evolutionary considerations, the shared fold between CP1 and Ave1 provides a framework for understanding their mode of action. Both proteins possess positively charged surface regions (Petti et al., 2026), including a structurally conserved region near the C-terminus. For Ave1, these charged regions are sufficient to disrupt microbial membranes, consistent with established mechanisms of membrane-active antimicrobial peptides (Petti et al., 2026, Chen et al., 2023). By analogy, we propose that CP1 employs a similar strategy, in which conserved positively charged surface protein regions mediate membrane disruption. Not all conserved features of CPs are expected to contribute directly to this activity. Several conserved motifs are buried within the protein core and are therefore likely to play a role in maintaining fold stability rather than mediating membrane interactions. However, two surface-exposed Leucine–Glycine pairs are located within positively charged regions and form amphipathic surfaces that could facilitate interactions with lipid bilayers, as observed in various other types of antimicrobial peptides (Oliveira Júnior et al., 2025). Although direct experimental validation will be required, these structural features strongly support a shared membrane-disruptive mechanism.

Membrane-active antimicrobial peptides often rely on interactions with cell wall components to concentrate at the microbial surface prior to membrane disruption (Malanovic & Lohner, 2016). Ave1 has been shown to bind lipoteichoic acid, facilitating its accumulation at bacterial membranes (Petti et al., 2026). While CP1 lacks the structural features implicated in lipoteichoic acid binding, several CPs have been reported to bind chitin (Gaderer et al., 2014; Zhang et al., 2017), suggesting an alternative mechanism for surface localization on fungal cells. In bacteria, the structurally related peptidoglycan may serve as a surface target (Vollmer, 2008), enabling CPs to accumulate at bacterial surfaces. Together, these observations support a hypothesis for a mechanistic framework in which CPs exploit conserved structural and surface features to target microbial membranes, providing a unified and plausible model for their antimicrobial activity.

Taken together, our findings identify a conserved protein fold shared by fungal CPs, fungal Ave1 and the Ave1-like homologs, and PNPs that likely originated as an antimicrobial scaffold and was subsequently repurposed for diverse biological functions. More broadly, our work supports the emerging view that many pathogen effectors that manipulate host physiology derive from ancestral antimicrobial proteins (Mesny et al., 2025). This evolutionary link between microbial competition and host manipulation suggests that many effectors did not evolve *de novo* as host-targeting molecules, but instead evolved from proteins originally involved in antagonistic interactions with other microbes (Mesny et al., 2024, 2025; Snelders et al., 2022). As the mechanisms of many antimicrobial effectors remain poorly understood (Chavarro-Carrero et al., 2024; Gómez-Pérez et al., 2023; Kraege et al., 2026; Mesny et al., 2025), further dissection of this conserved fold may reveal general principles governing the evolution and function of effectors across kingdoms.

Acknolegments

We thank Ceyda Ekin Hazir and Luca Weber for assistance. This work was supported by the Deutsche Forschungsgemeinschaft (DFG, German Research Foundation) through the funding of F.M.'s Walter Benjamin position (Project ID: ME 6064/1-1, Project number: 508411006). B.P.H.J.T acknowledges funding by the Alexander von Humboldt Foundation in the framework of an Alexander von Humboldt Professorship endowed by the German Federal Ministry of Education and Research is furthermore supported by the Deutsche Forschungsgemeinschaft under Germany´s Excellence Strategy – EXC 2048/1 – Project ID: 390686111 and by the DFG – Project ID 458090666 / CRC1535/1.

Author contributions

A.K. and B.P.H.J.T. conceived the project. A.K., V.W., F.M., G.P., J.Z., and B.P.H.J.T. designed the experiments. A.K., V.W., F.M., G.P., O.N., J.Z., and N.B. performed the experiments. A.K., V.W., F.M., and B.P.H.J.T. analyzed the data. A.K., and B.P.H.J.T. wrote the manuscript. All authors read and approved the final manuscript.

References

Altschul, S. F., Gish, W., Miller, W., Myers, E. W., & Lipman, D. J. (1990). Basic local alignment search tool. *Journal of Molecular Biology*, 215(3), 403–410. https://doi.org/10.1016/S0022-2836(05)80360-2

Baccelli, I., Luti, S., Bernardi, R., Scala, A., & Pazzagli, L. (2014). Cerato-platanin shows expansin-like activity on cellulosic materials. *Applied Microbiology and Biotechnology*, 98(1), 175–184. https://doi.org/10.1007/s00253-013-4822-0

Bastian, M., Heymann, S., & Jacomy, M. (2009). Gephi: an open source software for exploring and manipulating networks. *Proceedings of the 3rd International AAAI Conference on Weblogs and Social Media, ICWSM* 2009, 361–362. https://doi.org/10.1609/ICWSM.V3I1.13937

Berendsen, R. L., Pieterse, C. M. J., & Bakker, P. A. H. M. (2012). The rhizosphere microbiome and plant health. *Trends in Plant Science*, 17(8), 478–486. https://doi.org/10.1016/j.tplants.2012.04.001

Berman, H. M., Westbrook, J., Feng, Z., Gilliland, G., Bhat, T. N., Weissig, H., Shindyalov, I. N., & Bourne, P. E. (2000). The protein data bank. *Nucleic Acids Research*, 28(1), 235–242. https://doi.org/10.1093/nar/28.1.235

Bonazza, K., Gaderer, R., Neudl, S., Przylucka, A., Allmaier, G., Druzhinina, I. S., Grothe, H., Friedbacher, G., & Seidl-Seiboth, V. (2015). The fungal cerato-platanin protein EPL1 forms highly ordered layers at hydrophobic/hydrophilic interfaces. Soft Matter, 11(9), 1723–1732. https://doi.org/10.1039/C4SM02389G

Bulgarelli, D., Rott, M., Schlaeppi, K., Ver Loren van Themaat, E., Ahmadinejad, N., Assenza, F., Rauf, P., Huettel, B., Reinhardt, R., Schmelzer, E., Peplies, J., Gloeckner, F. O., Amann, R., Eickhorst, T., & Schulze-Lefert, P. (2012). Revealing structure and assembly cues for *Arabidopsis* root-inhabiting bacterial microbiota. *Nature* 2012 488:7409, 488(7409), 91–95. https://doi.org/10.1038/nature11336

Cao, Y., Kümmel, F., Logemann, E., Gebauer, J. M., Lawson, A. W., Yu, D., Uthoff, M., Keller, B., Jirschitzka, J., Baumann, U., Tsuda, K., Chai, J., & Schulze-Lefert, P. (2023). Structural polymorphisms within a common powdery mildew effector scaffold as a driver of coevolution with cereal immune receptors. *Proceedings of the National Academy of Sciences*, 120(32). https://doi.org/10.1073/pnas.2307604120

Chang, H. X., Noel, Z. A., & Chilvers, M. I. (2021). A β-lactamase gene of *Fusarium oxysporum* alters the rhizosphere microbiota of soybean. *The Plant Journal*, 106(6), 1588–1604. https://doi.org/10.1111/TPJ.15257

Chavarro-Carrero, E. A., Snelders, N. C., Torres, D. E., Kraege, A., López-Moral, A., Petti, G. C., Punt, W., Wieneke, J., García-Velasco, R., López-Herrera, C. J., Seidl, M. F., & Thomma, B. P. H. J. (2024). The soil-borne white root rot pathogen *Rosellinia necatrix* expresses antimicrobial proteins during host colonization. *PLOS Pathogens*, 20(1), e1011866. https://doi.org/10.1371/journal.ppat.1011866

Chen, E. H. L., Wang, C. H., Liao, Y. T., Chan, F. Y., Kanaoka, Y., Uchihashi, T., Kato, K., Lai, L., Chang, Y. W., Ho, M. C., & Chen, R. P. Y. (2023). Visualizing the membrane disruption action of antimicrobial peptides by cryo-electron tomography. *Nature Communications* 2023 14:1, 14(1), 5464-. https://doi.org/10.1038/s41467-023-41156-2

Cook, D. E., Mesarich, C. H., & Thomma, B. P. H. J. (2015). Understanding plant immunity as a surveillance system to detect invasion. *Annual Review of Phytopathology*, 53(1), 541–563. https://doi.org/10.1146/annurev-phyto-080614-120114

de Guillen, K., Mammri, L., Gracy, J., Padilla, A., Barthe, P., Hoh, F., Lahfa, M., Rouffet, J., Petit-Houdenot, Y., Kroj, T., & Lebrun, M. H. (2025). *Zymoseptoria tritici* effectors structurally related to killer proteins UmV-KP4 and UmV-KP6 inhibit fungal growth, and define extended protein families in fungi. *Molecular Plant Pathology*, 26(8), e70141. https://doi.org/10.1111/MPP.70141

de Guillen, K., Ortiz-Vallejo, D., Gracy, J., Fournier, E., Kroj, T., & Padilla, A. (2015). Structure analysis uncovers a highly diverse but structurally conserved effector family in phytopathogenic fungi. *PLOS Pathogens*, 11(10), e1005228. https://doi.org/10.1371/journal.ppat.1005228

de Jonge, R., Peter van Esse, H., Maruthachalam, K., Bolton, M. D., Santhanam, P., Saber, M. K., Zhang, Z., Usami, T., Lievens, B., Subbarao, K. V., & Thomma, B. P. H. J. (2012). Tomato immune receptor Ve1 recognizes effector of multiple fungal pathogens uncovered by genome and RNA sequencing. *Proceedings of the National Academy of Sciences*, 109(13), 5110–5115. https://doi.org/10.1073/pnas.1119623109

De Oliveira, A. L., Gallo, M., Pazzagli, L., Benedetti, C. E., Cappugi, G., Scala, A., Pantera, B., Spisni, A., Pertinhez, T. A., & Cicero, D. O. (2011). The structure of the elicitor Cerato-platanin (CP), the first member of the CP fungal protein family, reveals a double

ψβ-barrel fold and carbohydrate binding. *The Journal of Biological Chemistry*, 286(20), 17560–17568. https://doi.org/10.1074/JBC.M111.223644

Derbyshire, M. C., & Raffaele, S. (2023). Surface frustration re-patterning underlies the structural landscape and evolvability of fungal orphan candidate effectors. *Nature Communications*, 14(1), 5244. https://doi.org/10.1038/s41467-023-40949-9

Du, Y., Han, X., & Tsuda, K. (2024). Microbiome-mediated plant disease resistance: recent advances and future directions. *Journal of General Plant Pathology* 2024 91:1, 91(1), 1–17. https://doi.org/10.1007/S10327-024-01204-1

Eichfeld, R., Endeshaw, A. B., Hellmann, M. J., Moerschbacher, B. M., & Zuccaro, A. (2025). Domain gain or loss in fungal chitinases drives ecological specialization toward antagonism or immune suppression. *BioRxiv*, 2025.06.16.659886. https://doi.org/10.1101/2025.06.16.659886

Emms, D. M., & Kelly, S. (2018). STAG: species tree inference from all genes. *BioRxiv*, 267914. https://doi.org/10.1101/267914

Emms, D. M., & Kelly, S. (2019). OrthoFinder: phylogenetic orthology inference for comparative genomics. *Genome Biology*, 20(1), 238. https://doi.org/10.1186/s13059-019-1832-y

Faino, L., Seidl, M. F., Datema, E., van den Berg, G. C. M., Janssen, A., Wittenberg, A. H. J., & Thomma, B. P. H. J. (2015). Single-Molecule real-time sequencing combined with optical mapping yields completely finished fungal geno me. *MBio*, 6(4). https://doi.org/10.1128/mBio.00936-15

Fradin, E. F., & Thomma, B. P. H. J. (2006). Physiology and molecular aspects of Verticillium wilt diseases caused by *V. dahliae* and *V. albo-atrum*. *Molecular Plant Pathology*, 7(2), 71–86. https://doi.org/10.1111/J.1364-3703.2006.00323.X

Gaderer, R., Bonazza, K., & Seidl-Seiboth, V. (2014). Cerato-platanins: a fungal protein family with intriguing properties and application potential. *Applied Microbiology and Biotechnology*, 98(11), 4795–4803. https://doi.org/10.1007/s00253-014-5690-y

Gehring, C. A., & Irving, H. R. (2003). Natriuretic peptides—a class of heterologous molecules in plants. *The International Journal of Biochemistry & Cell Biology*, 35(9), 1318–1322. https://doi.org/10.1016/S1357-2725(03)00032-3

Gómez-Pérez, D., Schmid, M., Chaudhry, V., Hu, Y., Velic, A., Maček, B., Ruhe, J., Kemen, A., & Kemen, E. (2023). Proteins released into the plant apoplast by the obligate

parasitic protist *Albugo* selectively repress phyllosphere-associated bacteria. *New Phytologist*, 239(6), 2320–2334. https://doi.org/10.1111/nph.18995

Hacquard, S., Spaepen, S., Garrido-Oter, R., & Schulze-Lefert, P. (2017). Interplay between innate immunity and the plant microbiota. *Annual Review of Phytopathology*, 55(1), 565–589. https://doi.org/10.1146/annurev-phyto-080516-035623

Harbort, C. J., Hashimoto, M., Inoue, H., Niu, Y., Guan, R., Rombolà, A. D., Kopriva, S., Voges, M. J. E. E. E., Sattely, E. S., Garrido-Oter, R., & Schulze-Lefert, P. (2020). Root-secreted coumarins and the microbiota interact to improve iron nutrition in *Arabidopsis*. *Cell Host & Microbe*, 28(6), 825-837.e6. https://doi.org/10.1016/j.chom.2020.09.006

Jones, J. D. G., & Dangl, J. L. (2006). The plant immune system. *Nature* Vol. 444, Issue 7117, pp. 323–329. https://doi.org/10.1038/nature05286

Jones, J. D. G., Staskawicz, B. J., & Dangl, J. L. (2024). The plant immune system: from discovery to deployment. *Cell*, 187(9), 2095–2116. https://doi.org/10.1016/J.CELL.2024.03.045

Jones, P., Binns, D., Chang, H.-Y., Fraser, M., Li, W., McAnulla, C., McWilliam, H., Maslen, J., Mitchell, A., Nuka, G., Pesseat, S., Quinn, A. F., Sangrador-Vegas, A., Scheremetjew, M., Yong, S.-Y., Lopez, R., & Hunter, S. (2014). InterProScan 5: genome-scale protein function classification. *Bioinformatics*, 30(9), 1236–1240. https://doi.org/10.1093/bioinformatics/btu031

Jumper, J., Evans, R., Pritzel, A., Green, T., Figurnov, M., Ronneberger, O., Tunyasuvunakool, K., Bates, R., Žídek, A., Potapenko, A., Bridgland, A., Meyer, C., Kohl, S. A. A., Ballard, A. J., Cowie, A., Romera-Paredes, B., Nikolov, S., Jain, R., Adler, J., … Hassabis, D. (2021). Highly accurate protein structure prediction with AlphaFold. *Nature* 2021 596:7873, 596(7873), 583–589. https://doi.org/10.1038/s41586-021-03819-2

Katoh, K. (2002). MAFFT: a novel method for rapid multiple sequence alignment based on fast Fourier transform. *Nucleic Acids Research*, 30(14), 3059–3066. https://doi.org/10.1093/nar/gkf436

Kettles, G. J., Bayon, C., Sparks, C. A., Canning, G., Kanyuka, K., & Rudd, J. J. (2018). Characterization of an antimicrobial and phytotoxic ribonuclease secreted by the fungal wheat pathogen *Zymoseptoria tritici*. *New Phytologist*, 217(1), 320–331. https://doi.org/10.1111/nph.14786

Kombrink, A., & Thomma, B. P. H. J. (2013). LysM effectors: secreted proteins supporting fungal life. *PLoS Pathogens*, 9(12), e1003769. https://doi.org/10.1371/journal.ppat.1003769

Kraege, A., Punt, W., Doddi, A., Zhu, J., Schmitz, N., Snelders, N. C., & Thomma, B. P. H. J. (2026). Undermining the cry for help: the phytopathogenic fungus *Verticillium dahliae* secretes an antimicrobial effector protein to undermine host recruitment of antagonistic *Pseudomonas* bacteria. *New Phytologist*, 249(1), 406–417. https://doi.org/10.1111/nph.70686

Lin, Z., Akin, H., Rao, R., Hie, B., Zhu, Z., Lu, W., Smetanin, N., Verkuil, R., Kabeli, O., Shmueli, Y., dos Santos Costa, A., Fazel-Zarandi, M., Sercu, T., Candido, S., & Rives, A. (2023). Evolutionary-scale prediction of atomic-level protein structure with a language model. *Science*, 379(6637), 1123–1130. https://doi.org/10.1126/science.ade2574

Liu, Y., Chen, L., Wu, G., Feng, H., Zhang, G., Shen, Q., & Zhang, R. (2017). Identification of root-secreted compounds involved in the communication between cucumber, the beneficial *Bacillus amyloliquefaciens*, and the soil-borne pathogen *Fusarium oxysporum*. *Molecular Plant-Microbe Interactions®*, 30(1), 53–62. https://doi.org/10.1094/MPMI-07-16-0131-R

Lo Presti, L., Lanver, D., Schweizer, G., Tanaka, S., Liang, L., Tollot, M., Zuccaro, A., Reissmann, S., & Kahmann, R. (2015). Fungal effectors and plant susceptibility. *Annual Review of Plant Biology*, 66(1), 513–545. https://doi.org/10.1146/annurev-arplant-043014-114623

Luti, S., Sella, L., Quarantin, A., Pazzagli, L., & Baccelli, I. (2020). Twenty years of research on cerato-platanin family proteins: clues, conclusions, and unsolved issues. *Fungal Biology Reviews*, 34(1), 13–24. https://doi.org/10.1016/j.fbr.2019.10.001

Madeira, F., Madhusoodanan, N., Lee, J., Eusebi, A., Niewielska, A., Tivey, A. R. N., Lopez, R., & Butcher, S. (2024). The EMBL-EBI job dispatcher sequence analysis tools framework in 2024. *Nucleic Acids Research*, 52(W1), W521–W525. https://doi.org/10.1093/nar/gkae241

Malanovic, N., & Lohner, K. (2016). Antimicrobial peptides targeting gram-positive bacteria. *Pharmaceuticals*, 9(3), 59. https://doi.org/10.3390/ph9030059

Mesny, F., Bauer, M., Zhu, J., & Thomma, B. P. H. J. (2024). Meddling with the microbiota: fungal tricks to infect plant hosts. *Current Opinion in Plant Biology*, 82, 102622. https://doi.org/10.1016/j.pbi.2024.102622

Mesny, F., Hacquard, S., & Thomma, B. P. (2023). Co-evolution within the plant holobiont drives host performance. *EMBO Reports*, 24(9), EMBR202357455-. https://doi.org/10.15252/embr.202357455

Mesny, F., Wolf, V., López-Moral, A., Kraege, A., Punt, W., Park, J., Zhu, J., Sato, Y., & Thomma, B. P. (2025). Plant-associated fungi co-opt ancient antimicrobials for host manipulation. *BioRxiv*, 2024.01.04.574150. https://doi.org/10.1101/2024.01.04.574150

Ökmen, B., Katzy, P., Huang, L., Wemhöner, R., & Doehlemann, G. (2023). A conserved extracellular Ribo1 with broad-spectrum cytotoxic activity enables smut fungi to compete with host-associated bacteria. *New Phytologist*, 240(5), 1976–1989. https://doi.org/10.1111/nph.19244

Oliveira Júnior, N. G., Souza, C. M., Buccini, D. F., Cardoso, M. H., & Franco, O. L. (2025). Antimicrobial peptides: structure, functions and translational applications. *Nature Reviews Microbiology* 2025, 1–14. https://doi.org/10.1038/s41579-025-01200-y

Pazzagli, L., Cappugi, G., Manao, G., Camici, G., Santini, A., & Scala, A. (1999). Purification, characterization, and amino acid sequence of cerato-platanin, a new phytotoxic protein from *Ceratocystis fimbriata* f. sp*. platani*. *Journal of Biological Chemistry*, 274(35), 24959–24964. https://doi.org/10.1074/jbc.274.35.24959

Pennington, H. G., Jones, R., Kwon, S., Bonciani, G., Thieron, H., Chandler, T., Luong, P., Morgan, S. N., Przydacz, M., Bozkurt, T., Bowden, S., Craze, M., Wallington, E. J., Garnett, J., Kwaaitaal, M., Panstruga, R., Cota, E., & Spanu, P. D. (2019). The fungal ribonuclease-like effector protein CSEP0064/BEC1054 represses plant immunity and interferes with degradation of host ribosomal RNA. *PLOS Pathogens*, 15(3), e1007620. https://doi.org/10.1371/JOURNAL.PPAT.1007620

Petti G. C. (2026): Homologous antimicrobial proteins in plants and fungi: conserved mechanisms shaping the plant microbiota. PhD-Thesis; University of Cologne

Pieterse, C. M. J., Zamioudis, C., Berendsen, R. L., Weller, D. M., Van Wees, S. C. M., Bakker, P. A. H. M., Nl, C. M. J. P., Nl, C. Z., Nl, R. L. B., Nl, S. V., & Nl, P. A. H. M. B. (2014). Induced Systemic Resistance by Beneficial Microbes. *Annual Review of Phytopathology*, 52, 347–375. https://doi.org/10.1146/ANNUREV-PHYTO-082712-102340

Price, M. N., Dehal, P. S., & Arkin, A. P. (2009). FastTree: computing large minimum evolution trees with profiles instead of a distance matrix. *Molecular Biology and Evolution*, 26(7), 1641–1650. https://doi.org/10.1093/molbev/msp077

Punt, W., Kraege, A., Metzger, S., Schmitz, N., Zhu, J., Hacquard, S., Bonkowski, M., Snelders, N. C., & Thomma, B. P. H. J. (2025). Differential contributions of an antimicrobial effector from *Verticillium dahliae* to virulence and tomato microbiota assembly across natural soils. *BioRxiv,* 2025.09.30.679524. https://doi.org/10.1101/2025.09.30.679524

Quarantin, A., Castiglioni, C., Schäfer, W., Favaron, F., & Sella, L. (2019). The *Fusarium graminearum* cerato-platanins loosen cellulose substrates enhancing fungal cellulase activity as expansin-like proteins. *Plant Physiology and Biochemistry*, 139, 229–238. https://doi.org/10.1016/j.plaphy.2019.03.025

R Core Team. (2023). R: a language and environment for statistical computing. *https://www.R-project.org/.*

Rovenich, H., Boshoven, J. C., & Thomma, B. P. (2014). Filamentous pathogen effector functions: of pathogens, hosts and microbiomes. *Current Opinion in Plant Biology*, 20, 96–103. https://doi.org/10.1016/j.pbi.2014.05.001

Sakamoto, T., & Ortega, J. M. (2021). Taxallnomy: an extension of NCBI Taxonomy that produces a hierarchically complete taxonomic tree. *BMC Bioinformatics*, 22(1), 388. https://doi.org/10.1186/s12859-021-04304-3

Schneider, C. A., Rasband, W. S., & Eliceiri, K. W. (2012). NIH Image to ImageJ: 25 years of image analysis. *Nature Methods*, 9(7), 671–675. https://doi.org/10.1038/nmeth.2089

Seidl, M. F., & Van den Ackerveken, G. (2019). Activity and phylogenetics of the broadly occurring family of microbial Nep1-like proteins. *Annual Review of Phytopathology*, 57(1), 367–386. https://doi.org/10.1146/annurev-phyto-082718-100054

Seong, K., & Krasileva, K. V. (2023). Prediction of effector protein structures from fungal phytopathogens enables evolutionary analyses. *Nature Microbiology* 2023 8:1, 8(1), 174–187. https://doi.org/10.1038/s41564-022-01287-6

Snelders, N. C., Boshoven, J. C., Song, Y., Schmitz, N., Fiorin, G. L., Rovenich, H., van den Berg, G. C. M., Torres, D. E., Petti, G. C., Prockl, Z., Faino, L., Seidl, M. F., & Thomma, B. P. H. J. (2023). A highly polymorphic effector protein promotes fungal virulence through suppression of plant-associated Actinobacteria. *New Phytologist*, 237(3), 944–958. https://doi.org/10.1111/nph.18576

Snelders, N. C., Petti, G. C., van den Berg, G. C. M., Seidl, M. F., & Thomma, B. P. H. J. (2021). An ancient antimicrobial protein co-opted by a fungal plant pathogen for *in planta* mycobiome manipulation. *Proceedings of the National Academy of Sciences*, 118(49), e2110968118. https://doi.org/10.1073/pnas.2110968118

Snelders, N. C., Rovenich, H., Petti, G. C., Rocafort, M., van den Berg, G. C. M., Vorholt, J. A., Mesters, J. R., Seidl, M. F., Nijland, R., & Thomma, B. P. H. J. (2020). Microbiome manipulation by a soil-borne fungal plant pathogen using effector proteins. *Nature Plants*, 6(11), 1365–1374. https://doi.org/10.1038/s41477-020-00799-5

Snelders, N. C., Rovenich, H., & Thomma, B. P. H. J. (2022). Microbiota manipulation through the secretion of effector proteins is fundamental to the wealth of lifestyles in the fungal kingdom. *FEMS Microbiology Reviews*, 46(5). https://doi.org/10.1093/femsre/fuac022

Sperschneider, J., Dodds, P. N., Gardiner, D. M., Manners, J. M., Singh, K. B., & Taylor, J. M. (2015). Advances and challenges in computational prediction of effectors from plant pathogenic fungi. *PLOS Pathogens*, 11(5), e1004806. https://doi.org/10.1371/journal.ppat.1004806

Spooren, J., van Bentum, S., Thomashow, L. S., Pieterse, C. M. J., Weller, D. M., & Berendsen, R. L. (2024). Plant-driven assembly of disease-suppressive soil microbiomes. *Annual Review of Phytopathology*, 62(1), 1–30. https://doi.org/10.1146/annurev-phyto-021622-100127

Teufel, F., Armenteros, J. J. A., Johansen, A. R., Gíslason, M. H., Pihl, S. I., Tsirigos, K. D., Winther, O., Brunak, S., von Heijne, G., & Nielsen, H. (2021). SignalP 6.0 achieves signal peptide prediction across all types using protein language models. *BioRxiv*, 2021.06.09.447770. https://doi.org/10.1101/2021.06.09.447770

Thomma, B., Cammue, B., & Thevissen, K. (2002). Plant defensins. *Planta*, 216(2), 193–202. https://doi.org/10.1007/s00425-002-0902-6

Thompson, J. D., Higgins, D. G., & Gibson, T. J. (1994). CLUSTAL W: improving the sensitivity of progressive multiple sequence alignment through sequence weighting, position-specific gap penalties and weight matrix choice. *Nucleic Acids Research*, 22(22), 4673–4680. https://doi.org/10.1093/nar/22.22.4673

Todd, A. E., Orengo, C. A., & Thornton, J. M. (1999). Evolution of protein function, from a structural perspective. *Current Opinion in Chemical Biology*, 3(5), 548–556. https://doi.org/10.1016/S1367-5931(99)00007-1

Törönen, P., & Holm, L. (2022). PANNZER — A practical tool for protein function prediction. *Protein Science*, 31(1), 118–128. https://doi.org/10.1002/pro.4193

Trivedi, P., Leach, J. E., Tringe, S. G., Sa, T., & Singh, B. K. (2020). Plant–microbiome interactions: from community assembly to plant health. *Nature Reviews Microbiology*, 18(11), 607–621. https://doi.org/10.1038/s41579-020-0412-1

Troshin, P. V., Procter, J. B., & Barton, G. J. (2011). Java bioinformatics analysis web services for multiple sequence alignment—JABAWS:MSA. *Bioinformatics*, 27(14), 2001–2002. https://doi.org/10.1093/bioinformatics/btr304

Vandenkoornhuyse, P., Quaiser, A., Duhamel, M., Le Van, A., & Dufresne, A. (2015). The importance of the microbiome of the plant holobiont. *New Phytologist*, 206(4), 1196–1206. https://doi.org/10.1111/nph.13312

Vollmer, W. (2008). Structural variation in the glycan strands of bacterial peptidoglycan. FEMS *Microbiology Reviews*, 32(2), 287–306. https://doi.org/10.1111/j.1574-6976.2007.00088.x

Wagner, M. R., Lundberg, D. S., del Rio, T. G., Tringe, S. G., Dangl, J. L., & Mitchell-Olds, T. (2016). Host genotype and age shape the leaf and root microbiomes of a wild perennial plant. *Nature Communications*, 7(1), 12151. https://doi.org/10.1038/ncomms12151

Weiland, P., Dempwolff, F., Steinchen, W., Freibert, S., Tian, H., Glatter, T., Martin, R., Thomma, B. P. H. J., Bange, G., & Altegoer, F. (2023). Structural and functional analysis of the cerato-platanin-like protein Cpl1 suggests diverging functions in smut fungi. *Molecular Plant Pathology,* 24(7), 768–787. https://doi.org/10.1111/mpp.13349

Zhang, Y., Gao, Y., Liang, Y., Dong, Y., Yang, X., Yuan, J., & Qiu, D. (2017). The *Verticillium dahliae* SnodProt1-Like protein VdCP1 contributes to virulence and triggers the plant immune system. *Frontiers in Plant Science*, 8, 289292. https://doi.org/10.3389/fpls.2017.01880

Zhang, Y., & Skolnick, J. (2005). TM-align: a protein structure alignment algorithm based on the TM-score. *Nucleic Acids Research*, 33(7), 2302–2309. https://doi.org/10.1093/nar/gki524

Zhou, B.-J., Jia, P.-S., Gao, F., & Guo, H.-S. (2012). Molecular characterization and functional analysis of a necrosis- and ethylene-inducing, protein-encoding gene family from *Verticillium dahliae*. *Molecular Plant-Microbe Interactions®*, 25(7), 964–975. https://doi.org/10.1094/MPMI-12-11-0319

Supplementary information

Fusarium oxysporum MPI-CAGE-CH-0212 No.1/3

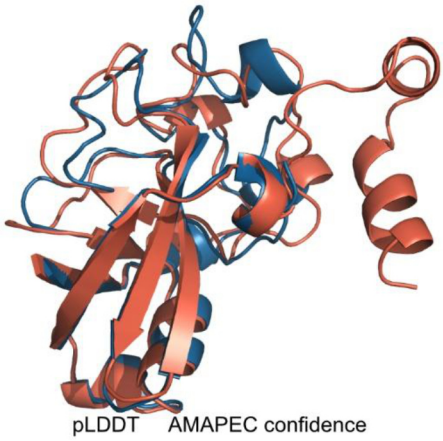

pLDDT AMAPEC confidence
59.09 0.15

Fusarium oxysporum MPI-CAGE-CH-0212 No.2/3

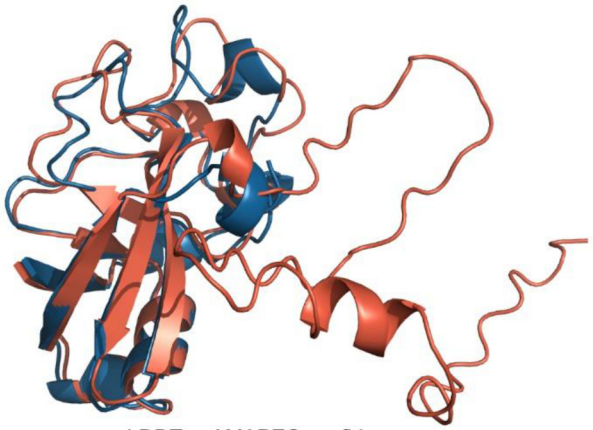

pLDDT AMAPEC confidence
64.78 0.26

Chaetomium globosum No.1/1

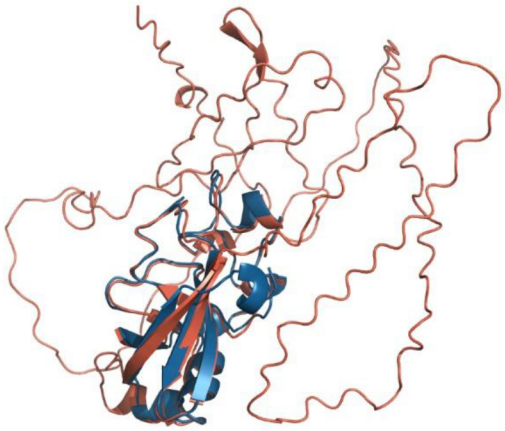

pLDDT AMAPEC confidence
52.62 0.47

Tuber aestivum var. *uncinatum* No.1/2

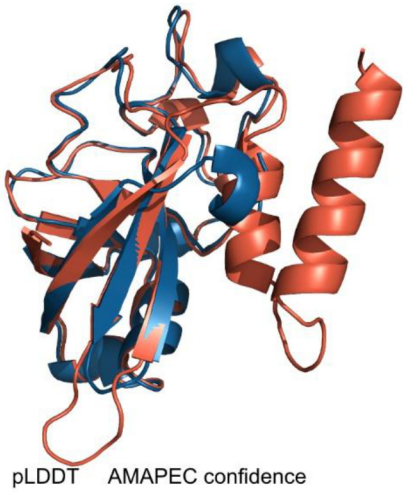

pLDDT AMAPEC confidence
77.42 0.43

Paxillus involutus ATCC 200175 No.1/5

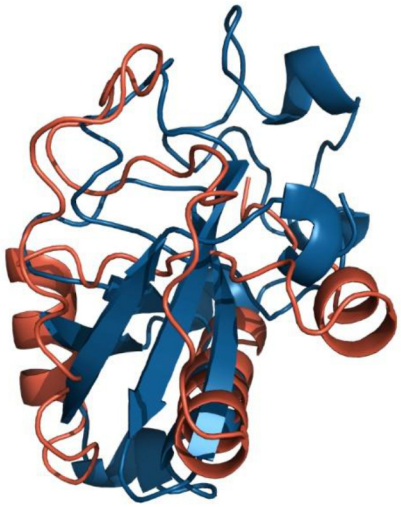

pLDDT AMAPEC confidence
32.04 0.04

Helotiales F229 No.1/1

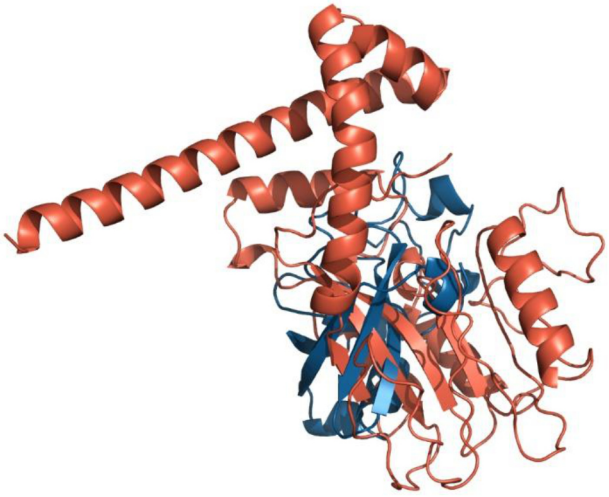

pLDDT AMAPEC confidence
53.44 0.08

Figure S1. Superposition of CP1 and the CP1 homologues that are predicted to lack antimicrobial activity. CP1 is colored in blue while the homologues are colored in red. Gene name and number of homologues in the same species is given above the protein fold and pLDDT score (1-100) and AMAPEC prediction confidence for antimicrobial activity (0-1) below the respective structure. AMAPEC confidence >0.5 is considered as predicted antimicrobial activity.

General Discussion

Introduction

Plants are continuously colonized by diverse microbial communities, collectively known as the plant microbiota, which inhabit all parts of the plant including roots, shoots, and leaves (Trivedi et al., 2020). The assembly of these communities is shaped by both environmental factors, such as soil properties and microbial pools, and host-derived factors, including root exudates that attract or repel specific taxa (Compant et al., 2019; Trivedi et al., 2020; Mesny et al., 2023). Together with their host, these microbes form a functional unit known as the holobiont, in which host and microbial activities are tightly interconnected (Vandenkoornhuyse et al., 2015; Mesny et al., 2023). The microbiota contributes to plant health by protecting against pathogens, for instance through direct antagonism or by stimulating host defences. Under pathogen attack, plants can recruit beneficial microbes from the bulk soil to enhance protection, a process termed the “cry for help” response (Rolfe et al., 2019; Du et al., 2025). Research over recent years has shown that plant pathogens have evolved sophisticated strategies to overcome not only plant immune responses, but also microbiota-mediated defences (Mesny et al., 2024). Many pathogens secrete antimicrobial effector proteins that manipulate host-associated microbial communities to facilitate niche establishment and disease development (Snelders et al., 2020; Mesny et al., 2024). In this thesis research I aimed to investigate the functional and evolutionary roles of antimicrobial effectors in shaping plant–microbe interactions and promoting pathogen success.

During my doctoral research, I studied antimicrobial effectors of the soil-borne vascular wilt fungus *Verticillium dahliae* to explore their roles in plant–microbe interactions as well as their evolutionary histories. In Chapter 2, we characterized the effector Av2 and showed that it suppresses the plant’s cry for help recruitment of antagonistic *Pseudomonas* bacteria, demonstrating that pathogens can actively sabotage microbiota-mediated host defences. Chapter 3 focused on the effector Ave1, revealing that while it consistently perturbs host microbiota, its contribution to fungal virulence varies depending on soil-derived microbial communities, highlighting the context-dependent nature of the effector activity. Chapter 4 investigates the evolutionary history of effectors, showing that many immunomodulatory effectors possess conserved antimicrobial properties, suggesting that fungi have repeatedly repurposed ancient antimicrobial proteins during evolution towards plant-associated lifestyles. Finally, Chapter 5 examined the cerato-platanin effector family, demonstrating conserved antimicrobial activity across all members of this protein family and across fungi that adopted diverse lifestyles. In the following sections, I will discuss these findings and place them into a broader context.

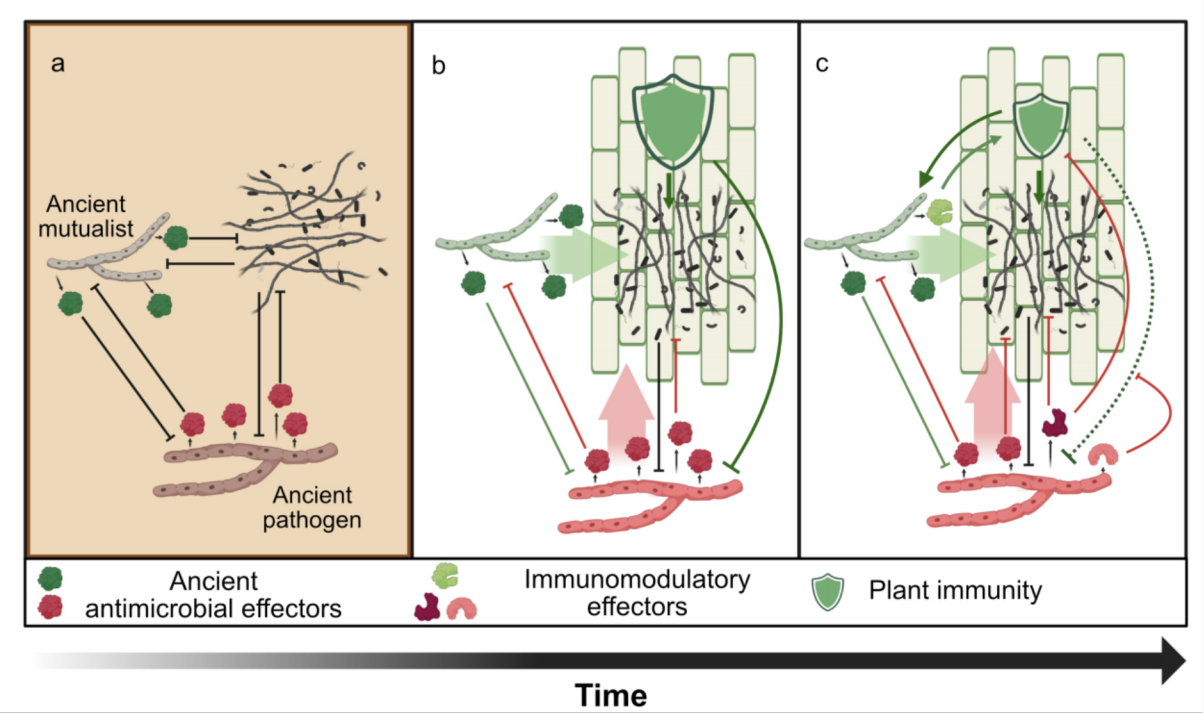

Figure 1. Evolutionary origin and functional diversification of fungal antimicrobial effectors. (**a**) Antimicrobial effectors likely originally arose as tools for microbial competition long before fungi engaged in interactions with terrestrial plants (**b**) During early colonization of terrestrial plants, ancestral fungi repurposed antimicrobial effectors to manipulate host-associated microbial communities, thereby possibly facilitating the earliest fungal associations with host organisms. (**c**) During host–fungus co-evolution, antimicrobial effectors were co-opted to facilitate colonization through the acquisition of immunomodulatory functions. Their secretion and stability in extracellular environments such as the plant apoplast likely predisposed these proteins to interact with host components, promoting functional diversification and giving rise to many of the immunomodulatory effectors observed today.

Many immunomodulating effectors evolved from ancient antimicrobial effectors

Several plant pathogens have been shown to deploy antimicrobial effectors that contribute to virulence by suppressing microbial competitors, yet the overall extent and diversity of antimicrobial effector repertoires across the fungal kingdom have remained poorly understood (Mesny et al., 2024). This gap has limited our ability to place antimicrobial effectors into an evolutionary context and to assess whether such strategies are specific adaptations to pathogenicity or reflect more general fundamentals of fungal biology. By applying large-scale computational analyses using AMAPEC, we demonstrate that fungi with diverse ecological lifestyles encode extensive repertoires of putative antimicrobial proteins (Chapter 4). Moreover, antimicrobial effectors are broadly conserved across the fungal phylogenetic tree, comprising numerous fungi that do not colonize plants. These observations indicate that

antimicrobial effector proteins are not niche innovations associated particularly with plant pathogenicity, but instead represent ancient and widespread components of fungal biology. Before the colonization of land by vascular plants approximately 500 million years ago, fungi primarily interacted with microbial communities in aquatic or semi-aquatic habitats, including bacteria and algae (Figure 1a; James et al., 2025; Snelders et al., 2022). In this context, microbial antagonism is likely to have been a key determinant of fitness, strongly favouring the evolution of antimicrobial strategies. The broad conservation of antimicrobial effector families across fungi, together with their presence in non-plant-associated lineages, supports the view that these proteins originally evolved as tools for microbial competition long before fungi engaged in interactions with terrestrial plants (Snelders et al., 2022; Mesny et al., 2024).

The widespread presence of antimicrobial effectors in extant fungi may reflect a long history of intermicrobial competition. Many fungi encode large repertoires of these effectors, yet each effector typically acts against a narrow set of microbial targets (Snelders et al., 2020, 2021, 2023, Mesny et al., 2024), indicating functional complementarity rather than redundancy among these repertoires. Moreover, given that many antimicrobials often have broadly conserved targets, such as phospholipid membranes, chitin, or peptidoglycan (Oliveira Júnior et al., 2025, Mesny et al., 2024), the observed insensitivity of certain microbes is unlikely to result from absence of the target, but may rather have from evolved resistance or insensitivity mechanisms. These can include modifications of the target site, such as cell wall decorations that protect or shield the target, or active countermeasures to degrade antimicrobial effectors or suppress the production of the effector. Consequently, intermicrobial competition may constitute an ongoing evolutionary arms race, analogous to the co-evolutionary arms race dynamics observed between plants and pathogens (Cook et al., 2015; Jones et al., 2024).

During interactions with early terrestrial plants, ancestral fungi likely secreted ancient antimicrobial effectors as they encounter microbial competitors (Figure 1b). The intrinsic properties of antimicrobial proteins, including their secretion and stability in extracellular environments such as the plant apoplast, may have made them particularly prone to acquiring additional functions to manipulate host physiology through interactions with host surface or apoplastic proteins. Such functional adaptation would have facilitated fungal adaptation to plant hosts and ultimately given rise to many of the immunomodulating effectors observed today (Figure 1c). Consistent with this evolutionary scenario, we find that many previously described effector proteins with immunomodulatory roles are predicted to possess antimicrobial activity, a prediction we experimentally validated for several effectors (Chapter 4 and 5). This suggests that immunomodulating effectors may have evolved through the co-option of ancestral antimicrobial proteins. Supporting this idea, we show in Chapter 4 that

changes in protein domain organization can repurpose effector function from antimicrobial to immunomodulatory. Specifically, acquisition of a nuclear localisation signal in the *V. dahliae* effector Vd424Y conferred the ability to enter plant cell nuclei and manipulate host immunity in addition to its antimicrobial activity. In addition, recent work has reported a similar functional repurposing in the chitinase effector SiCHIT2, where loss of a carbohydrate-binding domain shifted its activity from antimicrobial to immunomodulatory, facilitating evolutionary transition of *Serendipita indica* from saprotrophic lifestyle to plant symbiosis (Eichfeld et al., 2025).

Repurposing of antimicrobial proteins may have facilitated the earliest fungal associations with host organisms, enabling fungi to manipulate host-associated microbial communities. Importantly, because pathogens of animals may likewise depend on the ability to manipulate both host microbiota and immune responses (Stevens et al., 2025, Sexton et al., 2006), this evolutionary trajectory is unlikely to be restricted to plant-associated fungi and may instead represent a broader and recurrent pattern in fungal evolution (Snelders et al., 2022). Over time, this may have been followed by the evolution of more specialized host-directed virulence mechanisms, the extent and relative importance of which is likely to increase with higher degrees of co-evolution and host-specialisation (Möller et al., 2017; Mesny et al., 2024; Snelders et al., 2022). Consequently, it is important to recognize that not all fungal effectors share this ancient evolutionary origin. Fungal effector repertoires also include lineage-specific proteins, many of which likely arose independently of ancestral antimicrobial proteins, representing more recent innovations shaped by host-driven selection and co-evolutionary arms races with host immune systems (Cook et al., 2015; Jones et al., 2024).

The cerato-platanin family exemplifies an ancient protein fold that is conserved across fungi and plants, which has been co-opted as an antimicrobial effector in pathogenic fungi to contribute to virulence. By applying structural clustering to the *Verticillium dahliae* secretome we revealed an unexpected structural similarity between the cerato-platanins CP1, CP2, CP3, the previously characterized antimicrobial effectors Ave1 and Ave1L2 (Snelders et al., 2020; 2023), and plant natriuretic peptides (PNPs), all sharing a conserved three-dimensional fold (Chapter 5; Snelders et al, 2020; Snelders et al., 2023; Petti et al., 2026). The persistence of this fold across fungi and plants implies strong selective pressure to maintain this structure, pointing to an ancient and broadly relevant biological role. Functional assays support this notion: while CPs from fungi with diverse lifestyles exhibit broad antimicrobial activity, Ave1 and Ave1L2 display selective antimicrobial activity, and also PNPs can inhibit microbial growth (Snelders et al., 2020; Snelders 2023; Petti et al., 2026, Chapter 5). The presence of antimicrobial activity across such phylogenetically distant lineages suggests that this fold arose early in eukaryotic evolution as an effective antimicrobial scaffold and has been preserved due to its ability to suppress microbial growth. This pattern closely resembles that

of defensins, which likewise maintain structural conservation and antimicrobial function across multiple kingdoms (Thomma et al., 2002), suggesting that certain protein folds might be particularly well suited for antimicrobial activity.

While antimicrobial activity appears to be ancestral, our findings also highlight extensive functional diversification of this fold. In fungi, certain CPs contribute to virulence through immune modulation or interactions with host cell walls (Baccelli et al., 2014; Luti et al., 2020; Zhang et al., 2017). Similarly, Ave1 not only exhibits antimicrobial activity but is also capable to manipulate host physiology, as shown by its ability to induce stomatal opening (Punt et al., 2025). Together, these findings provide further evidence that ancestral antimicrobial proteins have been repeatedly co-opted for additional roles in host–pathogen interactions. This functional repurposing likely exploits intrinsic features of antimicrobial proteins, such as their secretion and stability in the plant apoplast, but possibly also the interaction with cell walls and membranes, which may facilitate the acquisition of additional functions (Snelders et al., 2022; Mesny et al., 2024). The acquisition of additional protein domains in CP2 and CP3 further supports this notion, as domain gain or loss can expand protein function, as exemplified by the previously discussed effectors Vd424Y and SiCHIT2, enabling adaptation to diverse ecological niches and host interactions (Chapter 4 & 5; Eichfeld et al., 2025; Todd et al., 1999).

Overall, based on the findings in this thesis, we show that fungi have co-opted antimicrobial effectors that originally evolved for microbial competition in ancestral environments and interactions to facilitate plant colonization. During this process, some of these ancestral antimicrobial effectors acquired additional immunomodulatory functions, explaining the evolutionary emergence of many immunomodulating effectors in plant-associated fungi. Importantly, this work highlights the power of structure-based approaches to uncover evolutionary relationships that are not apparent from sequence information alone. Together, these findings provide a new perspective on effector evolution, revealing a previously unrecognized ancient root in microbial antagonism.

Antimicrobial effector outcomes are highly dependent on environmental factors

Many fungal pathogens, including *V. dahliae*, transition through multiple ecological niches over the course of their life cycle, alternating between host colonization and extended persistence in soils or other environments outside the plan host (Fradin & Thomma, 2006; Guerreiro & Stuckenbrock, 2025; Katan, 2017). The plant-associated microbiota that these pathogens encounter is highly dynamic, shaped by both biotic and abiotic factors, and varies across plant tissues (Trivedi et al., 2020; Chapter 3). Importantly, this microbiota is largely assembled from

the microbial community of the bulk soil that the plant grows in, which acts as the primary microbial reservoir from which microbes are recruited. Soil microbial communities are typically more diverse than host-associated microbiota and differ substantially depending on physicochemical soil properties (Sokol et al., 2022; Fierer et al., 2017). As a result, pathogens must engage with a wide range of microbes and adjust their antimicrobial strategies to succeed in these distinct environments (Snelders et al., 2022, Mesny et al., 2024). For broad host-range pathogens such as *V. dahliae*, this challenge is amplified as it colonizes multiple plant species across diverse geographic regions while encountering and interacting with these highly variable microbiota (Trivedi et al., 2020; Snelders et al., 2022). These ecological complexities raise the question whether antimicrobial effectors function uniformly across environments or instead act in a context-dependent manner.

Many antimicrobial effectors influence multiple members of the microbiota, producing broader, system-level effects on community structure and function (Snelders et al., 2020; Chapter 2 & 3). Microbial communities operate as interconnected networks of interdependent species (Van der Heijden and Hartmann, 2016), meaning that changes that affect a single member can propagate through the entire community. Consequently, suppression or removal of particular microbes by fungal effectors can trigger cascading shifts in community composition due to these intermicrobial interactions. The specific outcomes of effector activity are therefore highly context-dependent, shaped by the unique structure of each microbiota. This context-dependency is evident from Chapter 3, where the antimicrobial effector Ave1 caused markedly different changes in the plant microbiota depending on the soil and its associated microbial community. These results illustrate that the effects of antimicrobial effectors on host microbiota are not uniform but vary according to environmental and community-specific factors.

Beyond their direct antimicrobial activity, we show that effectors contribute to fungal fitness in a highly context-dependent manner. The effector Ave1, for example, displays soil-specific functionality, with its contribution to virulence varying according to the composition of the local soil microbiota (Chapter 3). Similarly, it has been shown that Ave1L2 enhances virulence only in the presence of sensitive microbial antagonists, and experimental removal of these taxa abolishes its virulence contribution (Snelders et al., 2023; Punt et al., 2025). In addition, we demonstrate that Av2, previously considered dispensable for virulence, significantly increases *V. dahliae* pathogenicity under tested conditions by undermining host recruitment of beneficial *Pseudomonas* bacteria (Chavarro-Carrero et al., 2021; Chapter 2). Collectively, these observations illustrate that the virulence contributions of antimicrobial effectors are shaped by the dynamic interplay between the pathogen, the host, and the microbiota. Taken together, these results highlight the ecological versatility of antimicrobial effectors: their function is not fixed but depends on microbial context, environmental conditions, and host factors. Rather

than acting as static weapons, antimicrobial effectors serve as tools that fungi use to navigate and adapt to complex, fluctuating ecological niches.

The microbiota as a battleground for host pathogen interactions

Plants rely on their associated microbiota for protection against pathogens, often through a so-called “cry-for-help” mechanism, in which microbial antagonists are selectively recruited upon pathogen infection (Du et al., 2025; Spooren et al., 2024; Rolfe et al., 2019). For example, during infection by the soil-borne pathogen *Fusarium oxysporum* f. sp. *cucumerinum*, cucumber plants recruit beneficial *Bacillus amyloliquefaciens* bacteria, which reduces disease severity (Liu et al., 2017). Similarly, *Pseudomonas syringae pv*. tomato infections in *Arabidopsis thaliana* trigger the secretion of L-malic acid, which facilitates the recruitment of the beneficial rhizobacterium *Bacillus subtilis*, providing disease protection (Rudrappa et al., 2008). Antimicrobial effectors have so far been described as virulence factors that suppress antagonistic microbes within the plant associated microbiota, thereby indirectly facilitating pathogen establishment (Snelders et al., 2020; Snelders et al., 2021; Snelders et al., 2023; Gómez-Pérez et al., 2023 Mesny et al., 2024). The results presented in this thesis extend this understanding by demonstrating that antimicrobial effectors can directly interfere with host-driven microbiota recruitment. Specifically, characterization of Av2 shows for the first time that a pathogen can suppress the recruitment of microbial antagonists that are actively mobilized as part of the plant’s cry for help response (Chapter 2). By blocking the recruitment of protective microbes, Av2 undermines a critical layer of microbiota-mediated immunity. These findings provide direct experimental evidence that the plant microbiota is not merely a passive environment but a strategic battleground in host-pathogen interactions (Snelders et al., 2022; Mesny et al., 2024), in which pathogens evolve effectors that target not only host immune signalling but also host-mediated control over microbial community assembly. Consequently, disease outcome emerges from the combined interaction of pathogen virulence strategies, host defence responses, and microbiota composition, challenging host-centric views of plant immunity and positioning the microbiota as an active, evolvable component of plant defence that itself becomes subject to pathogen-driven selection.

Notably, sustained recruitment of beneficial microbes can, over time, lead to the formation of disease suppressive soils, in which susceptible plants remain healthy despite the continued presence of a virulent pathogen (Yin et al., 2021; Du et al., 2025). Arguably, the most famous example of such a legacy effect concerns the decline of the so-called take-all disease, caused by the fungal plant pathogen *Gaeumannomyces tritici*, in wheat fields over years of monoculture that has been associated with the recruitment of 2,4-diacetylphloroglucinol-

producing *Pseudomonas* spp. (Raaijmakers & Weller, 1998; Spooren et al., 2024). Given that pathogens are known to manipulate host microbiota via secreted antimicrobial effectors, it has been proposed that by actively interfering in host-mediated enrichment of antagonistic bacteria, pathogens may prevent or delay the establishment of disease-suppressive microbial communities (Mesny et al., 2024). Our findings provide a mechanistic basis for this hypothesis. By demonstrating that Av2 suppresses plant recruited microbial antagonists, this work suggests that pathogen derived antimicrobial effectors may contribute to both short term disease establishment and long-term pathogen persistence in soil. Consistent with this interpretation, disease suppressive soils typically require years of sustained pathogen pressure to develop (Weller et al., 2002; Kwak and Weller, 2013). This slow progression may be the consequence of a continuous suppression of beneficial microbes by pathogen effectors that is only gradually overcome by host-driven recruitment of the beneficials. These findings therefore suggest that suppression of microbiota recruitment may represent an important, yet underappreciated, function of antimicrobial effectors in ensuring the ecological and evolutionary success of soil-borne pathogens.

Conceptually, the work presented in this thesis supports a holobiont-centered view of plant–pathogen interactions, in which the host and its associated microbiota form an integrated ecological and evolutionary unit. By demonstrating that pathogens can directly interfere with cry for help-mediated microbial recruitment, this work positions the microbiota as an active and dynamic arena of host microbe interactions rather than a static background of infection. The existence of dual-function effectors with both antimicrobial and immunomodulating properties further blurs the line between microbiota-targeting and host-targeting activities, highlighting how evolutionary repurposing of ancient antimicrobial proteins integrates plant, pathogen, and microbiota interactions into a single, co-evolving system. Together, these insights raise important questions about how immune systems evolve to balance the management of pathogens and beneficial microbes, and how pathogens navigate complex microbial landscapes. More broadly, variation in microbial communities across soils, hosts, and environments likely acts as a major selective force shaping pathogen virulence strategies, emphasizing the need to further understand how pathogens detect and respond to these diverse microbial contexts.

General References

Almario, J., Mahmoudi, M., Kroll, S., Agler, M., Placzek, A., Mari, A., & Kemen, E. (2022). The leaf microbiome of *Arabidopsis* displays reproducible dynamics and patterns throughout the growing season. *MBio*, *13*(3). https://doi.org/10.1128/mbio.02825-21

Baccelli, I., Luti, S., Bernardi, R., Scala, A., & Pazzagli, L. (2014). Cerato-platanin shows expansin-like activity on cellulosic materials. *Applied Microbiology and Biotechnology*, *98*(1), 175–184. https://doi.org/10.1007/s00253-013-4822-0

Berendsen, R. L., Pieterse, C. M. J., & Bakker, P. A. H. M. (2012). The rhizosphere microbiome and plant health. *Trends in Plant Science*, *17*(8), 478–486. https://doi.org/10.1016/j.tplants.2012.04.001

Berendsen, R. L., Vismans, G., Yu, K., Song, Y., de Jonge, R., Burgman, W. P., Burmølle, M., Herschend, J., H M Bakker, P. A., & J Pieterse, C. M. (2018). Disease-induced assemblage of a plant-beneficial bacterial consortium. *The ISME Journal, 12*, 1496–1507. https://doi.org/10.1038/s41396-018-0093-1

Bozkurt, T. O., Schornack, S., Win, J., Shindo, T., Ilyas, M., Oliva, R., Cano, L. M., Jones, A. M. E., Huitema, E., Van Der Hoorn, R. A. L., & Kamoun, S. (2011). *Phytophthora infestans* effector AVRblb2 prevents secretion of a plant immune protease at the haustorial interface. *Proceedings of the National Academy of Sciences of the United States of America*, *108*(51), 20832–20837. https://doi.org/10.1073/PNAS.1112708109

Cao, Y., Kümmel, F., Logemann, E., Gebauer, J. M., Lawson, A. W., Yu, D., Uthoff, M., Keller, B., Jirschitzka, J., Baumann, U., Tsuda, K., Chai, J., & Schulze-Lefert, P. (2023). Structural polymorphisms within a common powdery mildew effector scaffold as a driver of coevolution with cereal immune receptors. *Proceedings of the National Academy of Sciences*, *120*(32). https://doi.org/10.1073/pnas.2307604120

Carlström, C. I., Field, C. M., Bortfeld-Miller, M., Müller, B., Sunagawa, S., & Vorholt, J. A. (2019). Synthetic microbiota reveal priority effects and keystone strains in the <i>Arabidopsis<i> phyllosphere. *Nature Ecology & Evolution*, *3*(10), 1445–1454. https://doi.org/10.1038/S41559-019-0994-Z

Chang, H. X., Noel, Z. A., & Chilvers, M. I. (2021). A β-lactamase gene of *Fusarium oxysporum* alters the rhizosphere microbiota of soybean. *The Plant Journal*, *106*(6), 1588–1604. https://doi.org/10.1111/TPJ.15257

Chavarro-Carrero, E. A., Snelders, N. C., Torres, D. E., Kraege, A., López-Moral, A., Petti, G. C., Punt, W., Wieneke, J., García-Velasco, R., López-Herrera, C. J., Seidl, M. F., & Thomma, B. P. H. J. (2024). The soil-borne white root rot pathogen *Rosellinia necatrix* expresses antimicrobial proteins during host colonization. *PLOS Pathogens*, *20*(1), e1011866. https://doi.org/10.1371/journal.ppat.1011866

Chen, L. Q., Hou, B. H., Lalonde, S., Takanaga, H., Hartung, M. L., Qu, X. Q., Guo, W. J., Kim, J. G., Underwood, W., Chaudhuri, B., Chermak, D., Antony, G., White, F. F., Somerville, S. C., Mudgett, M. B., & Frommer, W. B. (2010). Sugar transporters for intercellular exchange and nutrition of pathogens. *Nature*, *468*(7323), 527–532. https://doi.org/10.1038/nature09606

Chialva, M., Lanfranco, L., & Bonfante, P. (2022). The plant microbiota: composition, functions, and engineering. *Current Opinion in Biotechnology*, *73*, 135–142. https://doi.org/10.1016/j.copbio.2021.07.003

Compant, S., Mitter, B., Colli-Mull, J. G., Gangl, H., & Sessitsch, A. (2011). Endophytes of grapevine flowers, berries, and seeds: identification of cultivable bacteria, comparison with other plant parts, and visualization of niches of colonization. *Microbial Ecology*, *62*(1), 188–197. https://doi.org/10.1007/s00248-011-9883-y

Cook, D. E., Kramer, H. M., Torres, D. E., Seidl, M. F., & Thomma, B. P. H. J. (2020). A unique chromatin profile defines adaptive genomic regions in a fungal plant pathogen. *ELife*, *9*, 1–32. https://doi.org/10.7554/ELIFE.62208

Cook, D. E., Mesarich, C. H., & Thomma, B. P. H. J. (2015). Understanding plant immunity as a surveillance system to detect invasion. *Annual Review of Phytopathology*, *53*(1), 541–563. https://doi.org/10.1146/annurev-phyto-080614-120114

Debray, R., Herbert, R. A., Jaffe, A. L., Crits-Christoph, A., Power, M. E., & Koskella, B. (2022). Priority effects in microbiome assembly. *Nature Reviews. Microbiology*, *20*(2), 109–121. https://doi.org/10.1038/S41579-021-00604-W

de Guillen, K., Mammri, L., Gracy, J., Padilla, A., Barthe, P., Hoh, F., Lahfa, M., Rouffet, J., Petit-Houdenot, Y., Kroj, T., & Lebrun, M. H. (2025). *Zymoseptoria tritici* effectors structurally related to killer proteins UmV-KP4 and UmV-KP6 inhibit fungal growth, and define extended protein families in fungi. *Molecular Plant Pathology*, *26*(8), e70141. https://doi.org/10.1111/MPP.70141

de Guillen, K., Ortiz-Vallejo, D., Gracy, J., Fournier, E., Kroj, T., & Padilla, A. (2015). Structure analysis uncovers a highly diverse but structurally conserved effector family in phytopathogenic fungi. *PLOS Pathogens*, *11*(10), e1005228. https://doi.org/10.1371/journal.ppat.1005228

de Jonge, R., Bolton, M. D., Kombrink, A., Van Den Berg, G. C. M., Yadeta, K. A., & Thomma, B. P. H. J. (2013). Extensive chromosomal reshuffling drives evolution of virulence in an asexual pathogen. *Genome Research*, *23*(8), 1271–1282. https://doi.org/10.1101/GR.152660.112

de Jonge, R., Peter van Esse, H., Kombrink, A., Shinya, T., Desaki, Y., Bours, R., van der Krol, S., Shibuya, N., Joosten, M. H. A. J., & Thomma, B. P. H. J. (2010). Conserved fungal LysM effector Ecp6 prevents chitin-triggered immunity in plants. *Science*, *329*(5994), 953–955. https://doi.org/10.1126/science.1190859

de Jonge, R., Peter van Esse, H., Maruthachalam, K., Bolton, M. D., Santhanam, P., Saber, M. K., Zhang, Z., Usami, T., Lievens, B., Subbarao, K. V., & Thomma, B. P. H. J. (2012). Tomato immune receptor Ve1 recognizes effector of multiple fungal pathogens uncovered by genome and RNA sequencing. *Proceedings of the National Academy of Sciences*, *109*(13), 5110–5115. https://doi.org/10.1073/pnas.1119623109

Derbyshire, M. C., & Raffaele, S. (2023). Surface frustration re-patterning underlies the structural landscape and evolvability of fungal orphan candidate effectors. *Nature Communications*, *14*(1), 5244. https://doi.org/10.1038/s41467-023-40949-9

Dunken, N., Widmer, H., Balcke, G. U., Straube, H., Langen, G., Charura, N. M., Saake, P., De Quattro, C., Schön, J., Rövenich, H., Wawra, S., Khan, M., Djamei, A., Zurbriggen, M. D., Tissier, A., Witte, C.-P., & Zuccaro, A. (2024). A nucleoside signal generated by a fungal endophyte regulates host cell death and promotes root colonization. *Cell Host & Microbe*, *32*(12), 2161-2177.e7. https://doi.org/10.1016/j.chom.2024.10.020

Du, Y., Han, X., & Tsuda, K. (2024). Microbiome-mediated plant disease resistance: recent advances and future directions. *Journal of General Plant Pathology 2024 91:1*, *91*(1), 1–17. https://doi.org/10.1007/S10327-024-01204-1

Eichfeld, R., Endeshaw, A. B., Hellmann, M. J., Moerschbacher, B. M., & Zuccaro, A. (2025). Domain gain or loss in fungal chitinases drives ecological specialization toward antagonism or immune suppression. *BioRxiv*, 2025.06.16.659886. https://doi.org/10.1101/2025.06.16.659886

Faino, L., Seidl, M. F., Shi-Kunne, X., Pauper, M., Van Den Berg, G. C. M., Wittenberg, A. H. J., & Thomma, B. P. H. J. (2016). Transposons passively and actively contribute to evolution of the two-speed genome of a fungal pathogen. *Genome Research*, *26*(8), 1091–1100. https://doi.org/10.1101/GR.204974.116/-/DC1

Fierer, N. (2017). Embracing the unknown: disentangling the complexities of the soil microbiome. *Nature Reviews Microbiology*, *15*(10), 579–590. https://doi.org/10.1038/nrmicro.2017.87

Fradin, E. F., & Thomma, B. P. H. J. (2006). Physiology and molecular aspects of *Verticillium* wilt diseases caused by *V. dahliae* and *V. albo-atrum*. *Molecular Plant Pathology*, *7*(2), 71–86. https://doi.org/10.1111/J.1364-3703.2006.00323.X

Gómez-Pérez, D., Schmid, M., Chaudhry, V., Hu, Y., Velic, A., Maček, B., Ruhe, J., Kemen, A., & Kemen, E. (2023). Proteins released into the plant apoplast by the obligate parasitic protist *Albugo* selectively repress phyllosphere-associated bacteria. *New Phytologist*, *239*(6), 2320–2334. https://doi.org/10.1111/nph.18995

Guerreiro, M. A., & Stukenbrock, E. H. (2025). Fungal plant pathogens. *Current Biology*, *35*(11), R480–R484. https://doi.org/10.1016/J.CUB.2025.02.046

Hacquard, S., Spaepen, S., Garrido-Oter, R., & Schulze-Lefert, P. (2017). Interplay between innate immunity and the plant microbiota. *Annual Review of Phytopathology*, *55*(1), 565–589. https://doi.org/10.1146/annurev-phyto-080516-035623

Hu, Y., Ding, Y., Cai, B., Qin, X., Wu, J., Yuan, M., Wan, S., Zhao, Y., & Xin, X. F. (2022). Bacterial effectors manipulate plant abscisic acid signaling for creation of an aqueous apoplast. *Cell Host & Microbe*, *30*(4), 518-529.e6. https://doi.org/10.1016/J.CHOM.2022.02.002

James, T. Y., Kauff, F., Schoch, C. L., Matheny, P. B., Hofstetter, V., Cox, C. J., Celio, G., Gueidan, C., Fraker, E., Miadlikowska, J., Lumbsch, H. T., Rauhut, A., Reeb, V., Arnold, A. E., Amtoft, A., Stajich, J. E., Hosaka, K., Sung, G. H., Johnson, D., … Vilgalys, R. (2006). Reconstructing the early evolution of Fungi using a six-gene phylogeny. *Nature 2006 443:7113*, *443*(7113), 818–822. https://doi.org/10.1038/nature05110

Jones, J. D. G., & Dangl, J. L. (2006). The plant immune system. *Nature* Vol. 444, Issue 7117, pp. 323–329. https://doi.org/10.1038/nature05286

Jones, J. D. G., Staskawicz, B. J., & Dangl, J. L. (2024). The plant immune system: from discovery to deployment. *Cell*, *187*(9), 2095–2116. https://doi.org/10.1016/J.CELL.2024.03.045

Katan. (2017). Diseases caused by soilborne pathogens: biology, management and challenges. *Journal of Plant Pathology*, *99*(2), 305–315. https://doi.org/http://www.jstor.org/stable/44686775.

Kawchuk, L. M., Hachey, J., Lynch, D. R., Kulcsar, F., Van Rooijen, G., Waterer, D. R., Robertson, A., Kokko, E., Byers, R., Howard, R. J., Fischer, R., & Prüfer, D. (2001). Tomato Ve disease resistance genes encode cell surface-like receptors. *Proceedings of the National Academy of Sciences of the United States of America*, *98*(11), 6511–6515. https://doi.org/10.1073/PNAS.091114198

Kettles, G. J., Bayon, C., Sparks, C. A., Canning, G., Kanyuka, K., & Rudd, J. J. (2018). Characterization of an antimicrobial and phytotoxic ribonuclease secreted by the fungal wheat pathogen *Zymoseptoria tritici*. *New Phytologist*, *217*(1), 320–331. https://doi.org/10.1111/nph.14786

Klosterman, S. J., Atallah, Z. K., Vallad, G. E., & Subbarao, K. V. (2009). Diversity, pathogenicity, and management of *Verticillium* species. *Annual Review of Phytopathology*, *47*(1), 39–62. https://doi.org/10.1146/annurev-phyto-080508-081748

Kombrink, A., & Thomma, B. P. H. J. (2013). LysM effectors: secreted proteins supporting fungal life. *PLoS Pathogens*, *9*(12), e1003769. https://doi.org/10.1371/journal.ppat.1003769

Liu, Y., Chen, L., Wu, G., Feng, H., Zhang, G., Shen, Q., & Zhang, R. (2017). Identification of root-secreted compounds involved in the communication between cucumber, the beneficial *Bacillus amyloliquefaciens* , and the soil-borne pathogen *Fusarium oxysporum*. *Molecular Plant-Microbe Interactions®*, *30*(1), 53–62. https://doi.org/10.1094/MPMI-07-16-0131-R

Lo Presti, L., Lanver, D., Schweizer, G., Tanaka, S., Liang, L., Tollot, M., Zuccaro, A., Reissmann, S., & Kahmann, R. (2015). Fungal effectors and plant susceptibility. *Annual Review of Plant Biology*, *66*(1), 513–545. https://doi.org/10.1146/annurev-arplant-043014-114623

Lundberg, D. S., Lebeis, S. L., Paredes, S. H., Yourstone, S., Gehring, J., Malfatti, S., Tremblay, J., Engelbrektson, A., Kunin, V., Rio, T. G. Del, Edgar, R. C., Eickhorst, T., Ley, R. E., Hugenholtz, P., Tringe, S. G., & Dangl, J. L. (2012). Defining the core *Arabidopsis thaliana* root microbiome. *Nature 2012 488:7409*, *488*(7409), 86–90. https://doi.org/10.1038/nature11237

Luti, S., Sella, L., Quarantin, A., Pazzagli, L., & Baccelli, I. (2020). Twenty years of research on cerato-platanin family proteins: clues, conclusions, and unsolved issues. *Fungal Biology Reviews*, *34*(1), 13–24. https://doi.org/10.1016/j.fbr.2019.10.001

McLaughlin, S., Zhalnina, K., Kosina, S., Northen, T. R., & Sasse, J. (2023). The core metabolome and root exudation dynamics of three phylogenetically distinct plant species. *Nature Communications 2023 14:1*, *14*(1), 1649-. https://doi.org/10.1038/s41467-023-37164-x

Mesny, F., Bauer, M., Zhu, J., & Thomma, B. P. H. J. (2024). Meddling with the microbiota: fungal tricks to infect plant hosts. *Current Opinion in Plant Biology*, *82*, 102622. https://doi.org/10.1016/j.pbi.2024.102622

Mesny, F., Hacquard, S., & Thomma, B. P. (2023). Co-evolution within the plant holobiont drives host performance. *EMBO Reports*, *24*(9), EMBR202357455-. https://doi.org/10.15252/embr.202357455

Möller, M., & Stukenbrock, E. H. (2017). Evolution and genome architecture in fungal plant pathogens. *Nature Reviews Microbiology* 15, 765-771 https://doi.org/10.1038/nrmicro.2017.76

Ngou, B. P. M., Ahn, H. K., Ding, P., & Jones, J. D. G. (2021). Mutual potentiation of plant immunity by cell-surface and intracellular receptors. *Nature 2021 592:7852*, *592*(7852), 110–115. https://doi.org/10.1038/s41586-021-03315-7

Ökmen, B., Katzy, P., Huang, L., Wemhöner, R., & Doehlemann, G. (2023). A conserved extracellular Ribo1 with broad-spectrum cytotoxic activity enables smut fungi to compete with host-associated bacteria. *New Phytologist*, *240*(5), 1976–1989. https://doi.org/10.1111/nph.19244

Oliveira Júnior, N. G., Souza, C. M., Buccini, D. F., Cardoso, M. H., & Franco, O. L. (2025). Antimicrobial peptides: structure, functions and translational applications. *Nature Reviews Microbiology* 2025, 1–14. https://doi.org/10.1038/s41579-025-01200-y

Pennington, H. G., Jones, R., Kwon, S., Bonciani, G., Thieron, H., Chandler, T., Luong, P., Morgan, S. N., Przydacz, M., Bozkurt, T., Bowden, S., Craze, M., Wallington, E. J., Garnett, J., Kwaaitaal, M., Panstruga, R., Cota, E., & Spanu, P. D. (2019). The fungal ribonuclease-like effector protein CSEP0064/BEC1054 represses plant immunity and interferes with degradation of host ribosomal RNA. *PLOS Pathogens*, *15*(3), e1007620. https://doi.org/10.1371/journal.ppat.1007620

Petti G. C. (2026): Homologous antimicrobial proteins in plants and fungi: conserved mechanisms shaping the plant microbiota. PhD-Thesis; University of Cologne

Pieterse, C. M. J., Zamioudis, C., Berendsen, R. L., Weller, D. M., Van Wees, S. C. M., Bakker, P. A. H. M., Nl, C. M. J. P., Nl, C. Z., Nl, R. L. B., Nl, S. V., & Nl, P. A. H. M. B. (2014). Induced Systemic Resistance by Beneficial Microbes. *Annual Review Phytopathology.* 52:347–375. https://doi.org/10.1146/ANNUREV-PHYTO-082712-102340

Pruitt, R. N., Gust, A. A., & Nürnberger, T. (2021). Plant immunity unified. *Nature Plants 2021 7:4*, *7*(4), 382–383. https://doi.org/10.1038/s41477-021-00903-3

Pruitt, R. N., Locci, F., Wanke, F., Zhang, L., Saile, S. C., Joe, A., Karelina, D., Hua, C., Fröhlich, K., Wan, W. L., Hu, M., Rao, S., Stolze, S. C., Harzen, A., Gust, A. A., Harter, K., Joosten, M. H. A. J., Thomma, B. P. H. J., Zhou, J. M., … Nürnberger, T. (2021). The EDS1–PAD4–ADR1 node mediates Arabidopsis pattern-triggered immunity. *Nature 2021 598:7881*, *598*(7881), 495–499. https://doi.org/10.1038/s41586-021-03829-0

Punt, W., Park, J., Roevenich, H., Kraege, A., Schmitz, N., Wieneke, J., Snelders, N. C., Fiorin, G. L., López-Moral, A., Chavarro-Carrero, E. A., Petti, G. C., Wippel, K., & Thomma, B. P. H. J. (2025). A gnotobiotic system reveals multifunctional effector roles in plant-fungal pathogen dynamics. *BioRxiv*, 2025.03.27.645772. https://doi.org/10.1101/2025.03.27.645772

Raaijmakers, J. M., & Weller, D. M. (1998). Natural plant protection by 2,4-Diacetylphloroglucinol-producing *Pseudomonas* spp. in take-all decline soils. *Molecular Plant-Microbe Interactions MPMI*, *11*(2), 144–152.

Raffaele, S., & Kamoun, S. (2012). Genome evolution in filamentous plant pathogens: why bigger can be better. *Nature Reviews Microbiology 2012 10:6*, *10*(6), 417–430. https://doi.org/10.1038/nrmicro2790

Rolfe, S. A., Griffiths, J., & Ton, J. (2019). Crying out for help with root exudates: adaptive mechanisms by which stressed plants assemble health-promoting soil microbiomes. *Current Opinion in Microbiology*, *49*, 73–82. https://doi.org/10.1016/j.mib.2019.10.003

Roussin-Léveillée, C., Lajeunesse, G., St-Amand, M., Veerapen, V. P., Silva-Martins, G., Nomura, K., Brassard, S., Bolaji, A., He, S. Y., & Moffett, P. (2022). Evolutionarily conserved bacterial effectors hijack abscisic acid signaling to induce an aqueous environment in the apoplast. *Cell Host & Microbe*, *30*(4), 489-501.e4. https://doi.org/10.1016/j.chom.2022.02.006

Rovenich, H., Boshoven, J. C., & Thomma, B. P. (2014). Filamentous pathogen effector functions: of pathogens, hosts and microbiomes. *Current Opinion in Plant Biology*, *20*, 96–103. https://doi.org/10.1016/j.pbi.2014.05.001

Sánchez-Vallet, A., Tian, H., Rodriguez-Moreno, L., Valkenburg, D.-J., Saleem-Batcha, R., Wawra, S., Kombrink, A., Verhage, L., de Jonge, R., van Esse, H. P., Zuccaro, A., Croll, D., Mesters, J. R., & Thomma, B. P. H. J. (2020). A secreted LysM effector protects fungal hyphae through chitin-dependent homodimer polymerization. *PLOS Pathogens*, *16*(6), e1008652. https://doi.org/10.1371/journal.ppat.1008652

Sato, Y., Bex, R., Berg, G. C. M. van den, Höfte, M., Seidl, M. F., & Thomma, B. P. H. J. (2025). *Starship* giant transposons dominate plastic genomic regions in a fungal plant pathogen and drive virulence evolution. *Nat Commun* 16, 6806. https://doi.org/10.1038/s41467-025-61986-6

Seidl, M. F., & Van den Ackerveken, G. (2019). Activity and phylogenetics of the broadly occurring family of microbial Nep1-like proteins. *Annual Review of Phytopathology*, *57*(1), 367–386. https://doi.org/10.1146/annurev-phyto-082718-100054

Seong, K., & Krasileva, K. V. (2023). Prediction of effector protein structures from fungal phytopathogens enables evolutionary analyses. *Nature Microbiology 2023 8:1*, *8*(1), 174–187. https://doi.org/10.1038/s41564-022-01287-6

Sexton, A. C., & Howlett, B. J. (2006). Parallels in fungal pathogenesis on plant and animal hosts. *Eukaryotic Cell*, *5*(12), 1941–1949. https://doi.org/10.1128/EC.00277-06

Snelders, N. C., Boshoven, J. C., Song, Y., Schmitz, N., Fiorin, G. L., Rovenich, H., van den Berg, G. C. M., Torres, D. E., Petti, G. C., Prockl, Z., Faino, L., Seidl, M. F., & Thomma, B. P. H. J. (2023). A highly polymorphic effector protein promotes fungal virulence through suppression of plant-associated Actinobacteria. *New Phytologist*, *237*(3), 944–958. https://doi.org/10.1111/nph.18576

Snelders, N. C., Kettles, G. J., Rudd, J. J., & Thomma, B. P. H. J. (2018). Plant pathogen effector proteins as manipulators of host microbiomes? *Molecular Plant Pathology*, *19*(2), 257–259. https://doi.org/10.1111/mpp.12628

Snelders, N. C., Petti, G. C., van den Berg, G. C. M., Seidl, M. F., & Thomma, B. P. H. J. (2021). An ancient antimicrobial protein co-opted by a fungal plant pathogen for in planta mycobiome manipulation. *Proceedings of the National Academy of Sciences*, *118*(49), e2110968118. https://doi.org/10.1073/pnas.2110968118

Snelders, N. C., Rovenich, H., Petti, G. C., Rocafort, M., van den Berg, G. C. M., Vorholt, J. A., Mesters, J. R., Seidl, M. F., Nijland, R., & Thomma, B. P. H. J. (2020). Microbiome manipulation by a soil-borne fungal plant pathogen using effector proteins. *Nature Plants*, *6*(11), 1365–1374. https://doi.org/10.1038/s41477-020-00799-5

Snelders, N. C., Rovenich, H., & Thomma, B. P. H. J. (2022). Microbiota manipulation through the secretion of effector proteins is fundamental to the wealth of lifestyles in the fungal kingdom. *FEMS Microbiology Reviews*, *46*(5). https://doi.org/10.1093/femsre/fuac022

Sokol, N. W., Slessarev, E., Marschmann, G. L., Nicolas, A., Blazewicz, S. J., Brodie, E. L., Firestone, M. K., Foley, M. M., Hestrin, R., Hungate, B. A., Koch, B. J., Stone, B. W., Sullivan, M. B., Zablocki, O., Trubl, G., McFarlane, K., Stuart, R., Nuccio, E., Weber, P., … Pett-Ridge, J. (2022). Life and death in the soil microbiome: how ecological processes influence biogeochemistry. *Nature Reviews Microbiology*, *20*(7), 415–430. https://doi.org/10.1038/s41579-022-00695-z

Sperschneider, J., Dodds, P. N., Gardiner, D. M., Manners, J. M., Singh, K. B., & Taylor, J. M. (2015). Advances and challenges in computational prediction of effectors from plant pathogenic fungi. *PLOS Pathogens*, *11*(5), e1004806. https://doi.org/10.1371/journal.ppat.1004806

Spooren, J., van Bentum, S., Thomashow, L. S., Pieterse, C. M. J., Weller, D. M., & Berendsen, R. L. (2024). Plant-driven assembly of disease-suppressive soil microbiomes. *Annual Review of Phytopathology*, *62*(1), 1–30. https://doi.org/10.1146/annurev-phyto-021622-100127

Stevens, E. J., Li, J. D., Hector, T. E., Drew, G. C., Hoang, K., Greenrod, S. T. E., Paterson, S., & King, K. C. (2025). Within-host competition causes pathogen molecular evolution and perpetual microbiota dysbiosis. *The ISME Journal*, 19(1). https://doi.org/10.1093/ISMEJO/WRAF071

Tanaka, S., Brefort, T., Neidig, N., Djamei, A., Kahnt, J., Vermerris, W., Koenig, S., Feussner, K., Feussner, I., & Kahmann, R. (2014). A secreted *Ustilago maydis* effector promotes virulence by targeting anthocyanin biosynthesis in maize. *ELife*, *2014*(3), e01355. https://doi.org/10.7554/eLife.01355.001

Thomma, B., Cammue, B., & Thevissen, K. (2002). Plant defensins. *Planta*, *216*(2), 193–202. https://doi.org/10.1007/s00425-002-0902-6

Todd, A. E., Orengo, C. A., & Thornton, J. M. (1999). Evolution of protein function, from a structural perspective. *Current Opinion in Chemical Biology*, *3*(5), 548–556. https://doi.org/10.1016/S1367-5931(99)00007-1

Torres, D. E., Thomma, B. P. H. J., & Seidl, M. F. (2021). Transposable Elements Contribute to Genome Dynamics and Gene Expression Variation in the Fungal Plant Pathogen *Verticillium dahliae*. *Genome Biology and Evolution*, *13*(7). https://doi.org/10.1093/GBE/EVAB135

Trivedi, P., Leach, J. E., Tringe, S. G., Sa, T., & Singh, B. K. (2020). Plant–microbiome interactions: from community assembly to plant health. *Nature Reviews Microbiology*, *18*(11), 607–621. https://doi.org/10.1038/s41579-020-0412-1

Usami, T., Momma, N., Kikuchi, S., Watanabe, H., Hayashi, A., Mizukawa, M., Yoshino, K., & Ohmori, Y. (2017). Race 2 of *Verticillium dahliae* infecting tomato in Japan can be split into two races with differential pathogenicity on resistant rootstocks. *Plant Pathology*, *66*(2), 230–238. https://doi.org/10.1111/PPA.12576

Vandenkoornhuyse, P., Quaiser, A., Duhamel, M., Le Van, A., & Dufresne, A. (2015). The importance of the microbiome of the plant holobiont. *New Phytologist*, *206*(4), 1196–1206. https://doi.org/10.1111/nph.13312

Weiberg, A., Wang, M., Lin, F.-M., Zhao, H., Zhang, Z., Kaloshian, I., Huang, H.-D., & Jin, H. (2013). Fungal small RNAs suppress plant immunity by hijacking host RNA interference pathways. *Science*, *342*(6154), 118–123. https://doi.org/10.1126/science.1239705

Yuan, M., Jiang, Z., Bi, G., Nomura, K., Liu, M., Wang, Y., Cai, B., Zhou, J. M., He, S. Y., & Xin, X. F. (2021). Pattern-recognition receptors are required for NLR-mediated plant immunity. *Nature*, *592*(7852), 105–109. https://doi.org/10.1038/S41586-021-03316-6

Zhang, Y., Gao, Y., Liang, Y., Dong, Y., Yang, X., Yuan, J., & Qiu, D. (2017). The *Verticillium dahliae* SnodProt1-Like protein VdCP1 contributes to virulence and triggers the plant immune system. *Frontiers in Plant Science*, *8*, 289292. https://doi.org/10.3389/fpls.2017.01880

Zhou, J., & Ning, D. (2017). Stochastic community assembly: does it matter in microbial ecology? *Microbiology and Molecular Biology Reviews*, *81*(4). https://doi.org/10.1128/MMBR.00002-17

Zhou, J., Wu, S., Chen, X., Liu, C., Sheen, J., Shan, L., & He, P. (2014). The *Pseudomonas syringae* effector HopF2 suppresses Arabidopsis immunity by targeting BAK 1. *The Plant Journal*, *77*(2), 235–245. https://doi.org/10.1111/tpj.12381